PNWD-3552
WTP-RPT-114 Rev. 1

Final Report: Gas Retention and Release in Hybrid Pulse Jet Mixed Tanks Containing Non-Newtonian Waste Simulants

R. L. Russell
S. D. Rassat
S. T. Arm
M. S. Fountain
B. K. Hatchell
C. W. Stewart
C. D. Johnson
P. A. Meyer
C. E. Guzman-Leong

March 2005

Prepared for Bechtel National, Inc.
under Contract No. 24590-101-TSA-W000-00004

LEGAL NOTICE

WTP-RPT-114 Rev. 1

Final Report: Gas Retention and Release in Hybrid Pulse Jet Mixed Tanks Containing Non-Newtonian Waste Simulants

R. L. Russell	C. W. Stewart
S. D. Rassat	C. D. Johnson
S. T. Arm	P. A. Meyer
M. S. Fountain	C. E. Guzman-Leong
B. K. Hatchell	

March 2005

22 FWD 3/23/05

3/~~25~~/05

for W. Tamosaitis

ACCEPTED FOR

WTP PROJECT USE

Test specification: 24590-WTP-TSP-RT-03-010 Rev. 0
Test plan: TP-RPP-WTP-326 Rev. 0
Test exceptions: 24590-WTP-TEF-RT-03-082 and
24590-WTP-TEF-RT-04-00005
R&T focus area: Pretreatment
Test Scoping Statement(s): B-100

BATTELLE
75 YEARS OF INNOVATION

Battelle—Pacific Northwest Division
Richland, Washington, 99352

Completeness of Testing

This report describes the results of work and testing specified by Test Specification 24590-WTP-TSP-RT-03-010, Rev. 0 and Test Plan TP-RPP-WTP-326, Rev. 0. The work and any associated testing followed the quality assurance requirements outlined in the Test Specification/Plan. The descriptions provided in this test report are an accurate account of both the conduct of the work and the data collected. Test plan results are reported. Also reported are any unusual or anomalous occurrences that are different from expected results. The test results and this report have been reviewed and verified.

Approved:

Gordon H. Beeman, Manager
WTP R&T Support Project

3/16/05
Date

Testing Summary

The U.S. Department of Energy (DOE) Office of River Protection's Waste Treatment Plant (WTP) will process and treat radioactive waste that is stored in tanks at the Hanford Site. Pulse jet mixers (PJMs) along with air spargers and steady jets generated by recirculation pumps have been selected for use in mixing the high-level waste (HLW) slurries in several tanks [e.g., the lag storage (LS) vessels and the ultrafiltration feed process (UFP) vessels]. These mixing technologies are collectively called PJM/hybrid mixing systems.

A test program was established by Bechtel National, Inc. (BNI) to quantify gas-retention and release behavior in nonradioactive, non-Newtonian waste simulants (rheologically representative of actual waste) that are mixed with PJM/hybrid mixing systems. This report summarizes the results of numerous experiments in six different test stands. Table S.1 lists the test stands and key information for each one. In addition to reporting data, this report provides an assessment of the test results obtained with these PJM systems.

Table S.1. Summary of Test Stands Used in Gas-Retention and Release Testing

Test Stand **Parameter**	**UFP**	**LS**	**336 4PJM**	**APEL 4PJM**	**SRNL 4PJM**	**CBT**
WTP Process Vessel Being Represented	UFP Vessels UFP-VSL-00002A UFP-VSL-00002B	HLW LS Vessels HLP-VSL-0027A HLP-VSL-0027B HLP-VSL-0028	None; generic system to investigate general scaling and physical phenomena	None; generic system to investigate general scaling and physical phenomena	None; generic system to investigate general scaling and physical phenomena	None; generic system without PJMs to investigate air sparging
Scale	1:4.9	1:4.3	Large scale (approx. half - scale)	1:4.5 (relative to 336 4PJM system)	1:8.9 (relative to 336 4PJM system)	Large scale (approx. half - scale)
Number and Configuration of PJMs	4PJM trifoil configuration (3 PJMs around 1)	8PJM cluster configuration (7 PJMs around 1)	4PJM square configuration	4PJM square configuration	4PJM square configuration	No PJMs
Air Sparging Tubes	Four—three between PJMs, one near the center PJM (only center sparger used in tests)	Eight—near the tank wall between PJMs (only four spargers used in tests)	None	None	None	Nine—diamond-in-a-square pattern plus one tube in the center
Slurry Recirculation Capability	Four nozzles at 113 L/min each (used only in holdup tests)	One nozzle at 340 L/min (used only in holdup tests)	None	None	None	None
Gas-Holdup Test # (results discussed in Section 5)	Seq. 5, Run 3 Seq. 6, Run 3	Seq. 14, Run 3 Seq. 15A, Run 3	12/16/2003 test 07/22/2004 test	Tests on 12/15/2003 01/27/2004 02/19/2004 02/25/2004	031213R2A	N/A

N/A = not applicable.

Table S.1 (contd)

Test Stand / Parameter	UFP	LS	336 4PJM	APEL 4PJM	SRNL 4PJM	CBT
Gas-Release Test # (results discussed in Section 6)	Seq. 5, Run 2 Seq. 5, Run 4 Seq. 6, Run 2 Seq. 6, Run 4	Seq. 14, Run 2 Seq. 14, Run 4 Seq. 15, Run 2 Seq. 15A, Run 4	12/12/2003 03/23/2004 03/25/2004 07/20/2004 07/23/2004	12/02/2003 12/14/2003 01/26/2004 02/06/2004 02/10/2004 02/11/2004 02/12/2004 02/13/2004 02/18/2004 02/20/2004 02/25/2004	031212R1A 040227R1A	N/A
Air Sparger-Induced Gas-Release Test Numbers (results discussed in Section 7)	Seq. 5, Run 5 Seq. 6, Run 5	Seq. 15A, Run 5	None	None	None	CBT-040603 CBT-040608 CBT-040609 CBT-040614 CBT-040615 CBT-040707 CBT-040715 CBT-040611 CBT-040616

Objectives

During normal operation, PJM hybrid mixing systems in WTP vessels containing waste slurries exhibiting a non-Newtonian rheology must achieve safe, controllable release of flammable gas, hydrogen in particular. A main objective of this testing was to measure and report gas-holdup levels in simulants during steady-state PJM operation using vessels and conditions that have been shown to provide sufficient mobilization.(a) In addition, during loss-of-power events, PJMs may be operated intermittently on backup power. Excess retained gas above the steady-state holdup level is likely to accumulate in the slurry during periods of no mixing. Upon restart of the PJMs, the gas-release volume and rate must not create flammable conditions in the vessel headspace. Thus, the second objective of this testing was to measure experimentally and report gas-release characteristics (rates and volumes) in a scenario representing loss of power with intermittent mixing using backup power. It is important to demonstrate that an intermittent mixing protocol results in predictable and consistent release volumes and rates over a long period with many cycles of intermittent mixing. Thus, another objective was to measure and report the consistency of gas-release rates and volumes for a series of intermittent mixing cycles.

A further objective was to determine mass-transfer coefficients and gas holdup in kaolin-bentonite clay and pretreated AZ-101 slurry simulants in a bench-scale apparatus. In bubble-column holdup tests, the goal was to measure the retained gas fraction (holdup) as a function of sparged gas flow rate using several gas species, including oxygen and hydrogen. The purpose of mass-transfer tests was to evaluate

---

(a) The mixing performance of model WTP LS and UFP jet mixed vessels using configurations and operating conditions similar to those applied in gas retention and release tests is summarized in Johnson et. al. Hybrid Pulse Jet Mixer Test Results for Prototype Ultrafiltration Feed Process and High-Level Waste Lag Storage Vessels, WTP-RPT-128 (in processing) and Poloski et al. (2004).

oxygen mass-transfer coefficients in the non-Newtonian simulants using sparged air to strip oxygen from the initially oxygen-saturated slurries. Table S.2 summarizes these objectives and results.

Table S.2. Summary of Test Objectives and Results

Test Objective	Objective Met	Discussion
Measure and report gas-holdup volumes in simulant during steady-state PJM operation using vessels and conditions that have been demonstrated separately to provide sufficient mobilization.	Yes	Gas-holdup volumes were measured at several gas-generation rates and with various combinations of mixing methods (spargers, recirculation, and PJMs) in the LS and UFP prototypes in February 2004 using configurations and operating conditions determined in previous mixing studies to have acceptable performance. Gas-holdup tests were also successfully completed in a generic configuration of four PJMs in three test stands (336 Building 4PJM and Applied Process Engineering Laboratory [APEL] 4PJM at Battelle—Pacific Northwest Division [PNWD] and Savannah River National Laboratory [SRNL] 4PJM) representing different sizes (scaled) of the system (Table 5.1). Holdup varied from less than 1 to over 3 vol%, generally correlating with gas-generation rate, simulant depth and rheology, and PJM drive-cycle parameters (Table 5.2 and Section 5.4).
Experimentally measure and report gas-release characteristics (i.e., rates and volumes) in a loss-of-power scenario.	Yes	The transient decrease in gas-volume fraction was measured for restarting mixing systems after a period of gas accumulation in the LS and UFP prototypes with configurations similar to those used in the gas-holdup tests (see Figure 6.1, for example). Additional gas-release tests were completed in the 336 4PJM system, the APEL 4PJM system, and a small-scale 4PJM system at SRNL (Table 6.1). Sparging-only gas-release characteristics were investigated separately in the 336 cone-bottom tank (Table 7.1). The gas-release data show that gas-release behavior is influenced by simulant rheology (faster release for weaker slurry, Figure 6.16, for example), gas bubble size as deduced from the more rapid gas releases in tests that accumulated gas overnight (Figure 6.8), and somewhat by initial gas fraction (Figure 6.14). Full-coverage sparging was shown to be very effective at releasing retained gas (Figure 7.3, Table 7.3).
Measure and report consistency of gas-release rates and volumes for a series of intermittent mixing cycles.	Yes	A series of three repeated gas-release tests was completed in the APEL 4PJM system on consecutive days using the same ~100 gal (~380 L) batch of kaolin-bentonite clay and approximately the same initial gas fraction (3.7 to 4.3 vol%). Rates and volumes are reported. Results indicate release behavior is nominally repeatable (Figure 6.17).
Determine mass-transfer coefficients and gas holdup in kaolin-bentonite clay and pretreated AZ-101 slurry simulants in bench-scale apparatus.	Yes	Bench-scale bubble-column devices were used to measure gas holdup and mass-transfer coefficients in two kaolin-bentonite clay dilutions and a pretreated Tank AZ-101 slurry simulant. The gas holdup was a significant function of gas superficial velocity, slurry consistency, and the concentrations of sodium nitrate and anti-foaming agent. The scaled oxygen mass-transfer coefficients were in good agreement for the three simulants tested at the bench scale. A similar proof-of-concept gas-stripping test was conducted in the APEL UFP prototype vessel containing an initially oxygen-saturated kaolin-bentonite clay simulant. The mass transfer coefficient determined in the UFP test was approximately half that estimated from the correlation established in the bench-scale studies (1.27/hr).

The results presented in this report are for specific mixing-system configurations that were convenient to use in establishing the basis for scaled testing. Specific mixing results obtained from these tests should not be directly applied to WTP process vessels. Rather the test results verify the scaling laws for gas retention and release that are also developed in this document. These scaling laws must be applied in any interpretation of small-scale test results as applied to plant vessels.

Test Exceptions

The scope of testing was increased in Test Exceptions 24590-WTP-TEF-RT-03-082[(a)] and 24590-WTP-TEF-RT-04-00005.[(b)] Table S.3 describes the scope increase for this testing.

Table S.3. Test Exceptions

Test Exceptions	Discussion
24590-WTP-TEF-RT-03-082	Bubble-column gas-holdup and mass-transfer testing was added to the test matrix
24590-WTP-TEF-RT-04-00005	Gas-retention and release testing matrix was expanded

Results and Performance Against Success Criteria

For the most part, the gas-retention and release test success criteria provided in Test Specification 24590-WTP-TSP-RT-03-010 Rev. 0[(c)] and Test Plan TP-RPP-WTP-326[(d)] mirror the test objectives: the tests will be deemed successful if gas-holdup levels are measured during steady-state PJM operation using vessels that have demonstrated sufficient mobilization of the simulants under prototypic PJM operating conditions. In addition, these tests will be deemed successful if applicable gas-release characteristics are measured upon restart of PJMs following a simulated loss-of-power event, and measurements are made over several test cycles to assess the consistency of the release volume and rate.

(a) Smith GL. 2003. *Revised Test Matrix for Pulse Jet Mixer Gas Holdup and Release Testing.* 24590-WTP-TEF-RT-03-082, Bechtel National, Inc., Richland, WA.

(b) Smith GL. 2004. *Additional APEL and 336 4PJM Scaled Test Matrix for Pulse Jet Mixer Gas Holdup and Release Testing.* 24590-WTP-TEF-RT-04-00005, Bechtel National, Inc., Richland, WA.

(c) Smith GL. 2003. *Pulse Jet Mixer Gas Hold-Up and Release Testing.* 24590-WTP-TSP-RT-03-010 Rev. 0, Bechtel National, Inc., Richland, WA.

(d) Rassat SD and JW Brothers. 2003. *Test Plan for Pulse Jet Mixer Gas Hold-Up and Release Testing.* TP-RPP-WTP-326, Battelle—Pacific Northwest Division, Richland, WA.

Table S.4. Success Criteria

Success Criteria	How Testing Did or Did Not Meet Success Criteria
Measure gas-holdup levels (gas-volume fractions) during steady-state PJM operation using vessels that have demonstrated sufficient mobilization of the simulants under prototypic PJM operating conditions.	Success criterion met. Steady-state gas-holdup levels measured in LS and UFP vessels (prototypes) in February 2004 using configurations and operating conditions determined previously in mixing studies to have acceptable performance. Also, gas-holdup tests were successfully completed in the 336 Bldg 4PJM system (336 4PJM) and in several tests in the APEL 4PJM system.
These tests will be deemed successful if 1) applicable gas-release characteristics are measured upon restart of PJMs following a simulated loss-of-power event and 2) measurements are made over several test cycles to assess the consistency of the release volume and rate.	The transient decrease in gas-volume fraction measured on restarting mixing systems after a period of gas accumulation in the LS and UFP prototypes in February 2004 using configurations similar to those in the gas-holdup tests. Additional gas-release tests were successfully conducted in the 336 4PJM system, the APEL 4PJM system, and a small-scale 4PJM system at the SRNL. Three nearly identical release tests in the APEL 4PJM system demonstrated consistency of release volume and rate. Analysis of these data has determined the dominant release characteristics, consisting of time constants and release rates.

Quality Requirements

Battelle—Pacific Northwest Division (PNWD) implements the RPP-WTP quality requirements by performing work in accordance with the PNWD Waste Treatment Plant Support Project quality assurance project plan (QAPjP) approved by the RPP-WTP Quality Assurance (QA) organization. This work was performed to the quality requirements of NQA-1-1989 Part I, Basic and Supplementary Requirements, and NQA-2a-1990 Part 2.7. These quality requirements are implemented through PNWD's Waste Treatment Plant Support Project (WTPSP) Quality Assurance Requirements and Description Manual.

Experiments that were not method-specific were performed in accordance with PNWD's procedures QA-RPP-WTP-1101, "Scientific Investigations," and QA-RPP-WTP-1201, "Calibration Control System," ensuring that sufficient data were taken with properly calibrated measuring and test equipment (M&TE) to obtain quality results.

As specified in Test Specification 24590-WTP-TSP-RT-03-010 Rev. 0, "Pulse Jet Mixer Gas Hold-Up and Release Testing," BNI's QAPjP, PL-24590-QA00001, was not applicable because the work was not performed in support of environmental/regulatory testing, and the data will not be used as such.

PNWD addresses internal verification and validation activities by conducting an Independent Technical Review of the final data report in accordance with PNWD's procedure QA-RPP-WTP-604. This review verifies that the reported results are traceable, that inferences and conclusions are soundly based, and the reported work satisfies the Test Plan objectives. This review procedure is part of PNWD's WTPSP Quality Assurance Requirements and Description Manual.

Research and Technology Test Conditions

The test specification established extensive conditions to ensure that the results are valid for WTP project needs. Because of their extensive nature, the conditions are not listed here, but they essentially constitute the test methodology described later in this summary. The conditions, as modified by the test exceptions and test plan, were satisfied.

Simulant Use

The simulants used were selected based on actual waste slurry rheology measurements[(a)] that indicate the WTP non-Newtonian waste stream can be represented by a Bingham Plastic rheology model, which is represented by

$$\tau = \kappa\dot{\gamma} + \tau_y \tag{S.1}$$

where

τ = resulting shear stress

κ = consistency factor

$\dot{\gamma}$ = shear rate or strain rate

τ_y = Bingham yield stress; the assumed minimum stress required to initiate fluid movement as determined by a flow curve obtained by fitting rheological data using a Bingham Plastic rheological model.

The non-Newtonian waste stream bounding values of τ_y = 30 Pa and κ = 30 cP were identified based on limited data from actual waste slurries that can be represented by a Bingham Plastic rheology model (Poloski 2004). These values provide the basis for initially developing and selecting an upper bounding simulant used for this testing. Laponite and kaolin-bentonite simulant formulation changes established independently for PJM mixing studies were monitored and adopted as appropriate for the gas-retention and release tests. For the retention and release test strategy, simulant strength (yield stress and shear strength) and consistency factor, as determined by 24590-WTP-GPG-RTD-001 Rev. 0, are critical rheological properties. The limited data on shear strength (τ_{ss}, measured by a shear vane method) recorded for pretreated actual waste indicate that τ_{ss} exceeds the bounding τ_y obtained from Bingham plastic model fits of rheological data (rheograms) by a factor of ~2 where τ_{ss} is defined as the critical rheological parameter and ~70 Pa is used as an upper bounding value. The ratio τ_{ss}/τ_y for the kaolin-bentonite and Laponite simulants is typically 2 or greater, so a simulant with a bounding τ_y of 30 Pa is likely to provide a nearly bounding τ_{ss} as well.

Simulant selection criteria taken into consideration:

- Similarity to previous PJM test simulants
- Experience with previous PJM test simulants
- Stability of the material over the test duration
- Ease of preparation
- Compatibility with instrumentation and experimental detection methods for measuring gas content (as indicated by level)

(a) The development and selection of non-Newtonian waste simulants for use in WTP PJM testing are summarized in Poloski et al. (2004).

- Characterization of rheological properties
- Physical representation of WTP non-Newtonian waste stream
- Availability and procurement and disposal costs
- Health and environmental risks and hazards associated with material.

Test Methodology

Formulations for generating gas bubbles volumetrically *in situ* within simulant to represent the gas-generation process in actual waste were developed from initial bench-scale activities. The surface-catalyzed decomposition of hydrogen peroxide (H_2O_2) to generate oxygen gas bubbles was selected based on previous experience using this technique with clay waste simulant. Recipes were developed to allow target gas-volume fractions to be generated in the kaolin-bentonite clay and Laponite simulants used in PJM mixing studies. While bentonite clay surfaces are sufficiently catalytic to generate gas bubbles from H_2O_2 in kaolin-bentonite clay simulant, a manganese dioxide catalyst system was developed to allow more rapid gas generation for some tests. Laponite simulant requires an additive to produce the desired decomposition of H_2O_2 in a timely manner. Copper nitrate was selected for this purpose after screening several candidate catalysts.

Following successful development at the bench scale, the decomposition of nominal 30 wt% H_2O_2 solution was used to generate gas *in situ* in the kaolin-bentonite clay simulant contained in PJM vessels. The H_2O_2 solution was injected with a peristaltic pump through a single tube into the well-mixed cavern area adjacent to pulse-tube nozzles while the PJMs were operating under steady-state conditions. The amount of H_2O_2 introduced was quantified by weight. In the initial preparation for gas-release tests, a specified amount of H_2O_2 was introduced over a short period of time (e.g., 10 to 20 min). After some period of additional mixing (e.g., 10 to 30 min), the system was shut down to allow the H_2O_2 to decompose and gas bubbles to be retained in the quiescent simulant. The accumulated gas was typically released by operating the PJMs (and spargers if used) the following day.

In gas-holdup tests, H_2O_2 solution was added to simulant at a fixed rate over an extended period of time (2 to 3 hours) to continuously generate oxygen gas while the simulant was mixed in the PJM vessel using specified normal operating conditions. Injection continued until a new steady-state level was achieved in the test vessel. The rate of H_2O_2 injection was determined by recording the weight of a solution feed container as a function of time. The mixing system was shut down shortly after completion of the gas-holdup tests, resulting in simulant volume growth as residual H_2O_2 decomposed. After a short period of gas retention (30 minutes or less), a gas-release test was typically conducted. In some tests, the growth period was allowed to extend overnight for a release test the next morning.

In gas-retention and release experiments, retained gas-volume fractions in the vessels were assessed by changes in surface level, which were independently correlated to simulant volume. Several methods, including instrumental techniques (level probes) and visual/camera observations, were used to track changes in surface level over time. Ultrasonic level sensors were deployed in each of the vessels, and signals were output to a data acquisition and control system where they were recorded at a high frequency. Radio frequency admittance-level sensors were deployed to track the level within the PJMs of each vessel and to monitor tank surface level in some vessels. Typically, a single volume was determined for each pulse cycle using the sensor average minimum level obtained when the PJMs were drawn full (suction phase).

A simple, well-mixed slurry bubble migration in a theoretical model was derived to explain the basic elements of gas retention and release associated with PJM operation in non-Newtonian slurries, and the model was used as a tool to help interpret the test results. We assumed that gas-release rates and the rate of change of gas content represent averages such that the well-mixed model was applicable to the PJM system, that gas was retained in the slurry as bubbles, and that gas release occurred by bubbles rising to the slurry surface. Under these assumptions, a differential expression relating gas generation and release to the retained gas-volume fraction, α, was obtained. The general solution of the ordinary differential equation is

$$\alpha(t) = \alpha_0 e^{-Nt_C/\tau_R} + g_v \tau_R (1 - e^{-Nt_C/\tau_R}) \tag{S.2}$$

where α_0 = initial gas-volume fraction
N = number of PJM cycles
t_C = cycle period
τ_R = gas release time constant
g_v = volumetric gas-generation rate (at average *in situ* hydrostatic pressure) per unit volume of gas-free slurry

The time dependence of the average retained gas fraction α is completely characterized by the gas release number $N_R = t_C/\tau_R$ where $\tau_R = H/U_R$, H is the slurry fill depth, and U_R is the average bubble rise velocity at the slurry surface.

In the steady state, Eq. (S.2) reduces to

$$\alpha_{SS} = g_v \tau_R = g_v \frac{H}{U_R} \tag{S.3}$$

where α_{SS} is the steady-state retained gas-volume fraction or holdup. Eq. (S.3) is the fundamental statement of the relationship of the gas-generation, retention, and release parameters in the system. It can be used to predict the holdup from estimates of the release time constant and generation rate or to estimate the release time constant from the holdup and gas-generation rate.

Results

The tests described in this report were conducted in scaled test vessels with mixing systems similar, but not identical to, those anticipated for the full-scale plant. In addition, the operating modes of the test systems generally did not match plant conditions. For example, gas-generation rates were generally much higher than expected for the plant, and much less sparging than planned for the plant (or none at all) was applied. Because of these differences, the actual holdup gas fractions and gas-release rates recorded in these tests do not directly represent plant values or bounds. Extrapolation to full-scale conditions can only be attempted with careful consideration of established scaling principles for hybrid PJM-sparged systems.

Holdup Tests

Data are available for gas-holdup tests conducted in the LS and UFP prototype vessels as well as the scaled 4PJM systems in APEL, SRNL, and the 336 Building. The tests covered a range of gas generation rates (and simulant rheologies as well as prototype vessel mixing system configurations. The results are summarized in Table S.5 (see Tables 5.1 and 5.2 for more details). Results of holdup tests at three scales are shown by way of example in Figure S.1.

Table S.5. Gas-Holdup Results Summary

Test	Rheology, τ_y (Pa), κ (cP)	Generation Rate, g_v (mL/L-min)	Holdup α_{ss} (vol%)
LS Seq. 14, Run 3	36, 27	1.6 3.7	0.6 ± 0.1 1.2 ± 0.07
LS Seq. 15A, Run 3	35, 26	1.6 3.4	0.8 ± 0.06 1.4 ± 0.1
UFP Seq. 5, Run 3	36, 19	4.2	3.4 ± 0.3
UFP Seq. 6, Run 3	36, 20	3.7	3.5 ± 0.09
336 4PJM 12/16/03	44, 23	1.4	3.7 ± 0.05
336 4PJM 7/22/04	20, 18	0.8	1.6 ± 0.07
APEL 4PJM 12/15/03	40, 21	3.7	1.6 ± 0.2
APEL 4PJM 1/27/04	13, 22	3.7	0.9 ± 0.1
APEL 4PJM 2/19/04	7, 9	3.6	1.1 ± 0.04
APEL 4PJM 2/25/04	18, 14	3.6 7.2	0.9 ± 0.1 1.3 ± 0.07
SRNL 4PJM 12/13/03 R2A	16, 19	4.1	1.3 ± 0.01

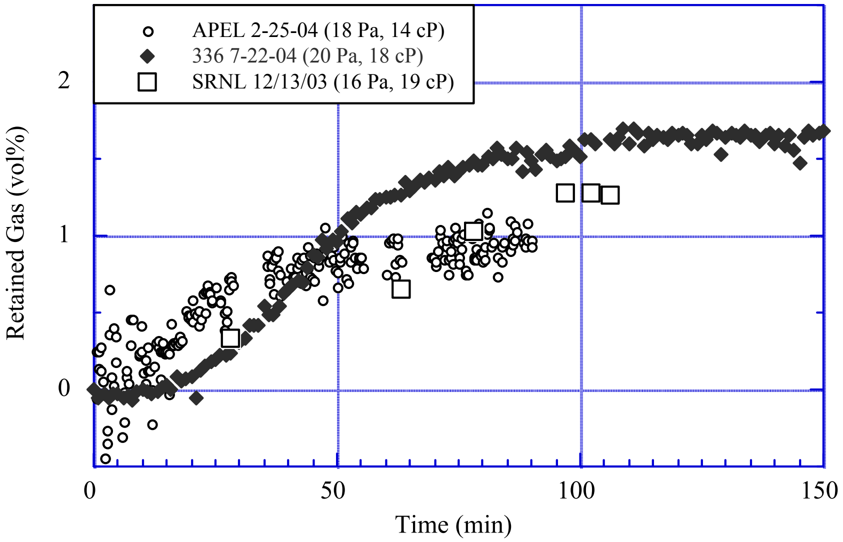

Figure S.1. 4PJM Holdup Scaling Example

The gas retention data show that gas holdup is influenced by the effectiveness of the mixing system, specifically PJM design, PJM drive cycle, gas generation rate, and simulant depth and rheology. Sparging and recirculation may have some effect, but the direct impact was not obvious in these tests. The steady-state holdup observed in these tests can be calculated to within a standard error of ±0.13 vol% using Eq. (S.3) where U_R is expressed by the following empirical model:[a]

$$U_R = -19.96 + 0.0415g_v - 22.27D + 4.85N_{PJM} + 0.1474U_0 + 820d_0 + 0.0436\tau_y + 0.0145\kappa + 0.00845(N_{PJM}\, g_v) - 0.00326(\kappa\, g_v) + 7.064(d_0\, D) - 0.0122(\tau_y\, N_{PJM}) \qquad (S.4)$$

where g_v = gas generation rate (mL gas/L simulant - min)
D = tank diameter (m)
U_0 = peak- average PJM nozzle drive velocity (m/s)
d_0 = PJM nozzle diameter (m)
N_{PJM} = number of PJMs
τ_y = Bingham yield stress (Pa) of the simulant
κ = Bingham consistency (cP) of the simulant.

The model of Eq. (S.3) substituted for U_R in Eq. (S.2) is plotted against all the holdup data in Figure S.2. Individual gas-fraction data points are shown with a "+", and the average holdup for each test is indicated by the symbols. The R^2 value for the model is 0.88.

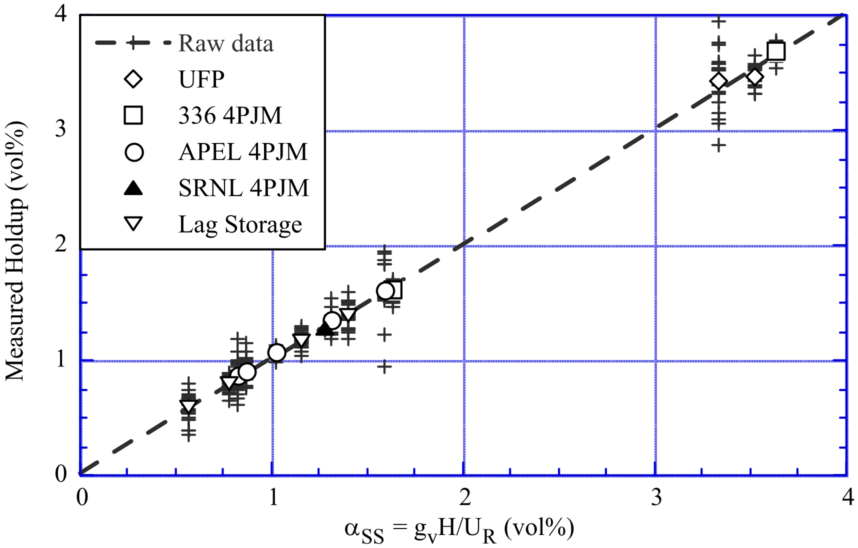

Figure S.2. Empirical Holdup Model Prediction Compared to Data

---

(a) The empirical holdup models given in this section must be used with careful consideration of scaling principles. They should only be applied to tank configurations, operational modes, and slurry conditions representative of the tests that were modeled.

Gas Release Tests

Gas-release test data were available for the LS and UFP prototype vessels as well as the scaled 4PJM systems at SRNL, APEL, and the 336 Building. Parameters that were varied include simulant rheology, initial gas fraction, mixing system, and, indirectly, bubble size by allowing the slurry to set overnight in many tests (creating larger bubbles) and less than 1 hour in a few tests (see Table 6.1).

Analysis of data from combined holdup and release tests showed that essentially all the H_2O_2 injected for the holdup tests had reacted before beginning the release tests, so gas generation was insignificant during the release. At the same time, this analysis showed that a single value for the time constant ($\tau_R = H/U_R$) predicted the gas volume fraction reasonably well through holdup tests, subsequent quiescent gas accumulation period, and initial rapid gas release. This confirms that scaling laws and the basic bubble rise model correctly portray the physical processes at work in the system. However, depending on the rheology, most release tests showed a persistent residual gas fraction that decayed much more slowly than the initial release, apparently following one or more additional longer time constants. Figure S.3 shows APEL 4PJM (1:4.5 scale relative to 336 4PJM) release tests for an example.

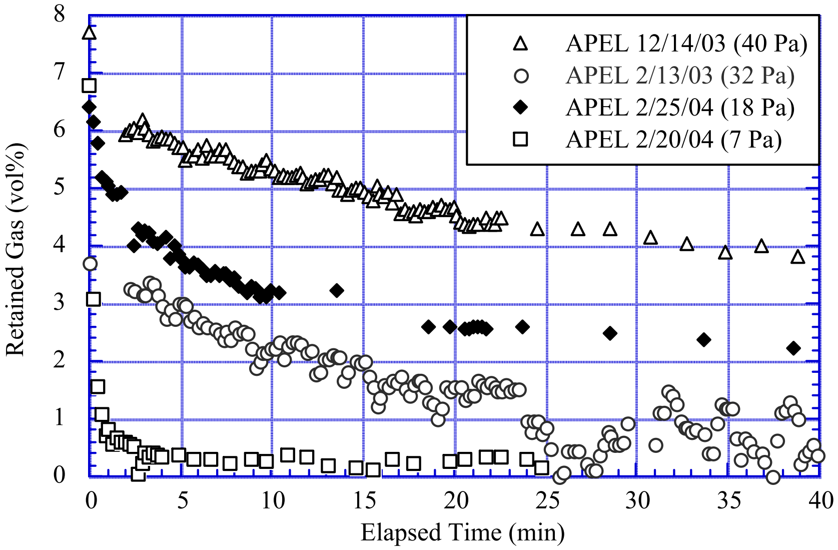

Figure S.3. APEL 4PJM Gas Release Tests: Effect of Simulant Rheology

The measured gas volume fractions during release could be predicted using three time constants and an expression similar to Eq. (S.2):

$$\alpha(t) = R_S \tau_S e^{-t/\tau_S} + R_M \tau_M e^{-t/\tau_M} + R_L \tau_L e^{-t/\tau_L} \quad \text{(S.5)}$$

where the six constants, R_S, τ_S, R_M, τ_M, R_L, and τ_L, are release rates and time constants for short, medium, and long duration components. The short time constant (fast release rate) roughly approximates that found to model the combined holdup-release tests. The long duration transient (slow release rate) often represents essentially a constant release rate. Most PJM release tests and all the sparger release tests were adequately modeled with only two time constants.

As yet, the physical phenomena represented by two or three distinct release rates have not been positively determined. However, the evidence suggests that the lower release rates and longer time constants may represent an erosion process where an unmixed or less well-mixed region of the simulant is slowly subsumed into, or recycled with, the well-mixed PJM cavern volume. Gas-release test conditions and results are summarized in Table S.6.

Table S.6. Gas Release Test Results Summary

Test/Date	α_0 (vol%)	τ_y (Pa)	κ (cP)	τ_S (min)	τ_M (min))	τ_L (min)
Lag Storage						
S14 R2 2/6/04	3.0	36	27	0.3	4.3	-
S14 R4 2/7/04	6.5			1.3	12	-
S15 R2 2/9/04	4.7	34-37	24-27	0.7	9	-
S15A R4 2/14/04	5.4			2.7	-	97
UFP						
S5 R2 2/12/04	3.2	34-39	19-20	3.3	-	50
S5 R4 2/12/04	6.8			0.6	13	1440
S6 R2 2/13/04	4.6	33-37	18-20	5.9	-	53
S6 R4 2/13/04	6.9			4.2	-	92
336 4PJM						
12/12/03	8.9	44	23	0.86	30	220
3/23/04	3.4	35	22	1.1	*73*	520
3/25/04	2.4			1.9	-	1100
7/20/04	1.9	20	18	2.1	-	280
7/23/04	3.8			1.3	36	670
SRNL 4PJM						
12/12/03	10.3	16	19	3.9	24	-
2/27/04	11.4	29	31	1.7	46	-
APEL 4PJM						
12/2/03	10.9	20	26	1.7	13.6	-
12/14/03	7.7	40	21	2.1	-	98
1/26/04	2.96	13	22	2.1	-	30
2/6/04	3.6	32-33	19	3.9	43	-
2/10/04	5.7			3.0	-	155
2/11/04	4.2			-	15	1440
2/12/04	4.3			-	8.2	585
2/13/04	3.7			-	16	-
2/18/04	5.0	7	10	1.6	-	-
2/20/04	6.8			0.25	19	-
2/25/04	6.4	18	14	2.8	-	134

The gas-release data show that release behavior is influenced by simulant rheology, gas-bubble size as deduced from the more rapid releases in tests that accumulated gas overnight, and somewhat by initial gas fraction. Extended-coverage sparging was very effective in releasing residual retained gas at the end of a test, but only partial sparging was used in the prototype vessel tests, so the full effect of sparging in hybrid PJM systems was not investigated. Gas-release behavior appears to scale well in the single series of tests that covers the full range of geometric scales (336, APEL, and SRNL 4PJM systems). Gas-release behavior is also quite repeatable, as demonstrated in a series of repeated tests within the APEL 4PJM test stand and as generally characterized by the gas-release model.

Sparging Gas-Release Tests

Sparger-induced gas-release tests were conducted in the LS and UFP vessels and in the 336 cone-bottom tank (CBT) equipped specifically for sparging tests. The sparging gas-release tests followed procedures similar to those used in PJM-induced gas-release tests. Besides the different dimensions and configurations of the test vessels themselves, the primary variables in the sparger gas-release tests were the number and location of spargers activated, the air flow rates, and the initial gas fraction. The simulant rheological properties varied only slightly over the test period, only becoming measurably stiffer in the CBT tests as water evaporated into the sparged air over the 2-month test period.

Within the test uncertainty, full-flow sparging released essentially all of the releasable gas over a period of about 10 minutes in every test. Application of the basic bubble-rise gas-release model from Section 2 gives gas-release time constants between 0.8 and 2.2 minutes for the cone-bottom tank tests and 0.6 to 2.4 minutes for more-or-less full sparging in UFP and LS tests.

Tests using sparging at one-third of full flow in the cone-bottom tank tests required a longer time, 40 to 60 minutes, compared with approximately 10 minutes for the full-flow tests. Time constants for the one-third flow tests ranged from 3 to 10 minutes compared with about 1 minute for the full-flow tests. Partial sparging in the UFP and LS tests resulted in incomplete gas release. The results of release tests in the CBT are summarized in Table S.7. An illustration of the effect of sparger air flow on gas-release behavior is shown in Figure S.4. Note that the gas fractions given in Table S.7 include a 0.3 to 0.5 vol% sparger holdup that exists only when spargers are operating.

Table S.7. Summary of Sparging Gas Release Tests in the CBT

Test ID	Air Flow (scfm)	Gas Fraction (vol%)		Release Time Const. (min)	
		Initial	Final	Fast	Slow
CBT-040603	204.2	1.5	-0.1	0.8	-
CBT-040608	202.1	2.0	0.2	0.8	88
CBT-040609	202.6	1.7	0.1	0.9	54
CBT-040614	203.3	1.4	0.4	1.0	241
CBT-040615	206.0	1.7	0.2	0.9	1440
CBT-040707	171.3	1.2	0	1.5	79
CBT-040715	206.3	0.8	0	2.2	1440
CBT-040611	68.2	2.4	0.7	2.8	218
CBT-040616	57.8	0.7	-0.1	6.3	-

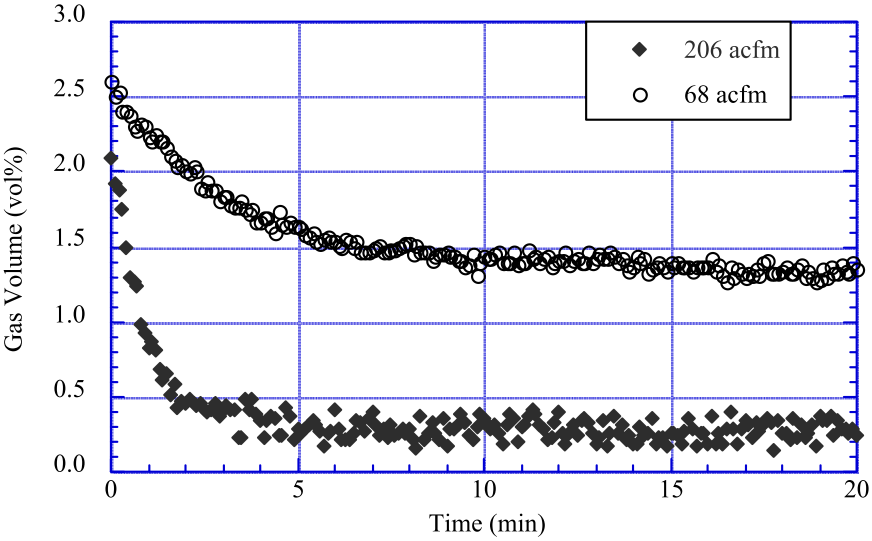

Figure S.4. Effect of Sparger Air Flow (CBT 6/15 and 6/11)

Bubble Column Holdup Tests

Hydrogen gas was not used in the majority of gas-retention and release tests because of the experimental difficulties associated with generating hydrogen *in situ* in relatively large quantities and the potential safety issues. Therefore, bench-scale tests in a bubble-column were completed to compare the relative holdup of oxygen, hydrogen, and other gases in various simulants.

A parametric study was performed to determine gas holdup (α_i) in the bubble column tests as a function of gas type, yield stress, consistency (κ), sodium nitrate ($NaNO_3$) and anti-foaming agent (AFA) concentrations and gas superficial velocity (u, cm/s, defined as volumetric gas flow rate divided by column cross-sectional area). A statistical analysis on the results provided the following correlation:

$$\alpha_i = \exp\begin{pmatrix} -2.93 - 0.152\kappa + 2.99[\mathrm{NaNO_3}] + 0.0171[\mathrm{AFA}] + 0.256\kappa[\mathrm{NaNO_3}] - \\ 4.67\times10^{-4}\kappa[\mathrm{AFA}] - 0.0187[\mathrm{AFA}][\mathrm{NaNO_3}] + 3.72\times10^{-3}\kappa^2 - 1.91[\mathrm{NaNO_3}]^2 \end{pmatrix} u^{0.743} \quad \text{(S.6)}$$

The residual square value is 80%, indicating that this percentage of the data variability is explained by the correlation, which shows yield stress and gas type to have no significant impact on the holdup. Increasing consistency and sodium nitrate and AFA concentrations increase gas holdup, the latter because bubble coalescence is reduced, and bubbles are smaller. Gas type was experimentally observed to affect holdup and the statistical analysis probably failed to capture this observation because three of the four gases (air, argon and oxygen) have very similar molecular weights. The correlation predicts gas holdup in pretreated AZ-101 HLW simulant containing AFA for gas velocities less than 0.8 cm/s very well, assuming a value for [$\mathrm{NaNO_3}$] equivalent to the total salt concentration in the slurry. Gas holdup was observed to decrease with increasing velocities above 0.8 cm/s for reasons unclear at present and for which the correlation does not predict. In the absence of AFA, the correlation significantly over-predicts gas holdup although holdup is empirically equivalent (i.e. disregarding differences in salt concentrations) for slurries of similar rheology.

Mass Transfer Tests

Oxygen mass transfer tests were also completed using a bench-scale bubble column with clay (two different strengths) and pretreated AZ-101 slurry simulants. Dissolved oxygen probes were placed in the simulant, which was initially concentrated in oxygen by sparging oxygen gas through the bubble column. Subsequently, the excess dissolved oxygen was stripped from the simulant by sparging with air. The change in dissolved oxygen content over time at different heights in the column was used to calculate mass-transfer coefficients as a function of superficial gas velocity (flow rate). The scaled mass-transfer coefficients were in good agreement for the three simulants tested. A similar proof-of-concept gas-stripping test was conducted in the UFP prototype vessel containing partially oxygen-saturated kaolin-bentonite clay simulant. In the demonstration, air flowed continuously at a controlled rate through four sparge tubes while the PJMs were operated using prototypic cyclic conditions. The mass-transfer coefficient determined in the UFP test was approximately half that estimated from the correlation established in the bench-scale studies (1.27/hr), possibly due to differences in the bubble sizes or uniformity of sparged air in the two test stands.

Discrepancies and Follow-on Tests

None.

References

Poloski AP, PA Meyer, LK Jagoda, and PR Hrma. 2004. *Non-Newtonian Slurry Simulant Development and Selection for Pulsed Jet Mixer Testing.* WTP-RPT-111 Rev 0, PNWD-3495, Battelle—Pacific Northwest Division, Richland, WA.

Acknowledgments

The authors want to thank all the other individuals who contributed to the success of this task. Several staff contributed to the gas-retention and release testing in both the 336 Building and the Applied Process Engineering Laboratory. These include Bill Buchmiller, Jagan Bontha, Harry Smith, Dale Wallace, Bill Combs, Carl Enderlin, Michele Friedrich, Mike Johnson, Rich Hallen, Mark Gerber, Jim Bates, Jim Alzheimer, Joe Brothers, Franz Nigl, Adam Poloski, Tom Loftus, Richard Ehlers, Wayne Wilcox, and David Blanchard.

The following contributors from Savannah River National Laboratory are also to be thanked for the data that they provided to help support this task: David Wilson, Hector Guerrero, Michael Restivo, Tim Steeper, Russell Eibling, Erich Hansen, Tim Jones, and Kurt Eberl.

Several more staff provided assistance by manually observing the levels in the tank, including Jessica Vucelick, Kate Deters, Abby Capetillo, Jackie Newell, Spiro Tzemos, Lawrence Schienbein, Brent Barnett, and Sergei Sinkov.

The authors would also like to thank Lynette Jagoda and Bryan Cook for their analysis of the rheology samples. We also appreciate the efforts of Jim Fort, Wassana Yantasee, and Sato Yokuda in providing the velocity information. Beric Wells must be thanked for his data and videotape review and SK Sundaram for his data review. Dean Kurath is to be thanked for his invaluable oversight of this project. Lenna Mahoney is to be thanked for her thorough review of this report. And, as always, we thank Sheila Bennett for her valuable editorial support.

Nomenclature

4PJM	Four pulse jet mixers
A	Cross-sectional area of the slurry surface
acfm	Actual cubic feet per minute
AFA	Anti-foaming agent
atm	Atmosphere (unit of pressure)
APEL	Applied Process Engineering Laboratory
ASME	American Society of Mechanical Engineers
a	Interfacial area per unit volume of slurry
A_g	H_2O_2 reaction rate constant
A_R	Gas release rate constant
BNI	Bechtel National, Inc.
C	Instantaneous concentration
C*	Saturated solution concentration
C^o	Initial concentration at time zero
CBT	Cone-bottom tank
cm/s	Velocity units expressed in distance per time
C_p	H_2O_2 concentration
cP	Centipoise
D	Tank diameter
DACS	Data acquisition and control system
DB	Drexelbrook level probes
DOE	U.S. Department of Energy
d_b	Average bubble diameter (m)
d_{bt}	Distance between the top and bottom pressure transducers
d_{db}	Distance between the diffuser and bottom pressure transducer
d_0	PJM nozzle diameter (m)
d_y	Cylinder thickness
D_L	Gas diffusivity
$D_{L,H}$	H_2 diffusivities
$D_{L,O}$	O_2 diffusivities

F_k	Fraction of total gas release
F_L	Fraction of gas release described by long time constant
F_M	Fraction of gas release described by medium time constant
F_S	Fraction of gas release described by short time constant
Fe_2O_3	Iron oxide
g_c	Standard acceleration of gravity (= 32.x174 ft/s^2 = 9.80665 m/s^2)
g_m	Moles of gas generated per unit volume of gas-free slurry per unit time
g_v	Specific volumetric gas-generation rate at the average *in situ* hydrostatic pressure and gas-bubble (slurry) temperature (m^3 gas/m^3 gas-free slurry/s)
$g_{m,O2}$	Specific molar O_2 gas-generation rate
$g_{v,a}$	Specific volumetric gas-generation rate
$g_{v,a,O2}$	Steady state specific volumetric O_2 gas generation rate at the slurry surface resulting from H_2O_2 decomposition at ambient pressure
$g_{v,O2}$	*In situ* volumetric O_2 gas-generation rate
G_m	Total molar gas-generation rate
$G_{m,O2}$	Total steady-state molar O_2 gas-generation rate
$G_{v,O2}$	Total *in situ* volumetric rate of O_2 generation from H_2O_2 decomposition
GR&R	Gas retention and release
h_{wet}	Wetted height above the bottom of the tank part
H	Slurry level in the tank; assumed constant for small gas fractions (α <10 vol%)
H_2	Hydrogen
H_{max}	Tank liquid level when PJMs are empty
H_{min}	Height of the fluid surface in a tank when the PJMs are full of fluid
H_{pjm}	Average height of fluid within the PJMs of a test stand
H_{static}	Tank liquid level under static conditions
$H_{surface}$	Height of the fluid surface in the tank
H'_{pjm}	Average height of fluid within the PJMs, minus an 8 cm offset
H/D	Height-to-diameter ratio
HLW	High-level waste
H_2O_2	Hydrogen peroxide
ID	Inside diameter
K	Kelvin (unit of absolute temperature)
k	Mass-transfer coefficient

k_l	Liquid side mass-transfer coefficient
$(k_la)_H$	k_la products for H_2
$(k_la)_O$	k_la products for O_2
L	Liter (unit of volume)
LAW	Low-activity waste
LRB	Laboratory record book
LS	HLW lag storage vessel
M	Molarity (moles chemical per L solution)
MnO_2	Manganese dioxide
M_p	Molecular weight of H_2O_2 (34.0 g/mol)
MSE	Mean square error
M&TE	Measuring and test equipment
min	Minute (unit of time)
mol	Quantity of chemical in gram-moles
N	Number of PJM cycles
$NaNO_3$	Sodium nitrate
n_b	Number density of bubbles
n_g	Number of moles of gas present in the bubbles per unit volume of slurry
N_c	Number of PJM cycles
N_g	Total number of moles of gas in the slurry
N_{O2}	Number of moles of O_2 present in the simulant as gas bubbles
N_p	Gram-moles of hydrogen peroxide
N_{pjm}	Number of PJMs in a tank for a specific test configuration
N_R	Gas release number
nm	Nanometer
O_2	Oxygen
OD	Outside diameter
p	Average *in situ* pressure at H/2 (Pa)
P_0	Pressure head in the bubble column at zero gas flow
p_a	Ambient headspace pressure (Pa)
P_b	Pressure recorded by the bottom pressure transducer
ps	Hydrogen peroxide solution

P_t	Pressure recorded by the top pressure transducer without gas
P_{tg}	Pressure recorded by the top pressure transducer with gas
Pa	Pascal
PCD	Pitch circle diameter
PJM	Pulse jet mixer
PNWD	Battelle—Pacific Northwest Division
ppm	Parts per million
PVC	Polyvinyl chloride
QA	Quality assurance
QAPjP	PNWD Waste Treatment Plant Support Project Quality Assurance project plan
Q_{ps}	Average volumetric flow rate of H_2O_2 solution
r	Radius
r_{pjm}	Radius of the PJM
R	Ideal gas constant (0.08206 L-atm/mol-K)
R^2	Residual square
R_L	Release rate constant for long duration component
R_m	Total molar gas-release rate (moles of gas released per second)
R_M	Release rate constant for medium duration component
R_0	Initial (maximum) volumetric gas-release rate from the slurry (m^3 gas/s)
R_S	Release rate constant for short duration component
R_v	Volumetric gas-release rate from the slurry at the surface (m^3 gas/s)
RF	Radio frequency
ROB	Region of bubbles
scfm	Standard cubic feet per minute—14.7 pounds per square inch absolute (psia), 68°F, and 0% relative humidity
SRNL	Savannah River National Laboratory
t	Time
t_c	Cycle period
t_C	PJM cycle time
t_D	PJM drive time
T	Slurry and gas bubble temperature (K)
t_w	Cone wall thickness

u	Gas superficial velocity (cm/s)
	u_{cr} Average bubble rise velocity throughout bubble column
U_0	Peak average PJM nozzle drive velocity (m/s)
U_R	Average bubble rise velocity at the slurry surface (m/s)
UFP	Ultrafiltration feed process vessel
US	Ultrasonic level sensors
V	Tank volume
VS	Video level scale
V_R	Total release volume
v_{bH}	Average bubble volume at the slurry surface (m^3)
V_{bs}	Total bubbly-slurry volume (m^3)
V_g	Volume of gas retained in bubbly simulant
V_{O2}	Volume of O_2 gas
V_{pjm}	Total volume in all PJMs above H_{min}
V_{ps}	Volume of hydrogen peroxide solution
V_s	Gas-free or initial slurry volume (m^3)
$V_{s,0}$	Gas-free slurry volume before adding H_2O_2 solution
V_{static}	Tank volume under static conditions (PJMs vented to atmosphere)
V_{tank}	Tank volume when the PJMs are full of fluid
w_{ps}	Mass flow rate of H_2O_2 solution
W_p	Mass of unreacted H_2O_2 in simulant
$\overline{W}_p$	Integral time average of the unreacted H_2O_2
W_{ps}	Total mass of H_2O_2 solution
W_s	Mass of the simulant
WTP	Waste Treatment Plant
WTPSP	Waste Treatment Plant Support Project
x_p	Weight fraction of H_2O_2 in solution
ZOI	Zone of influence
α	Average retained gas-volume fraction (m^3 gas/m^3 bubbly slurry)
α_H	Gas-volume fraction at the slurry surface
	α_i – Average retained gas volume fraction (m^3 gas/m^3 gas-free slurry)
α_0	Initial gas-volume fraction prior to a gas-release test

α_{ss}	Steady-state gas-volume fraction; gas holdup (m^3 gas/m^3 bubbly slurry)
$\alpha(t)$	Time-varying gas volume fraction
ΔP_{bt}	Differential pressure between the two pressure transducers in the bubble column
$\dot{\gamma}$	Shear rate or strain rate
κ	Bingham plastic consistency (mPa-s)
ρ	Density
ρ_{ps}	Density of the hydrogen peroxide solution
ρ_s	Gas-free slurry density (kg/m^3); assumes well-mixed slurry with no settling
τ	Shear stress in rheology measurements
τ_0	Yield stress
τ_L	Time constant for long duration component
τ_M	Time constant for medium duration component
τ_R	Gas release time constant
τ_S	Time constant for short duration component
τ_{ss}	Shear strength measured by a shear vane
τ_y	Bingham yield stress

Contents

Figures

Tables

1.0 Introduction

A test program was established by Bechtel National, Inc. (BNI) to quantify the gas-retention and release behavior of pulse jet mixer (PJM) systems using nonradioactive, non-Newtonian waste simulants. This report summarizes the results of numerous experiments in six different test stands. In addition to reporting data, this report provides an assessment of the test results obtained with these PJM systems. Section 1.1 provides the background of the need for this gas-retention and release testing, and Section 1.2 presents an outline of the report.

1.1 Background

The Hanford Site has 177 single- and double-shell tanks containing radioactive waste. The U.S. Department of Energy (DOE) Office of River Protection's Waste Treatment Plant (WTP) is being designed and built to pretreat and then to vitrify a large portion of these wastes. The WTP consists of three primary facilities: a pretreatment facility, a low-activity waste (LAW) vitrification facility, and a high-level waste (HLW) vitrification facility. The pretreatment facility receives waste feed from the Hanford tank farms and separates it into 1) a high-volume, low-activity, liquid process stream stripped of most solids and radioisotopes and 2) a much smaller-volume of HLW slurry containing most of the solids and most of the radioactivity. In the pretreatment facility, solids and radioisotopes are removed from the waste by precipitation, filtration, and ion exchange processes to produce the LAW streams. The slurry of filtered solids is blended with two ion exchange eluate streams containing soluble radioisotopes to produce the HLW stream. The HLW and LAW vitrification facilities convert these process streams into glass, which is poured directly into stainless steel canisters.

Several vessels through which the HLW pretreated sludge stream will be processed will be mixed using PJM technology. This technology has been selected for use in so called "black cell" regions of the WTP. Within these regions of the plant, maintenance capability will not be available for the operating life of the WTP. PJM technology was selected for use in these regions because the technology lacks moving mechanical parts that require maintenance.

The concept behind PJM mixing technology involves a pulse tube coupled with a jet nozzle. One end of the tube is immersed in the tank while periodic vacuum, vent, and pressurized air are supplied to the opposite end. This creates various operating modes for the pulse tube, including the drive cycle (pressure), where the contents of the PJM tube are discharged at high velocity through the nozzle; the refill mode (vacuum), where the tank contents refill the pulse tube; and an equilibration mode (vent), where the pulse tube and tank fill levels approach the same level. The PJM system uses these operating modes to produce a sequence of drive cycles that provide mixing in the vessel. PJM operating parameters, velocity, nozzle diameter, and drive time, along with the rheological properties of the fluid being mixed, all contribute to the effectiveness of mixing within the vessel.

Many of the waste slurries to be received and processed in the WTP exhibit non-Newtonian behavior. In particular, when stationary, the fluid can develop gel-like properties and behave like a very weak solid. When an applied force exceeds its shear strength, it acts like a fluid and begins to flow. The majority of available knowledge for mixing non-Newtonian fluids is associated with mechanical agitators. The subject of jet mixing in non-Newtonian fluids is a relatively new and developing field, with some theoretical analysis and applied research being pursued in industry and academia. The field of non-steady jet mixing in non-Newtonian fluids is essentially in its infancy.

The generation and retention of flammable gases in and their subsequent release from radioactive waste contained in Hanford waste tanks has long been studied (see, for example, Johnson et al. 2001). In particular, the mechanisms of gas-bubble retention and release in non-Newtonian tank waste were the subject of several investigations by Gauglitz, Stewart, and colleagues (Gauglitz et al. 1995, 1996; Stewart et al. 1996; Rassat et al. 1998). These studies developed relationships between gas-retention and release behavior and the physical properties (e.g., rheology) of actual and simulated waste, including bentonite clay/water slurries. While these and other investigations give a fundamental understanding of the phenomena, they do not provide sufficient information to predict a priori the gas-retention and release characteristics for non-Newtonian waste-slurries in WTP vessels mixed with PJMs and possibly with auxiliary spargers or recirculation pumps.

Therefore, a test program was established to quantify the gas-retention and release behavior of PJM systems using nonradioactive, non-Newtonian waste simulants. This report summarizes the results of numerous experiments in five test stands operated by Battelle—Pacific Northwest Division (PNWD): 1) a reduced-scale model of the WTP ultrafiltration feed process (UFP) vessel; 2) a reduced-scale model of the WTP lag storage (LS) vessel; 3) a large-scale 4PJM vessel located in the 336 Building (336 4PJM); 4) a smaller, geometrically scaled version of the 336 4PJM system in the Applied Process Engineering Laboratory (APEL), referred to as the APEL 4PJM system; and 5) the 336 Building cone-bottom tank (CBT) that was used for the sparging tests. Wilson et al. (2004) provides limited data for a still smaller scale 4PJM system housed and operated at the Savannah River National Laboratory (SRNL). In addition to reporting data, this report provides an assessment of the test results obtained with these PJM systems.

The gas-retention and release test criteria were initially provided by BNI in Test Specification 24590-WTP-TSP-RT-03-010 Rev. 0,(a) and PNWD issued the corresponding Test Plan TP-RPP-WTP-326,(b) identifying a matrix of tests to provide the required information. Further gas-retention and release testing guidance was given by BNI in Test Exceptions 24590-WTP-TEF-RT-03-082(c) and 24590-WTP-TEF-RT-04-00005.(d)

During normal operation, PJMs in WTP vessels with non-Newtonian waste must achieve safe, controllable release of flammable gas. A main objective of this testing was to measure and report gas-holdup levels in rheologically representative simulants during steady-state PJM operation using LS and

---

(a) Smith GL. 2003. *Pulse Jet Mixer Gas Hold-Up and Release Testing.* 24590-WTP-TSP-RT-03-010 Rev. 0, Bechtel National, Inc., Richland, WA.

(b) Rassat SD and JW Brothers. 2003. *Test Plan for Pulse Jet Mixer Gas Hold-Up and Release Testing.* TP-RPP-WTP-326, Battelle – Pacific Northwest Division, Richland WA.

(c) Smith GL. 2003. *Revised Test Matrix for Pulse Jet Mixer Gas Holdup and Release Testing.* 24590-WTP-TEF-RT-03-082, Bechtel National, Inc., Richland, WA.

(d) Smith GL. 2004. *Additional APEL and 336 4PJM Scaled Test Matrix for Pulse Jet Mixer Gas Holdup and Release Testing.* 24590-WTP-TEF-RT-04-00005, Bechtel National, Inc., Richland, WA.

UFP model vessels (prototypes) and conditions that were separately demonstrated to provide sufficient mobilization.[(a)]

During loss-of-power events, PJMs may be operated intermittently on backup power. Excess retained hydrogen (H_2) above the steady-state holdup level is likely to accumulate in the waste slurry during periods of no mixing. Upon restart of the PJMs, the gas-release volume and rate must not result in flammable conditions in the vessel headspace. Additionally, in the case of a slow gas-release process, it is necessary to understand how long to operate the mixing system to reduce the retained gas fraction to acceptable levels. Therefore, the second objective of this testing was to experimentally measure and report gas-release characteristics (rates and volumes) in a loss-of-power scenario. Because it is important to demonstrate that an intermittent mixing protocol results in a predictable and consistent release behavior over a long period involving many cycles of mixing, a final objective was to measure and report the gas-release rates and volumes for a series of repeated intermittent mixing cycles.

The proposed use of spargers in combination with PJMs to enhance the effectiveness of mixing and gas release in the non-Newtonian waste vessels in the WTP has a further potential benefit. Air sparging may help mitigate the buildup of flammable gas in waste contained in PJM vessels. Proof-of-concept tests were conducted to demonstrate gas-stripping mass transfer in non-Newtonian simulants, and the results are reported in this document.

The mass-transfer coefficients and gas holdup in kaolin-bentonite clay and pretreated AZ-101 slurry simulants were also determined in a bench-scale apparatus to compare the gas holdup in different types of simulants with different types of gases. This was important so correlations could be made from the kaolin-bentonite clay to the actual waste.

1.2 Outline

The major thrust of the testing summarized in this document is oxygen (O_2) gas retention in and release from kaolin-bentonite clay waste-slurry and Laponite simulants in PJM systems. Hydrogen gas was not used in the majority of gas-retention and release tests because of the experimental difficulties associated with generating it *in situ* in relatively large quantities and the potential safety issues. As described below, several bench-scale tests were completed to compare the relative gas holdup of O_2, H_2, and other gases in various simulants. Before presenting the PJM test results and data analysis in Sections 5 and 6, theoretical and experimental background information is provided in Sections 2 through 4.

Section 2 outlines a theoretical and experimental framework to aid our understanding of gas-retention and release phenomena in PJM slurry systems. The theory is predicated on a model of gas-bubble migration in well-mixed non-Newtonian slurry. The model addresses normal PJM operations in which a steady-state retained gas fraction (gas holdup) is attained, and gas is released during both normal operations and restart of the mixing system after a quiescent period. Several important parameters are

---

(a) The mixing performance of model WTP LS and UFP PJM vessels using configurations and operating conditions similar to those applied in gas retention and release tests are summarized in Johnson et. al. Hybrid Pulse Jet Mixer Test Results for Prototype Ultrafiltration Feed Process and High-Level Waste Lag Storage Vessels, WTP-RPT-128 (in processing) and Poloski et al. (2004).

identified in the bubble-migration model development, and this section addresses how to produce and quantify many of them (e.g., gas-volume fraction) from an experimental perspective.

The principle of generating O_2 gas bubbles volumetrically in waste slurry simulants by decomposition of added hydrogen peroxide (H_2O_2), which is the method of gas generation used in gas-retention and release tests discussed in later sections of this report, is also discussed in Section 2. In preparation for tests in the large-volume PJM systems (~380 to 38,000 L), bench-scale O_2 gas-generation and retention scoping tests were completed with both kaolin-bentonite clay and Laponite simulants. Section 3 describes the testing to demonstrate and quantify O_2 generation resulting from H_2O_2 decomposition in small amounts (<1 L) of the kaolin-bentonite clay and Laponite simulants. Of particular interest are the quantities of H_2O_2 solution required to achieve target gas-volume fractions in the PJM-scale gas-release tests (i.e., provide recipes) and to develop an understanding of the O_2 generation rates as a function of H_2O_2 concentration and simulant/catalyst properties.

Section 4 describes the configuration details of the four PNWD-operated PJM test stands and the experimental methods used to obtain the gas-retention and release data in the APEL and 336 4PJMs and UFP and LS tanks. The section summarizes universal system operations, test stand-specific equipment and instrumentation, and the details for determining contained simulant volume from surface level measurements in each vessel. The experimentally determined variation in simulant volume as a function of time due to gas-bubble retention and release is the key to assessing gas-holdup and release volumes and rates in PJM systems.

The results of gas-holdup tests in the UFP and LS prototype vessels during February 2004 and tests in the scaled 4PJM test stands in APEL, SRNL, and the 336 Building are presented in Section 5. Steady gas generation was achieved by continuously adding H_2O_2 solution during routine operation of the PJM mixing system, which also included either sparger or recirculation pump operation in the prototype vessel tests. Increases in the simulant surface level over numerous PJM cycles were a measure of the accumulating gas volume in the simulant; an approximately constant level indicated an approach to steady state. The reported gas-holdup values are the gas-volume fraction measured at steady state.

In the gas-holdup tests described in Section 5, multiple generation rates were achieved by changing the H_2O_2 solution flow rate. This allowed us to determine the variation in gas holdup as a function of gas-generation rate. In each prototype vessel experiment, relatively thick kaolin-bentonite clay simulant was used (Bingham Plastic rheology model: >30 Pa yield stress; 19 to 27 cP consistency). However, in APEL 4PJM tests, the clay simulant rheology was varied by diluting thick clay with water. Gas-holdup tests were completed in APEL 4PJM with clay as thin as 7 Pa yield stress and 9 cP consistency and as thick as 40 Pa yield stress and 21 cP consistency, providing information on the variation in gas holdup with rheology. Two gas-holdup tests were completed in the 336 4PJM system using thick clay (44 Pa yield stress, 23 cP) and thinner clay (20 Pa yield stress, 18 cP) comparable to that used in two of the APEL 4PJM tests. The SRNL test used a clay simulant similar to the other 4PJM systems with a rheology of 16 Pa yield stress and 19 cP consistency.

Gas-release test results and data analysis are presented in Section 6. These experiments were completed with the same batches of clay used in the gas-holdup tests and provide essentially the same rheology in the specified test stands for gas-release tests. Gas-release tests were generally conducted by restarting the mixing system after some quiescent gas-accumulation period ranging from ~10 minutes to overnight. In the prototype vessels, a gas-release test often followed within ~30 minutes of a gas-holdup test because decomposition of residual H_2O_2 caused a rapid increase in the retained gas-volume fraction after the mixing system was shut down. However, evaluation of the data in Section 6 suggests that gas-generation rates during these gas-release tests are small.

As summarized in Section 6, the gas-release data were analyzed to determine the functional form and parameter dependencies that describe the gas-release process (gas-release time constants and peak release rates). The data show that gas-release behavior is influenced by simulant rheology, gas-bubble size as deduced from the more rapid releases in tests that accumulated gas overnight, and somewhat by the initial gas fraction. Extended-coverage sparging was very effective in releasing residual retained gas at the end of a test, but only partial sparging was used in the prototype vessel tests, so the full effect of sparging remains to be investigated. Gas-release behavior appears to scale well in the single series of tests that cover the full range of geometric scales (336, APEL, and SRNL 4PJM systems). Gas-release behavior is also quite repeatable, as demonstrated in a series of repeated tests within the APEL 4PJM test stand and as generally characterized by the gas-release model.

Sparger-induced gas-release test results are presented in Section 7. These tests followed procedures similar to those used in PJM-induced gas-release tests. Besides the different dimensions and configurations of the test vessels themselves, the primary variables in the sparger gas-release tests were the number and location of spargers activated, the air flow rates, and the initial gas fraction. The simulant rheological properties also varied somewhat over the test period, generally becoming stiffer as water evaporated into the sparged air.

As noted above, this report focuses on gas-retention and release behavior in PJM mixed systems (Sections 2 through 7). Sections 8 and 9 are self-contained discussions of bench-scale tests, comparing the relative gas holdup of O_2, H_2, and other gases in various simulants and O_2 mass transfer in non-Newtonian slurry simulants, respectively.[a] Section 8 briefly summarizes the experimental methods used and how the data were analyzed. The test results showing that there is a significant impact on gas holdup related to the gas type are then presented.

Section 9 briefly summarizes important mass-transfer theory before presenting experimental methods and the results of proof-of-concept tests. Bench-scale experiments demonstrate the stripping of O_2 from O_2-saturated kaolin-bentonite clay and pretreated AZ-101 chemical waste simulant resulting from air sparging at different flow rates. The results are used to calculate mass-transfer coefficients. A similar proof-of-concept gas-stripping test was also conducted in December 2003 in the UFP prototype vessel containing partially O_2-saturated kaolin-bentonite clay simulant. The simulant was sparged with air while the PJMs were operated using prototypic cyclic conditions. Section 10 contains the cited references, and appendixes contain supporting material.

(a) Mass transfer and bubble-column gas holdup testing is called for in Test Exception 24590-WTP-TEF-RT-03-082, "Revised Test Matrix for Pulse Jet Mixer Gas Holdup and Release Testing," by GL Smith, Bechtel National, Inc., Richland, WA.

2.0 Gas-Retention and Release Principles and Scaling

This section provides the theoretical and experimental framework needed to aid our understanding of gas-retention and release phenomena in PJM slurry systems. The theory is predicated on a model of gas-bubble migration in well-mixed non-Newtonian slurry (Section 2.1). The model addresses normal operations in which a steady-state retained gas fraction (gas holdup) is attained, and gas is released during normal operations and upon restart of the mixing system after a quiescent period. Several important parameters are identified in the model development. Section 2.2 considers from an experimental perspective how to produce and quantify many of these key parameters. The method of generating O_2 gas in waste slurry simulant using H_2O_2, which is the foundation of the gas-retention and release tests discussed in later sections, is described.

2.1 Theory

A model for gas retention and release based on bubble migration in well-mixed slurry is developed in Section 2.1.1. From the general model, more specific expressions for gas retention and holdup and gas release are derived in Sections 2.1.2 through 2.1.4. Important parameters and nondimensional groups resulting from the derivation and PJM system considerations are summarized in Section 2.1.5.

2.1.1 Bubble Migration in Well-Mixed Slurry

A simple well-mixed slurry bubble migration model is presented that helps explain the basic elements of gas retention and release associated with PJM operation in non-Newtonian slurries. Though a PJM system (except for air spargers and recirculation pumps) is actually intermittently mixed due to the cyclic nature of PJM operation, we assume that gas-release rates and the rate of change of gas content represent averages such that the well-mixed model is applicable to the pulsed system. This assumption and the validity of the development that follows are supported by comparisons of model predictions with experimental results presented in Sections 5 and 6.

Gas is generated continuously within the waste slurry. Gas molecules are generated in solution in the liquid phase, but the solution quickly supersaturates, bubbles nucleate, and existing bubbles grow. The gas-retention and release model considers only the gas in bubbles. The gas-generation rate, g_v, is the volume of gas in the form of bubbles generated per unit volume of gas-free slurry per unit time referenced to the vessel headspace pressure and the gas-bubble (i.e., slurry) temperature. The retained gas fraction, α, is defined as the average gas-volume fraction existing as bubbles in the slurry. The gas holdup is the gas-volume fraction retained at steady state during normal operation and continuous gas generation, α_{ss}.

We begin by assuming that the gas is well mixed throughout the slurry on a mole basis. If n_g is the number of moles of gas present in bubbles per unit volume of slurry, the gas-volume fraction is determined from the Ideal gas law:

$$\alpha = \frac{RT}{p} n_g \qquad (2.1)$$

where R is the gas constant (0.08206 L-atm/gram-mole-K), T is the local waste temperature, and p is the local pressure. Because n_g is uniform throughout the mixed waste, the gas fraction varies with local temperature and pressure (though the temperature will also likely be uniform in a well-mixed system). If T and p are taken as average quantities in the slurry, α is the average gas fraction. The average pressure, p, is approximately given by

$$p = p_a + \rho_s g_c H / 2 \tag{2.2}$$

where p_a = headspace pressure
ρ_s = average density of gas-free slurry
g_c = standard acceleration of gravity
H = slurry depth (assumed equal to the gas-free slurry depth for a small gas fraction, α <10 vol%).

Applying molar gas conservation to the slurry results in

$$\frac{dN_g}{dt} = G_m - R_m \tag{2.3}$$

where N_g is the total number of moles of gas in the slurry, G_m is the total molar gas-generation rate (moles of gas generated per second), and R_m is the total molar gas-release rate (moles of gas released per second). Eq. (2.3) can be written in terms of specific quantities as

$$\frac{d(n_g V_{bs})}{dt} = g_m V_s - R_v \frac{p_a}{RT} \tag{2.4}$$

where V_{bs} = volume of bubbly slurry (i.e., total slurry volume including retained gas bubbles)
V_s = volume of gas-free slurry (or initial volume)
g_m = moles of gas generated per unit volume of gas-free slurry per unit time
R_v = total volumetric release rate of gas at the surface.

If the gas fraction is small (α <10 vol%), the slurry volume is approximately constant ($V_{bs} \approx V_s$) and Eq. (2.4) can be written as

$$V_s \frac{dn_g}{dt} = g_m V_s - R_v \frac{p_a}{RT} \tag{2.5}$$

Substituting the gas-volume fraction α for n_g using Eq. (2.1) and rearranging, this can be written as

$$\frac{p}{p_a}\frac{d\alpha}{dt} = g_m \frac{RT}{p_a} - \frac{R_v}{V_s} \tag{2.6}$$

The grouping in Eq. (2.6), which includes the molar generation rate, g_m, is the specific volumetric gas-generation rate, $g_{v,a}$, at headspace pressure (~1 atm) and slurry (gas-bubble) temperature:

$$g_{v,a} = g_m \frac{RT}{p_a} \tag{2.7}$$

Using this expression, Eq. (2.6) simplifies to

$$\frac{p}{p_a}\frac{d\alpha}{dt} = g_{v,a} - \frac{R_v}{V_s} \tag{2.8}$$

If the gas release occurs as bubbles rise and break at the surface, the volumetric release rate is defined by

$$R_v = n_b v_{bH} U_R A = \alpha_H U_R A \tag{2.9}$$

where n_b = bubble number density (number of bubbles per unit total slurry volume)
v_{bH} = average bubble volume at the simulant surface
α_H = gas-volume fraction at the slurry surface ($\alpha_H = n_b v_{bH}$)
U_R = rise velocity of the bubbles at the surface
A cross-sectional area of the slurry surface.

In a predominantly cylindrical tank, $A \approx V_s/H$. Substituting Eq. (2.9) into Eq. (2.8) and using the tank area approximation gives

$$\frac{p}{p_a}\frac{d\alpha}{dt} = g_{v,a} - \alpha_H \frac{U_R}{H} \tag{2.10}$$

The tank average gas-volume fraction, α, and surface gas-volume fraction, α_H, are related by $\alpha = (p_a/p)\alpha_H$. Likewise, the gas-generation rate, g_v, at the *in situ* average hydrostatic pressure and $g_{v,a}$ are related by $g_v = (p_a/p)\ g_{v,a}$. Applying these definitions reduces Eq. (2.10) to a first-order ordinary differential equation for the average gas fraction:

$$\frac{d\alpha}{dt} + \frac{\alpha U_R}{H} - g_v = 0 \tag{2.11}$$

which has the general solution,

$$\alpha(t) = \alpha_0 \exp(-\frac{U_R}{H}t) + g_v \frac{H}{U_R}(1 - \exp(-\frac{U_R}{H}t)) \tag{2.12}$$

where α_0 is the initial gas fraction at t = 0. The time dependence of the gas fraction α is completely characterized by the time constant $\tau_R = H/U_R$. The bubble rise velocity U_R cannot be calculated or directly measured but can be determined empirically as a function of the slurry mixing system (e.g., PJM duty cycle, PJM nozzle diameter and velocity, slurry rheology). Empirical models for U_R are discussed in Section 5. Several other useful solutions can be derived from Eq. (2.11) and (2.12).

2.1.2 Gas Retention in Gelled Slurry

When the mixing system is not operating, small bubbles are held in place by the strength of the gelled slurry, and the bubble rise velocity is zero. Solving Eq. (2.11) for $U_R = 0$ gives

$$\alpha(t) = \alpha_0 + g_v t \tag{2.13}$$

Hence, when the mixing system is not operating, gas accumulates at a rate given directly by the *in situ* volumetric generation rate, g_v.

2.1.3 Gas Holdup

As previously defined, the gas holdup is the gas-volume fraction retained at steady state during normal operation and continuous gas generation. From Eq. (2.12) the holdup at long times, α_{ss}, is given by

$$\alpha_{ss} = g_v \frac{H}{U_R} = g_v \tau_R \tag{2.14}$$

Hence, for the well-mixed slurry with rising bubbles, the steady-state holdup increases with increasing generation rate and slurry depth and decreases with increasing bubble rise velocity and average slurry pressure. While the molar flammable gas inventory within the slurry is the primary concern, the volume of retained gas is most readily quantified in experiments. Eq. (2.14) provides a basis for comparing experimental gas-holdup results at different geometric scales (e.g., slurry depths) and gas-generation rates. Also, because bubbles can be expected to be roughly the same size and rise at roughly the same speed, Eq. (2.14) implies that the gas-generation rate must vary inversely with the length scale to achieve the same holdup.

The bubble rise velocity in Eq. (2.14) is expected to be a function of the gas-bubble diameter d_b and the non-Newtonian slurry density and rheology (expressed as the yield stress, τ_y, and consistency, κ, following the Bingham model). Because bubbles can rise only during the time the slurry is mobile, the effective bubble rise velocity should also vary with the extent and intensity of slurry mobilization produced by the mixing system.(a) Important parameters affecting mobilization effectiveness could include the ratio of PJM drive time to total cycle time (t_D/t_C), the number of PJMs, the PJM nozzle diameter, d_0, nozzle velocity, U_0, the tank diameter, D, and the depth of the simulant, H. Empirical models relating the bubble rise velocity to these parameters is given in Section 5.4. The most accurate determination of average bubble rise velocity is obtained from steady-state holdup test data using Eq. (2.14).

(a) The term "mixing" in this context refers to the hydraulic mobilization or fluidization of a non-Newtonian slurry, not necessarily to homogenization.

2.1.4 Gas Release

To model the gas-release process during a restart of the mixing system, consider a gelled slurry with initial retained gas fraction, α_0. If the slurry mobilization process and gas release are relatively fast, i.e., the time constant $\tau_R = H/U_R$ is small, then gas generation can be neglected, and the transient gas fraction is found by setting $g_v = 0$ in Eq. (2.12):

$$\alpha(t) = \alpha_0 \exp(-\frac{U_R}{H} t) = \alpha_0 \exp(-\frac{t}{\tau_R}) \tag{2.15}$$

Substituting Eq. (2.15) into Eq. (2.9), the total volumetric gas-release rate is given by

$$R_v(t) = \alpha_0 U_R \frac{p}{p_a} A \exp(-\frac{t}{\tau_R}) \tag{2.16}$$

which has the form

$$R_v(t) = R_0 e^{-t/\tau_R} \tag{2.17}$$

where $R_0 = \alpha_0 U_R A(p/p_a)$ is the release rate at t = 0 and, as noted above, $\tau_R = H/U_R$ is the time constant for the release. The total release volume, V_R, can be found by integrating Eq. (2.17) from t = 0 to ∞, which results in

$$V_R = R_0 \tau_R \tag{2.18}$$

2.1.5 Important Parameters and Nondimensional Groups

The following list summarizes waste properties and system parameters relevant to gas-retention and release phenomena as noted in the development above.

Slurry properties-

τ_y	Bingham plastic yield stress (Pa)
κ	Bingham plastic consistency (mPa-s)
ρ_s	Gas-free slurry density (kg/m^3); assumes well-mixed slurry with no settling.

Gas and bubble properties-

α	Average retained gas-volume fraction (m^3 gas/m^3 bubbly slurry)
α_{ss}	Gas holdup (m^3 gas/m^3 bubbly slurry)
d_b	Average bubble diameter (m)
g_m	Specific molar gas-generation rate (mole gas/m^3 gas-free slurry/s)

g_v	Specific volumetric gas-generation rate at the average *in situ* hydrostatic pressure and gas-bubble (slurry) temperature (m^3 gas/m^3 gas-free slurry/s)
n_b	Number density of bubbles (#/m^3 bubbly slurry)
R_v	Volumetric gas-release rate from the slurry at the headspace pressure (m^3 gas/s)
R_0	Initial (maximum) volumetric gas-release rate from the slurry (m^3 gas/s)
U_R	Average bubble rise velocity at the slurry surface (m/s)
v_{bH}	Average bubble volume at the slurry surface (m^3).

Physical parameters-

H	Slurry fill level in the tank (m); assumed constant for small gas fractions (α <10 vol%)
D	Nominal tank diameter (m)
N_{PJM}	Number of PJMs
d_0	PJM nozzle diameter (m)
U_0	PJM nozzle velocity (average or peak-average over the drive cycle)
t_D, t_C	PJM drive time (s) and total cycle time (s)
p_a	Ambient headspace pressure (Pa)
p	Average *in situ* pressure at H/2 (Pa)
T	Slurry and gas-bubble temperature (K)
V_s	Gas-free or initial slurry volume (m^3)
V_{bs}	Total bubbly-slurry volume (m^3).

Many of these parameters and properties will be used in the subsequent analysis of experimental data. They are also the basis of key groups and nondimensional parameters that aid our understanding of how the gas-retention and release phenomena scale. Of particular importance is the bubble rise time, the time constant of the gas-release process in the well-mixed slurry bubble migration model:

$$\tau_R = \frac{H}{U_R}$$

Some relevant nondimensional parameter groups for the physical system follow. The gas-holdup number represents the ratio of gas generated to gas leaving by virtue of bubble rise. It is considered a dominant nondimensional parameter:

Gas-holdup number: $$N_\alpha = \frac{g_v H}{U_R} = g_v \tau_R$$

The ratio of PJM cycle time, t_C, or any relevant system time, to bubble rise time is defined as the gas-release number. It directly affects gas-release rates and other transients and is also considered a dominant nondimensional parameter:

Gas-release number: $$N_R = \frac{t_C U_R}{H} = \frac{t_C}{\tau_R}$$

2.2 Experimental Considerations

In situ generation of O_2 gas bubbles by H_2O_2 decomposition in kaolin-bentonite-water (clay) and Laponite-water simulants has been used to investigate gas retention and release in WTP PJM vessels. This section summarizes the calculation of the equivalent O_2 gas-generation rate resulting from a steady addition of H_2O_2 solution (solution denoted by the subscript "ps" and H_2O_2 itself by subscript "p"). It also demonstrates the calculation of the theoretical maximum volume of O_2 gas and the gas-volume fraction expected in the simulant for a fixed amount of H_2O_2. Gas-volume fractions are defined in terms of known or measured experimental quantities.

The gas-bubble generation technique is based on the decomposition of H_2O_2 on catalytic surfaces (e.g., iron-containing species in bentonite clay). Two moles of H_2O_2 decompose to yield two moles of water and one mole of O_2 according to the following reaction:

$$2H_2O_2 \rightarrow 2H_2O + O_2 \tag{2.19}$$

Once enough H_2O_2 has decomposed to supersaturate the simulant in dissolved O_2, bubbles nucleate, and existing bubbles grow. Further decomposition of H_2O_2 generally contributes mostly to bubble growth as dissolved O_2 diffuses through the liquid to the existing bubbles, reducing the supersaturation below that necessary for nucleating new bubbles. Generated gas will be retained or released depending on many factors, including the degree of slurry mobilization in the system, the retained gas-volume fraction, the size of bubbles, and simulant rheology.

2.2.1 Gas-Volume Fraction

In many gas-retention and release tests, a specific gas-volume fraction in the simulant was targeted and assumed to result from complete H_2O_2 solution decomposition according to Eq. (2.19) and O_2 liberation to the gas phase. The average retained gas-volume fraction, α, referenced to the total bubbly-slurry volume, V_{bs}, is defined as

$$\alpha = \frac{V_g}{V_{bs}} = \frac{V_g}{V_s + V_g} \tag{2.20}$$

where the total volume is the sum of V_g, the volume of retained gas (O_2 bubbles), and V_s, the gas-free slurry volume defined previously.[a] The gas-free slurry volume includes the volume of H_2O_2 solution, V_{ps}. In most cases V_{ps} is negligible compared with the large initial volume of gas-free simulant. However, in gas-holdup experiments where H_2O_2 solution is added continuously for an extended period, a correction for the added solution volume is applied. To a close approximation,[b] the extra water volume resulting from the H_2O_2 solution is obtained directly from the volume of solution added or may be calculated from the H_2O_2 solution density, ρ_{ps}, and mass, W_{ps}:

$$V_{ps} = \frac{W_{ps}}{\rho_{ps}} \tag{2.21}$$

The gas-free simulant volume is typically obtained from surface-level measurements in the PJM vessel before H_2O_2 solution is added, but it may also be estimated from the mass of simulant added to the vessel, W_s, and its gas-free bulk density ρ_s ($V_s = W_s/\rho_s$).

The volume of gas retained in the bubbly simulant at a given time is determined as the difference of the total bubbly slurry volume in the vessel and the initial volume of additives (gas-free slurry and H_2O_2 solution):

$$V_g = V_{bs} - V_s = V_{bs} - \left(V_{s,0} + V_{ps}\right) \tag{2.22}$$

In Eq. (2.22), $V_{s,0}$ is the gas-free slurry volume before adding H_2O_2 solution. As with the initial simulant volume, the total bubbly slurry volume in the vessel at any time is typically determined from surface-level measurements and associated correlations of volume contained as a function of surface level (see Section 4). Substituting Eq. (2.22) into Eq. (2.20) gives the gas-volume fraction in terms of measured and/or known volumes:

$$\alpha = \frac{V_g}{V_{bs}} = \frac{V_{bs} - (V_{s,0} + V_{ps})}{V_{bs}} = 1 - \frac{V_{s,0} + V_{ps}}{V_{bs}} \tag{2.23}$$

(a) GH Beeman sent the following letter to the WTP PDC submittal coordinator: *Information on Gas Retention and Release for Bechtel Report "Hybrid Mixing System Test Data Supporting the Ultrafiltration Feed Process (UFP-VSL-00002A/2B) and HLW Lag Storage (HLP VSL 00027A/B) and HLW Blend (HLP-VSL-00028) Vessel Configurations.* RPP-WTP-04-472 (2004). In this letter, the gas-free simulant volume was used to approximate the total bubbly slurry volume to calculate the reported gas-volume fractions (α_i). As indicated in Eq. (2.20), the difference in gas fraction determined by the two methods increases as the volume of gas increases. At 10 vol%, the error is approximately 1 vol%; at 4 vol%, the error is 0.15 vol%. The true gas volume fraction can be computed from the approximate value as follows:

$$\alpha = \frac{V_g/V_s}{1 + V_g/V_s} = \frac{\alpha_i}{1 + \alpha_i}$$

(b) For a nominal 30 wt% hydrogen peroxide solution, it is estimated that, upon complete decomposition of the H_2O_2, the total water volume from the original solution and decomposition is ~95% of the added hydrogen peroxide solution volume. Because the difference is small, the added hydrogen peroxide solution volume is used directly.

2.2.2 Oxygen Gas-Volume

Assuming 100% decomposition of the H_2O_2 according to Eq. (2.19) and neglecting dissolved O_2 and any loss of O_2 by chemical reaction, evaporation, or early bubble release, the theoretical amount of H_2O_2 needed to produce a given volume of O_2 gas, V_{O2}, is readily calculated from the ideal gas law:

$$V_{O2} = \frac{N_{O2}RT}{p} = \frac{N_p RT}{2p} \tag{2.24}$$

where R is the ideal gas constant, T is the absolute temperature of the gas (taken to be in thermal equilibrium with the slurry), and p is the average hydrostatic pressure on the gas bubbles. At a room temperature of 22ºC (295.15K) and 1 atm (101.235 kPa) pressure, the grouping of constants RT/p is 24.2 L/mol gas. The right side of Eq. (2.24) gives V_{O2} in terms of the gram-moles of H_2O_2, N_p, where the stoichiometry of the H_2O_2 decomposition reaction given in Eq. (2.19) is applied.

For preparing O_2-bubble laden slurries, it is convenient to convert Eq. (2.24) to a basis of H_2O_2 solution mass or volume. Using a H_2O_2 solution of concentration x_p, the weight fraction H_2O_2 in solution, the mass of H_2O_2 solution W_{ps} in grams and the theoretical *in situ* volume of O_2 given in Eq. (2.24) are related as follows:

$$V_{O2} = \frac{RT}{p}\left(\frac{W_{ps}x_p}{2M_p}\right) = \frac{RT}{p}\left(\frac{V_{ps}\rho_{ps}x_p}{2M_p}\right) \tag{2.25}$$

where M_p is the molecular weight of H_2O_2 (34 g/mol). The right-hand expression of Eq. (2.25) is given in terms of the H_2O_2 solution volume using Eq. (2.21) to convert solution mass to volume. Nominal 30-wt% H_2O_2 solution was used in gas-retention and release experiments described in this report. (Fisher Scientific, the brand we used, provided an assay concentration on its label [30.6 wt%], and a solution density of ρ_{ps} = 1.114 kg/L was measured.)

In many tests, specific initial O_2 gas-volume fractions α_0 in the slurry were targeted and assumed to result from total H_2O_2 decomposition and O_2 liberation to the gas phase. Recasting Eq. (2.23) in terms of the target initial O_2 gas-volume fraction and neglecting the contribution of the small volume of H_2O_2 solution added on the total slurry volume gives

$$\alpha_0 = \frac{V_{O2}}{V_{bs}} \approx \frac{V_{O2}}{V_{s,0} + V_{O2}} \tag{2.26}$$

Combining Eq. (2.25) and (2.26) and rearranging in terms of the H_2O_2 solution mass gives

$$W_{ps} = V_{s,0}\frac{\alpha_0}{(1-\alpha_0)}\frac{p}{RT}\frac{2M_p}{x_p} \tag{2.27}$$

The actual mass of H_2O_2 needed to achieve an initial retained gas fraction, α_0, for gas-release experiments is generally greater than that calculated by Eq. (2.27) to account for the excess needed to saturate the slurry with O_2 and losses (gas release) while the H_2O_2 solution was mixed into the simulant. Generally, the H_2O_2 solution quantity was calculated for a gas fraction a few volume percent higher than the actual target, α_0.

2.2.3 Oxygen Gas Generation Rates

In gas-holdup tests, H_2O_2 solution was added to simulant slurry at a fixed rate over an extended period of time to continuously generate O_2 gas while the simulant was mixed in the PJM vessel using specified "normal" operating conditions. At steady state, the rate of gas release from the vessel is equal to the rate of gas generation, and a steady-state gas-volume fraction defined as the gas holdup, α_{ss}, is retained in the simulant (Section 2.1). The time-varying gas-volume fraction, $\alpha(t)$, is determined experimentally from changes in simulant volume due to retained gas while gas is continuously generated by H_2O_2 addition and decomposition:

$$\alpha(t) = \frac{V_{O2}(t)}{V_{bs}(t)} = \frac{V_{bs}(t) - \left[V_{s,0} + V_{ps}(t)\right]}{V_{bs}(t)} = \frac{V_{bs}(t) - \left[V_{s,0} + Q_{ps}t\right]}{V_{bs}(t)} \tag{2.28}$$

In this equation, the time-varying volume of gas-free simulant is corrected for the total volume of H_2O_2 solution added over an elapsed time t, which is given by

$$V_{ps}(t) = Q_{ps}t = \frac{w_{ps}t}{\rho_{ps}} \tag{2.29}$$

Here, Q_{ps} and w_{ps} are, respectively, the average volumetric and mass flow rates of the H_2O_2 solution.

The total *in situ* volumetric rate of O_2 generation, $G_{v,O2}$, from H_2O_2 decomposition is derived from Eq. (2.25) where the mass of H_2O_2 solution is replaced by its mass or volumetric flow rate:

$$G_{v,O2} = \frac{RT}{p}\left(\frac{w_{ps}x_p}{2M_p}\right) = \frac{RT}{p}\left(\frac{Q_{ps}\rho_{ps}x_p}{2M_p}\right) \tag{2.30}$$

Eq. (2.30) applies if O_2 gas is generated at a rate equivalent to H_2O_2 introduction, as would be expected for instantaneous decomposition or a steady-state process where a steady-state concentration of H_2O_2 is established in the slurry. The latter is achieved (or approached) in gas-holdup experiments (Sections 5 and 6).

For assessing O_2 mass balance in the mixed-slurry system, it is preferred to cast Eq. (2.30) in terms of the total steady-state molar O_2 gas-generation rate, $G_{m,O2}$:

$$G_{m,O2} = \frac{w_{ps}x_p}{2M_p} = \frac{Q_{ps}\rho_{ps}x_p}{2M_p} \tag{2.31}$$

To compare experiments in PJM vessels containing different amounts of simulant, it is convenient to normalize the rate of gas generation by the initial volume of gas-free simulant. The steady-state specific volumetric gas (O_2) generation rate at the tank headspace (slurry surface) ambient pressure, $g_{v,a,O2}$, resulting from H_2O_2 decomposition is

$$g_{v,a,O2} = \frac{G_{v,a,O2}}{V_s} = \frac{RT}{p_a V_s}\left(\frac{w_{ps} x_p}{2M_p}\right) = \frac{RT}{p_a V_s}\left(\frac{Q_{ps}\rho_{ps} x_p}{2M_p}\right) \tag{2.32}$$

As noted in Section 2.1, the *in situ* volumetric gas-generation rate, $g_{v,O2}$, is given by $g_{v,a,O2}(p_a/p)$.(a) The equivalent specific molar gas-(O_2) generation rate, $g_{m,O2}$, is

$$g_{m,O2} = \frac{G_{m,O2}}{V_s} = \frac{w_{ps} x_p}{2M_p V_s} = \frac{Q_{ps}\rho_{ps} x_p}{2M_p V_s} \tag{2.33}$$

In Eq. (2.32) and (2.33), the gas-free simulant volume has not been corrected by the small excess volume of water introduced by adding the H_2O_2 solution. The gas-generation rate terms defined here are applied to the analysis of gas-holdup test results in Sections 5 and 6.

Gas generation by decomposition of H_2O_2 behaves differently from the radiolytic and thermal gas-generation processes expected to occur in the actual process slurry. The primary difference is that H_2O_2 decomposes so rapidly that the resulting gas-generation rate in the test slurry varies widely. Hydrogen peroxide decomposition can produce a constant gas-generation rate only in carefully controlled steady-state holdup tests. In radioactive waste, however, the gas-generation rate is nearly constant for a given temperature and dilution. The gas-generation rates used in the holdup tests were generally much higher than those expected in the waste. However, gas generation in the waste is expected to be extremely sensitive to temperature, and the hotter vessels may have very high gas-generation rates.

Another fundamental limitation of tests generating gas by H_2O_2 decomposition is that gas is generated only in regions where H_2O_2 can be delivered by the mixing system. In holdup tests starting from a zero gas state, gas retention may be underestimated if there is a large region not mobilized by the mixing system that does not receive any H_2O_2. On the other hand, series holdup tests where the intensity of mixing decreases (e.g., PJM-only mixing immediately following one with PJMs and spargers) will overestimate the holdup. The volume of a mobilized region can be fairly accurately quantified from the unreleased gas left after release tests with an initial gas fraction produced by homogeneous distribution of H_2O_2.

The gas-retention and release behavior of process vessels with PJM systems, as defined by the fundamental model in Section 2.1, with release models derived from the data as shown in Sections 5 and 6, will help investigate the effects of different gas-generation rates and functionalities.

(a) In letter report RPP-WTP-04-472, Eq. (2.32) was used to calculate reported experimental volumetric gas generation rates.

3.0 Bench-Scale Gas-Generation and Retention Scoping Tests

In preparation for gas-retention and release tests in PJM systems, bench-scale gas-generation and retention scoping tests were completed with both kaolin-bentonite clay and Laponite simulants. This section describes the testing to demonstrate and quantify O_2 gas generation resulting from H_2O_2 decomposition in small amounts of the kaolin-bentonite clay and Laponite simulants. Section 3.1 describes the experimental methods used, Section 3.2 summarizes the kaolin-bentonite clay simulant test results, and Section 3.3 summarizes the Laponite simulant test results. The development and selection of these non-Newtonian waste simulants for use in WTP PJM testing are summarized in Poloski et al. (2004). Using the kaolin-bentonite clay simulant was emphasized in the PJM gas-retention and release test program (Sections 5 and 6); however, a few tests were completed using a Laponite simulant.

3.1 Experimental Methods

Several bench-scale gas-generation tests were completed with kaolin-bentonite and Laponite simulants using the H_2O_2 decomposition technique and targeting a range of retained gas-volume fractions, α_0 (see Section 2.2). These bench-scale tests were intended to provide information needed to support the PJM system gas-retention and release experiments. Of particular interest were the quantities of H_2O_2 required to achieve target gas fractions in the larger-scale gas-release tests (i.e., to provide recipes) and to develop an understanding of the O_2 gas-generation rates as a function of H_2O_2 concentration (i.e., varying target gas fraction) and simulant/catalyst properties.

The base kaolin-bentonite clay simulant was nominally a 27 wt% solids (80 wt% kaolin:20 wt% bentonite) and water mixture prepared by Quadra Chemical Company in Portland, Oregon. Rheograms of the base simulant were fit to a Bingham plastic model, giving a yield stress of ~20 Pa and a consistency factor of ~40 cP. A bulk density of 1180 g/L was determined for the material by weighing 100 mL of the simulant in a graduated cylinder on a Mettler PC4400 balance. This compares well with the 1200 g/L density calculated from clay particle and water densities. Over the course of testing, some dilution of the clay simulant occurred, and more than one batch of clay simulant was used. Two different catalysts, manganese dioxide and iron oxide, were evaluated in screening experiments to enhance H_2O_2 decomposition and increase the gas-bubble generation rate. The manganese dioxide (MnO_2, Alfa AESAR) produced a significantly greater effect than the iron oxide and therefore was chosen for further testing.

The base Laponite simulant—also prepared by Quadra Chemical Company in Portland, Oregon—was initially ~2.0 wt% solids in water. The particular batch of Laponite simulant used in the bench-scale scoping tests described here was a portion of the material already used in several 336 Building large-scale (~10,000 gal tank) PJM tests. During a series of large-scale tests, the Laponite received additions of blue dye and was intentionally diluted with small quantities of water. After gelling ~25 hours, this base Laponite simulant had a measured shear strength of ~90 Pa using a shear vane method of measurement. The base density was determined by weighing 100 mL of the Laponite simulant in a graduated cylinder on a Mettler PC4400 balance and found to be only slightly greater than water (~1010 g/L). A catalyst was added to the Laponite simulant to enhance H_2O_2 decomposition and increase the gas-bubble generation rate. Several catalysts, including copper and iron powders, nitrate salts of copper and iron, and

50 wt% sodium hydroxide solution, were evaluated in screening experiments. Except for the iron powder and the sodium hydroxide solution, each produced a noticeable effect. Of these, copper nitrate trihydrate [$Cu(NO_3)_2 \bullet 3H_2O$, Alfa Aesar] was selected for bench-scale tests because of its efficacy in relatively low concentrations and the ease of handling and distributing it in the simulant.

To minimize the effects of dilution on the base simulant rheology, a relatively concentrated H_2O_2 solution was used in the bench-scale tests (30 wt% H_2O_2, unstabilized, Fisher Scientific). In a typical experiment, a mixture of simulant, H_2O_2 solution, and catalyst (if used) was prepared as follows: 1) an aliquot of simulant (generally $\leq$ 0.6 L) was weighed into a beaker or other vessel and mixed with a spatula; 2) the appropriate quantity of catalyst (if any) was weighed into a weigh boat or other container, added to the simulant, and mixed for a minute or more with a spatula; 3) the calculated quantity of H_2O_2 solution was weighed into a separate container; and 4) the H_2O_2 solution was quickly added to the simulant and mixed thoroughly with a spatula for ~1 minute.

Immediately after preparation, an aliquot of the nearly gas-free simulant/H_2O_2 mixture was placed in either a 100-mL or 250-mL graduated cylinder, allowing for expected volume expansion. The initial volume was noted and the sample volume recorded over time, usually for a day or more. The volume could be read to 1 mL in the 100-mL and 2 mL in the 250-mL graduated cylinders, which is ~1 vol%. The volume increase was attributed to the volume of gas generated, and these data were subsequently used to calculate the retained gas-volume fraction, α, as a function of time. Where observable, bubble sizes and shapes were also noted. Larger quantities of simulant mixtures were prepared for shear strength and rheology measurements in some cases. These samples were placed in loosely covered containers shortly after preparation and were aged 18 to 24 hours before analysis.

3.2 Kaolin-Bentonite Clay Simulant Results

Testing related to the gas-retention and generation rate are presented in Section 3.2.1. Composition effects on the gas-generation rate, including the effect of different clay batches, commercially stabilized H_2O_2, catalyst addition, and recycled clay, are discussed in Section 3.2.2. Section 3.2.3 shows the simulant rheology effects.

3.2.1 Gas-Retention and Generation Rate

Testing was performed with various target gas fractions in the clay simulant to compare measured maximum retained gas fractions with expected values and to determine the rate of gas generation as a function of initial H_2O_2 concentration in the simulant (i.e., H_2O_2 amount added/initial simulant amount). The gas-generation rate data presented here are further evaluated in Section 6.2. Table 3.1 summarizes the quantities of simulant and H_2O_2 solution used and the final measured gas fraction for each test. Two batches of clay simulant were used in these tests with the 4.9, 9.9, 19.8, 40.3, and 82.5 vol% expected gas-fraction tests using a batch of “old” clay, and the 15, 24.9, 30, and 49.8 vol% expected gas-fraction tests using a batch of “new” clay. As the expected gas fraction increased, the gas-generation rate increased, as determined from the initial slope of the growth curve in Figure 3.1. A significant increase appeared in the gas-generation rate between 19.8 and 24.9 vol% and between 40.3 and 49.8 vol% expected gas fractions. It is unknown whether this was due to the different clay simulant batches or the amount of H_2O_2 added.

Table 3.1. Measured Gas Fractions in Clay Simulant with Various Expected Gas Fractions

Expected Gas Fraction (vol%)	Simulant Batch Used	Actual Base Simulant Mass (g)	Actual H_2O_2 Solution Mass (g)	Maximum Measured Gas Fraction (vol %)
4.9	"old" clay	720.1	0.2957	3.4
9.9	"old" clay	640.3	0.5582	8.7
15.0	"new" clay	106.3	0.1489	12.7
19.8	"old" clay	719.5	1.4094	19.2
24.9	"new" clay	94.4	0.2484	22.9
30.0	"new" clay	94.5	0.3203	27.5
40.3	"old" clay	204.8	1.0907	35.3
49.8	"new" clay	70.9	0.5591	47.9 [a]
82.5	"old" clay	179.1	1.2440	28.5 [b]

(a) There was a column-width spanning bubble supporting the clay with a height of ~14 mL. When this volume is subtracted, the measured gas fraction is 39 vol%.

(b) The volume grew and then collapsed overnight so the true maximum gas fraction was not recorded. However, from the height of the clay on the cylinder walls, it was estimated to be ~35 vol%.

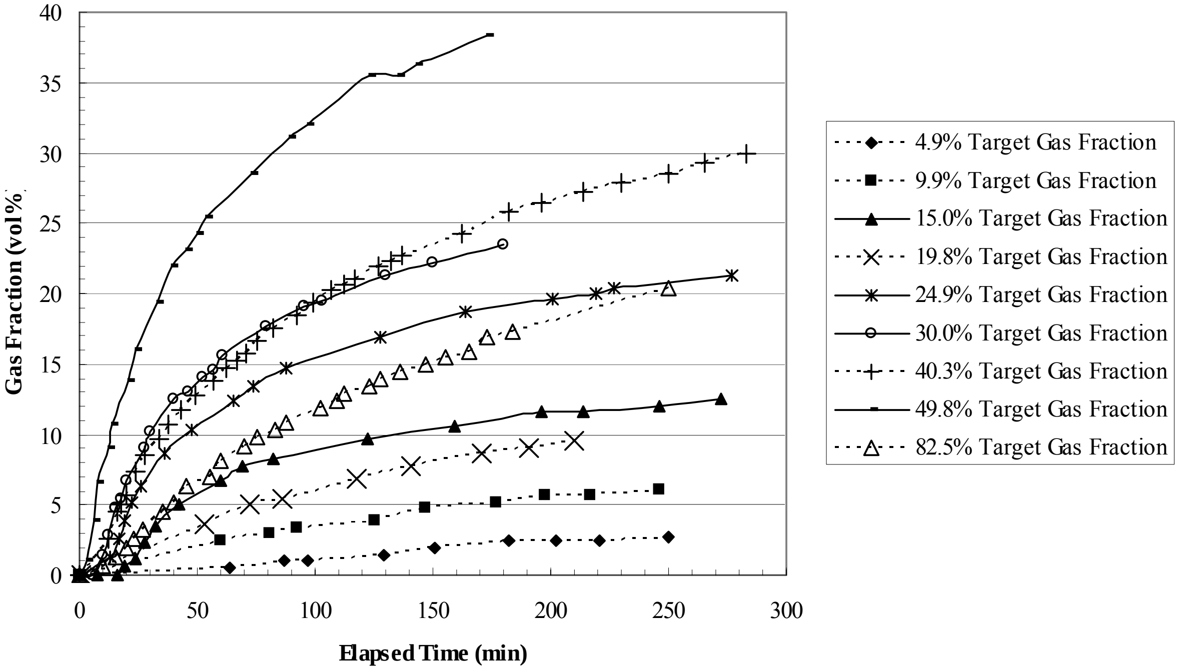

Figure 3.1. Comparison of Reaction Rate with Varying Expected Gas Fractions in Kaolin-Bentonite Clay Simulant (dotted lines represent tests performed using the "old" clay and solid lines represent tests using the "new" clay)

This test also showed agreement to within 2.5 vol% of the expected and measured gas fractions until the maximum gas retention of ~35 vol% was achieved, confirming the expected reaction stoichiometry. The slight difference between the expected and measured gas fractions is due to the O_2 needing to saturate the liquid before being retained as gas in the clay and the unreacted H_2O_2. Figure 3.2 shows the long-term growth and retention of the varying expected gas fractions, indicating that nearly 100% of the gas is retained in the clay at small scale, with none being released until maximum gas retention is achieved. After the maximum gas retention is achieved, gas loss through the simulant surface or a collapse of the retained gas occurred.

The bubbles were predominantly round and evenly distributed and grew in size proportional to the expected gas fraction in the clay simulant. As the concentration and size of the bubbles increased, they tended to form bubble trails in the simulant, causing a higher concentration of bubbles near the top. Most of the bubbles grew to ~2 mm in diameter at the wall. However, in the 49.8 vol% expected gas fraction sample, the bubbles grew to >3 mm diameter, and a vessel-spanning bubble formed, supporting the simulant above it and not allowing the simulant to collapse. Figure 3.3 is an example of the bubbles seen in the bench-scale testing of the kaolin-bentonite simulant.

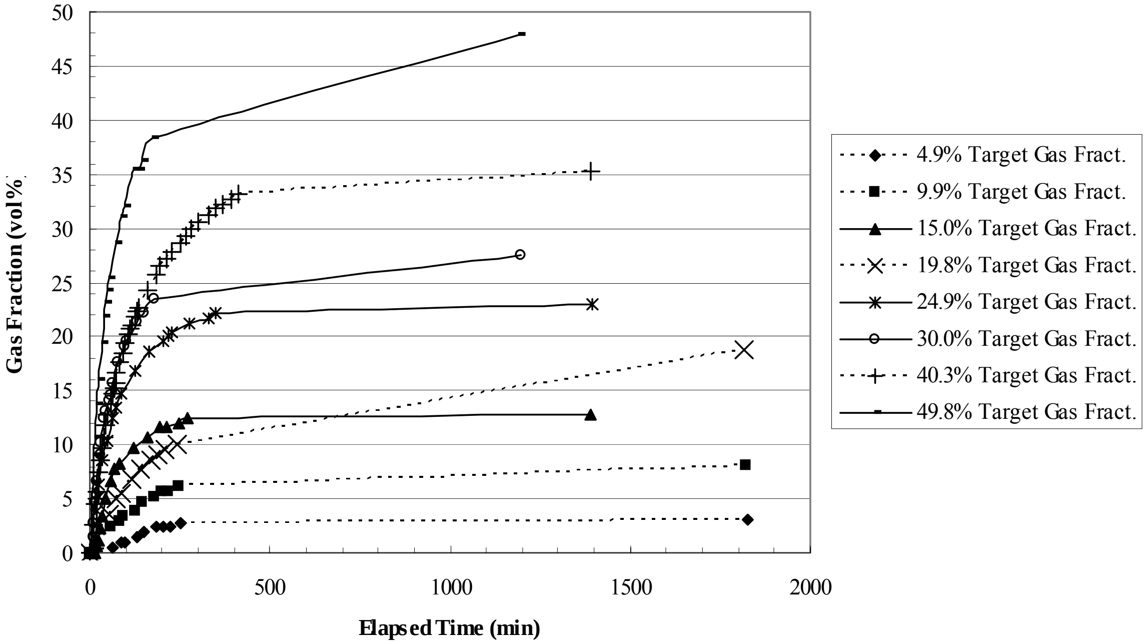

Figure 3.2. Gas-Retention Profiles of Expected Gas Fractions in Kaolin-Bentonite Clay Simulant (dotted lines represent tests performed using the "old" clay and solid lines represent tests using the "new" clay)

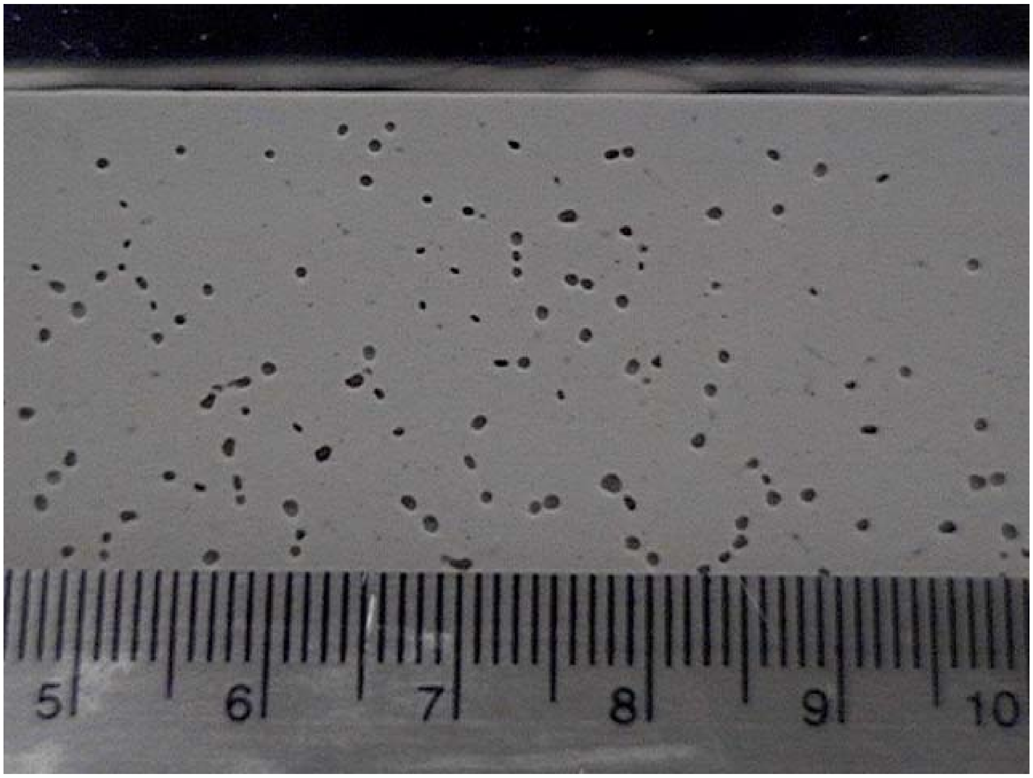

Figure 3.3. Approximately 9 vol% *in Situ* Generated Oxygen Gas Bubbles in Kaolin-Bentonite Simulant at a Clear Vessel Wall. Scale demarcations are 1 mm; numbers are cm.

3.2.2 Composition Effects on Gas-Generation Rate

A test was performed to compare the gas-generation rates of commercially stabilized and unstabilized H_2O_2 because 30 wt% commercially stabilized H_2O_2 was available. Both tests were performed with an approximately 20-vol% expected gas fraction. However, the unstabilized H_2O_2 was tested in a 250-mL graduated cylinder and the commercially stabilized H_2O_2 in a 100-mL graduated cylinder. In the first 200 minutes, the commercially stabilized H_2O_2 was found to have a slightly higher gas fraction than the unstabilized H_2O_2 (12.5 vol% versus 9.5 vol%). However, the final gas fraction was slightly higher with unstabilized H_2O_2 than with commercially stabilized H_2O_2 (19.2 vol% versus 17.2 vol%). Therefore, it was decided to continue using the unstabilized H_2O_2 in the testing.

A second batch of clay simulant was received and a gas-retention test performed to confirm that the "new" clay simulant had gas-retention properties similar to the previous batch, or "old" clay. The bulk density of the new batch of clay simulant was measured using a 50-mL graduated cylinder and found to be the same as the previous batch (old clay), 1.18 g/mL. Table 3.2 summarizes the quantities of simulant and H_2O_2 solution used along with the final measured gas fraction for each test. As can be seen in Figure 3.4, there were no real differences in maximum gas retention between the two batches of kaolin-bentonite clay simulants for 9.9 and 19.8 vol% expected gas fractions. However, as Figure 3.5 shows, there was a significant difference in the rates of reaction to achieve the maximum gas retention. This shows that each batch of clay simulant may have a different gas-generation rate that needs to be considered in testing. This is further evaluated in Section 6.2.

Table 3.2. Comparison of Different Batches of Clay Simulant with Varying Expected Gas Fractions

Simulant Batch	Expected Gas Fraction (vol%)	Actual Base Simulant Mass (g)	Actual H_2O_2 Solution Mass (g)	Maximum Measured Gas Fraction (vol %)
First Batch ("old")	9.9	640.3	0.5582	8.7
Second Batch ("new")	9.9	269.8	0.2344	8.7
First Batch ("old")	19.8	719.5	1.4094	19.2
Second Batch ("new")	19.7	269.8	0.5260	19.1

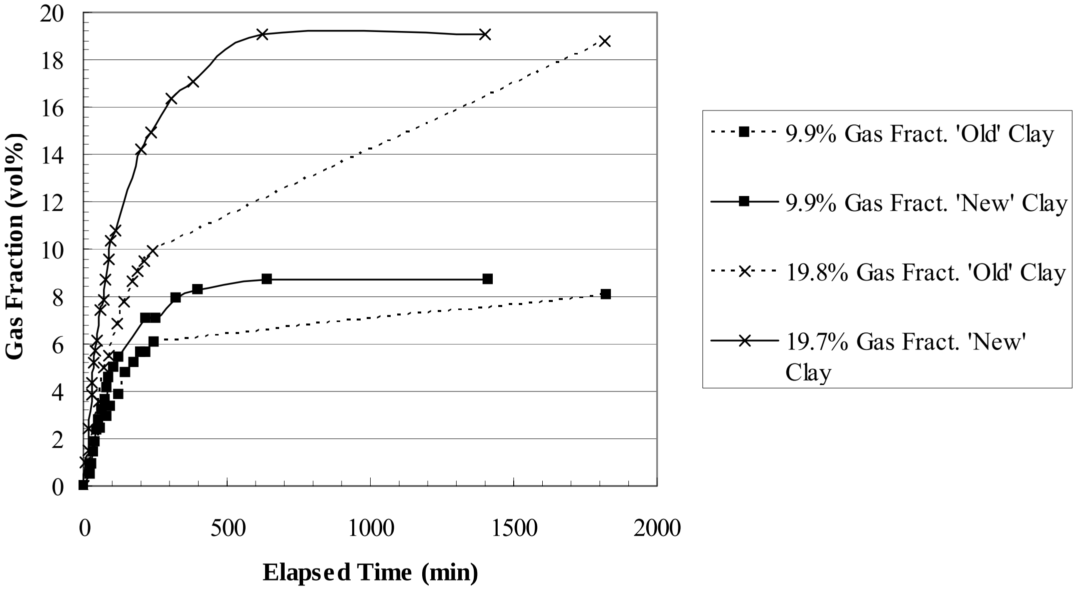

Figure 3.4. Maximum Gas-Retention Comparison for Two Batches of Kaolin-Bentonite Clay Simulant

To determine whether the kaolin-bentonite clay simulant could be reused in large-scale testing, a recycle experiment was performed using the 19.8 vol% expected gas-fraction rheology testing sample from the "old" clay simulant batch. Approximately 3 weeks after the rheology testing was completed, the sample was degassed by stirring, and more 30 wt% unstabilized H_2O_2 was added to the sample for another 19.7 vol% expected gas fraction. The H_2O_2 and simulant were well mixed by stirring and poured into a 100-mL graduated cylinder. Maximum gas retention of approximately 24 vol% was achieved in less than 21 hours. There were lots of bubbles throughout of varying sizes up to approximately 1.5 mm in diameter at the wall. This indicates that the kaolin-bentonite clay simulant can be reused in the large-scale testing and may even react faster and more fully the second time. The results of each H_2O_2 addition are shown in Figure 3.6. No testing was performed to determine the effect of a third addition or more of H_2O_2.

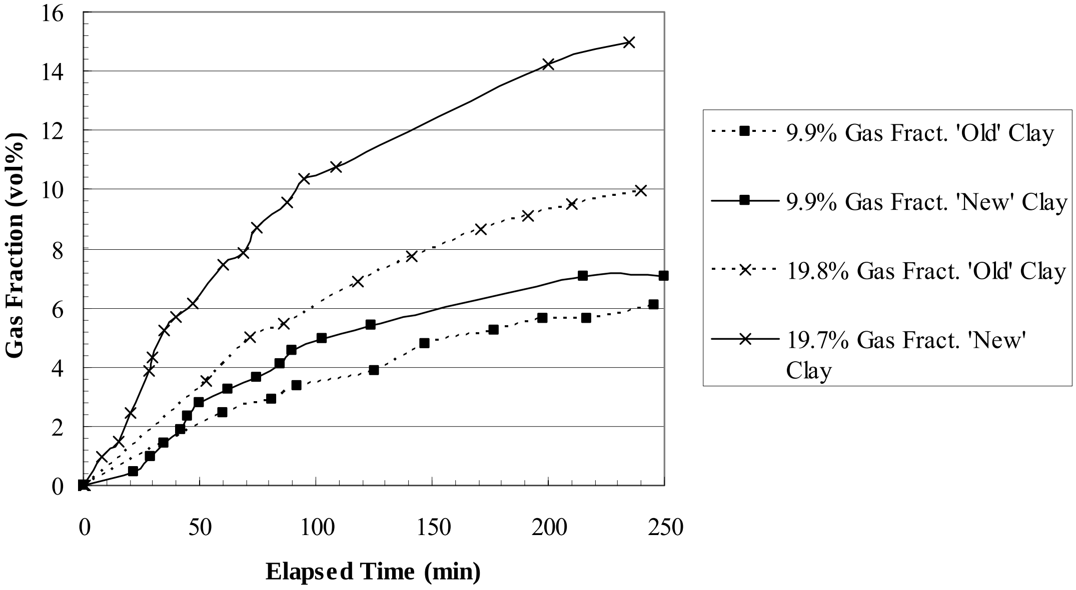

Figure 3.5. Gas-Retention and Generation Rate Comparison for Two Batches of Kaolin-Bentonite Clay Simulant

To increase the decomposition rate of the H_2O_2 in clay simulant for possible use in large-scale gas-holdup (retention) tests, the addition of catalysts was investigated. To determine the most effective catalyst, two tests were performed. Initially, 500 ppm of -200-mesh MnO_2 was added to one column and 500 ppm of Fe_2O_3 was added to the other column along with enough 30 wt% unstabilized H_2O_2 to provide a 19.7 vol% expected gas fraction in the Quadra clay simulant. It was determined that MnO_2 increased the decomposition rate of the H_2O_2, but the Fe_2O_3 did not. The results are shown in Figure 3.7.

The particle size of the MnO_2 catalyst was then varied to determine whether it had an effect on the catalytic activity. Three different MnO_2 particle sizes were tested: –325 mesh powder (smallest), –200 mesh powder, and a sand-sized granular particle. As expected, it was found that the smaller the particle size, the greater the catalytic activity. The smaller particle sizes were selected for additional investigation to minimize the amount required because of potential rheology and waste disposal effects.

Several different concentrations of –200-mesh MnO_2 were tested to determine the effect of catalyst concentration on the rate of gas generation in the clay simulant with a 19.7 vol% expected gas fraction. As expected, it was found that the greater the catalyst concentration, the greater the rate of gas generation. However, there was no significant difference between the 250- and the 500-ppm catalyst concentrations, as shown in Figure 3.8. Based on this information, it was decided to use 250-ppm MnO_2 as a catalyst in the larger scale testing.

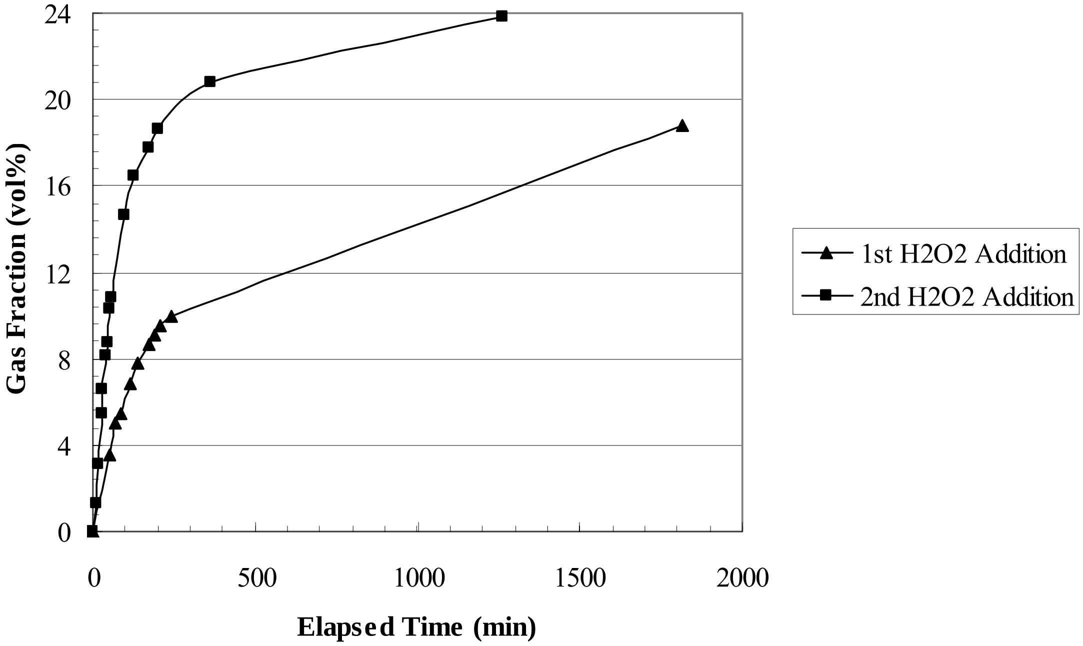

Figure 3.6. Kaolin-Bentonite Clay Simulant Recycle Results at ~20 vol% Expected Gas Fraction

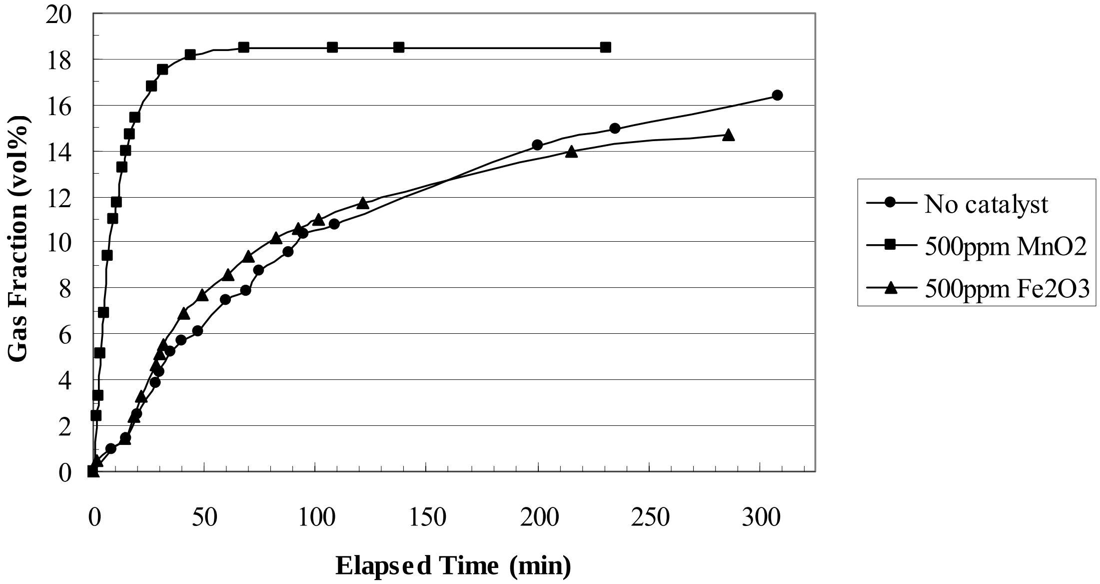

Figure 3.7. Catalyst Evaluation in Quadra Kaolin-Bentonite Clay Simulant with a 19.7-vol% Expected Gas Fraction

The concentration of –325-mesh MnO_2 was also varied in the clay simulant with 19.7-vol% expected gas fraction to determine whether a lower concentration of MnO_2 could be used with a smaller particle size. It was found that 50- and 100-ppm MnO_2 had very similar rates of gas generation, and 250- and 500-ppm MnO_2 had very similar rates of gas generation.

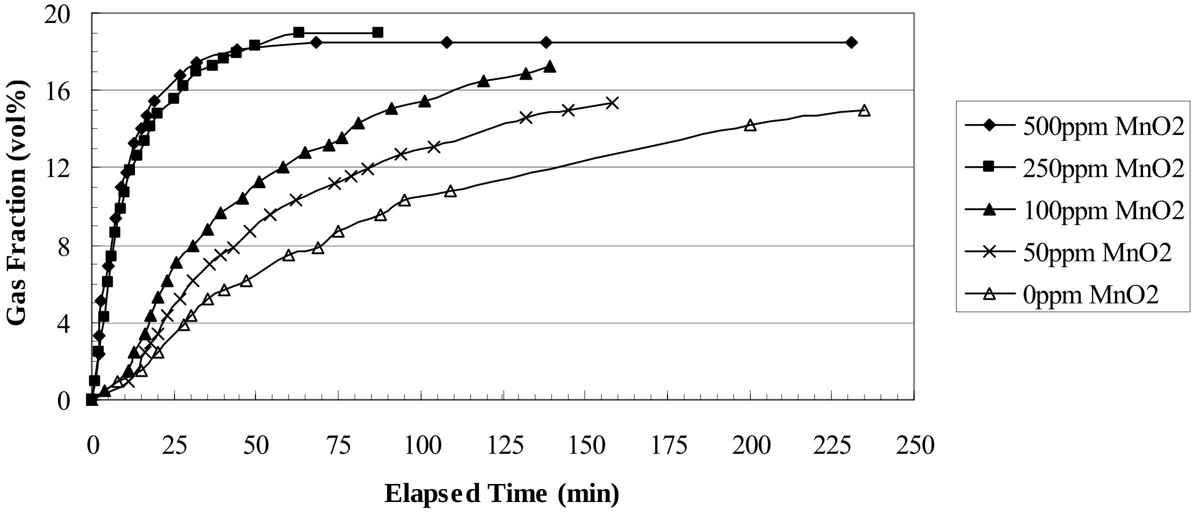

Figure 3.8. Gas-Generation Rate with Varying–200 Mesh MnO_2 Concentrations in Kaolin-Bentonite Simulant with 19.7 vol% Expected Gas Fraction

The two different MnO_2 particle size gas-generation rates were compared, as shown in Figure 3.9. At 500-ppm MnO_2, both MnO_2 particle sizes had very similar rates of gas generation. However, at 100-ppm and 50-ppm MnO_2, the –325 mesh MnO_2 had significantly higher rates of gas generation than the –200 mesh MnO_2. This indicated that a lower concentration of MnO_2 could be used to obtain the same gas-generation rate if a smaller MnO_2 particle size was used.

3.2.3 Simulant Rheology

Shear strengths were measured to determine the effect of the H_2O_2 and gas bubbles on the old clay simulant rheology after aging (growth time) for 3 days. Table 3.3 shows the average shear strengths obtained. As the measured gas fraction increased, the shear strength decreased, which was expected. This means the H_2O_2 and gas bubbles create weaker slurry with less cohesion between particles. Gauglitz et al. (1995) also found that shear and tensile strengths of bentonite clay simulant were reduced with increasing gas fraction.

Rheograms were obtained for the baseline (no H_2O_2 added) sample and the 19.8-vol% expected gas-fraction sample, both with and without gas bubbles. The measurement with gas bubbles present was obtained by carefully pouring simulant into the rheology sample cup, but it might have partially degassed in the transfer. The sample shrank in the cup during the run as it degassed. With the first down curve fit to a Bingham plastic model, shown in Table 3.4, the baseline sample and the 19.8-vol% expected gas-fraction sample with gas bubbles present had essentially the same yield stress and consistency factor. This could be caused by the degassing of the sample as it was poured and tested. However, after the 19.8-vol% expected gas-fraction sample was degassed by stirring, both yield stress and consistency factor were different than in both previous samples; yield stress was ~6.4 Pa and consistency factor ~47 cP. The yield stress may have decreased from stirring and measuring without any aging time.

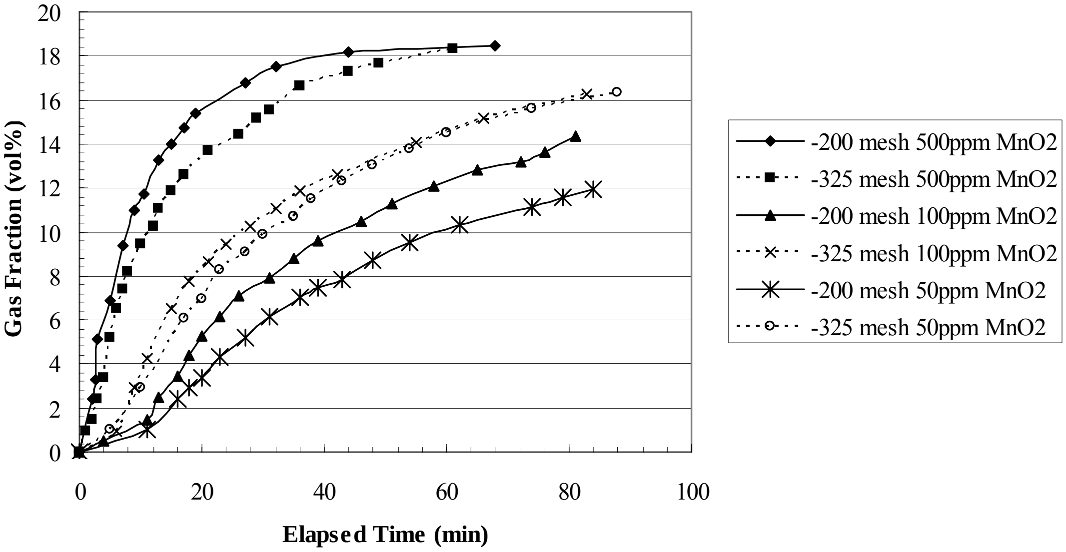

Figure 3.9. Comparison of –200 and –325 mesh MnO_2 Gas-Generation Rates in Kaolin-Bentonite Simulant with Varying MnO_2 Concentrations and 19.7-vol% Expected Gas Fraction

Table 3.3. Shear Strengths of the Clay Simulant with Varying Expected Gas Fractions

Expected Gas Fraction (vol%)	Measured Gas Fraction (vol%)	Actual Base Simulant Mass (g)	Actual H_2O_2 Solution Mass (g)	Avg. Shear Strength (Pa)
0	0	~700	0	68.1
4.9	3.4	720.1	0.2957	59.6
9.9	8.7	640.3	0.5582	58.3
19.8	19.2	719.5	1.4094	52.3

Table 3.4. Curve Fit to Bingham Plastic Model for 0 and 19.8 vol% Expected Gas Fractions in Clay Simulant

	0% Expected Gas Fraction	19.8% Expected Gas Fraction with Gas Bubbles	19.8% Expected Gas Fraction Without Gas Bubbles
Simulant Mass Used, g	~700	719.5	719.5
H_2O_2 Mass Used, g	0	1.4094	1.4094
Yield Stress, Pa	11.4	13.2	6.4
Consistency Factor, cP	42.3	42.8	47.0

3.3 Laponite Simulant Scoping Test Results

Several different catalysts were evaluated using ~100-mL samples of Laponite simulant in 250-mL beakers spiked with enough 30-wt% H_2O_2 to theoretically obtain >50-vol% gas. The catalysts evaluated were copper powder, 50-wt% sodium hydroxide solution, iron powder, copper nitrate, and iron nitrate.

The approximate gas fractions observed ranged from 0 to 20 vol%. The copper nitrate produced the largest gas fraction; it turned the Laponite dark brown when added, but overnight the color changed from dark brown to clear with a band of golden yellow near the top. The iron powder added as both -100 mesh and -325 mesh powders and the sodium hydroxide solution did not produce any measurable volume increase.

Based on the various catalyst evaluations, it was decided to continue using the copper nitrate trihydrate [$Cu(NO_3)_2 \cdot 3H_2O$, Alfa Aesar] and to vary the concentration from 100 to 1000 ppm in the Laponite simulant. Five tests were performed using 100-, 250-, 500-, 750-, and 1000-ppm copper nitrate. Bubbles began forming in the Laponite within 5 minutes of H_2O_2 addition in all of the samples. The samples turned a range of colors immediately from dark orange-brown in the 1000-ppm sample to golden yellow in the 100-ppm sample. As time progressed, a band of color was noticed moving toward the top of the sample. Within 24 hours, all of the samples were completely clear with no color remaining. This indicated that a chemical reaction between the H_2O_2 and the copper nitrate was occurring. All of the copper nitrate concentrations created about the same volume fraction of gas in the Laponite simulant, but the data were more qualitative than quantitative.

Because 100-ppm copper nitrate appeared to be sufficient to create a target gas fraction, it was decided to try lower copper nitrate concentrations of 25-, 50-, and 75-ppm in the Laponite simulant. The 25-ppm copper nitrate sample did have a slight volume increase, and the bubbles that formed were oblong and large at the top of the sample with rounder, smaller bubbles near the bottom. The 50-ppm copper nitrate sample behaved like the 25-ppm sample. The 75-ppm copper nitrate sample had a greater volume increase with bubbles widely dispersed and irregularly shaped. After five days, all three of these samples were stirred to remove all bubbles present and to observe whether any more bubbles formed. Bubbles appeared to regrow in all of the samples. The bubbles were larger, oblong, and fairly well dispersed.

It was then decided to add dye to the Laponite simulant so mixing in the large-scale tank could be observed more easily. A screening test was performed to determine whether the dye would act as a catalyst and cause gas generation when H_2O_2 was added. It was observed that after ~1 day there were a few very tiny (<1-mm diameter) bubbles evenly distributed throughout the samples but no significant volume change. Therefore, it was decided that the Laponite simulant would continue to require the addition of catalyst even in the presence of the dye.

The expected gas fraction was varied in the Laponite with 100-ppm copper nitrate catalyst. Table 3.5 summarizes the quantities of simulant, copper nitrate catalyst, and H_2O_2 solution used to prepare Laponite simulants with expected gas fractions of 10, 19.9, and 49.5 vol%. The table also indicates the observed vol% gas fraction after ~6 hours of growth, and Figure 3.10 shows the retained gas fraction as a function of time in the three tests. The expected 49.5 vol% gas-fraction sample peaked at ~31 vol% retained gas, and then bubbles burst and gas was released down to ~23 vol%. Then the retained gas slowly increased to ~29 vol% and began to release again with bubbles popping at the surface. After ~6 hours, gas was still releasing, and the amount of gas retained was about the same as the expected 19.9 vol% gas-fraction sample. This indicates that the maximum gas retention under these conditions in the Laponite simulant is ~31 vol%.

Table 3.5. Laponite Simulant (~90 Pa shear strength after aging 25 hours) Formulations Using 100-ppm Copper Nitrate Catalyst and Three Different Expected Gas Fractions

Expected Gas Fraction (vol%)	Actual Base Simulant Mass m_{sim} (g)	Actual Catalyst Mass m_{cat} (mg)	Actual H_2O_2 Solution Mass m_{sol} (g)	Measured Gas Fraction after ~6 hours (vol%)
10.0	100.88	10.9	0.1043	7.7
19.9	101.72	10.3	0.2340	18
49.5	76.01	7.7	0.6970	19

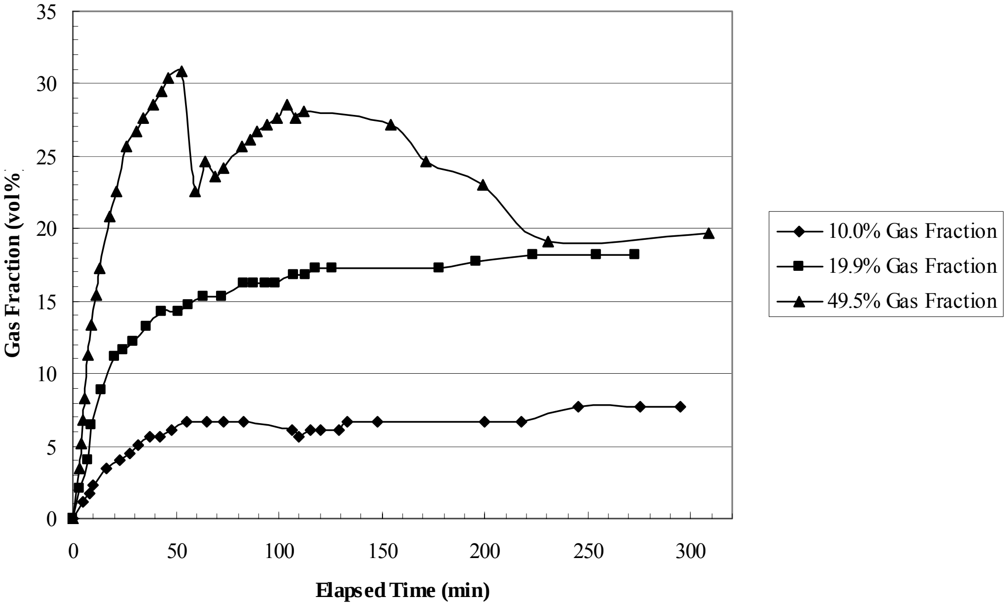

Figure 3.10. *In Situ* Gas Generation in Laponite Simulant (~90 Pa shear strength after aging 25 hr) Using 100-ppm Copper Nitrate with Three Different Expected Gas Fractions

Both the 10 and 19.9 vol% samples continued to retain gas as it was generated with no visual indication of gas release. As the gas was being generated, the color of the Laponite simulant changed from brown to faint yellow in the 49.5 vol% gas-fraction sample and from golden yellow to colorless in the 10 vol% gas-fraction sample.

3.3.1 Gas Generation

A test was performed to compare the gas-generation rates of unstabilized and commercially stabilized 30 wt% H_2O_2 (Aldrich) because 30 wt% commercially stabilized H_2O_2 was available. Both tests were performed under the same conditions in 100-mL graduated cylinder columns with a ~20 vol% expected gas fraction, as shown in Table 3.6. No significant difference was found between the two, especially in the first 200 minutes. The final gas fraction was only slightly higher with the unstabilized than with commercially stabilized H_2O_2 (~18 vol% versus ~17 vol%). Although no significant performance difference was noted, it was decided to continue to use the unstabilized H_2O_2.

Table 3.6. Dyed Laponite Simulant (~90 Pa Shear Strength after aging 25 hours) with ~20-vol% Expected Gas Fraction Using Commercially Stabilized and Unstabilized H_2O_2

	Expected Gas Fraction (vol%)	Actual Base Simulant Mass m_{sim} (g)	Actual Catalyst Mass m_{cat} (mg)	Actual H_2O_2 Solution Mass m_{sol} (g)	Maximum Measured Gas Fraction (vol%)
Stabilized H_2O_2	19.9	104.9	2.6	0.2371	~17
Unstabilized H_2O_2	19.5	101.7	2.8	0.2340	~18

In situ gas-generation experiments were completed with Laponite simulant. Table 3.7 summarizes the quantities of simulant, copper nitrate catalyst, and H_2O_2 solution used to prepare the Laponite simulants with 0-, 10-, 25-, and 100-ppm target catalyst concentrations. In each sample, sufficient H_2O_2 solution was added to achieve an expected gas fraction of ~20-vol%. Table 3.7 also indicates the observed vol% gas retention after ~1 day of growth, and Figure 3.11 shows the retained gas fraction as a function of time in the tests. The samples without catalyst only reached between 4- and 6-vol% gas retention before leveling out within a few hours whereas the samples with catalyst reached between 15 and 17 vol% gas retention in the same timeframe. The catalyst concentration clearly affects the gas-generation rate and the ability to reach target gas fractions in a convenient experimental time frame (e.g., ~1 day). Catalyst concentrations in the range of 25- to 100-ppm appear most likely to provide a combination of manageable rheology and acceptable gas-generation rate and were further tested.

Bubble size varied with the amount of catalyst and gas fraction also. Without catalyst, the bubbles were fairly evenly distributed, approached 1 mm in diameter near the end of the test, and remained round throughout. With catalyst present, the bubbles grew to ~4 mm in diameter, became oblong, and joined together.

To determine whether Laponite could be reused in the large-scale testing, dyed Laponite with 25-ppm copper nitrate added was degassed, and after enough 30 wt% H_2O_2 had been added to obtain an initial 20 vol% expected gas fraction, allowed to achieve equilibrium. Then enough 30 wt% H_2O_2 was added to the Laponite to achieve another 20 vol% expected gas fraction with no additional copper nitrate. It took much longer for gas to be generated the second time (144 hr versus 5 hr), but a higher final gas fraction was reached the second time (11 versus 9 vol%). The H_2O_2 seems to have reacted with the dye and the copper nitrate because the color became very light and then disappeared, leaving the Laponite clear with no trace of dye or copper nitrate. If the copper nitrate had decomposed during the first test, it would account for the longer gas-generation time during the second test. The Laponite also became very fluid at the top of the column. There were few bubbles, but those present joined together and were quite large (~5-6 mm in diameter at the wall). No testing was performed to determine the effect of adding H_2O_2 a third time or more to the Laponite.

Table 3.7. Laponite Simulant (~90 Pa shear strength after aging 25 hr) with Varying Amounts of Catalyst Targeting a 20 vol% Gas Fraction

Target Catalyst Conc. (ppm)	Expected Gas Fraction (vol%)	Actual Base Simulant Mass m_{sim} (g)	Actual Catalyst Mass m_{cat} (mg)	Actual H_2O_2 Solution Mass m_{sol} (g)	Measured Gas Fraction After ~1 day (vol%)
0	16.0	82.77	0	0.1534	4.1
0	19.9	100.62	0	0.2322	5.4
10	20.1	100.56	1.1	0.2342	~16
25	19.9	101.70	2.8	0.2340	~18
100	15.3	84.72	8.9	0.1498	~14

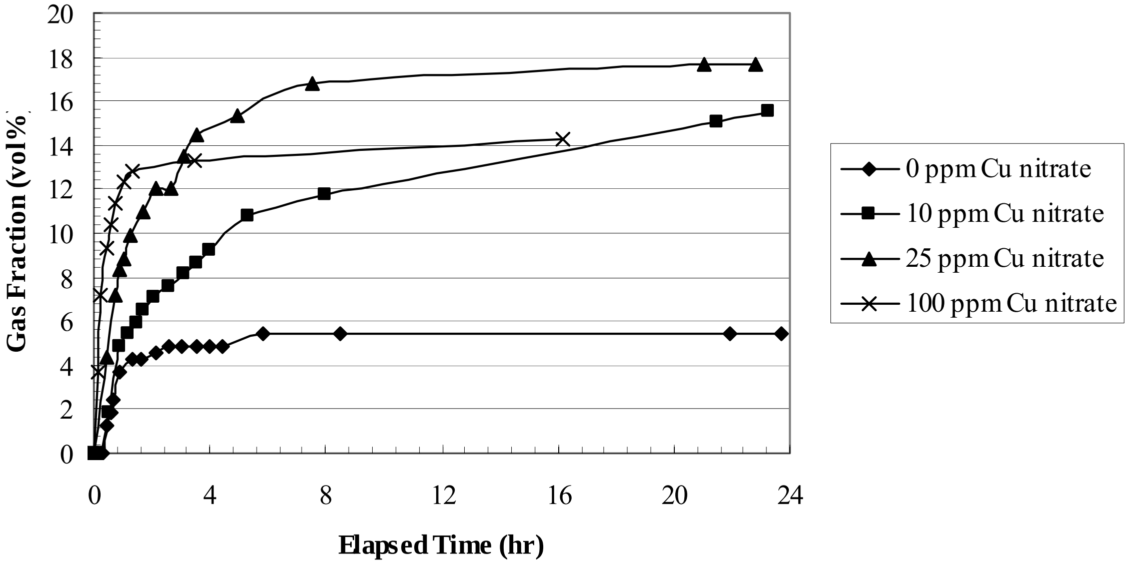

Figure 3.11. *In Situ* Gas Generation in Laponite (~90 Pa shear strength after aging 25 hr) with Varying Amounts of Copper Nitrate Catalyst and Expected Gas Fractions of 15 to 20 vol%

3.3.2 Simulant Rheology

Two different rheology studies were performed with the Laponite simulant. One focused on the effect of copper nitrate with dye present, and one focused on the effect of gas fraction (i.e., H_2O_2 amount) with dye and copper nitrate present.

Shear strengths were measured on four Laponite samples with dye present. The amount of copper nitrate added was varied to determine its effect on Laponite rheology. Table 3.8 shows the average shear strengths obtained after 24 hours. The shear strength of Laponite increased with copper nitrate concentration; at 100 ppm the shear strength was significantly greater than the baseline, indicating that copper nitrate does affect the shear strength of the simulant. This must be accounted for in testing because adding polar compounds (copper nitrate) to Laponite reduces the osmotic pressure that is holding sodium ions away from particle surfaces. This causes the electrical double layer to thin and allows the weaker positive charge on the edge of the crystals to interact with negative surfaces of adjacent crystals. The process may continue to give a "house of cards" structure, which, in a simple system of Laponite, water, and salt, is seen as a highly thixotropic gel, resulting in viscosity increase *in situ*.

Table 3.8. Shear Strengths of Dyed Laponite Simulant with Varying Amounts of Copper Nitrate

Amount of Cu Nitrate (ppm)	Avg. Shear Strength (Pa)	Yield Stress (Pa)	Consistency Factor (cP)
0	88.2	14.6	14.6
10	110.2	16.4	14.1
25	124.9	20.2	13.4
100	125.6	19.1	12.6

Rheograms were obtained for all of the samples. With the first down curve (when the shear rate decreases from maximum) fit to a Bingham plastic model, as shown in Table 3.8, the baseline sample had a yield stress of ~14.6 Pa compared with ~19 Pa for the 100-ppm copper nitrate sample. The baseline sample had a consistency factor of ~14.6 cP compared with ~12.6 cP for the 100-ppm copper nitrate sample. Based on these data, it appears that copper nitrate does increase yield stress and slightly decreases the consistency factor. The reason for the slight decrease in the consistency factor is unknown.

Another rheology study was performed to determine the effect of varying gas fraction on shear strength. This was done by maintaining a constant catalyst concentration (25 ppm copper nitrate) and aging time (24 hr) while varying the amount of H_2O_2 added to the simulant. Table 3.9 shows the range of shear strengths obtained. Several blanks were also tested to determine the effect of the gas, of the copper nitrate, and of the Laponite simulant alone. As expected, the copper nitrate significantly increased shear strength while the retained gas decreased it.

Rheograms were then obtained on the blanks as well as on the expected 20 vol% sample. With the first down curve fit to a Bingham plastic model, it was observed that the consistency factor was not significantly altered by any of the additives ranging from 12.2 to 13.4 cP. However, the yield stress was affected significantly, ranging from 4.9 Pa in the Laponite with no additives to 18.6 Pa with 25-ppm copper nitrate and no gas fraction. The sample with no catalyst and an expected gas fraction of 20 vol% may have had a lower actual gas fraction than the sample with catalyst and the same target gas fraction. This indicates that Laponite additives significantly affect yield stress and only slightly affect the consistency factor, which needs to be taken into account during testing.

Table 3.9. Shear Strengths of Dyed Laponite Simulant with Varying Copper Nitrate and H_2O_2 Concentrations

Expected Gas Fraction (vol%)	**Actual Base Simulant Mass m_{sim} (g)**	**Amount of 30 wt% H_2O_2 Added (g)**	**Amount of Cu Nitrate (ppm)**	**Avg. Shear Strength (Pa)**
0	~600	0	0	114.7
0	571.3	0	25	127.7
20	399.0	0.9332	0	95.3
5	606.0	0.2959	25	109.6
10	606.0	0.6230	25	88.6
20	555.5	1.2841	25	61.3

4.0 Gas-Retention and Release Test Vessels and Methods

This section describes each of the PJM test stands and the measurement methods used to obtain the gas-retention and release data at PNWD facilities. Section 4.1 provides an overview of how PJMs work and the components common to the test stands. Section 4.2 summarizes the testing procedures. Section 4.3 describes the configurations of the 4PJM test stands (composed of the tank, PJMs, ancillary systems, and instrumentation). Section 4.4 explains the data reduction methods for the gas-retention and release tests.

Gas-retention and release tests were performed by PNWD in five different systems. Two systems, each using four PJMs for mixing, investigated general scaling and physical phenomena and did not model specific full-scale process vessels. These are the full-scale 4PJM system in the 336 Building (336 4PJM) and the 1:4.5-scale 4PJM system in the APEL facility (APEL 4PJM). Two systems were also built to model specific full-scale process vessels and are thus termed “scaled prototypes”; these are the 1:4.9-scale UFP prototype system and the 1:4.3-scale LS prototype system. The fifth test stand operated by PNWD was without PJMs and is called the cone-bottom tank (CBT) test stand. Gas-retention and release tests were also performed in a 1:9-scale 4PJM system (SRNL 4PJM) operated by SRNL. The SRNL test stand is briefly described here; full details are in Wilson et al. (2004). Key features of these six test stands are listed in Table 4.1.

Table 4.1. Summary of Test Stands Used for Gas-Retention and Release Testing

Test Stand **Parameter**	**UFP**	**LS**	**336 4PJM**	**APEL 4PJM**	**SRNL 4PJM**	**CBT**
WTP Process Vessel Being Represented	UFP Vessels UFP-VSL-00002A UFP-VSL-00002B	HLW LS Vessels HLP-VSL-0027A HLP-VSL-0027B HLP-VSL-0028	None; generic system to investigate general scaling and physical phenomena	None; generic system to investigate general scaling and physical phenomena	None; generic system to investigate general scaling and physical phenomena	None; generic system without PJMs to investigate air sparging
Scale	1:4.9	1:4.3	Large scale (approx. half - scale)	1:4.5 (relative to 336 4PJM system)	1:8.9 (relative to 336 4PJM system)	Large scale (approx. half -scale)
Number and Configuration of PJMs	4PJM trifoil configuration (3 PJMs around 1)	8PJM cluster configuration (7 PJMs around 1)	4PJM square configuration	4PJM square configuration	4PJM square configuration	No PJMs
Air Sparging Tubes	Four—three between PJMs, one near the center PJM (only center sparger used in tests)	Eight—near the tank wall between PJMs (only four spargers used in tests)	None	None	None	Nine—diamond-in-a-square pattern plus one tube in the center
Slurry Recirculation Capability	Four nozzles at 113 L/min each (used only in holdup tests)	One nozzle at 340 L/min (used only in holdup tests)	None	None	None	None

N/A = not applicable.

4.1 PJM/Test Stand Overview

Specifics of each test stand are given in Section 4.2, but all PJM test stands have the same basic components. Four to eight PJM assemblies are suspended in a round-bottomed tank. PJM assemblies consist of a cylindrical section (comprising most of the length), a rounded shoulder (header) at the top with riser piping for connecting to air and/or vacuum supplies, and a 60° cone section at the bottom with a nozzle at the tip of the cone (either as a truncated cone or as a piece of pipe attached to the tip of the cone). In some cases (LS and UFP), wiring for instrumentation within the PJMs may be routed through the riser pipes. Flexible hoses connect to the top of the riser piping to provide air pressure, vacuum, and venting capabilities for each PJM. Test stands may have separate riser pipes in the tank for sample collection, air sparging, and recirculation of the simulant.

Operation of the PJMs includes a fill or suction phase and a drive or discharge phase. During the fill phase, fluid is drawn up into the PJM (from the tank) by applying a vacuum. During the drive phase, the PJM is pressurized to expel fluid through the nozzle at high velocity to induce mixing in the tank. The total time for a complete fill-drive cycle ranges from 7 seconds (SRNL 4PJM) to 1 minute (336 4PJM) following the geometric scale of the tank. The drive time is generally on the order of one-fourth of the total pulse cycle time.

The PJM nozzle exit velocity is a test-specific parameter that is obtained by manually manipulating the durations of the suction and discharge phases, the supply pressure, and the amount of vacuum. PJM drive cycle nomenclature and nozzle velocity calculation methods are described in Section 3.2.1 of WTP-RPT-113.(a)

In addition to PJMs, the scaled prototype systems (LS and UFP) were equipped with recirculation pumps and air spargers that were used in various combinations in some tests to enhance mixing and gas release. Recirculation was done with centrifugal recirculation pumps that are controlled manually using variable frequency drives. In some cases, a diaphragm pump was also used in line with the centrifugal pumps to avoid pump cavitation. The pneumatic diaphragm pump flow rate was regulated by manually adjusting the air supply pressure to the pump. Air spargers consisted of small-diameter stainless steel tubes with an open end submerged in the simulant. Air was expelled through the air sparging tubes to create large bubbles that agitate the simulant as they rise to the surface. The flow rate of air through these tubes was controlled with rotameters.

Each test stand is instrumented to measure and record the height of the simulant surface level, which is used to determine the volume of gas held up within or released from the simulant. In the UFP, LS, and APEL 4PJM test stands, heights were measured on a scale affixed to the outer wall of the tank at an arbitrary vertical location; for the 336 4PJM test stand, heights were measured as distance down from the top of the tank rim. Primary among the tank simulant surface level sensors is an ultrasonic-type sensor stationed a fixed distance above the simulant surface. The ultrasonic sensor projects ultrasonic waves in a cone shape (8 degrees from vertical) from the face of the sensor, requiring attention to sensor placement to avoid obstructions. Some tests also used a micropower impulse radar (guided wave radar) sensor to measure the tank simulant surface level. This waveguide level sensor consists of dual solid rods that

---

(a) Bamberger JA et al. 2004. *Technical Basis for Testing Scaled Pulse Jet Mixing Systems for Non-Newtonian Slurries*. WTP-RPT-113 Rev. A, Battelle—Pacific Northwest Division, Richland, WA.

sense immersion in fluid based on the time of flight between sending a microwave pulse and receiving the reflected signal. A third level sensor used in some tests is a radio frequency (RF) admittance sensor rod like those used within the PJMs. Additional sensors are used to determine temperature (of simulant and ambient air), pressure (pressure delivered to the PJMs), flow rate (for air sparging, H_2O_2 injection, or simulant recirculation), and density (of H_2O_2 or recirculated simulant). Level probes are also installed within the PJMs to provide data for control of PJM operation. These level probes consist of a long sensor rod that uses RF admittance technology to determine the simulant level (i.e., how much of the sensor rod is immersed), regardless of any buildup of material on the sensor rod.

4.2 Gas-Retention and Release Test Procedures

Gas-retention and release tests were conducted by PNWD according to Test Instructions TI-RPP-WTP-337 and TI-RPP-WTP-338, which describe the purpose of the testing and the specific steps to take for a test. Gas-release tests occur after introducing H_2O_2 to generate O_2 gas bubbles and when simulant level has reached a predetermined value indicating the desired initial gas-volume fraction, at which point the mixing system (PJM operation plus specified recirculation and/or sparging, as applicable) is started to release the gas. The simulant level is measured during the test to track the release. Gas-holdup tests are initiated by introducing H_2O_2 to the simulant at a specified rate with the mixing system operating, and the simulant level is tracked to a steady state. In some tests, the H_2O_2 injection rate was increased and the system operated until a second steady-state gas holdup occurred.

Testing was performed as a sequence of runs where the sequence defined the test parameters/system configuration, and each run was either a gas-holdup or gas-release test. The conditions for the test sequences and runs are listed in Table 5.1 (gas holdup) and Table 6.1 (gas release). An entire sequence could last about 24 hours, part of which was unmanned (e.g., when performing a quiescent long-term gas-holdup test prior to a gas-release test). After a gas-release test, any remaining gas was purged from the simulant by aggressively agitating the simulant (e.g., PJM overblow and sparging) to prepare the simulant for the subsequent gas-holdup test.

The decomposition of a nominally 30-wt% H_2O_2 solution was used to generate gas *in situ* in the kaolin-bentonite clay simulant. The H_2O_2 solution was injected while the PJMs and other equipment were operating. A peristaltic pump was used to feed the H_2O_2 solution through a single tube into the well-mixed cavern near the center of the tank at approximately the level of the pulse-tube nozzles. The rate of H_2O_2 injection was measured with a MicroMotion (Boulder, CO) model RFT 9739 Coriolis mass flow meter.

In the preparation for gas-release tests, a specified mass of H_2O_2 was introduced over a short period of time (10 to 20 minutes). After 10 to 30 minutes of additional mixing, the system was shut down to allow the H_2O_2 to decompose and gas bubbles to be retained in the quiescent simulant.

In gas-holdup tests, H_2O_2 solution was added to the simulant at a fixed rate over 2 to 3 hours to continuously generate O_2 gas while the simulant was mixed in the PJM vessel using specified normal operating conditions. Injection continued until a new steady-state level was achieved in the test vessel.

Before starting a test sequence (at least once daily), a level sensor performance check was completed so that scaling factors could be confirmed or updated. During testing, observers periodically took manual measurements of tank simulant level (backup measurements to the electronically logged data) and operated video cameras to document the testing. Air sparger flow rates and line pressures were recorded manually during tests in which air sparging took place. Hydrogen peroxide solution injection information was recorded manually by the peristaltic pump operator (as well as electronically by the data acquisition control system [DACS]). All other data were recorded electronically by the DACS, including tank simulant level, PJM simulant levels, temperature (tank and ambient air), recirculation flow rate, recirculated simulant density, and system pressures.

4.3 PJM Test Stand Descriptions

4.3.1 UFP Prototype Test Stand

The UFP test stand is a nominally 1:4.94 linearly scaled version of the 168-in. (427-cm) diameter full-scale UFP tank. Nominal dimensions of the scaled UFP tank and PJMs are listed in Table 4.2. The UFP tank used in gas-retention and release testing is constructed of clear acrylic and has a round-bottomed, stainless steel insert. Figures 4.1 and 4.2 show plan and section view diagrams, respectively, of the UFP system. The difference between the UFP-tank-diameter scale factor and the pulse-tube-height scale factor (noted in Table 4.2) was the result of using standard pipe sizes (for procurement expediency). However, by adjusting the length of the stroke, the volume expelled from the PJMs was set to be consistent with the UFP vessel scale factor of ~ 4.94.

Table 4.2. Approximate Dimensions of the Scaled UFP System

Item	Approximate Diameter	Approximate Length/Height	Other
UFP Tank	34 ± 1 in. (86 ± 2 cm) ID	91 ± 1 in. (230 ± 2 cm)	Diameter corresponds to a scale of about 1:4.94; ~2:1 elliptical stainless steel dish
PJM Tube	6.065 in. (15.41 cm) ID	37 ± 1 in. (94 ± 2 cm)	6-inch schedule 40 stainless steel pipe; height corresponds to a scale of 1:4.32
Center PJM Nozzle	0.824 in. (2.09 cm) ID	N/A	¾-inch schedule 40 stainless steel pipe; pointed straight down; nose of nozzle is ~ 2 in. (5 cm) above the tank bottom
Perimeter PJM Nozzles	0.824 in. (2.09 cm) ID	N/A	¾-inch schedule 40 stainless steel pipe; angled at 45° (using a standard 45° elbow fitting) radially outwards; nose of nozzle is ~ 2 in. (5 cm) above the tank bottom (at the nozzle lateral location)

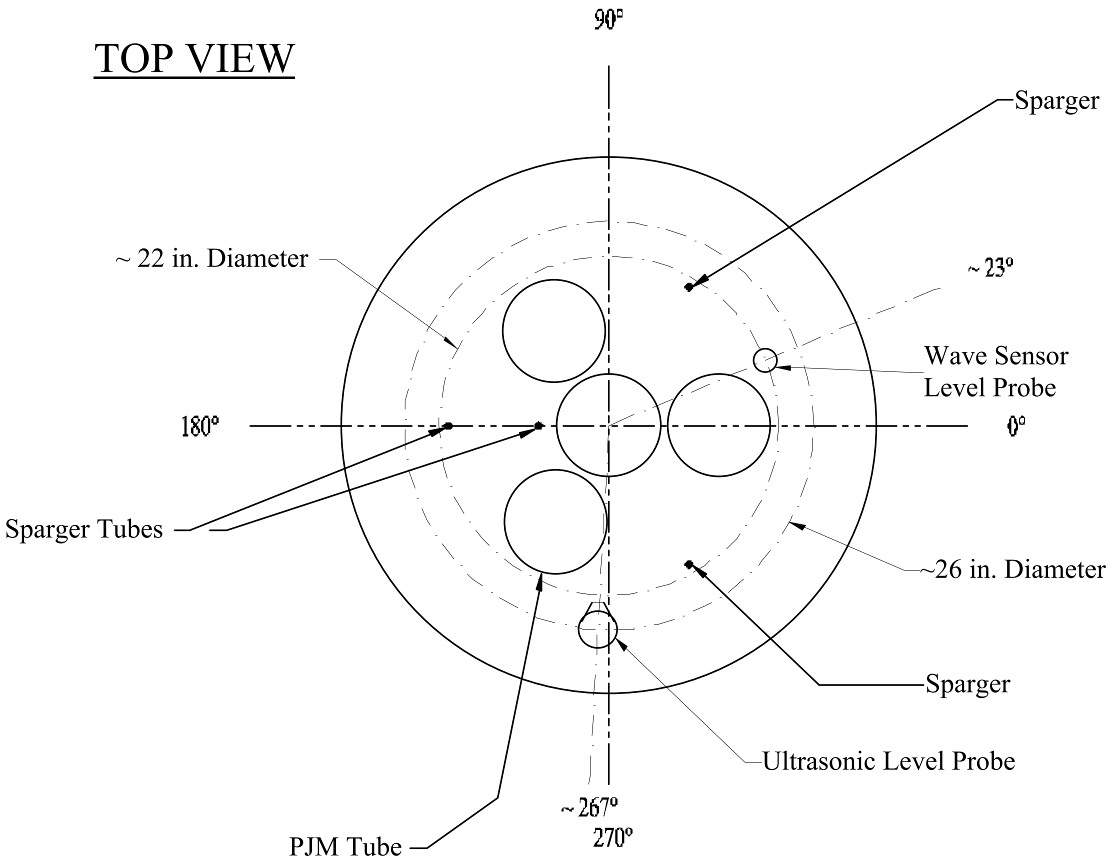

Figure 4.1. Top View of the UFP Prototypic Test Stand Showing Lateral Locations

Testing in the UFP tank was performed using different combinations of PJMs, air sparging, and/or simulant recirculation. The configuration of PJMs for which results are presented in this document was a 4PJM trifoil configuration (often referred to in operator logs as a "chandelier 3+1" configuration) with one PJM in the center and the other three spaced nearly evenly around it. The three perimeter nozzles were oriented at 45° radially outward, and the center nozzle was vertical. Two simulant fill heights were used in testing: ~1.4 height-to-diameter ratio (H/D) and ~1.8 H/D, corresponding to ~170 gal (~644 L) and ~221 gal (~837 L), respectively. At an H/D of ~1.8, the equilibrium tank simulant level was above the top of the PJM shoulder.

UFP gas-retention and release tests with spargers were performed using one to four air sparger tubes (one in the center and/or three at the perimeter). The center air sparger was about midway between adjacent perimeter PJMs at a radial position of approximately 4.5 inches (~11 cm) from the tank centerline. The perimeter air spargers were placed approximately midway between adjacent perimeter PJMs at a pitch circle diameter (PCD) of 20 ± 1 inches (50 ± 2 cm). All sparger tubes were made of 0.5-inch (1.3-cm) OD (0.37-inch [0.94-cm] ID) stainless steel tubing. The lower ends of the sparger tubes were approximately 4 inches (~10 cm) above the bottom of the tank (i.e., approximately 2 inches [~5 cm] above the tip of the nozzle), as measured from the tank floor.

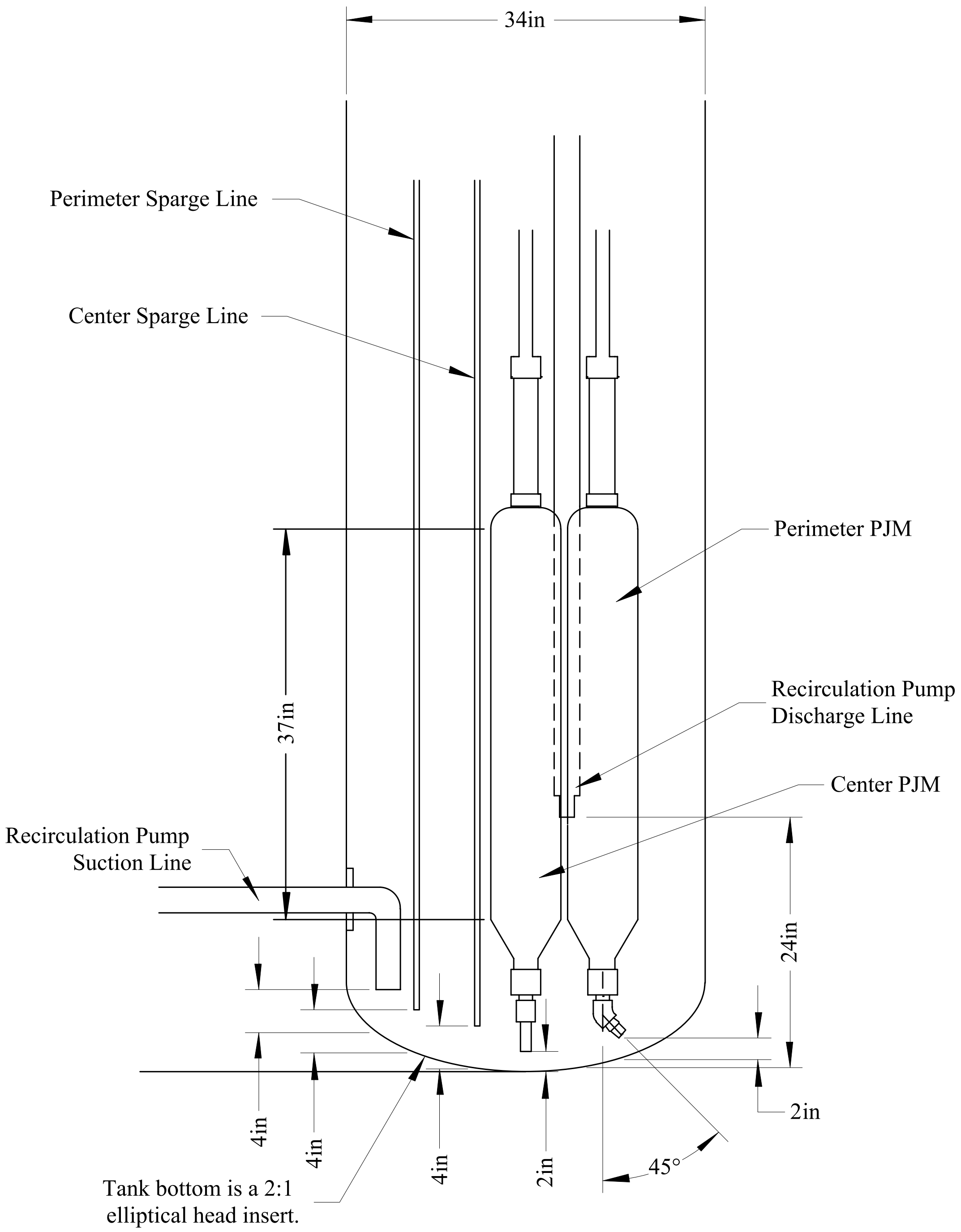

Figure 4.2. Side View of the UFP Test Stand Showing Nominal Dimensions

A peristaltic pump was used to feed the H_2O_2 solution through a single tube into the well-mixed cavern near the tank center. The ¼-inch OD stainless steel injection tubing was strapped to the outside of the center PJM, and the outlet ended about 1 inch (2.54 cm) above the center PJM nozzle outlet. The rate of H_2O_2 injection was measured with a 0.25-inch MicroMotion (Boulder, CO) model RFT 9739 Coriolis mass flow meter.

The recirculation pump system consisted of two centrifugal pumps placed in parallel and connected in series with a diaphragm pump that was used to prime the centrifugal pumps before startup and eliminate cavitation during operations. Recirculation for the UFP tank used a single 2-inch schedule 40 stainless steel pipe for the discharge line (2.067-inch [5.25-cm] ID) with a 1-inch schedule 40 stainless steel nozzle (1.049-inch [2.66-cm] ID) pointing straight down. The recirculation discharge line was laterally about midway between two of the perimeter PJMs at a radial position approximately 5.5 inches (~14 cm) from the tank centerline and an elevation of about 24 inches (~61 cm) from the center of the tank floor. The pump suction line consisted of a 2-inch schedule 40 polyvinyl chloride (PVC) pipe (2.067 inch [5.25 cm] ID) at a radial position approximately 4 inches (~10 cm) from the tank wall on the opposite side of the tank from the discharge line at an elevation of about 4 inches (~10 cm), measured from the center of the intake to the tank floor beneath it.

Table 4.3 lists the instrumentation and process control software that were used with the UFP test stand. The lateral locations of the sensors are shown in Figure 4.1. The ultrasonic level sensor was placed in the annular region between the PJMs and the tank wall, ~13 inches (~33 cm) from the center at an angle of ~267° and mounted nominally 20 inches (0.5 m) above the simulant surface. A micropower impulse radar sensor was placed in the annular region between the PJMs and the tank wall, ~11 inches (~28 cm) from the center of the vessel at an angle of ~23°.

There were three observer stations around the UFP test stand at 0° (~east), 90° (~north), and 270° (~south); the west station was inaccessible because of the test skid and ancillary equipment. A flexible measuring tape was affixed to the outer wall of the tank with clear tape at each observer station. The vertical placement of the measuring tapes was arbitrary, and the tapes were not precisely aligned. The affixed measuring tape at the 270° station is the primary reference. See Attachment C of Appendix A for the relationship between the 270° station affixed tape and the distance down from the top of the tank rim.

Table 4.3. Instrumentation in the UFP System

Parameter	Equipment Name/Model	Manufacturer
Process control/data collection	DASYLab, Version 7.0	DASYTEC USA (Bedford, NH)
Fluid level within the PJMs	Universal II level transmitter	Ametek Drexelbrook (Horsham, PA)
Pressure/vacuum at system manifold	Cerabar T PMP 135 pressure transducer	Endress + Hauser (Greenwood, IN)
Fluid level within the tank	UCL-200 ultrasonic liquid level sensor	Gems Sensors, Inc. (Plainville, CT)
Fluid level within the tank	MIR-800 micropower impulse radar “waveguide” level probe	Gems Sensors, Inc. (Plainville, CT)
Temperature of fluid/ambient air	Type K thermocouple	Omega Engineering, Inc. (Stamford, CT)

4.3.2 LS Prototype Test Stand

The LS test stand is a nominally 1:4.29 linearly scaled version of the 300-inch (760-cm) diameter full-scale LS tank. Nominal dimensions of the LS tank and PJMs are listed in Table 4.4. The LS tank used in gas-retention and release testing is constructed of clear acrylic and has a round-bottom stainless steel insert. Figures 4.3 and 4.4 show plan and section view diagrams of the LS system, respectively.

Table 4.4. Approximate Dimensions of the Scaled LS System

Item	Approximate Diameter	Approximate Length/Height	Other
LS Tank	70 ± 1 in. (180 ± 2 cm) ID	91 ± 1 in. (230 ± 2 cm)	Diameter corresponds to a scale of about 1:4.29; ~100:6 elliptical stainless steel dish
PJM tube	12.0 in. (30.0 cm) ID	31 ± 1 in. (79 ± 2 cm)	12-in. schedule 40 stainless steel pipe; height corresponds to a scale of 1:4.93
Center PJM nozzle	1.049 in. (2.66 cm) ID	N/A	1-in. schedule 40 stainless steel pipe pointed straight down; nose of nozzle is ~ 2 in. (5 cm) above tank bottom
Perimeter PJM nozzles	0.957 in. (2.43 cm) ID	N/A	1-in. schedule 80 PVC pipe; angled at 45° (using a standard 45° elbow fitting) radially outwards; nose of nozzle is ~ 2 in. (5 cm) above the tank bottom (at the nozzle lateral location)
Even-numbered perimeter PJM nozzles for test sequence 14 only	0.957 in. (2.43 cm) ID	N/A	1-in. schedule 80 PVC pipe; angled upward at 135° (using standard fittings)

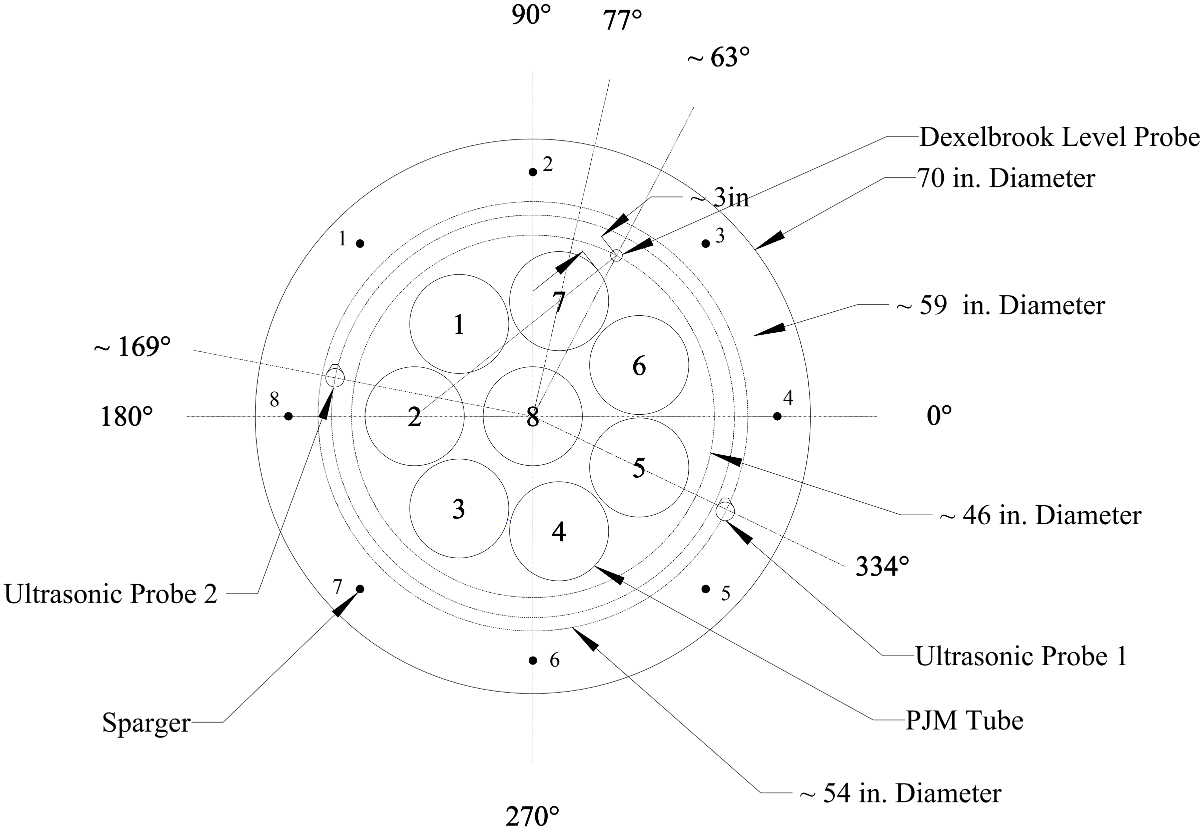

Figure 4.3. Top View of the LS Prototype Test Stand Showing Lateral Locations

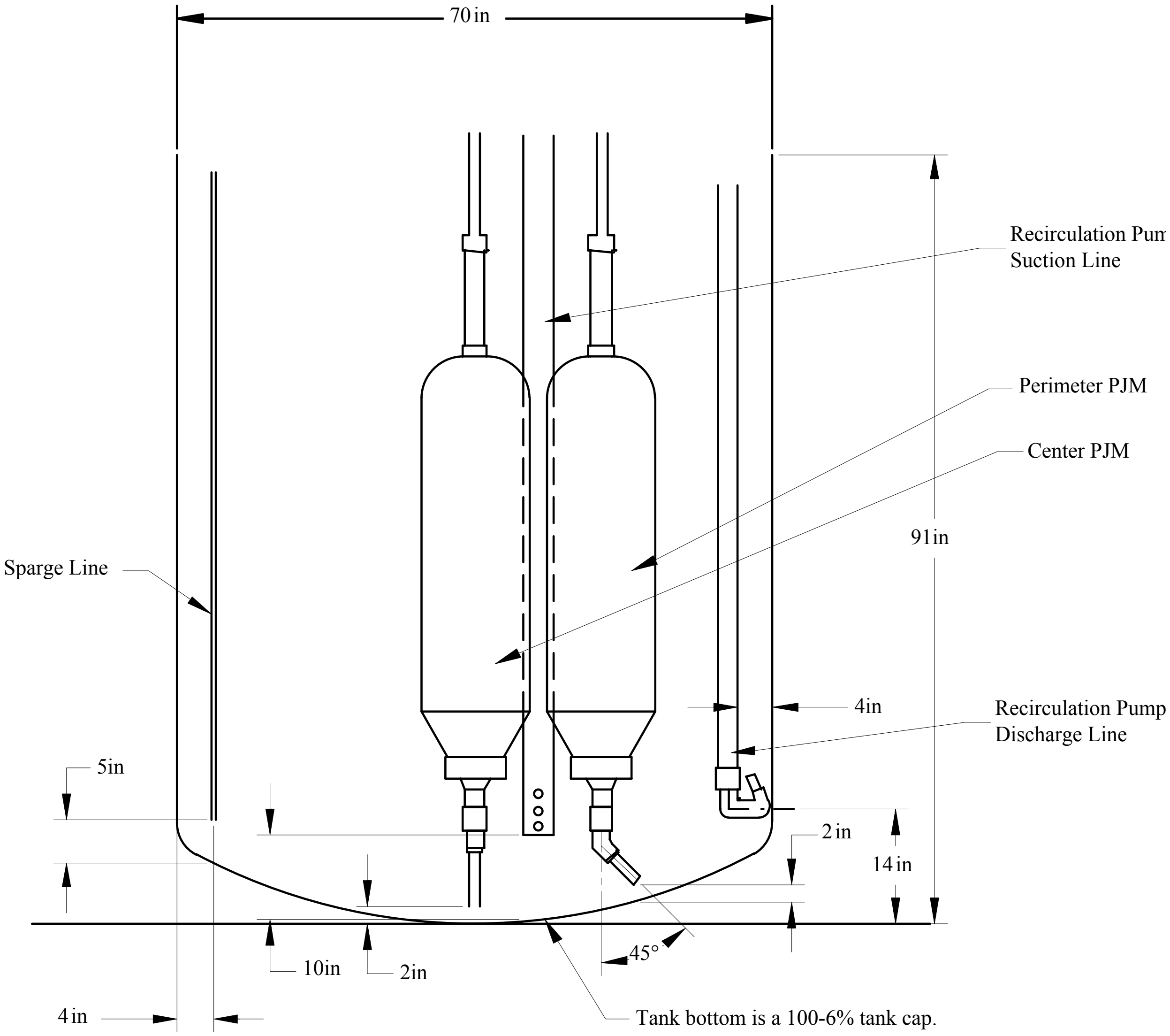

Figure 4.4. Side View of the LS Prototype Test Stand Showing Nominal Dimensions

The difference between the LS-tank-diameter scale factor and the pulse-tube-height scale factor (noted in Table 4.4) was the result of using standard pipe sizes for procurement expediency. By adjusting the length of the stroke, the volume expelled from the PJMs was set consistent with the LS vessel scale factor of ~ 4.29.

Testing in the LS tank used different combinations of PJMs, air sparging, and/or simulant recirculation. The configuration for which results are presented in this document was an 8PJM cluster configuration (often referred to in operator logs as a “chandelier 7+1” configuration) with one PJM in the center of the tank and the other seven equally spaced around the center PJM on a PCD of 30 ± 1 inches (76 ± 2 cm). The seven perimeter nozzles were oriented at 45° angles radially outward (except in test sequence 14, where the even-numbered PJMs had nozzles angled radially outward and upward at 135°, and the others were angled outward at 45°), and the center nozzle was oriented vertically. A simulant fill height of ~0.74 H/D, corresponding to ~759 gal (~2873 L), was used. At an H/D of ~0.74, the equilibrium tank level was at the top of the cylindrical PJM tube section (just below the PJM shoulder).

The LS test stand had an array of eight air sparging tubes distributed equally around the tank circumference at a PCD of 62 ± 1 inches (157 ± 2 cm). All sparger tubes were made of 0.5-inch (1.3-cm) OD (0.37-inch [0.94-cm] ID) stainless steel tubing. The lower ends of the sparger tubes were approximately 5 inches (~13 cm) above the bottom of the tank (i.e., approximately 3 inches [~8 cm] above the tip of the 45° nozzles), as measured from the tank floor. When using air sparging, gas-retention and release tests used either all eight sparging tubes or only the four odd-numbered tubes.

A peristaltic pump was used to feed the H_2O_2 solution through a single tube into the well-mixed cavern near the tank center. The ¼-inch OD stainless steel injection tubing was strapped to the outside of the center PJM, and the outlet ended about 1 inch (2.54 cm) above the center PJM nozzle outlet. The rate of H_2O_2 injection was measured with a 0.25-inch MicroMotion (Boulder, CO) model RFT 9739 Coriolis mass flow meter.

The recirculation pump system consisted of two centrifugal pumps placed in parallel and connected in series with a diaphragm pump that was used to prime the centrifugal pumps before startup and eliminate cavitation during operations. The pump suction line consisted of a 3-inch schedule 80 PVC pipe (2.90-inch [7.4-cm] ID). The end of the suction line had several 1.5-inch (3.8-cm) holes drilled along its side to provide additional simulant flow. The suction line was in the space between the center and two adjacent perimeter PJMs, as shown in Figure 4.4. The elevation of the suction line varied from 4 to 12 inches (10 to 30 cm) above the tank floor; the elevation was selected to minimize cavitation during testing caused by proximity of the suction line to the air sparging tubes. Four 2-inch schedule 40 stainless steel pipes (2.067-inch [5.25-cm] ID) were used for recirculation discharge in test sequence 15 (and 15A). The discharge lines were laterally located along the four corners of a rectangle at a PCD of 60 ± 1 inch (150 ± 2 cm). Each discharge line had a nozzle made of ½-inch schedule 40 stainless steel pipe (0.622-inch [1.58-cm] ID). The nozzles were pointed up at an angle of 30º at an elevation approximately 16 inches (~41 cm) above the bottom center of the tank. The nozzles were pointed approximately tangential to the tank wall. The recirculation pump system was not used in test sequence 14.

Table 4.5 lists the instrumentation and process control software used with the LS test stand. The lateral locations of the sensors are shown in Figure 4.3. The ultrasonic level sensor #1 was ~27 inches (~69 cm) from the center of the vessel at an angle of ~334°, and the ultrasonic level sensor #2 was ~25 inches (~64 cm) from the center of the vessel at ~169°. The ultrasonic level sensors were mounted nominally 20 inches (0.5 m) above the simulant surface. Although not used to obtain data during the gas-retention and release tests, a Drexelbrook level probe was located in the annular region between the PJMs and the tank wall, ~23 inches (~58 cm) from the center of the vessel at an angle of ~63°.

There were three observer stations around the LS test stand at 90° (~north), 180° (~west), and 270° (~south); the east station was inaccessible because of the test skid and ancillary equipment. A flexible measuring tape was affixed to the outer wall of the tank with clear tape at each observer station. The vertical placement of the measuring tapes was arbitrary, and the tapes were not precisely aligned. The affixed measuring tape at the 270° station is the primary reference. See Attachment C of Appendix A for the relationship between the 270° station affixed tape and the distance down from the top of the tank rim.

Table 4.5. Instrumentation in the LS System

Parameter	Equipment Name/Model	Manufacturer
Process control/data collection	DASYLab, version 7.0	DASYTEC USA (Bedford, NH)
Fluid level within the PJMs	Universal II level transmitter	Ametek Drexelbrook (Horsham, PA)
Pressure/vacuum at system manifold	Cerabar T PMP 135 pressure transducer	Endress + Hauser (Greenwood, IN)
Fluid level in tank	UCL-200 ultrasonic liquid level sensors	Gems Sensors, Inc. (Plainville, CT)
Temperature of fluid/ambient air	Type K thermocouple	Omega Engineering, Inc. (Stamford, CT)

4.3.3 APEL 4PJM Test Stand

The APEL 4PJM test stand is a linearly scaled version of the 336 4PJM test stand (see Section 4.3.4) and thus has the same arrangement of four PJMs within a round-bottomed tank. Nominal dimensions of the APEL 4PJM tank and PJMs are listed in Table 4.6. Figures 4.5 and 4.6 show plan and section view diagrams, respectively, of the APEL 4PJM system. The PJMs are situated in a square around the center of the tank, along a PCD of 21 ± 1 inches (53 ± 2 cm). In the gas-holdup and release tests, the nominal simulant fill height in the APEL 4PJM system was ~0.9 H/D, corresponding to ~100 gal (~380 L). The nozzles are approximately 2 inches (5 cm) above the tank floor at the PJM lateral location.

Table 4.6. Approximate Dimensions of the APEL 4PJM System

Item	Approximate Diameter	Approximate Length/Height	Other
APEL 4PJM Tank	33.8 ± 0.5 in. (85.8 ± 1 cm) ID	83.5 ± 1 in. (212 ± 2 cm)	Diameter corresponds to a scale of about 1:4.53;~2:1 elliptical stainless steel dish
PJM Tube	5.29 in. (13.4 cm) ID	48 ± 1 in. (120 ± 2 cm)	5-in. schedule 10 stainless steel pipe; ID is a measured value
PJM Nozzle	0.88 ± 0.01 in. (2.2 ± 0.02 cm) ID	N/A	Discharges vertically downward

A peristaltic pump was used to feed the H_2O_2 solution through a single tube into the well-mixed cavern near the tank center. The ¼-inch OD stainless steel injection tubing ran down the wall of the APEL 4PJM tank to the center of the tank bottom where it angled directly upward, and the tubing outlet ended about 1 ft above the bottom of the center of the tank floor. The rate of H_2O_2 injection was measured with a 0.25-inch MicroMotion (Boulder, CO) model RFT 9739 Coriolis mass flow meter.

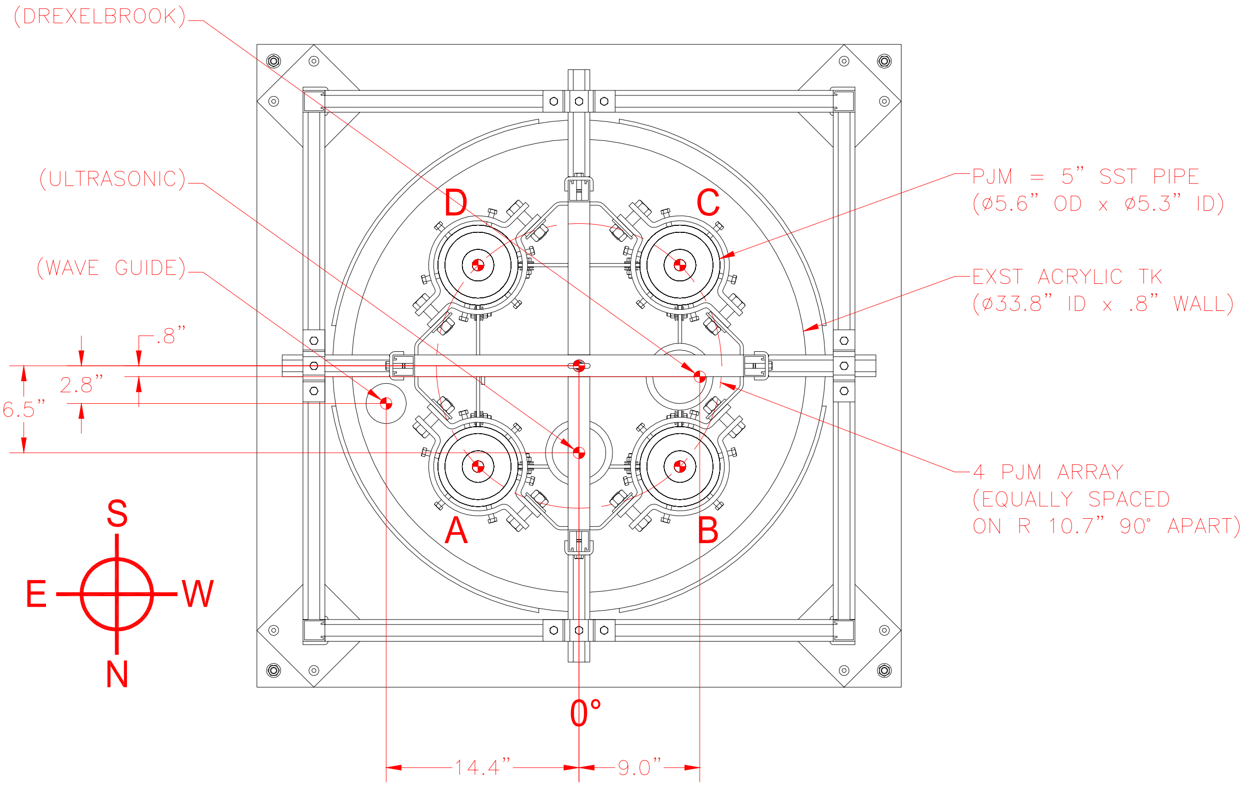

Figure 4.5. Top View of the APEL 4PJM Test Stand Showing Lateral Locations

Table 4.7 lists the instrumentation and process control software used with the APEL 4PJM test stand. The lateral locations of the sensors are shown in Figure 4.5. The Drexelbrook level probes for the tank level were mounted within the operating range of the tank level. The ultrasonic level sensor was mounted nominally 20 inches (0.5 m) above the simulant surface between PJMs A and B, as shown in Figure 4.6.

There were four observer stations around the APEL 4PJM test stand at 0° (north), 90° (west), 180° (south), and 270° (east). At each observer station, a flexible measuring tape was affixed vertically to the outer wall of the tank with clear tape. The vertical placement of the measuring tapes was arbitrary, and the tapes were not precisely aligned. The measuring tape at the 0° station is used as the reference for all height measurements (e.g., PJM level probes, tank level from the ultrasonic sensor).

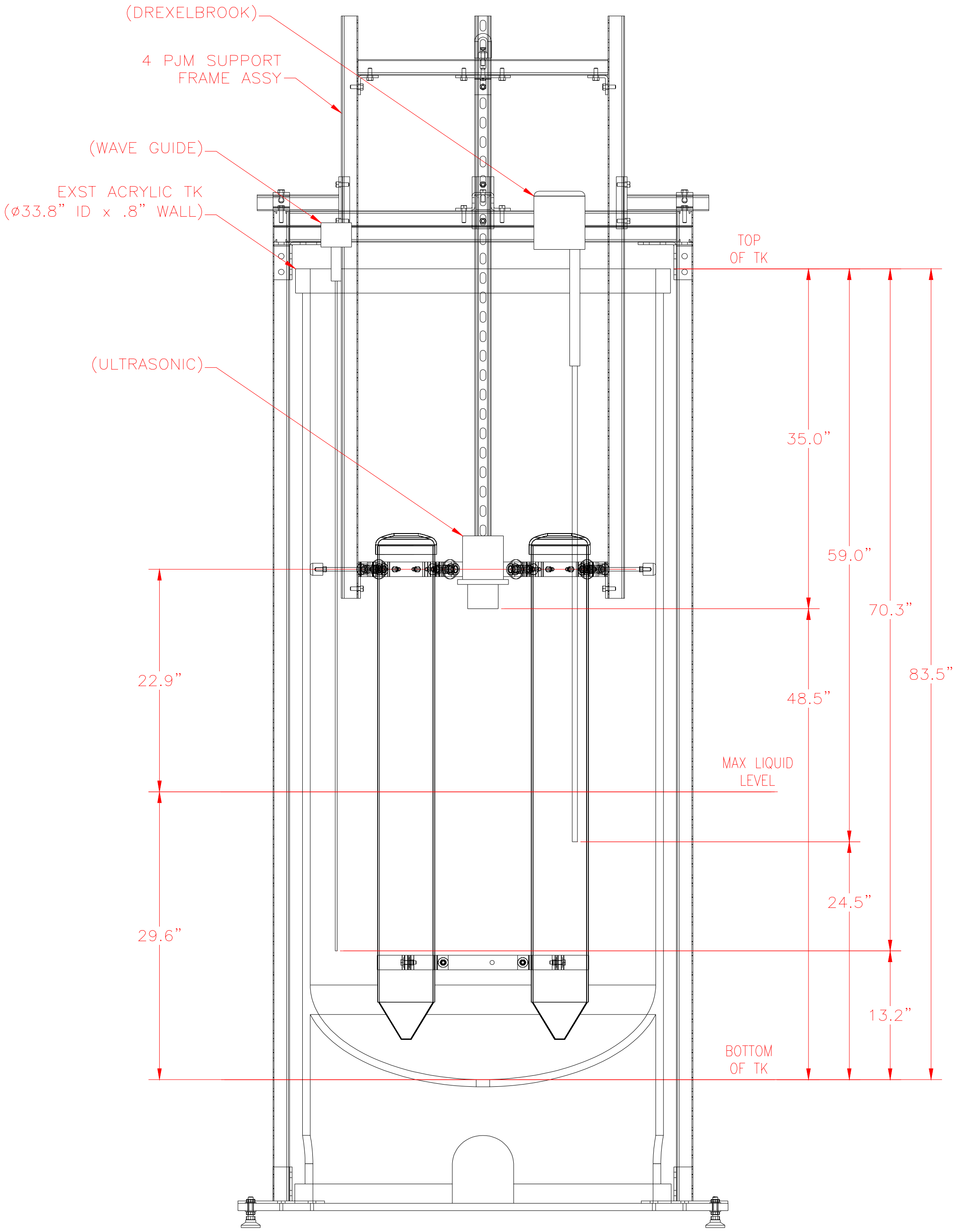

Figure 4.6. Side View of the APEL 4PJM Test Stand Showing Nominal Dimensions

Table 4.7. Instrumentation in the APEL 4PJM System

Parameter	Equipment Name/Model	Manufacturer
Process control & data collection	DASYLab, version 7.0	DASYTEC USA (Bedford, NH)
Fluid level within the PJMs	Universal II level transmitter	Ametek Drexelbrook (Horsham, PA)
Pressure within the PJMs	PMP 135 pressure transducer	Endress + Hauser (Greenwood, IN)
Fluid level within the tank	UCL-200 ultrasonic liquid level sensor	Gems Sensors, Inc. (Plainville, CT)
Fluid level within the tank	MIR-800 micropower impulse radar “waveguide” level probe	Gems Sensors, Inc. (Plainville, CT)
Fluid level within the tank	Universal II level transmitter	Ametek Drexelbrook (Horsham, PA)
Temperature of the fluid and ambient air	Type K thermocouple	Omega Engineering, Inc. (Stamford, CT)

4.3.4 336 4PJM Test Stand

The full-scale PJM test stand installed in the 336 Building test facility has been described extensively in previous reports (e.g., Bontha et al. 2003a, 2003b). Therefore, only a brief description is included here.

The 336 4PJM system consists of four PJMs within a round-bottom tank. Nominal dimensions of the tank and PJMs are listed in Table 4.8. Figures 4.7 and 4.8 show plan and section view diagrams of the 336 4PJM system, respectively (see Bontha et al. 2003a for as-built diagrams and dimensions). The tank has a nominal operating volume of about 10,000 gal (~38,000 L) at an H/D of ~0.9. PJMs are held in place by cross beams welded to the side of the tank. Additionally, tie beams connect each PJM to the two nearest PJMs to provide support to the tubes and prevent vibration during operation. The tie beams are ~6 ft (~1.8 m) from the tank floor (measured from the center). Laterally, the PJMs were positioned approximately at the centers of the four quadrants of the tank. Vertically, the tips of the PJM nozzles were ~10 inches (~25 cm) above the tank bottom (at a point directly below the PJM). The overall length of the PJM assembly (excluding the 2-inch pipe and flange connection at the top) is approximately 12 ft (~3.6 m).

Table 4.8. Approximate Dimensions of the 336 4PJM System

Item	Approximate Diameter	Approximate Length/Height	Other
336 4PJM tank	12.75 ft (3.90 m) ID	15 ft (4.6 m) height	Bottom of tank is a nominally 2:1 elliptical dish with a height of about 38.4 in. (0.98 m)
PJM tube	2 ft (0.6 m) ID	10 ft (3 m) length	Custom made tube (rolled/welded steel)
PJM nozzle	~ 4 in. (~10 cm) ID	N/A	Discharges vertically downward

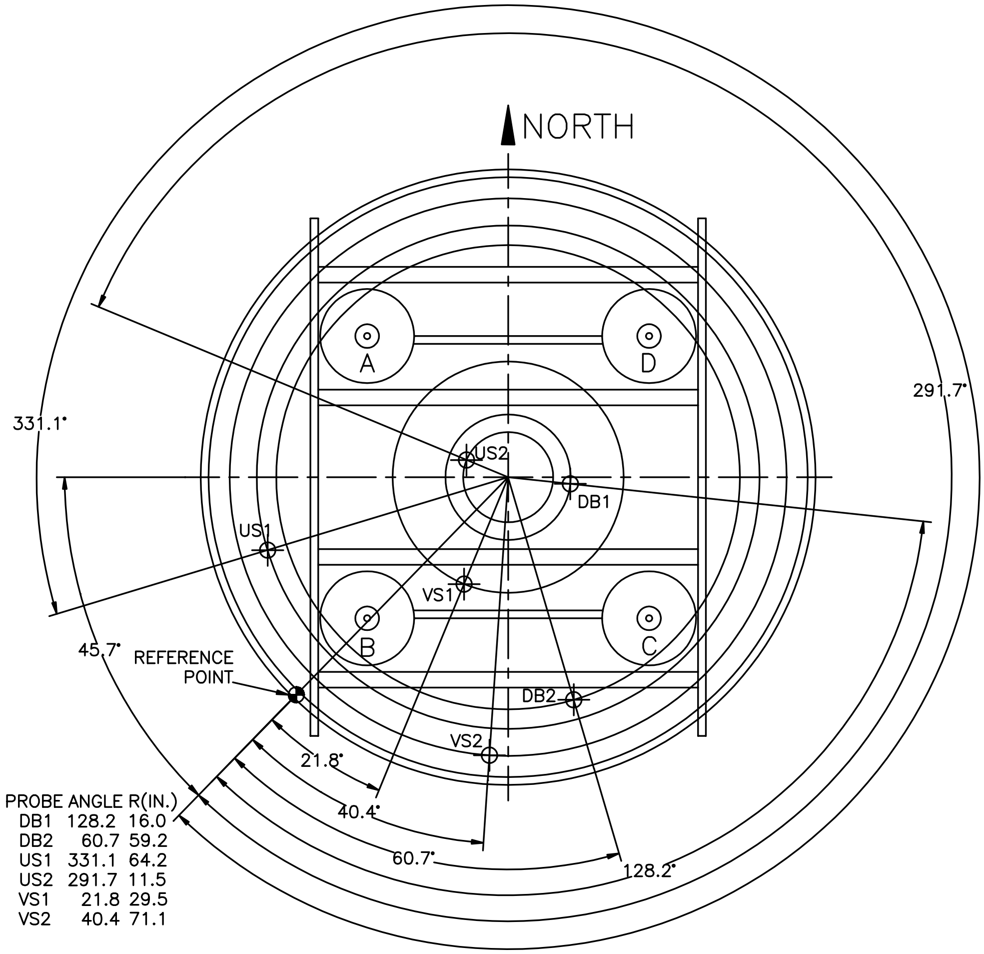

PROBE	ANGLE	R(IN.)
DB1	128.2	16.0
DB2	60.7	59.2
US1	331.1	64.2
US2	291.7	11.5
VS1	21.8	29.5
VS2	40.4	71.1

Figure 4.7. Top View of the 336 4PJM Test Stand Showing Lateral Locations of Drexelbrook (DB) Level Probes, Ultrasonic (US) Level Sensors, and Video Level Scales (VS)

A peristaltic pump was used to feed the H_2O_2 solution through a single tube into the well-mixed cavern near the tank center. The ½-inch OD stainless steel injection tubing was routed up through a bulkhead fitting in the tank drain (at the lateral center of the tank) and ended about 8 inches (20.3 cm) above the bottom of the tank floor. The rate of H_2O_2 injection was measured by monitoring the change in mass of the H_2O_2 supply jugs, which were stationed on a platform scale.

Table 4.9 lists the instrumentation and process-control software that are used with the 336 4PJM test stand. The lateral locations of the sensors are shown in Figures 4.7 and 4.9. The Drexelbrook level probes for the tank level were mounted within the operating range of the tank level. The ultrasonic level sensors were mounted nominally 20 inches (0.5 m) above the simulant surface. Slurry surface height observations for PJM level probes, tank level sensors, and manual measurements were measured as the distance down from the top of the tank rim at the reference point shown in Figure 4.9.

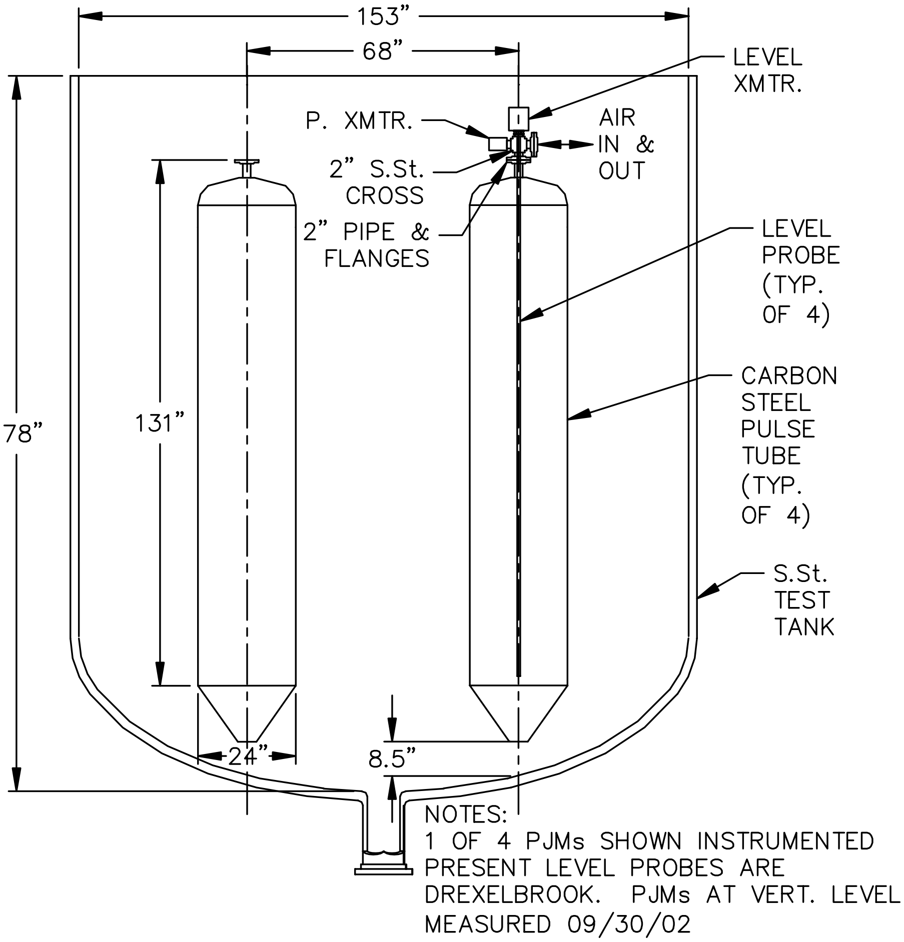

Figure 4.8. Side View Schematic of the 336 4PJM Test Stand Showing Nominal Dimensions

Table 4.9. Instrumentation in the 336 4PJM System

Parameter	Equipment Name/Model	Manufacturer
Process Control & Data Collection	DASYLab, version 7.0	DASYTEC USA (Bedford, NH)
Fluid Level within the PJMs	Universal Lite level transmitter	Ametek Drexelbrook (Horsham, PA)
Pressure within the PJMs	DPG100 pressure transducer	Cecomp Electronics (Libertyville, IL)
Fluid Level within the Tank	UCL-200 ultrasonic liquid level sensor	Gems Sensors, Inc. (Plainville, CT)
Fluid Level within the Tank	Universal II level transmitter	Ametek Drexelbrook (Horsham, PA)
Temperature of the fluid and the ambient air	Type K thermocouple	Omega Engineering, Inc. (Stamford, CT)

Video cameras inserted into camera wells tracked the elevation of the simulant/air interface during testing. Camera well locations are shown in Figure 4.9. To record the interface elevation, a small video camera was moved up and down in the camera well and the images recorded. Two metal measuring tapes were affixed to rigid support rods and submerged vertically into the simulant next to specific camera wells (lateral locations shown in Figures 4.7 and 4.9 as “video scales” VS1 and VS2) so the video cameras could record the elevation of the simulant surface on the metal tapes when the tank surface level was at a minimum elevation (i.e., during the PJM suction phase).

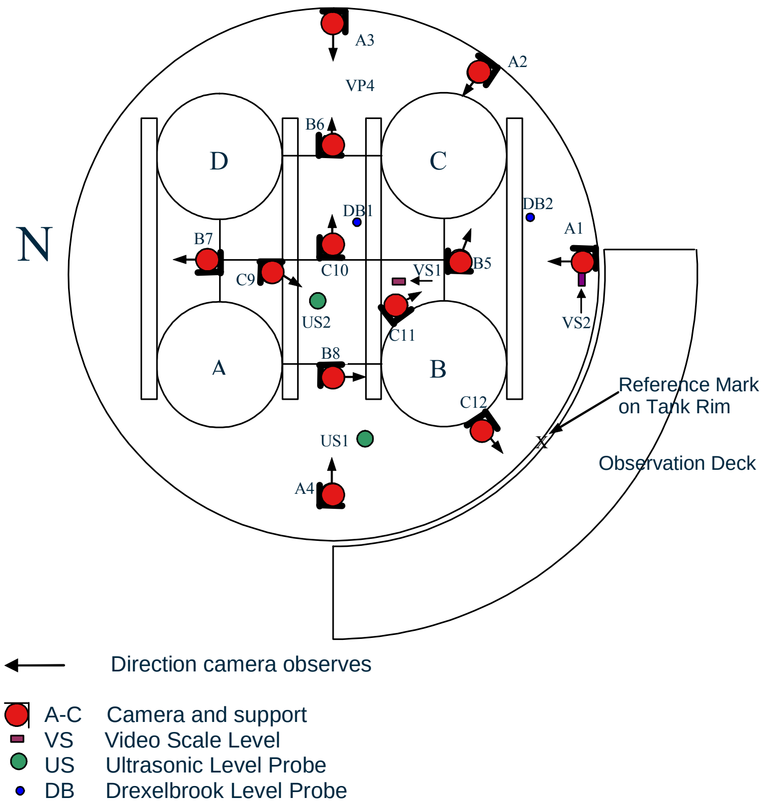

Figure 4.9. Plan View of the Instrument Locations for the 336 Building 4PJM Test Stand

4.3.5 SRNL 4PJM Test Stand

The 4PJM test stand operated by SRNL is described by Wilson et al. (2004). A brief description is included here for convenience. Wilson et al. (2004) do not provide tolerances on dimensions, which could be expected to range from 0.125 to 0.5 inch, depending on the item being measured.

The SRNL 4PJM test stand is a linearly scaled version of the 336 4PJM test stand and thus has the same arrangement of four PJMs within a round-bottomed tank. Nominal dimensions of the SRNL 4PJM tank and PJMs are listed in Table 4.10. Figures 4.10 and 4.11 show plan and section view diagrams, respectively, of the SRNL 4PJM system. The PJMs are situated in a square around the center of the tank, along a PCD of 10.64 inches (27.0 cm). In the gas-holdup and release tests, the nominal simulant fill height in the SNRL 4PJM system was ~0.9 H/D, corresponding to ~14 gallons (~53 L). The nozzles are approximately 2 inches (5 cm) above the tank floor at the PJM lateral location.

Table 4.10. Approximate Dimensions of the SNRL 4PJM System

Item	Approximate Diameter	Approximate Length/Height	Other
SRNL 4PJM Tank	17.25 in. (43.8 cm) ID	43.0 in. (109 cm)	Diameter corresponds to a scale of about 1:8.87 Tank walls are clear acrylic; bottom is a ~2:1 elliptical dish
PJM Tube	2.625 in. (6.67 cm) ID	48 ± 1 in. (120 ± 2 cm)	2½-inch schedule 10 stainless steel pipe; ID is a measured value
PJM Nozzle	0.445 in. (1.13 cm) ID	N/A	Discharges vertically downward

Hydrogen peroxide solution was injected into the simulant at a location about 1 inch (2.54 cm) above the center of the tank bottom. Wilson et al. (2004) report the duration of the H_2O_2 injection and the total mass of 30 wt% H_2O_2 solution that was injected for each test.

Table 4.11 lists the instrumentation and process control software used with the SNRL 4PJM test stand. The lateral location of the thermocouple is shown in Figure 4.10. The thermocouple is on the north side of the test tank, 11¾ inches from bottom of the tank and ½ inch from the inside wall. The DACS used only the level probe in the north PJM (PJM1) to control the system pulse cycle, although data for all four PJM level probes were logged.

There were four observer stations around the SNRL 4PJM test stand at nominally the northeast, northwest, southeast, and southwest sides of the tank. At each observer station, an adhesive-backed flexible measuring tape ($^1/_{16}{}^{th}$ inch graduations) was affixed vertically to the outer wall of the tank. The affixed tapes enabled tank level measurements over the span of 6.25 inches (at the rim of the stainless steel dish) to 36 inches. Wilson et al. (2004) do not provide specifics, but it is presumed that the vertical placement of the measuring tapes was arbitrary, and the tapes were all aligned at 6.25 inches. Fluid height in the tank is reported by Wilson et al. (2004) as the average of the observations at all four observer stations. The primary measurements of fluid surface height in the SRNL 4PJM tank were the manual observations taken with the system quiescent and the PJMs vented to atmosphere (which differs from the majority of measurements in the tests conducted by PNWD in the other test stands). For some longer-term events (e.g., overnight gas holdup before a gas-release test), the PJM level probes were used to log the fluid level in the tank (with the level probe output scaled to match the affixed tape scale).

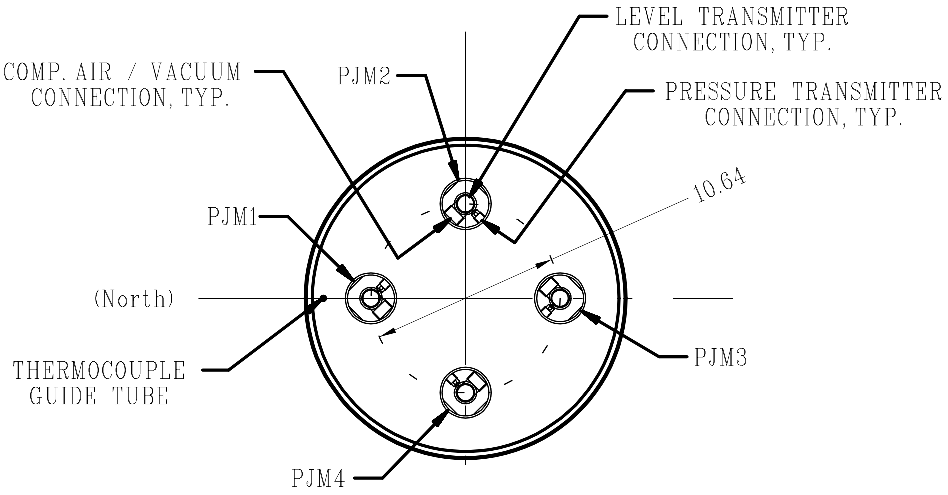

Figure 4.10. Top View of the SNRL 4PJM Test Stand Showing Lateral Locations

4.3.6 CBT Test Stand

The CBT test stand is a large-scale tank used for testing gas release from air spargers alone. Nominal dimensions of the CBT tank and the air sparging tubes are listed in Table 4.12. Figures 4.12 and 4.13 show plan and section view diagrams, respectively, of the CBT system. The air sparging tubes are situated in a diamond-in-a-square pattern with an additional tube at the center of the tank; lateral positions are shown in Figure 4.12. The air sparging tubes are approximately 6 inches (15.2 cm) above the tank floor. In the gas-holdup and release tests, the nominal simulant fill height in the CBT system was nominally two-thirds of the full-scale system.

Because of the minimal equipment in the CBT, H_2O_2 was added to the slurry in a sequence of steps. After an initial mass reading of quiescent slurry in the CBT, the fluid was transferred to the 336 4PJM system, where H_2O_2 was added to the slurry and thoroughly mixed with the PJMs in that test stand. After mixing, the amended slurry was transferred back to the CBT and weighed to account for any fluid loss during transfers. The slurry was allowed to stand until all or most of the H_2O_2 had decomposed, providing a starting point for CBT gas-release tests. After completion of a CBT gas-release test, the slurry was transferred to the 336 4PJM test stand and back again for thorough degassing (via PJM overblow).

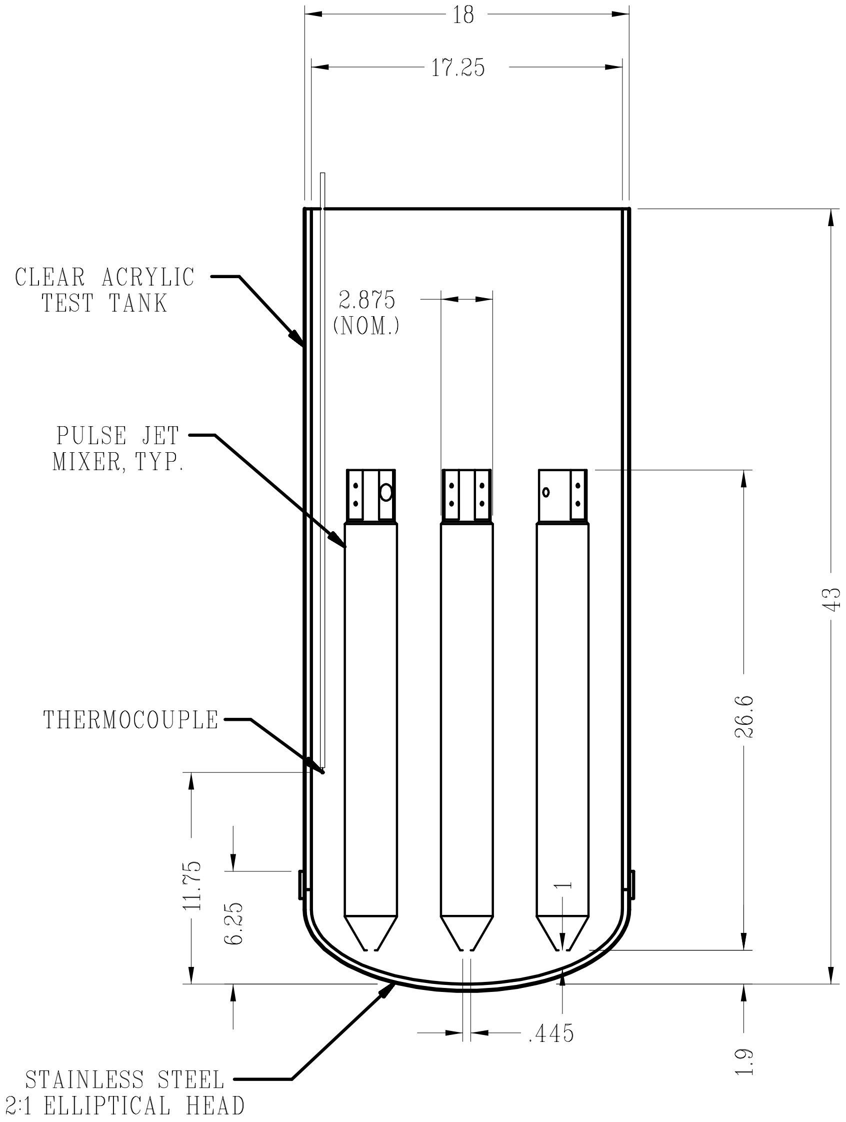

Figure 4.11. Side View of the SRNL 4PJM Test Stand Showing Nominal Dimensions

Table 4.11. Instrumentation in the SNRL 4PJM System

Parameter	Equipment Name/Model	Manufacturer
Process control & data collection	LabView	National Instruments (Austin, TX)
Sensor/Control Hardware Interface	PCI bus card Analog input board NI 6011E (PCI-MIO-16XE-50)	National Instruments (Austin, TX)
Sensor/Control Hardware Interface	NI SCXI-1000 input/output chassis	National Instruments (Austin, TX)
Sensor/Control Hardware Interface	Power supply Model 515	Rosemount Analytical (Orrville, OH)
Sensor/Control Hardware Interface	NI SCXI-1303 terminal block and NI SCXI-1102 input module	National Instruments (Austin, TX)
Sensor/Control Hardware Interface	NI SCXI-1161 relay switching output module	National Instruments (Austin, TX)
Fluid level within the PJMs	Universal II level transmitter (with manufacturer's modification 91-133)	Ametek Drexelbrook (Horsham, PA)
Pressure within the PJMs	Pressure Transducer Model 3051CD	Rosemount (Chanhassen, MN)
Temperature of the fluid and ambient air	Type E thermocouple	Omega Engineering, Inc. (Stamford, CT)

Table 4.12. Approximate Dimensions of the CBT System

Item	Approximate Diameter	Approximate Length/Height	Other
CBT	152 in. (386 cm) ID	166.0 in. (421.6 cm)	Conical tank bottom has a nominal height of 70 in. (177.8 cm)
"A" Air Sparger Tubes	0.824 in. (2.1 cm) ID	99.7 in. (253.2 cm)	¾-in. schedule 40 steel pipe Length is measured from tank rim downward
"B" Air Sparger Tubes	0.824 in. (2.1 cm) ID	119.4 in. (303.3 cm)	¾-in. schedule 40 steel pipe Length is measured from tank rim downward
"C" Air Sparger Tubes	0.824 in. (2.1 cm) ID	160.0 in. (406.4 cm)	¾-in. schedule 40 steel pipe Length is measured from tank rim downward

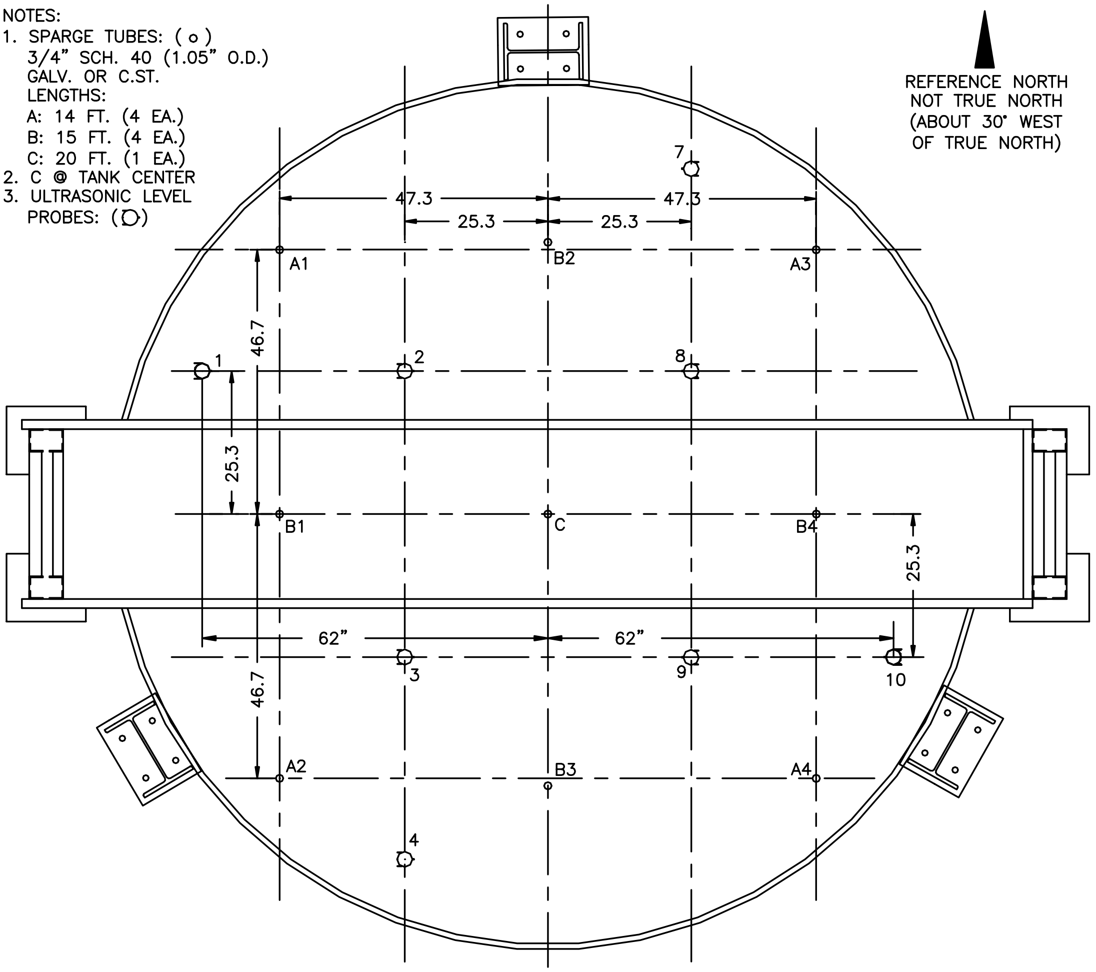

Figure 4.12. Top View of the CBT Test Stand Showing Lateral Locations (all dimensions in inches)

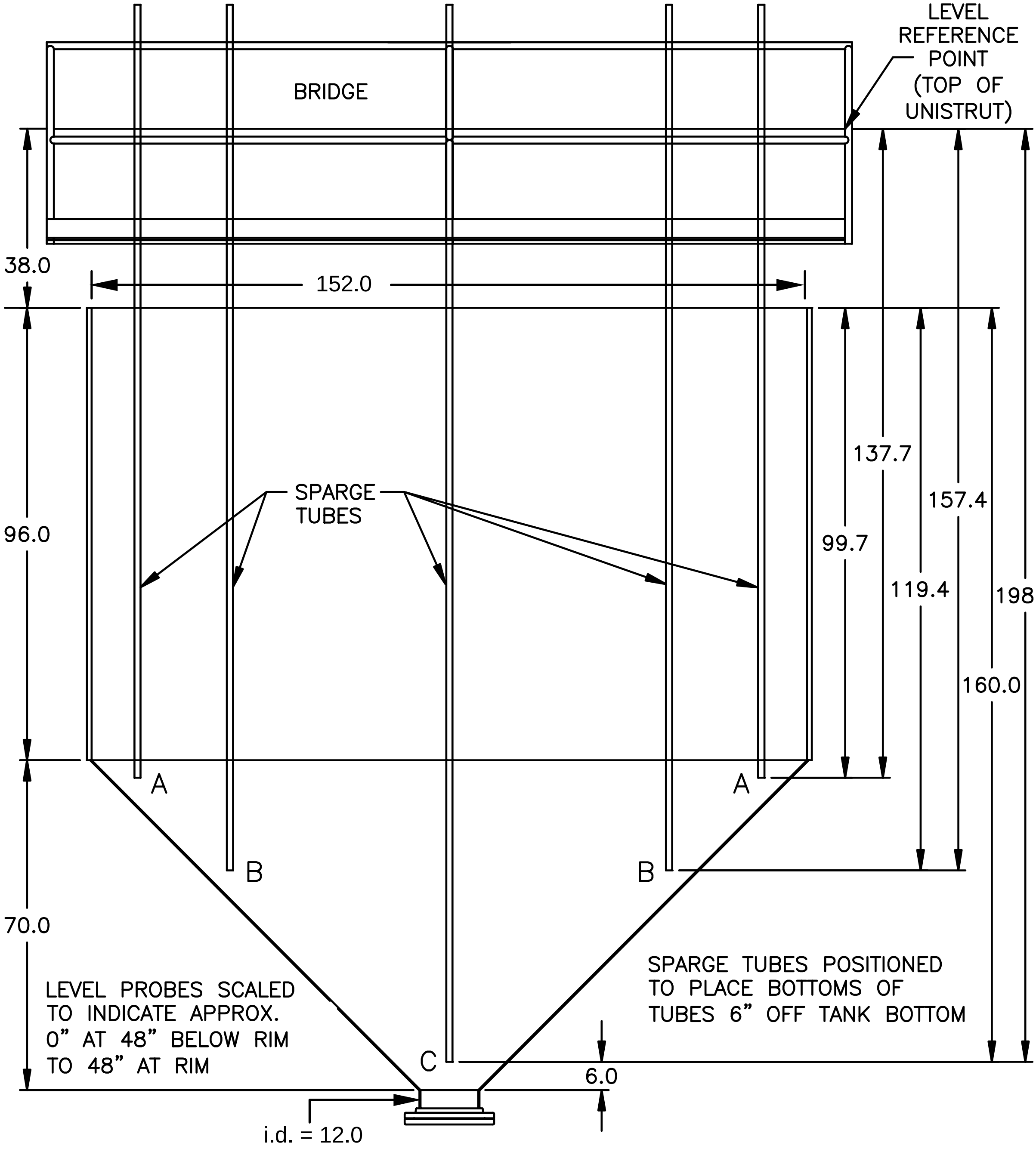

Figure 4.13. Side View of the CBT Test Stand Showing Nominal Dimensions (all dimensions in inches)

Table 4.13 lists the instrumentation and process control software used with the CBT test stand. The lateral locations of the sensors are shown in Figure 4.12. Slurry surface height observations for tank level sensors were measured on a scale of 0 equals 48 inches down from the top of the tank rim, and the top of the tank rim equals a height of 48 inches. Manual height observations for the slurry surface were measured as the distance down from the top of the middle unistrut beam on the bridge above the tank (Figure 4.12). The manual height measurements are the primary values used for determining the volume of gas entrained in the slurry.

Table 4.13. Instrumentation in the CBT System

Parameter	Equipment Name/Model	Manufacturer
Process control & data collection	DASYLab, version 7.0	DASYTEC USA (Bedford, NH)
Fluid level within the tank (information only)	UCL-200 ultrasonic liquid level sensor	Gems Sensors, Inc. (Plainville, CT)
Temperature of the fluid	Type K thermocouple	Omega Engineering, Inc. (Stamford, CT)
Temperature of air sparger air	Type J thermometers	Omega Engineering, Inc. (Stamford, CT)
Air flow rates for air spargers	VFC-122 manometers	Dwyer (Michigan City, IN)
Sparger air pressure	Air pressure gauge	Ashcroft (Stratford, CT)

4.4 Gas-Retention and Release Data Reduction

The amount of gas in the simulant was assessed by tracking the change in surface height of the simulant in the tank during the testing, applying independently developed correlations to calculate the simulant volume from the surface height and calculating the gas-volume fraction as the change in simulant volume relative to the volume at a reference “zero-gas” state.

As discussed in previous sections, changes in tank simulant level over time were tracked using one or more sensors for electronic data collection (from one or more level sensors), manual observation, and video recording equipment. The electronic data from the level sensors deployed in each of the vessels (Section 4.3) were used as the primary data in calculating gas-volume fractions (except the SRNL test stand, which primarily used manual observations). For tanks with multiple sensors, the results are presented as the average of the calculated gas-fraction values.

The reduction of logged data to gas-fraction results consists of three major steps: extraction of tank simulant level (height) values from the logged data, conversion of height values to volume, and calculation of the gas fractions.

Two approaches were used when extracting height values from the DACS logged data, depending on whether the system was operating or quiescent. During operations, the minimum tank simulant level for each cycle (when PJMs are full) is extracted from the logged data. When the system is quiescent (and the PJMs are full), an average over a time period of one cycle is used for the height value. Thus, the extracted height data consist of one minimum tank fluid level per pulse cycle where the cycle length depends on the test stand involved.

The extracted height values are converted to total tank volume using correlations that were derived independently (see Appendix A). The correlation of tank liquid surface level height to total tank volume under PJM-full conditions for each test stand was obtained from a summation of the volume within the

PJMs above the liquid surface height (from PJM geometry/position) plus the volume below the liquid surface height (from a static correlation). The tank-specific level-volume correlation under static conditions (PJMs vented to atmosphere) was determined empirically by adding a known mass of water in steps and measuring the resulting liquid surface level height. Occasionally, measurements of height were taken under static conditions when the static correlation alone determines the total tank volume.

The gas fraction is calculated as the change in simulant volume relative to the volume at a reference “zero-gas” state, as shown in Eq. 2.23 (Section 2.2 discusses calculation of gas-fraction further).

4.4.1 Summary of Height/Tank Volume Correlations

Calculations to obtain the height/tank volume correlations were generally performed in three stages. First, linear least-squares regression was applied to the height/tank volume data for water under static conditions to obtain a linear curve fit (static correlation). Second, the geometry/dimensions and vertical position of the PJMs were used to get a piece-by-piece description of the volume within a PJM assembly. These two volume calculations were combined and curve-fit to obtain equations describing the height/tank volume relationship when the PJMs are full. This relationship is not linear (over the whole length of the PJM assembly) because of changes in diameter of the various parts of the PJM. However, large segments of the curve can be simplified to a linear or cubic curve fit equation. The manner in which the APEL 4PJM system was operated resulted in a sufficiently simple system and enough data to calculate the total tank volume (with the PJMs full) directly rather than obtaining a correlation through regression. Table 4.14 lists static correlations and Table 4.15 the correlations for tank volume when the PJMs are full. Because the SRNL test-stand-height observations were taken under static conditions, there is not a correlation for the case where PJMs are full. The CBT test stand did not have PJMs, so it also does not have a PJM full correlation. For a more detailed discussion of these correlations, see Appendix A.

For some gas-retention and release tests in the LS tank, the minimum tank fluid surface-level height intersected both the PJM tube and shoulder as the volume changed over time. Linear regressions were conducted to determine whether the applicable range for the correlation in the LS PJM shoulder region could be extended 1.6 cm into the PJM tube part, resulting in a single equation that could be used for a test. Based on the R^2 statistic, the curve fit was deemed acceptable; hence, the overlap in the valid range of Eq. 4.9 and 4.10.

For the APEL 4PJM tank, the PJM level probe data were electronically logged at 8 cm less than the 0° station affixed tape reading. This 8-cm offset was implemented for convenience during operations to prevent driving the fluid level in the PJMs down too far. Before calculating the tank volume with Eq. 4.12, the 8 cm must be added back to the PJM level probe data, H'_{pjm}, to obtain the PJM level probe data on the 0° station affixed tape scale, H_{pjm}.

Table 4.14. Height/Volume Correlations for Test Stands under Static Conditions

Tank	**Height/Volume Correlation under Static PJM Conditions** Applicable above top of tank dish section. V_{static} = Tank volume under static conditions (L) $H_{surface}$ = Tank fluid surface level height on the scale of: UFP – affixed tape height on south side (cm) LS – affixed tape height on south side (cm) APEL 4PJM – affixed tape height at 0° station (cm) 336 4PJM – distance down from top of tank rim (in.) SRNL 4PJM affixed tape height (in.) CBT – distance down from top of tank rim (in.)	**R^2**	**Eq. #**
UFP	$V_{static} = 5.67571 \times H_{surface} + 144.37745$	0.999980	(4.1)
LS	$V_{static} = 24.04534 \times H_{surface} + 416.71567$	0.999969	(4.2)
APEL 4PJM	$V_{static} = 5.72254 \times H_{surface} + 45.99564$	0.999961	(4.3)
336 4PJM	$V_{static} = -296.26055 \times H_{surface} + 49485.23$	0.999987	(4.4)
SRNL 4PJM	$V_{static} = 3.70677 \times H_{surface} - 5.10251$	0.999995	(4.5)
CBT	$V_{static} = -295.82382 \times H_{surface} + 47309.22$	0.999987	(4.6)

Table 4.15. Height/Volume Correlations for Height Observations Taken when PJMs Are Full

Tank	**Applicable Height Range**	**Height/Volume Correlation under Full PJM Conditions** V_{tank} = Tank Volume under PJM Full Conditions (L) $H_{surface}$ = Tank Fluid Surface Level Height on the Scale of: UFP affixed tape height on south side (cm) LS affixed tape height on south side (cm) APEL 4PJM affixed tape height at 0° station (cm) 336 4PJM distance down from top of tank rim (in.)	$\mathbf{R^2}$	**Eq. #**
UFP	11.5 cm to 101.0 cm	$V_{tank} = 4.94161 \times H_{surface} + 218.81407$	0.999998	(4.7)
	101.0 cm to 196.5 cm	$V_{tank} = 5.66061 \times H_{surface} + 147.23645$	1.000000	(4.8)
LS	52.6 cm to 102.6 cm	$V_{tank} = 18.23469 \times H_{surface} + 1071.5948$	1.000000	(4.9)
	101.0 cm to 117.6 cm	$V_{tank} = 0.0096806 \times (H_{surface})^3 - 2.98630 \times (H_{surface})^2 + 325.32031 \times H_{surface} - 9454.7612$	1.000000	(4.10)
	117.6 cm to 201.0 cm	$V_{tank} = 24.01227 \times H_{surface} + 423.1228$	1.000000	(4.11)
APEL 4PJM	6.0 cm (just above top of tank dish) to 110.0 cm (within PJM tube section)	$V_{tank} = V_{static} + N_{pjm} \cdot \left(\pi \cdot r_{pjm}^2 - \pi \cdot r_{probe}^2\right) \cdot \left(H_{pjm} - H_{surface}\right)$	Not Applicable	(4.12)
336 4PJM	0.0 in. to 20.5 in.	$V_{tank} = -296.05543 \times H_{surface} + 49509.95$	1.000000	(4.13)
	20.5 in. to 26.25 in.	$V_{tank} = -0.274568 \times (H_{surface})^3 + 21.62222 \times (H_{surface})^2 - 834.22346 \times H_{surface} + 53821.27$	1.000000	(4.14)
	26.25 in. to 147.75 in.	$V_{tank} = -266.64017 \times H_{surface} + 48854.91$	1.000000	(4.15)

5.0 Gas-Holdup Tests

Reviewed data are available from gas-holdup tests in the UFP and LS PJM scaled prototype vessels performed in the APEL during February 2004, for tests in the scaled 4PJM test stands in the 336 Building (approximately one-half scale relative to the plant) and APEL (1:4.5 scale relative to 336), and for one small-scale (1:9 scale relative to 336) test performed at SRNL. Kaolin-bentonite clay simulant was used in these gas-holdup experiments. Decomposition of H_2O_2 into O_2 and water supplied the gas generation.

The tests were planned to achieve equilibrium between gas generation and release. A constant gas-generation rate was provided by injecting a 30 wt% H_2O_2 solution at a steady rate with the mixing system operating. The accumulating gas volume in the simulant was calculated from the increasing simulant surface level measured at the minimum point in each PJM cycle (PJMs full before starting the drive cycle), assuming the initial level represented a totally gas-free state. (Simulant volume relation to the measured surface level in each test vessel is discussed in Section 4.4 and Appendix A.) After H_2O_2 injection started, the level rose with accumulating gas until it achieved a constant level in which the gas-release rate closely matched the gas-generation rate. The gas holdup is defined as the average gas-volume fraction in the simulant at this steady state. The holdup was computed by averaging the gas-volume fractions calculated from level data over the last 20 PJM cycles of H_2O_2 injection at each rate. This number of cycles occupies from 20 minutes for the 336 4PJM tests to 4.4 minutes in the 1:4.5 scale APEL 4PJM tests.[a]

The steady-state gas holdup is defined as a function of the gas-generation rate and the U_R/H parameter in Eq. (2.14). The volumetric rate of gas generation at steady state is calculated from the rate of H_2O_2 addition and the chemistry of the decomposition reaction using the Ideal gas law and is expressed by Eq. (2.32). Substituting Eq. (2.32) into Eq. (2.14), converting to the *in situ* pressure, and rearranging gives an expression that allows the quantity U_R/H to be calculated from gas-holdup test data:

$$\left(\frac{U_R}{H}\right) = \frac{g_{v,O2}}{\alpha_{SS}} = \frac{1}{\alpha_{SS}} \frac{x_p \rho_{ps} Q_{ps}}{2M_p} \frac{RT}{pV_s} \tag{5.1}$$

The parameter U_R/H controls depletion or accumulation of gas. The inverse, H/U_R, represents the average bubble transit time, which is the time constant for the exponential gas-release model expressed by Eq. (2.12). In a steady-state holdup test, it is a measure of the effectiveness of the mixing system in mobilizing the simulant, allowing bubbles to rise and release. In the pulsed PJM mixing system, the simulant is fully fluid for only some fraction of time in some fraction of the total volume. Therefore, the calculated U_R/H represents the effective time- and volume-averaged slurry mobilization that actually causes gas release. The larger the average U_R/H, or the smaller the average bubble transit time, the more effective the mixing system is at gas release.

(a) This method was not applicable to the SRNL 4PJM test where measurements were made periodically by pausing the PJMs. Only three data points separated by 4 and 5 minutes were obtained after approximate steady state was achieved.

5.1 Test Summary

Table 5.1 summarizes the conditions defining the gas-holdup tests presented in this section. The details of the PJM, sparger, and recirculation systems are given in Section 4. There were important differences in the various mixing systems that appeared to influence the holdup. In LS test sequence 14, three of the seven outer PJM nozzles were canted upward at 135° and four downward at 45°, while all seven outer PJM nozzles were set at 45° downward in sequence 15A. At the same time, LS sequence 14 operated four of eight air spargers without recirculation, while LS sequence 15A used recirculation through four nozzles instead of spargers. Both UFP tests used the same PJM system, but sequence 5 used single-nozzle recirculation, while sequence 6 had a single sparger. Sequence 6 also used a deeper simulant. All 4PJM tests in 336 (approximately half scale), APEL (1:4.5 scale relative to 336), and SRNL (1:9 scale relative to 336) used only their four PJMs without sparging or recirculation.

The target PJM peak average nozzle velocity was 12 m/s in the LS and UFP tests and 10.5 m/s in the 4PJM system tests. However, based on the rate of change of measured simulant level, the actual peak average nozzle velocities during the drive cycle were significantly different than the target values.[(a)] As listed in Table 5.1, the LS and UFP systems actually achieved higher peak average drive velocities, from 16 to 17 m/s, while the APEL and 336 4PJM systems produced generally lower peak average velocities ranging from 8.3 to 10.5 m/s. The PJM cycle times ranged from 0.11 minutes in the SRNL 4PJM system to 1 minute in the 336 4PJM vessel in proportion to their geometric scale. The actual duration of the drive portion was 7 to 15% of the cycle time.

The simulant in all the LS and UFP tests was relatively stiff (~36 Pa Bingham yield stress) while the large-scale 336 4PJM test on 12/13/03 and the APEL 4PJM test on 12/15/03 used the stiffest simulant (40 to 44 Pa Bingham yield stress). The other three APEL 4PJM tests, the SRNL 4PJM test on 12/13/03, and the 336 4PJM test on 7/22/04 used relatively weaker simulants with yield stress ranging from 7 to 20 Pa and consistency from 9 to 22 cP.

All tests used volumetric O_2 generation rates in one or two of four nominal ranges: a very low rate of 0.8 mL of O_2 gas at average bubble hydrostatic pressure per liter of gas-free simulant per minute, a low rate of 1.4–1.7 mL/L-min, a medium rate of 3.4–4.2 mL/L-min, and a high rate of 7.2–8.0 mL/L-min. A gas-generation rate of 1 mL/L-min is approximately equivalent to a 0.1 vol%/min expansion rate if all the gas were retained.

(a) PJM drive cycle nomenclature and nozzle velocity calculation methods are described in Section 3.2.1 of WTP-RPT-113 Rev. A (Bamberger et al. 2004).

Table 5.1. Gas-Holdup Test Description

Test/Date	Simulant Depth & Volume	Rheology		PJM Layout and Drive Parameters[(a)]	Spargers Operating	Recirc. Nozzles	H_2O_2 (mL/min) [O_2 (mL/L-min)]
		τ (Pa)	κ (cP)				
LS Seq. 14, Run 3 2/6/04	H = 1.31 m H/D = 0.74 V_s = 2,862 L	36	27	Cluster 7 (3-135° and 4-45°) around 1 (0°) @ 17 m/s, t_C = 0.75 min, t_D/t_C = 0.093	4 (#1, 3, 5, 7) @ ~3 acfm	None	42.7 (1.6) 98 (3.7)
LS Seq. 15A, Run 3 2/14/04	H = 1.31 m H/D = 0.74 V_s = 2,935 L	35	26	Cluster 7 (all-45°) around 1 (0°) @ 16 m/s, t_C = 0.75 min, t_D/t_C = 0.11	None	4 @ ~454 L/min total (~6.5 min V_s exch. time)	43.9 (1.6) 91.5 (3.4)
UFP Seq. 5, Run 3 2/12/04	H = 1.20 m H/D = 1.4 V_s = 633 L	36	19	Trifoil (3-45°) around 1 (0°) @ 16 m/s, t_C = 0.45 min, t_D/t_C = 0.073	None	1 @ ~340 L/min (~1.9 min V_s exch. time)	24.4 (4.2)
UFP Seq. 6, Run 3 2/13/04	H = 1.55 m H/D = 1.8 V_s = 833 L	36	20	Trifoil (3-45°) around 1 (0°) @ 16 m/s, t_C = 0.45 min, t_D/t_C = 0.073	One center @ ~3 acfm	None	28.6 (3.7)
336 4PJM 12/16/03	H = 3.45 m H/D = 0.9 V_s = 37,230 L	44	23	4 (0°) @ 8.5 m/s, t_C = 1.0 min, t_D/t_C = 0.15	None	None	530 (1.4)
336 4PJM 7/22/04	H = 3.45 m H/D = 0.9 V_s = 37,700 L	20	18	4 (0°) @ 8.3 m/s, t_C = 1.0 min, t_D/t_C = 0.16			292 (0.82) *618 (1.7)*[(b)]
APEL 4PJM 12/15/03	H = 0.77 m H/D = 0.9 V_s = 379 L	40	21	4 (0°) @ 10.3 m/s, t_C = 0.22 min, t_D/t_C =0.11			12.6 (3.7)
APEL 4PJM 1/27/04	H = 0.77 m H/D = 0.9 V_s = 375 L	13	22	4 (0°) @ 10.4 m/s, t_C = 0.22 min, t_D/t_C = 0.11			12.5 (3.7)
APEL 4PJM 2/19/04	H = 0.77 m H/D = 0.9 V_s = 393 L	7	9	4 (0°) @ 9.9 m/s, t_C = 0.22 min, t_D/t_C = 0.12			12.8 (3.6) *26.4 (8.0)* [(b)]
APEL 4PJM 2/25/04	H = 0.77 m H/D = 0.9 V_s = 385 L	18	14	4 (0°) @ 10.5 m/s, t_C = 0.22 min, t_D/t_C = 0.11			12.3 (3.6) 24.9 (7.2)
SRNL 4PJM 12/13/03 R2A	H = 0.4 m H/D = 0.9 V_s = 54 L	16	19	4 (0°) @ 8.7 m/s, t_C = 0.11 min, t_D/t_C = 0.18			1.9 (4.1)

(a) The peak-average PJM nozzle velocities and associated drive time-to-cycle time ratio are listed.
(b) This result was not used because the actual H_2O_2 injection rate is inconsistent with the measured holdup.

5.2 Gas-Retention Test Results

The variations in the mixing systems, gas-generation rates, and the simulant rheology all affected the holdup to various degrees. Figure 5.1 shows the retained gas-volume fraction history for LS test sequence 15A, run 3 as an example of the conduct of the test and of the presentation of results for subsequent tests. Hydrogen peroxide injection corresponding to the low gas-generation rate began at time zero after the mixing system (eight PJMs and recirculation in this case) had already homogenized the simulant. There was an approximately 10-minute delay in gas accumulation as the dissolved O_2 generated in solution became sufficiently concentrated to begin forming and growing bubbles.

Steady-state equilibrium between gas generation and release at a holdup of about 0.9 vol% occurred after about 50 minutes in this test. Doubling the H_2O_2 solution injection rate at 65 minutes gave a holdup of about 1.5 vol% after 120 minutes. Hydrogen peroxide injection ceased at 156 minutes. The steady-state bubble transit times (inverse of U_R/H from Eq. 5.1) for the two gas-generation rates are 5.7 and 4.5 minutes, respectively. The holdup and standard deviation, gas-generation rate, and transit time for each test are summarized in Table 5.2.

A gas-release test was scheduled to follow the run 3 holdup test. Accordingly, after inadvertently overblowing the PJMs, which mixed the remaining H_2O_2 solution in the simulant, the mixing system was shut down at 164 minutes to let the retained gas build up to the target of 5 to 6 vol%. The gas-accumulation period represented in Figure 5.1 is not shown on plots for other tests.

Table 5.2. Gas-Holdup Results Summary

Test	Generation Rate (mL/L-min)	Holdup (vol%)$^{(a)}$	Bubble Transit Time (H/U_R) (min)	Note
LS Seq. 14, Run 3	1.6 3.7	0.6 ± 0.1 1.2 ± 0.07	3.7 3.2	135˚ PJM nozzles, spargers
LS Seq. 15A, Run 3$^{(b)}$	1.6 3.4	0.8 ± 0.06 1.4 ± 0.1	4.9 4.2	45˚ PJM nozzles, recirculation
UFP Seq. 5, Run 3	4.2	3.4 ± 0.3	8.5	H/D = 1.4, recirculation
UFP Seq. 6, Run 3	3.7	3.5 ± 0.09	9.8	H/D = 1.8, sparger
336 4PJM 12/16/03	1.4	3.7 ± 0.05	26.6	Stiff clay
336 4PJM 7/22/04	0.8 *1.7*	1.6 ± 0.07 *2.0*	20.1 *12*	Nominal clay, results at 1.7 mL/L-min suspect
APEL 4PJM 12/15/03	3.7	1.6 ± 0.2	4.4	Stiff clay. Gas retention increased with H_2O_2 off.
APEL 4PJM 1/27/04	3.7	0.9 ± 0.1	2.3	Weak clay. Holdup varies.
APEL 4PJM 2/19/04	3.6 *8.0*	1.1 ± 0.04 *~0.8*	3.0 ~1	Very weak clay. Holdup unchanged at 8 mL/L-min.
APEL 4PJM 2/25/04$^{(c)}$	3.6 7.2	0.9 ± 0.1 1.3 ± 0.07	2.6 1.9	Weak clay
SRNL 4PJM 12/13/03	4.1	1.3 ± 0.01	3.2	Atypical approach to steady state.

(a) Uncertainties are ± one standard deviation.
(b) Gas fractions corrected down 0.12 vol% to start at zero.
(c) Gas fractions corrected down 1.01 vol% to start at zero.

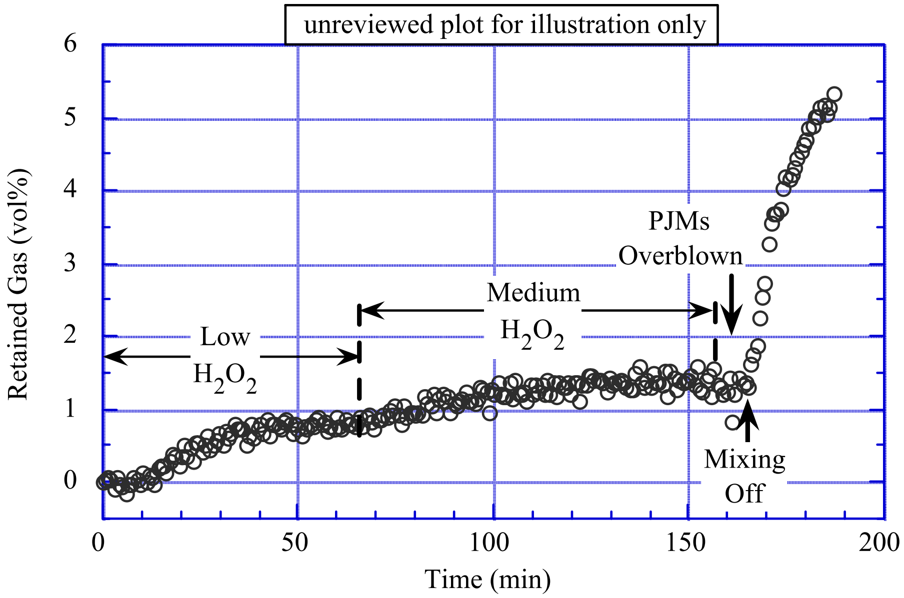

Figure 5.1. Lag Storage Sequence 15A, Run 3 Gas-Retention Test Results

Holdup tests necessarily assume that the initial gas-volume fraction in the simulant is zero. However, due to measurement uncertainties, such as unevenness of the simulant surface, simulant held up inside the PJMs, or simple measurement error, the calculated initial gas-volume fraction may differ enough from zero to warrant a correction. The LS sequence 15A example was one such test. As shown in Figure 5.2, the average gas-volume fraction over the first 10 minutes before the simulant saturated with O_2 and gas began to accumulate was 0.123 vol%. The correction was made by subtracting this average from each calculated gas fraction to bring the initial average back to zero. Only one other holdup test, the APEL 4PJM test on 2/25/04, required correction and was similarly adjusted down by 1.06 vol%.

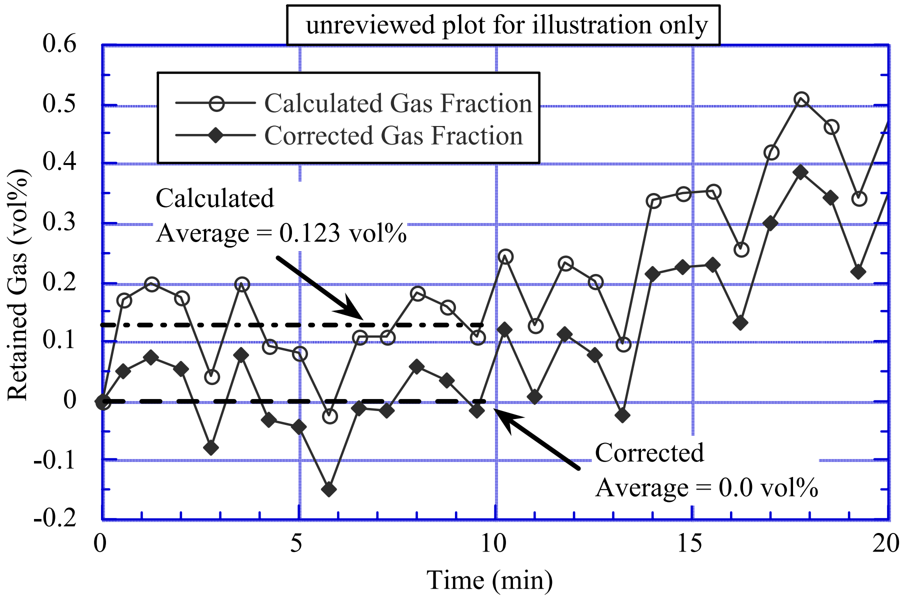

Figure 5.2. Correction for Zero Initial Gas-Volume Fraction (LS Sequence 15A, Run 3)

5.2.1 Scaled Prototype Retention Tests

The retained gas-volume fraction histories for both LS and UFP tests are shown in Figure 5.3. The holdup is much higher in the UFP tests, apparently the result of less efficient slurry mobilization with a corresponding lower gas-release rate. Though all four tests used essentially the same simulant, the calculated bubble transit times in the UFP tests are two to three times that of the LS tests for the same gas-generation rate. While the H/D ratio for the UFP tests is more than double that of the LS tests (1.4 to 1.8 versus 0.74), the absolute simulant depth is essentially equivalent (1.2 to 1.55 m versus 1.3 m). On the other hand, the UFP tests used four PJMs with a single sparger or recirculation nozzle compared with eight PJMs with four spargers or recirculation nozzles in the LS vessel. The slightly higher holdup and greater bubble transit time in UFP sequence 6 relative to sequence 5 is probably more a result of the deeper simulant than a difference in mobilization effectiveness between the single recirculation nozzle and single sparger.

Holdup is also noticeably higher in LS sequence 15A than in sequence 14. Sequence 14 may have lower holdup either because sparging is more effective than recirculation or because the 135° PJM nozzles are more effective than 45° PJM nozzles. The gas-release test results discussed in Section 6 imply that the PJM nozzle angles are the dominant influence.

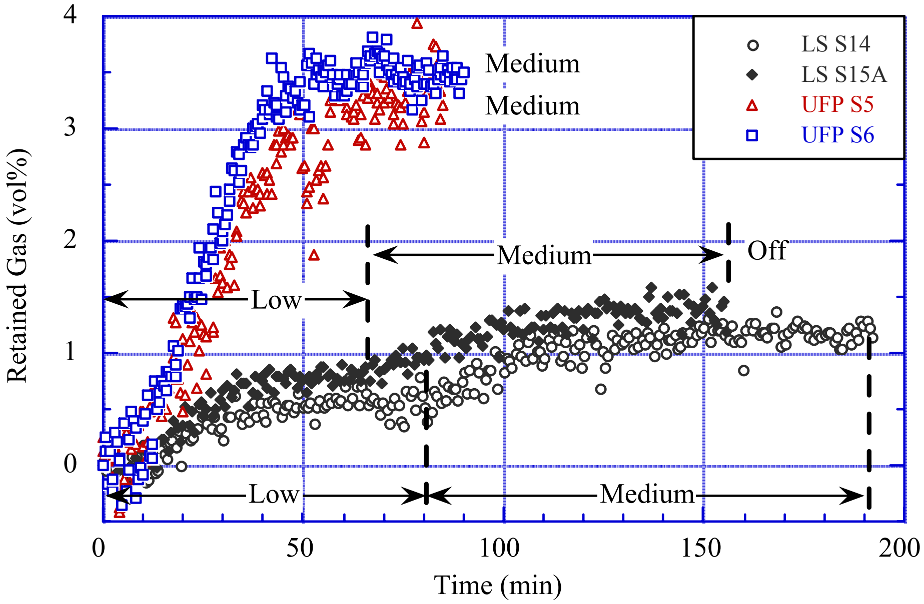

Figure 5.3. LS and UFP Prototype Gas-Retention Test Results

5.2.2 4PJM Retention Tests

The holdup test results in 4PJM systems in the 336 Building, APEL, and SRNL are compared in Figures 5.4 and 5.5. Figure 5.4 compares results of the 12-16-03 test in 336, the 12-15-03 test in APEL, and the 12-13-03 experiment at SRNL. To produce the same holdup according to Eq. (2.14), the gas-generation rates should be inversely proportional to the length scale of the three test stands. Thus the APEL and SRNL tests should have 4.5 and 9 times the gas-generation rates of the 336 tests, respectively.

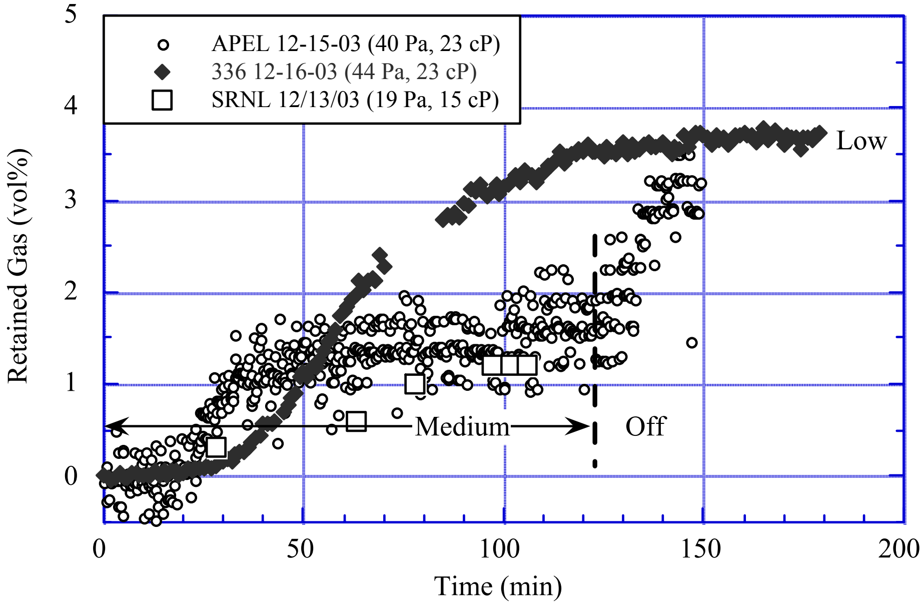

Figure 5.4. APEL (12-15-03), 336 (12-16-03) and SRNL (12-13-03) 4PJM Holdup Test Results

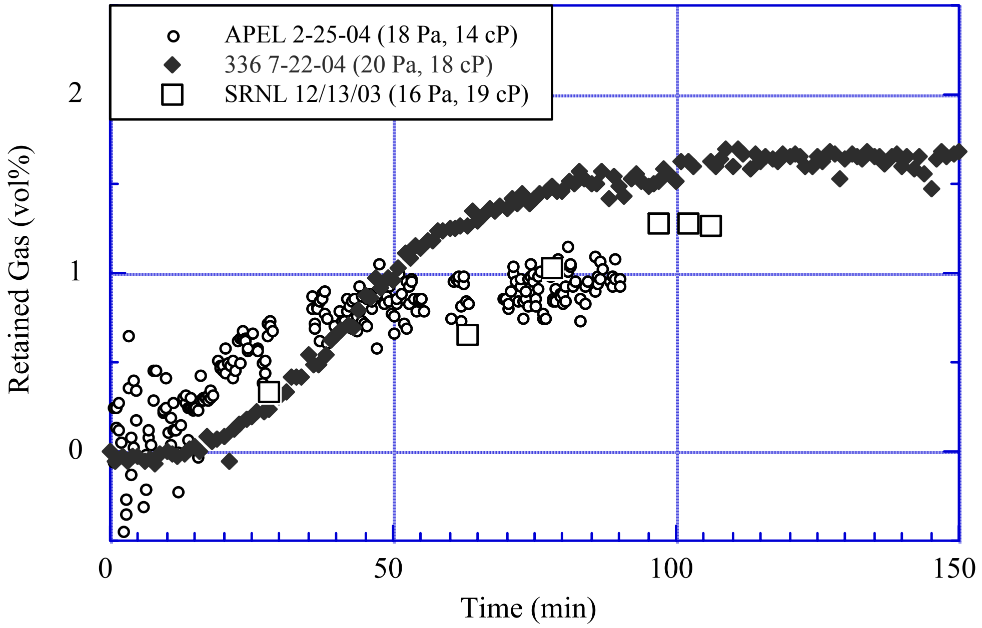

Figure 5.5. APEL (2-25-04), 336 (7-22-04) and SRNL (12-13-03) 4PJM Holdup Test Results

Because the APEL and SRNL tests used only 2.6 times the gas-generation rate of the 336 test, the holdup should be less, especially since the SRNL clay simulant also had less than half the Bingham yield stress of the stiff clay used in larger scale tests. Accordingly, the 3.7 vol% holdup in the 336 test is higher as the scaling law implies. The smaller APEL test showed an unexpected increase in holdup starting just before H_2O_2 injection ceased, though the PJMs continued to operate. This might imply that a region of stiff simulant began to gel, possibly in narrow gaps between structures (between the PJMs and vessel wall). Gauglitz and colleagues noticed a similar effect in bench-top gas-release tests and used a weaker simulant to model tank-scale behavior (Stewart et al. 1996). This might also be a factor in the high holdup seen in the 336 test.

Figure 5.5 compares results of three more closely scaled tests. The 7-22-04 test in the 336 facility, the 2-25-04 test in APEL, and the 12-13-03 SNRL test all used similar simulant rheology, and the gas-generation rates, at least in 336 and APEL, were in the correct proportion according the length scale. As a result, holdups are in the same range, though the approach to steady state occurred at different speeds.

Three holdup tests in the APEL 4PJM system using weak simulant are summarized in Figure 5.6. The weak simulants had Bingham yield stresses ranging from 7 to 18 Pa and consistencies from 9 to 22 cP. Each of the three tests began with the medium generation rate, while the 2-19-04 and 2-25-04 transitioned to the high gas-generation rate in the second half of the run. Except for the stiffest clay of the 12-15-03 test, simulant rheology had little observable effect for the medium gas-generation rate part of the tests. However, the 2-25-04 run clay produced a slightly higher holdup than the test on 2-19-04 with the weakest simulant, which appeared able to retain no more gas at the high generation rate.

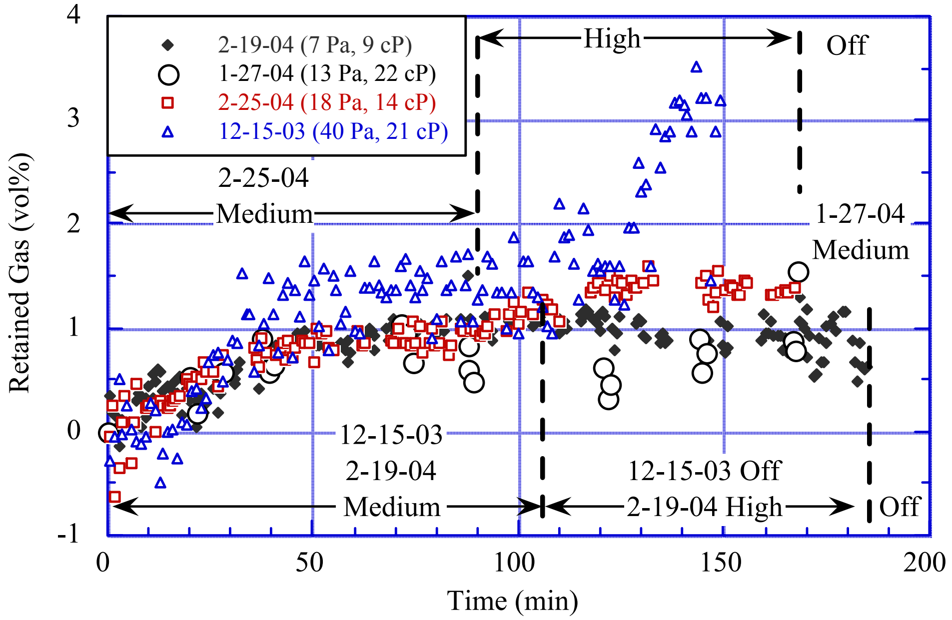

Figure 5.6. APEL 4PJM Holdup Test Results (12-15-03, 1-27-04, 2-19-04, and 2-25-04)

5.3 Uncertainties

The calculation of gas holdup in the simulant from changes in surface level while it fluctuates during PJM operation is subject to variability caused by several identifiable factors as well as random uncertainty. A 1-inch level change implied a change of 0.8 vol% in retained gas in the 336 4PJM tests, 1.5 to 2 vol% in LS and UFP scaled prototype tests, and 3.8 vol% in the APEL 4PJM vessel. Surface irregularities during operation may be on the order of 1 inch, as shown in Figure 5.7. Transient fluctuations in the surface level cause corresponding fluctuations in the gas-volume fraction of as much as 1 vol%, as shown in the preceding plots.

Simulant coats the tank walls and other structures as the surface level moves up and down each PJM cycle. An example is shown in Figure 5.8. This "cake out" of simulant has the effect of lowering the active surface level for an apparent loss in gas volume. In a test run in an initially "clean" APEL 4PJM tank, the static simulant level dropped 0.75 cm, equivalent to about 1.1 vol%, after about 8 hours of intermittent PJM operation with no H_2O_2 addition. It is not known whether simulant continues to deposit indefinitely or reaches some steady state where the rate at which material sloughs off matches the rate of deposition. A similar deposition may also be occurring inside the PJM tubes though symptoms (e.g., reduction in nozzle velocity, changes in cycle timing) have not been detected. The cake-out effect is aggravated in gas-release tests where the average level drops, as opposed to a holdup test where the level is rising.

Figure 5.7. Example of Uneven Simulant Surface (UFP Sequence 5)

Figure 5.8. Example of Simulant Cake out and Uneven Surface (LS Sequence 15A)

The initial surface level before H_2O_2 injection is assumed to represent simulant with a zero gas fraction. Simulant that has been used in previous tests may still contain a small amount of gas, and sparging introduces a small (less than 0.5 vol%) short-term air holdup that needs to be separated from the gas generated *in situ*. Fortunately, it is easy to apply a correction in holdup tests to force the starting gas-volume fraction to zero and isolate the effects of H_2O_2 injection. This correction was needed in LS sequence 15A, run 3 (-0.123 vol%) and in the APEL 4PJM test on 2/25/04 (-1.06 vol%).

Though the surface fluctuation and nonuniformity discussed above makes the relative accuracy of the point level measurements largely irrelevant, the electronic level sensors sometimes drift or exhibit other problems that compromise data reduction. Problems with ultrasonic sensors were particularly severe in the APEL 4PJM system. The ultrasonic sensors generally performed well in the UFP and LS scaled prototype tests and in the 336 4PJM system.

It is difficult to combine all the factors that contribute to uncertainty, most of which are complex or impossible to quantify individually, into a precisely defined overall value. However, a general uncertainty range can be estimated. While a gas-volume fraction calculated from a single surface-level data point may be uncertain by as much as ± 1 vol%, depending on the test, the data behavior as a whole can be estimated to within ± 0.5 vol% or less. Averaging over 20 data points to compute holdup gives typical standard deviations ranging from less than ± 0.1 to ±0.3 vol%. The empirical model of the full set of holdup results has a standard error of ± 0.12 as described in Section 5.4. A conservative (~95% confidence, assuming normality) overall estimate for uncertainty for these holdup results would be double the standard deviation of a typical average or to ± 0. 5 vol%.

5.4 Analysis[a]

The scaled prototype tests (LS and UFP) and 4PJM holdup tests represent two distinct populations of data. The scaled prototype LS and UFP tests used different combinations of PJM nozzle design, simulant depth, sparging and recirculation in each test (see Table 5.1). It could be said that each of these tests used some manner of enhanced mixing in addition to PJMs, though the data are insufficient to isolate the effectiveness of individual methods directly. The 4PJM tests were designed specifically to investigate the effects of scale. Each test system is not only geometrically equivalent, but the PJM cycle time also followed the length scale. The simulant rheology and gas generation rate were varied within both the 336 and APEL 4PJM tests. Only one SRNL holdup test was chosen to demonstrate scaling with the 336 and APEL vessels. Though intended to be uniform, the PJM nozzle velocities and drive times varied enough within tests and between tests to qualify as potential influence on the holdup and bubble rise velocity.

Taking the features of these two groups of data into consideration, the gas-retention data presented in this section show that gas holdup is strongly influenced by the effectiveness of the mixing system, specifically PJM design (see Figure 5.3), gas-generation rate (see Figures 5.1 and 5.3), and simulant depth (see Figure 5.4). Sparging and recirculation may have some effect, but the test matrix did not isolate these factors so they could be quantified. The APEL 4PJM data (see Figure 5.6) indicate only a small effect of simulant rheology (i.e., Bingham plastic model yield stress and consistency factors) at a given gas-generation rate.

The basic relationship of holdup to the gas-generation rate, bubble-rise velocity and simulant depth is expressed by Eq. (2.14). The gas-generation rate and the simulant height are known and the bubble-rise velocity can be determined empirically using Eq. (5.1). The bubble-rise velocity should vary with the extent and intensity of mobilization. Potentially important parameters affecting mobilization effectiveness include the tank diameter, the PJM drive time to total cycle time, the number of PJMs, the PJM nozzle diameter and drive velocity, and the rheology, density, and depth of the simulant. An empirical equation ($R^2 = 0.88$) representing the rise velocity, U_R, was derived by least-squares regression on all of the holdup test data as follows:

$$\begin{aligned} U_R = &- 19.96 + 0.0415g_v - 22.27D + 4.85N_{PJM} + 0.1474U_0 + 820d_0 + 0.0436\tau_y \\ &+ 0.0145\kappa + 0.00845(N_{PJM}\, g_v) - 0.00326(\kappa\, g_v) + 7.064(d_0\, D) - 0.0122(\tau_y\, N_{PJM}) \end{aligned} \tag{5.2}$$

where U_0 = peak-average PJM nozzle velocity (m/s)
d_0 = PJM nozzle diameter (m)
D = tank diameter (m)
τ_y = Bingham yield stress of the simulant (Pa)
κ = Bingham consistency (cP) of the simulant
N_{PJM} = number of PJMs in the system.

A model ($R^2 = 0.91$) similarly derived only from data from the geometrically identical 4PJM tests (336, APEL, and SNRL) is expressed by:

(a) The empirical holdup models given in this section must be used with careful consideration of scaling principles. They should only be applied to tank configurations, operational modes, and slurry conditions representative of the tests that were modeled.

$$U_R = -4.111 + 0.155g_v + 103t_D + 0.435U_0 + 0.0197\tau_y - 0.00162\kappa - 0.00693(\tau_y\, g_v) - 12.23(U_0\, t_D) \quad (5.3)$$

where t is the peak-average PJM drive time (min).

The details of the data selection and regression analyses are given in Appendix B.

Figure 5.9 shows the result of substituting the model for bubble-rise velocity based on all holdup data, Eq. (5.2), for the average rise velocity, U_R, in Eq. (2.14) to predict the holdup. The symbols represent the average holdup computed from the raw data while the actual raw data are shown with a "+". The dotted line represents the prediction from the model equations. The standard error in the holdup predicted by the model is ± 0.13 vol%, and the R^2 value for the holdup prediction is 0.98. Figure 5.10 shows the holdup predictions from the model for bubble-rise speed based only on the 4PJM data, Eq. (5.3). The standard error in the predicted holdup is ± 0.12 vol%, and the R^2 value for the holdup prediction is 0.98.

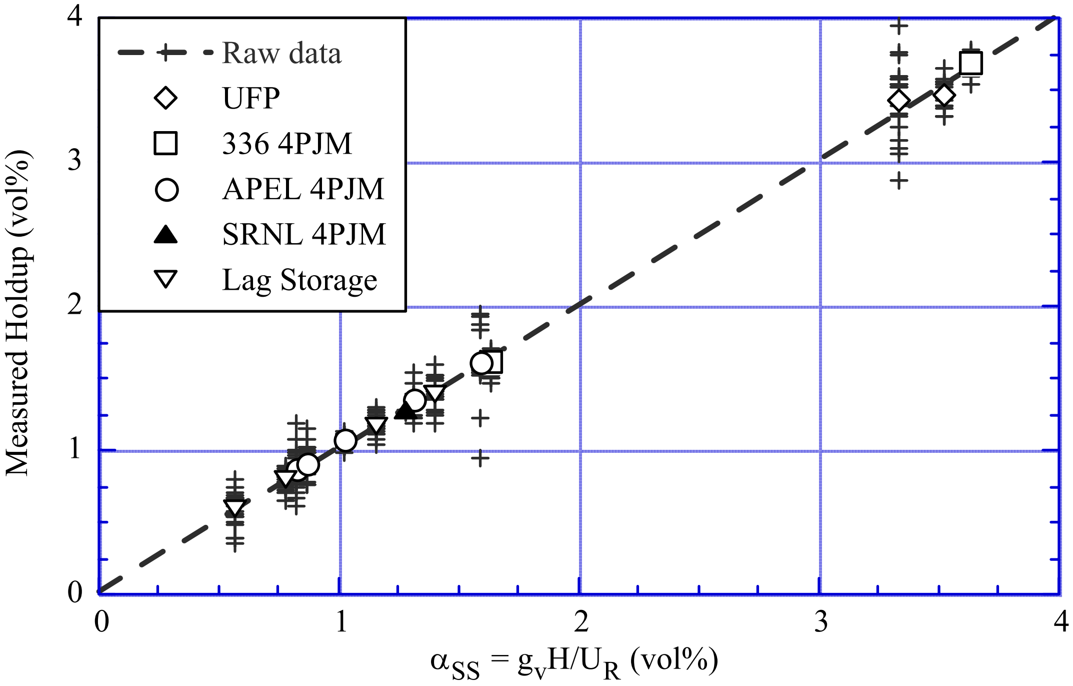

Figure 5.9. Empirical Holdup Prediction Based on All Holdup Data

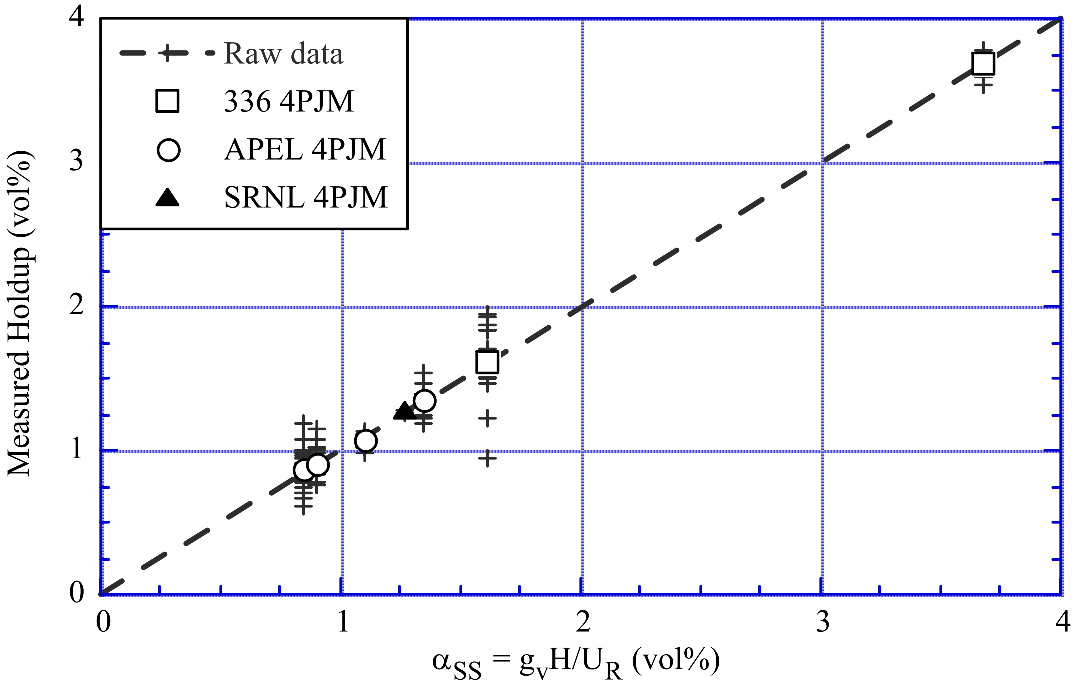

Figure 5.10. Empirical Holdup Prediction Based on 4PJM Holdup Data

5.5 Conclusions on Holdup Tests

The holdup tests discussed in this section covered tests stands ranging from the 12-ft. diameter 336 4PJM system at approximately half of full scale down to the SRNL vessel at 1:9 336 4PJM scale. There were variations on three different PJM configurations, including partial sparging and recirculation nozzles. The holdup data over the full range of test conditions were well correlated with the gas-generation rate, system dimensions, simulant properties, and PJM drive cycle parameters. The holdup data also provide a reliable method to characterize the overall gas-retention and release behavior of PJM-driven mixing systems.

6.0 Gas-Release Tests

Reviewed data are available for gas-release tests in the UFP and LS PJM scaled prototype vessels in the APEL during February 2004 and in the scaled 4PJM test stands in the 336 Building (approximately half-scale relative to the plant), APEL (1:4.5-scale relative to 336), and SRNL (1:9-scale relative to 336). Kaolin-bentonite clay simulant was used in these gas-holdup experiments. Decomposition of H_2O_2 into O_2 and water supplied the gas generation. These data were analyzed to determine the functional form that describes the gas-release process to help predict gas-release behavior in the full-scale plant. The tests are described in Section 6.1. Section 6.2 assesses the amount of gas generation during the release tests, and gas-release test results are presented in Section 6.3. Uncertainty analysis is presented in Section 6.4, data analysis methods are derived and applied in Section 6.5, and conclusions are given in Section 6.6.

Gas-release tests were generally conducted by restarting the mixing system after some quiescent gas-accumulation period ranging from 10 minutes to overnight (~18 hours) that followed a mixing period during which a predetermined mass of H_2O_2 was injected to achieve the desired initial gas-volume fraction. Several gas-release tests followed a gas-holdup test (see Section 5). An example of two combined holdup and gas-release tests in the UFP test stand is given in Figure 6.1. The first PJM pulse typically released a large volume of the retained gas, and each subsequent pulse released progressively less gas, causing the level to drop in an exponential trend.

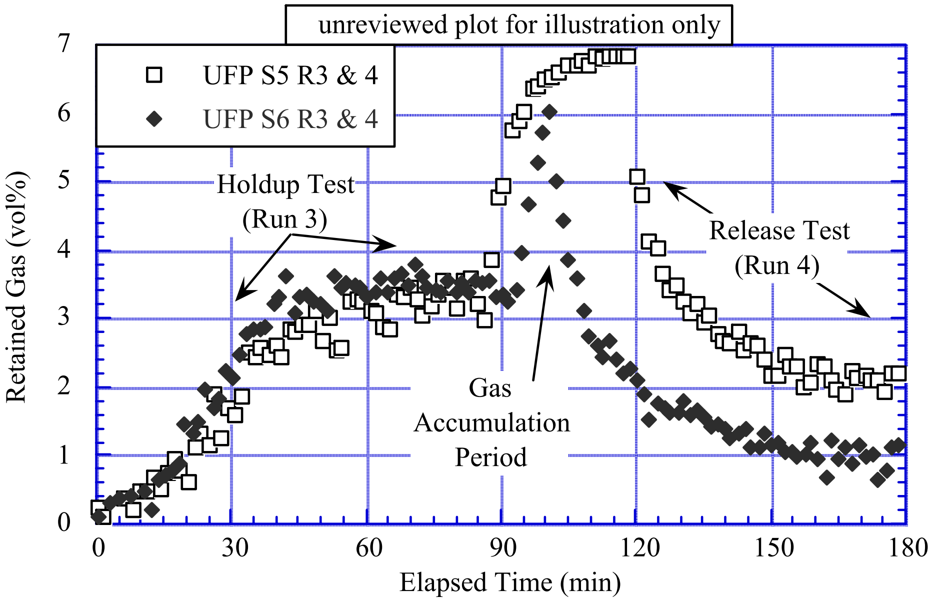

Figure 6.1. Gas-Fraction Histories for UFP Gas-Holdup and Release Tests

Like the gas-holdup tests, the initial gas-volume fraction in the simulant before H_2O_2 injection is assumed to be zero. Then, after gas accumulation and release, the retained gas-volume fraction calculated from the surface level at the end of the test should decrease to slightly greater than or, at best, zero. However, because of the same measurement uncertainties and errors discussed in Section 5, the calculated ending gas-volume fraction may be less than zero. While a positive gas-volume fraction indicates less than total gas release, a negative average gas fraction (as opposed to an occasional negative data point) is unphysical and warrants a correction. For example, consider UFP sequence 6, run 4. Full sparging was used to degas the simulant at the end of the test. When the spargers were shut down, the average gas-volume fraction dropped to –0.53 vol%. The calculated gas fractions were corrected by this average to bring the final average back up to zero, as shown in Figure 6.2. Four other release tests required correction: LS sequence 14, run 2 (-0.68 vol%), LS sequence 15, run 2 (-0.40 vol%), the APEL 4PJM test on 12/2/03 (–0.21 vol%), and the APEL 4PJM test on 2/18/04 (–0.19 vol%). The actual gas-volume fraction may have been slightly positive, as observed in the other tests, so these corrections are lower bounds.

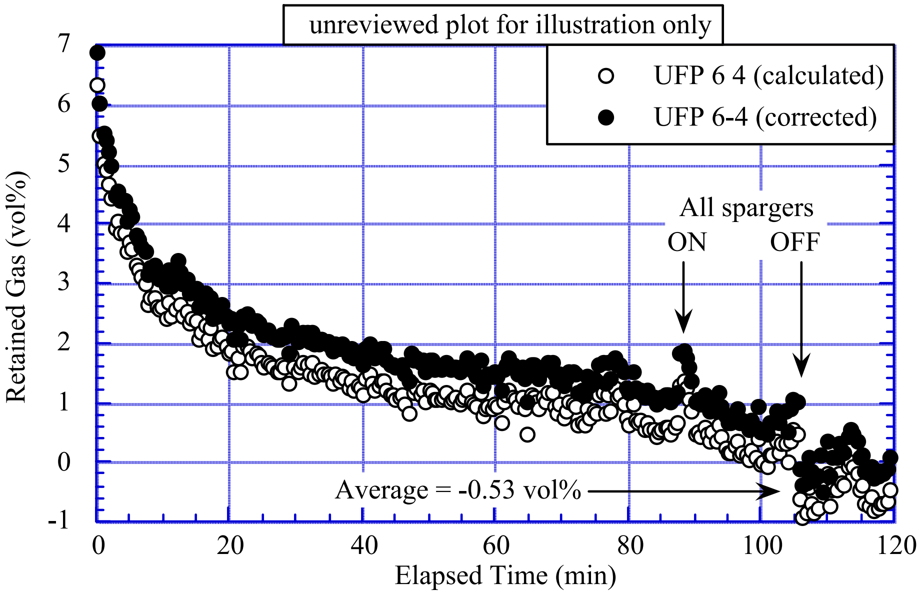

Figure 6.2. Example of Gas-Volume Fraction Correction in UFP Sequence 6, Run 4

6.1 Test Summary

Table 6.1 summarizes the gas-holdup and release tests presented and analyzed in this section. The simulant used in the LS tests has the same nominal 36-Pa Bingham yield stress as the UFP tests but a slightly higher consistency, 24 to 27 cP versus 18 to 20 cP. The 12/12/03 336 4PJM test and the 12/14/03 APEL 4PJM test used the same relatively stiff simulant with a Bingham yield stress of 40 to 44 Pa and consistency of 21 cP. The other APEL 4PJM tests used a range of rheology with yield stress ranging from 7 to 34 Pa and consistency from 9 to 27 cP. Four additional 4PJM tests were run in the large-scale 336 Building vessel. Two tests used simulant with a 35 Pa yield stress and 22 cP consistency, and two had a 20 Pa yield stress and 18 cP consistency.

Table 6.1. Gas-Release Test Description

Test Sequence	Run	Initial Gas (vol%)	Simulant		Rheology		PJM Layout and Drive Cycle (a)	Spargers Operating
			Volume (L)	Depth (m)	τ (Pa)	κ (cP)		
LS Seq. 14	2	3.0 (overnight)	2,850	1.3 (H/D≈0.7)	36	27	Cluster 7 (3-135° and 4-45°) around 1 (0°) @ 16.9 m/s, $t_C = 0.75$ min, $t_D/ t_C = 0.09$	4 (#1, 3, 5, 7) @ ~3 acfm
	4	6.5	2,870					
LS Seq. 15, 15A	2	4.7 (overnight)	2,840	1.3 (H/D≈0.7)	34-37	24-27	Cluster 7 (all-45°) around 1 (0°) @ 15 m/s, $t_C = 0.75$ min, $t_D/ t_C = 0.09$	4 (#1, 3, 5, 7) @ ~3 acfm
	4	5.4	2,950					
UFP Seq. 5	2	3.2 (overnight)	633	1.2 (H/D≈1.4)	34-39	19-20	Tri-foil (3-45°) around 1 (0°) @ 15.4 m/s, $t_C = 0.45$ min, $t_D/ t_C = 0.09$	One center @ ~3 acfm
	4	6.8	643					
UFP Seq. 6	2	4.6 (overnight)	833	1.6 (H/D≈1.8)	33-37	18-20	Tri-foil (3-45°) around 1 (0°) @ 16.3 m/s, $t_C = 0.45$ min, $t_D/ t_C = 0.07$	One center @ ~3 acfm
	4	6.9	839					
336 4PJM 12/12/03		8.9	37,150	3.45 (H/D≈0.9)	44	23	8.5 m/s, $t_C = 1.0$ min, $t_D/ t_C = 0.14$	None
3/23/04		3.4	37,500	3.45 (H/D≈0.9)	35	22	8.4 m/s, $t_C = 1.0$ min, $t_D/ t_C = 0.15$	None
3/25/04		2.4	37,500	3.45 (H/D≈0.9)	35	22	8.4 m/s, $t_C = 1.0$ min, $t_D/ t_C = 0.15$	None
7/20/04		1.9	37,600	3.45 (H/D≈0.9)	20	18	8.3 m/s, , $t_C = 1.0$ min, $t_D/ t_C = 0.15$	None
7/23/04		3.8	37,400	3.45 (H/D≈0.9)	20	18	8.4 m/s, , $t_C = 1.0$ min, $t_D/ t_C = 0.15$	None
SRNL 4PJM 12/12/03		10.3	52	0.4 (H/D≈0.9)	16	19	Four @ 8.7 m/s, $t_C = 0.11$ min, $t_D/ t_C = 0.18$	None
2/27/04		11.4	52	0.4 (H/D≈0.9)	29	31	11.5 m/s, $t_C = 0.11$ min, $t_D/ t_C = 0.13$	None

Table 6.1 (contd)

Test Sequence	Run	Initial Gas (vol%)	Simulant		Rheology		PJM Layout	Spargers Operating
			Volume (L)	Depth (m)	τ (Pa)	κ (cP)		
APEL 4PJM	12/2/03	10.9	380	0.77 (H/D≈0.9)	20	26	9.7 m/s, t_C = 0.22 min, t_D/ t_C = 0.13	None
	12/14/03	7.7	380	0.77 (H/D≈0.9)	40	21	10.2 m/s, t_C = 0.22 min, t_D/ t_C = 0.12	None
	1/26/04	2.9	380	0.77 (H/D≈0.9)	13	22	10.3 m/s, t_C = 0.22 min, t_D/ t_C = 0.13	None
	2/6/04	3.6	380	0.77 (H/D≈0.9)	33	19	9.1 m/s, t_C = 0.22 min, t_D/ t_C = 0.12	None
	2/10/04	5.7	380	0.77 (H/D≈0.9)	33	19	10.0 m/s, t_C = 0.22 min, t_D/ t_C = 0.11	None
	2/11/04	4.2	380	0.77 (H/D≈0.9)	33	19	9.1 m/s, t_C = 0.22 min, t_D/ t_C = 0.11	None
	2/12/04	4.3	370	0.77 (H/D≈0.9)	32	19	9.4 m/s, t_C = 0.22 min, t_D/ t_C = 0.11	None
	2/13/04	3.7	370	0.77 (H/D≈0.9)	32	19	9.0 m/s, t_C = 0.22 min, t_D/ t_C = 0.11	None
	2/18/04	5.0	390	0.77 (H/D≈0.9)	7	10	10.0 m/s, t_C = 0.22 min, t_D/ t_C = 0.11	None
	2/20/04	6.8	390	0.77 (H/D≈0.9)	7	10	11.3 m/s, t_C = 0.22 min, t_D/ t_C = 0.11	None
	2/25/04	6.4	390	0.77 (H/D≈0.9)	18	14	10.1 m/s, t_C = 0.22 min, t_D/ t_C = 0.12	None

(a) The peak-average PJM nozzle velocities and associated drive time-to-cycle time ratios are given.

All 4PJM tests used only their four PJMs while the LS and UFP tests added sparging. Neither vessel used the installed recirculation nozzles in release tests. Sparger design and operation were selected before further sparger testing showed that more spargers or increased sparger air flow rates were needed to provide effective mobilization. The LS gas-release tests in sequence 14 used four spargers and eight PJMs with three nozzles canted upward at 135º, four downward at 45º°, and one vertical. In sequence 15 (and 15A), all seven outer PJM nozzles were set at 45º, and one was vertical; four spargers were used. Both UFP tests used four PJMs and a single central sparger. The UFP sequence 5 tests used a height-to-diameter ratio (H/D) of 1.4, while sequence 6 had an H/D = 1.8.

6.2 Gas Generation During Release

The steady gas fraction in the latter part of the accumulation period in UFP sequence 5, runs 3 and 4, shown in Figure 6.1, indicates that the unreacted H_2O_2 was depleted, and the gas (O_2) generation rate fell almost to zero before the release test began. In the UFP sequence 6 tests shown in the same figure, however, the gas-volume fraction was still rising steeply when the gas-release test started. Thus the gas-release tests that followed the gas-holdup tests may initially be complicated by gas generation that would need to be accounted for in the gas-release data analysis.

To quantify whatever latent gas generation might be occurring, the amount of H_2O_2 remaining at the start of the gas-release tests must be estimated. This requires solving mass conservation equations for both H_2O_2 and retained gas through the gas-holdup test (run 3), a gas-accumulation phase, and the gas-release test (run 4). Assuming the gas bubbles in the slurry consist only of O_2 and all the O_2 is generated by H_2O_2 decomposition with no losses to the atmosphere, the conservation equations for H_2O_2 mass and moles of O_2 gas are expressed as

$$\frac{dW_p}{dt} = x_p \rho_{ps} Q_{ps} - 2M_p V_s g_m \tag{6.1}$$

and

$$\frac{dN_{O2}}{dt} = V_s g_m - \frac{V_{bs} p}{RT} R_v \tag{6.2}$$

where W_p = mass of unreacted H_2O_2 in the simulant (g)
g_m = molar generation rate of O_2 gas bubbles per liter of simulant (moles/L-min)
V_s = initial volume of degassed simulant (liters)
N_{O2} = number of moles of O_2 present in the simulant as gas bubbles
V_{bs} = volume of bubbly simulant (liters), equal to V_s plus accumulated gas
R_v = gas-volume release rate per unit volume of bubbly simulant (volume fraction/min).

The gas-volume fraction is calculated from the number of moles of O_2 gas in the simulant by

$$\alpha = N_{O2}\frac{RT}{pV_{bs}} = \frac{1}{\dfrac{V_s}{N_{O2}}\dfrac{p}{RT}+1} \tag{6.3}$$

Eq. (6.1) through (6.3) require expressions for the gas-volume release rate, R_v, and the O_2 molar generation rate, g_m. Based on bubble migration theory from Section 2, the gas-release rate should be a linear function of the gas-volume fraction of the form:

$$R_v = A_R \alpha \tag{6.4}$$

where A_R is the U_R/H parameter discussed in Section 2.

The O_2 generation rate should be functionally dependent on the concentration of H_2O_2. A brief review of abstracts on catalyzed H_2O_2 decomposition, which includes kaolin-bentonite clay, indicates that the reaction should be first order for low concentrations and zeroth-order for high concentrations (Tachiev et al. 2000, for example). Therefore, for the relatively low concentrations of H_2O_2 used in the gas-release tests, the average O_2 generation rate should be directly proportional to the H_2O_2 concentration, C_p, similar to the gas-release rate in Eq. (6.4):

$$g_m = A_g C_p \tag{6.5}$$

where A_g is a constant.

Substituting parameter definitions Eq. (6.3) through (6.5) into the H_2O_2 and O_2 gas mass conservation, Eq. (6.1) and (6.2) produce

$$\frac{dW_p}{dt} = x_p \rho_{ps} Q_{ps} - 2A_g W_p \tag{6.6}$$

and

$$\frac{dN_{O2}}{dt} = A_g \frac{W_p}{M_p} - A_R N_{O2} \tag{6.7}$$

The solutions to Eq. (6.1) and (6.2) are obtained by integrating between times t_1 and t_2 and are expressed, respectively, as follows:

$$W_p(t_2) = W_p(t_1) e^{-2A_g(t_2-t_1)} + \frac{x_p \rho_{ps} Q_{ps}}{2A_g}\left[1 - e^{-2A_g(t_2-t_1)}\right] \tag{6.8}$$

$$N_{O2}(t_2) = N_{O2}(t_1) e^{-A_R(t_2-t_1)} + \frac{\overline{W}_p A_g}{M_p A_R}\left[1 - e^{-A_R(t_2-t_1)}\right] \tag{6.9}$$

where $\overline{W}_p$ is the integral time average of Eq. (6.8) between t_1 and t_2, given by

$$\overline{W}_p = \frac{x_p \rho_{ps} Q_{ps}}{2A_g} - \frac{W_p(t_2) - W_p(t_1)}{2A_g(t_2 - t_1)} \tag{6.10}$$

The constants for the gas-release and gas-generation functions in Eq. (6.4) and (6.5) were determined for each gas-release test that followed a gas-holdup test by minimizing the error between the predictions of the solutions to the two conservation equations (6.8 and 6.9) and the test data during and after the gas-holdup test up to the beginning of the ensuing gas-release test. The constants were adjusted with the SOLVER function in Microsoft Excel.(a)

Figures 6.3 through 6.6 show the measured and predicted gas-volume fractions and the total H_2O_2 mass for combined gas holdup (retention)-release tests in LS sequences 14 and 15A and UFP sequences 5 and 6. In the first minutes of the retention tests, dissolved O_2 apparently builds in solution before bubbles can nucleate. Because the model does not treat dissolved gas, H_2O_2 injection was held to zero until the measured gas-volume fraction began rising. Gas release was set to zero during the accumulation period when the mixing system was not operating. The constants A_R and A_g determined from the error minimization for each test are listed in Table 6.2. The results show that 1) the H_2O_2 inventory is well depleted by the time the gas-release test begins, and gas generation can be ignored in analyzing the release data; 2) the gas-release function with constants fit to the gas-holdup test also follows the gas-accumulation period and the initial part of the gas release, sometimes quite well; but 3) in most cases, the actual gas release at later times is generally much slower, apparently following a longer time constant.

The observation that the simple conservation equations with a single gas-release coefficient predicted gas-volume fractions that match the data during both retention and the initial gas-release periods supports the gas-bubble migration model derived in Section 2 as the fundamental description of the gas-retention and release process. However, the relatively abrupt departure of the predicted and measured gas-volume fractions after the initial release show that additional effects come into play as the gassy simulant is remobilized after the gas-accumulation period.

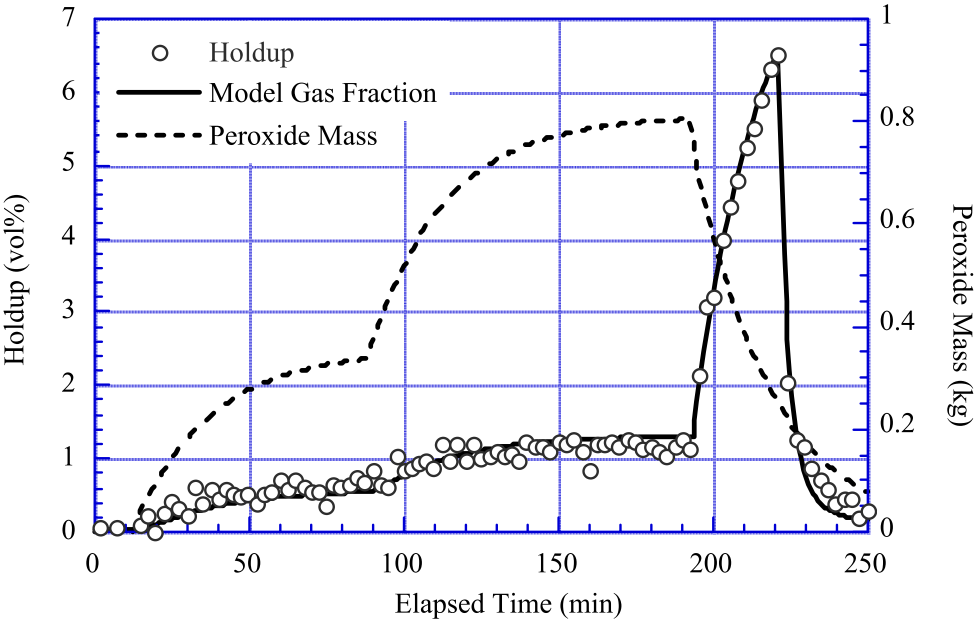

Figure 6.3. Gas-Retention and Release Model Results: LS Sequence 14, Runs 3 and 4

(a) Microsoft Excel 2004 for Mac®, Version 11.1, on a Macintosh PowerBook G4 running OS 10.3.5.

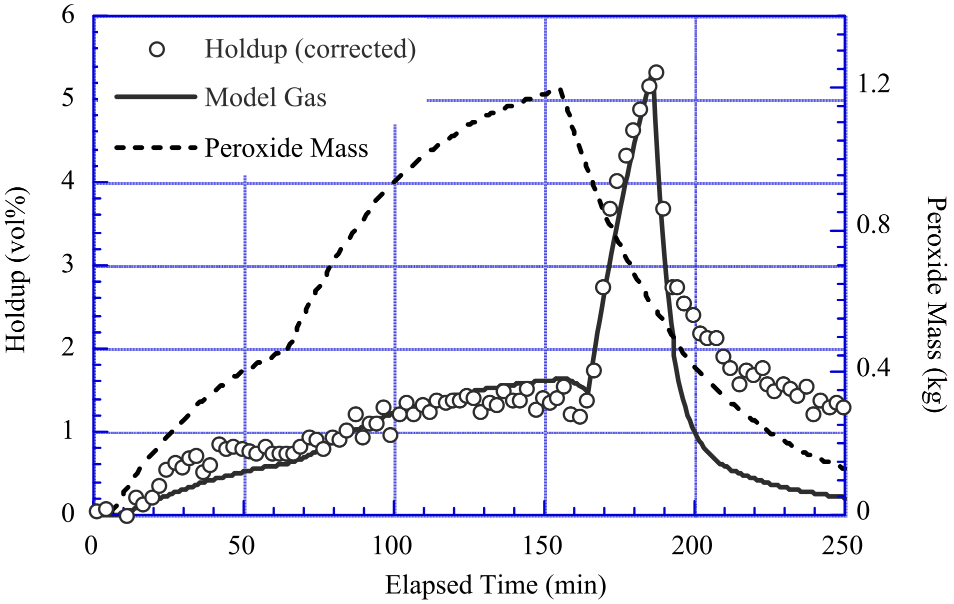

Figure 6.4. Gas-Retention and Release Model Results: LS Sequence 15A, Runs 3 and 4

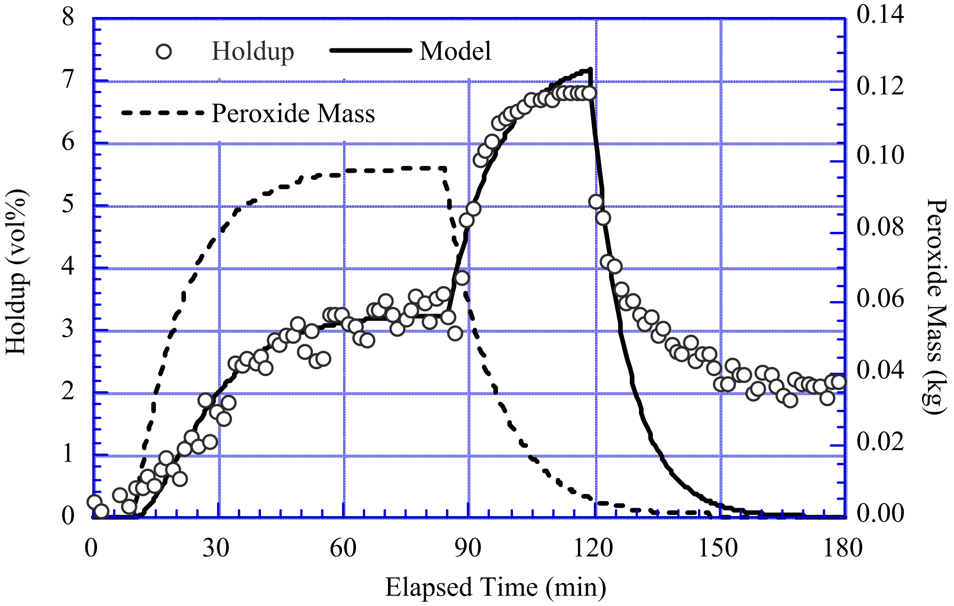

Figure 6.5. Gas-Retention and Release Model Results: UFP Sequence 5, Runs 3 and 4

Evidence suggests that the slow, steady release of gas after the initial rapid release may be the result of a persistent region of less-than-fully mobilized simulant slowly eroding away. In fact, the solution of a system of equations describing an erosion process has the same exponential form as the basic bubble rise model. Apparently, the first few PJM cycles may release gas rapidly from a fully mobilized cavern in the lower part of the tank, leaving most or all of the retained gas above it. This unreleased gas may create a buoyant cap on top of the now heavier degassed cavern that slows further mobilization. The slow-releasing region is not a permanent, un-mobilized heel. It is simply mobilized more slowly, apparently by a different process. The time constants for the slower releases are described and quantified in Section 6.5.

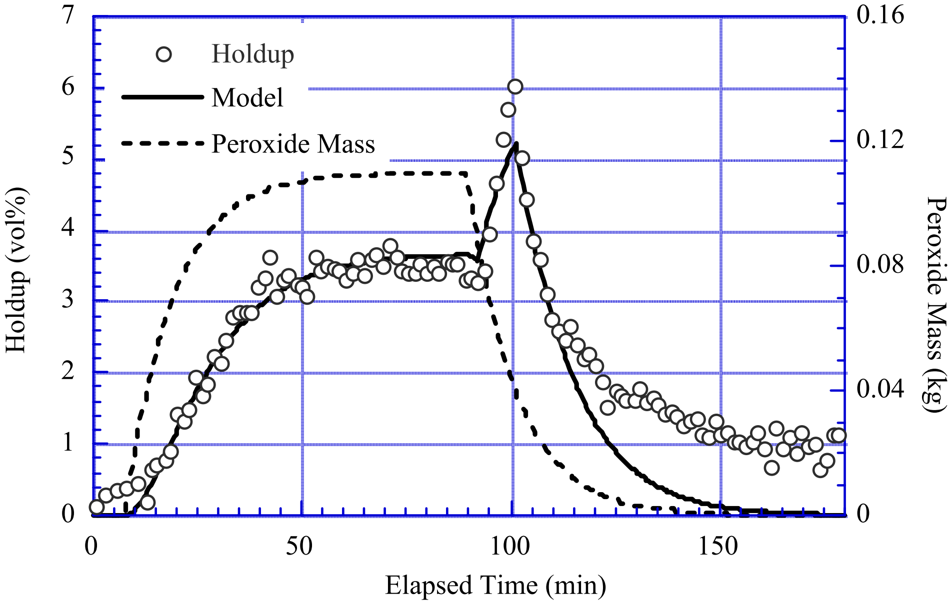

Figure 6.6. Gas-Retention and Release Model Results: UFP Sequence 6, Runs 3 and 4

Table 6.2. Coefficients of Generation and Release Functions Determined by Error Minimization

Gas-Holdup and Release Test	Gas Generation	Gas Release
	A_g (mol/L-min)	A_R (min^{-1})
LS Seq. 14, Runs 3 & 4	0.020	0.28
LS Seq. 15A, Runs 3 & 4	0.012	0.19
UFP Seq. 5, Runs 3 & 4	0.042	0.12
UFP Seq. 6, Runs 3 & 4	0.043	0.10

One clue is that the LS sequence 14 tests had half the PJM nozzles angled upward at 135° while all nozzles pointed downward at 45° in sequence 15 (and 15A). It may be that the upward jets from the PJMs in sequence 14 mobilized most of the simulant, allowing the well-mixed model to predict the release (Figure 6.3) much better than sequence 15A (Figure 6.4). The same effect may have occurred in the UFP tests, where a larger aspect ratio (H/D from 1.4 to 1.8 in UFP compared with 0.74 for the LS vessel) would make formation of a buoyant cap more likely. The higher values of the coefficient (A_R) on the gas-release function for LS sequence 14 versus sequence 15 and UFP sequence 5 versus sequence 6 in Table 6.3 are consistent with this argument.

The formation of the postulated buoyant cap may have been mitigated somewhat by partial sparging in the LS and UFP tests. In the 4PJM tests, which had no spargers, a slow release of residual gas was generally observed in all tests with simulant yield stress of ~20 Pa and higher. The thinner clay tests generally released their gas as fast as or faster than predicted by the well-mixed model. These tests and the effects of sparging and simulant rheology are discussed in Section 6.3.

6.3 Gas-Release Test Results

The gas-release test data set shows the effects of initial gas-volume fraction and simulant rheology and the differences between test stands for similar conditions. Two sets of scaled prototype tests compare the effects of letting simulant stand overnight versus starting the gas-release tests after letting gas accumulate less than an hour (as introduced in Section 6.2). Tests in the three 4PJM vessels also show the effect of scale for the same rheology, approximately the same initial gas fraction, and the same mixing system. Results are presented in terms of gas-volume fraction versus time. Section 6.3.1 covers scaled prototype tests, Section 6.3.2 discusses 4PJM scaling test results, Section 6.3.3 covers the 336 4PJM tests, and Section 6.3.4 presents the results of the APEL 4PJM tests.

6.3.1 Scaled Prototype Gas-Release Tests

Data from four gas-release tests are available in both the LS and UFP vessels. Figure 6.7 shows the results for the four LS tests. The simulant rheology was essentially the same for all tests, but run 2 in sequences 14 and 15 (and 15A) ran after accumulating gas overnight, while run 4 took place after about half an hour of gas buildup following a gas-holdup test (see Figures 6.3 and 6.4).

The overnight tests (run 2) began with a lower gas volume, much lower in sequence 14, and released their gas more quickly than the run 3 tests with short accumulation periods. In theory, because large bubbles have the lowest internal pressure and scavenge dissolved O_2 to grow at the expense of small bubbles, the overnight tests should begin with larger bubbles, even with a lower initial gas-volume fraction. Because the gas-release rate is proportional to the bubble rise speed, the overnight tests with the largest, fastest-rising bubbles should release gas more rapidly and completely.

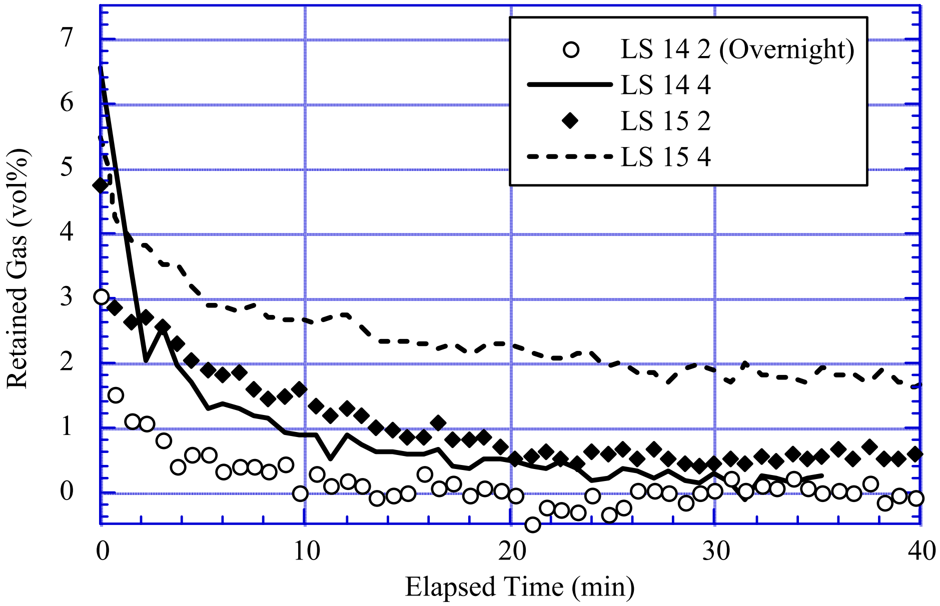

Figure 6.7. Results of Gas-Release Tests in the LS Vessel

The improved mobilization provided by the four up-angled PJMs in sequence 14 is also obvious. Results of sequence 15, run 2 are almost identical to those of sequence 14, run 4, even though the former had the benefit of larger overnight bubble size and 2 vol% less initial retained gas. Likewise, sequence 15A, run 4 retains about 2 vol% more gas than sequence 14, run 4 over the entire test.

Figure 6.8 compares the gas-release test results for UFP sequences 5 and 6. Again, run 2 of each sequence accumulated gas overnight, while both run 4 tests began only 10 to 30 minutes after a gas-holdup test (see Figures 6.5 and 6.6). While LS sequences 14 and 15 used different mixing systems, UFP sequences 5 and 6 used different simulant depths with the same mixing system. UFP sequences 5 and 6 had a simulant H/D of 1.4 and 1.8, respectively.

Like the LS tests, a marked difference exists between the overnight (run 2) and 30-minute (run 4) gas accumulation in sequence 5, with the latter holding a residual 2 vol% out to the end of the test. However, there is less than 1 vol% difference between overnight (run 2) and 10-minute (run 4) accumulation in sequence 6. It may be that the reduced mobilization of the deeper simulant also reduces the effect of larger bubbles that accumulate overnight.

Figure 6.9 shows how sparging released residual gas at the end of LS sequence 15A, run 4. At 87 minutes elapsed time, all eight spargers and the PJMs started up after a 7-minute rest during which the entire mixing system was shut down. Starting the spargers appears to have produced a gas holdup of about 0.5 vol%, which released quickly when they were shut down 10 minutes later. This brief sparger run reduced the residual retained gas from 1.4 to 0.3 vol%.

Figure 6.10 shows a similar release of 2 vol% residual gas release during the last hour of UFP sequence 5, run 4. After shutting down the PJMs, all four spargers were activated. After about 10 minutes, the PJMs were turned on also and ran until the end of the test. The spargers were shut down at 95 minutes elapsed time, having run a little over 20 minutes. The sparging induced a temporary gas holdup of about 0.5 vol% on startup without PJMs and almost 1 vol% on shutdown with PJMs operating.

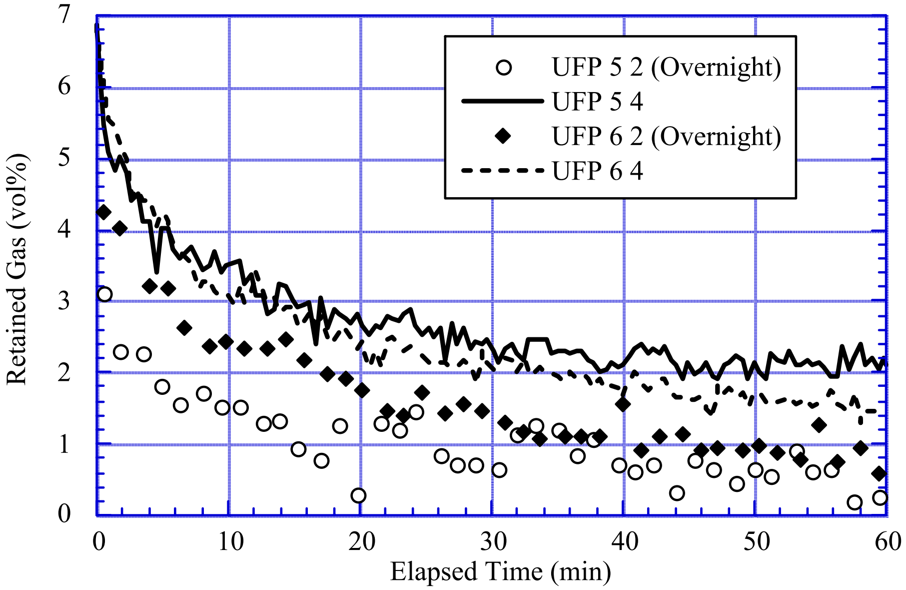

Figure 6.8. Results of Gas-Release Tests in the UFP Vessel

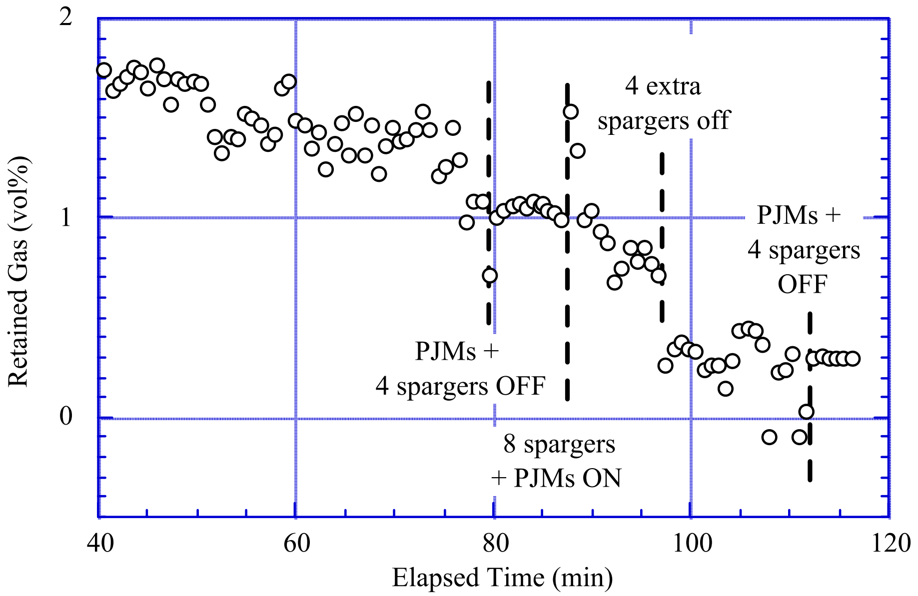

Figure 6.9. Effect of Spargers on Residual Gas Release in LS Sequence 15A, Run 4

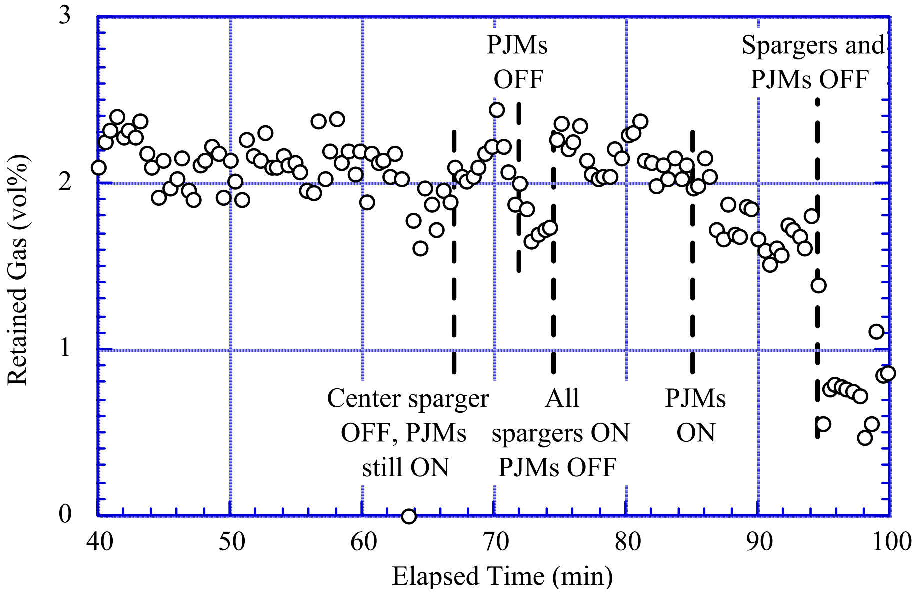

Figure 6.10. Effect of Spargers on Residual Gas Release in UFP Sequence 5, Run 4

This may be evidence of a complex bubble transport interaction between spargers and PJMs in the deep simulant. The 20-minute sparger run reduced the residual gas holdup from 2 vol% to less than 1 vol%.

6.3.2 4PJM Gas-Release Tests—Scaling Comparison

The 4PJM tests include test stands of three geometric scales from the large scale system in the 336 Building, the 1:4.5 scale (with respect to 336) test stand at APEL, and a 1:9 scale (with respect to 336) vessel at the SRNL. The 4PJM design differs from the UFP and LS scaled prototype vessels in that the four PJMs are spaced more uniformly in the tank instead of clustered in the center. No spargers or recirculation pumps were used in these tests.

In a gas-release test from an initial gas fraction, α_0, without gas generation, the decreasing gas-volume fraction is described by

$$\alpha(t) = \alpha_0 e^{-tU_R/H} = \alpha_0 e^{-N_c(t_c U_R/H)} \tag{6.11}$$

where N_c is the number of PJM cycles and t_c is the PJM cycle period. The exponent contains the gas-release number described in Section 2. Because t_c is scaled with H, and U_R does not vary widely, the gas-release number will be similar for all scales, and curves of gas fraction versus the number of PJM cycles should follow similar trends.

Figure 6.11 plots gas fraction versus the number of PJM cycles for gas-release tests in each of the three scales. Test conditions were equivalent except that the SRNL test started with a higher gas fraction, and the simulant Bingham yield stress was considerably lower (16 Pa versus 40–44 Pa; see Table 6.2). The results of all three tests are similar, but the APEL test showed a slower release rate in the latter stages. Figure 6.12 presents the results of three tests with similar simulant rheology, though the 336 test had a much lower initial gas fraction. This time the SRNL test exhibits a much slower initial release than the larger vessels, but matches the 336 4PJM trend well in the latter stages.

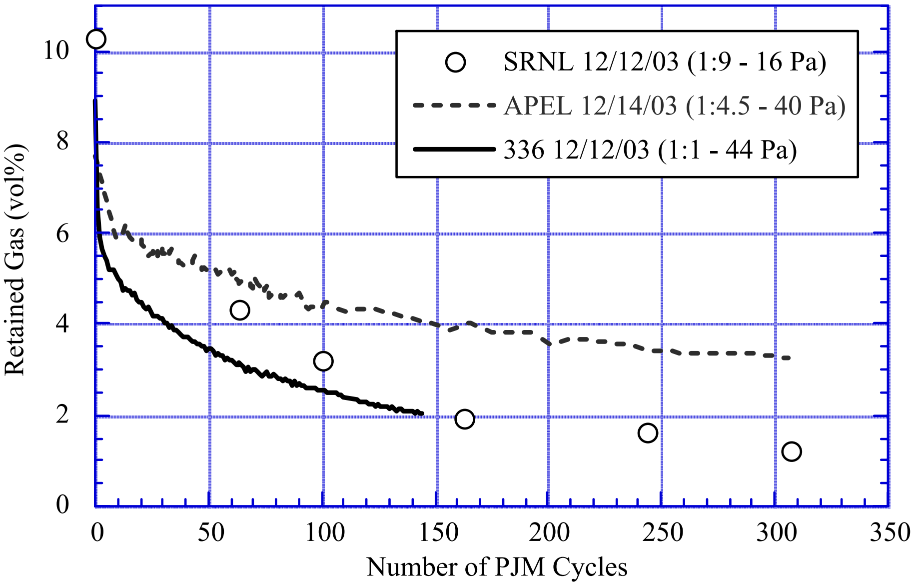

Figure 6.11. Scaled 4PJM Gas-Release Test Comparison

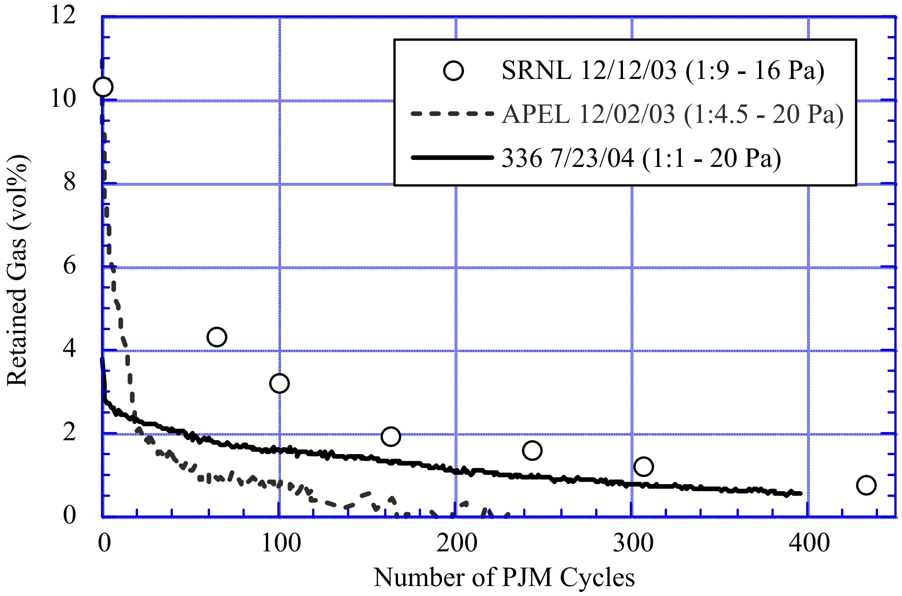

Figure 6.12. Scaled 4PJM Gas-Release Tests with Similar Rheology (kaolin:bentonite clay)

6.3.3 336 4PJM Gas-Release Test Results

Comparing all five kaolin-bentonite tests in the 336 4PJM system shows the effect of simulant rheology on gas-release behavior (Figure 6.13). The December 2003 test, also plotted in Figure 6.11, used the stiffest clay with a Bingham yield stress of 44 Pa and a consistency of 23 cP while the simulant for the two March 2004 tests had a Bingham yield stress of 35 Pa with a consistency of 22 cP. The July tests had a Bingham yield stress of 20 Pa and a consistency of 18 cP. While the high initial gas fraction makes it difficult to compare the December test directly, it is clear that the trend is toward a 1 to 2 vol%

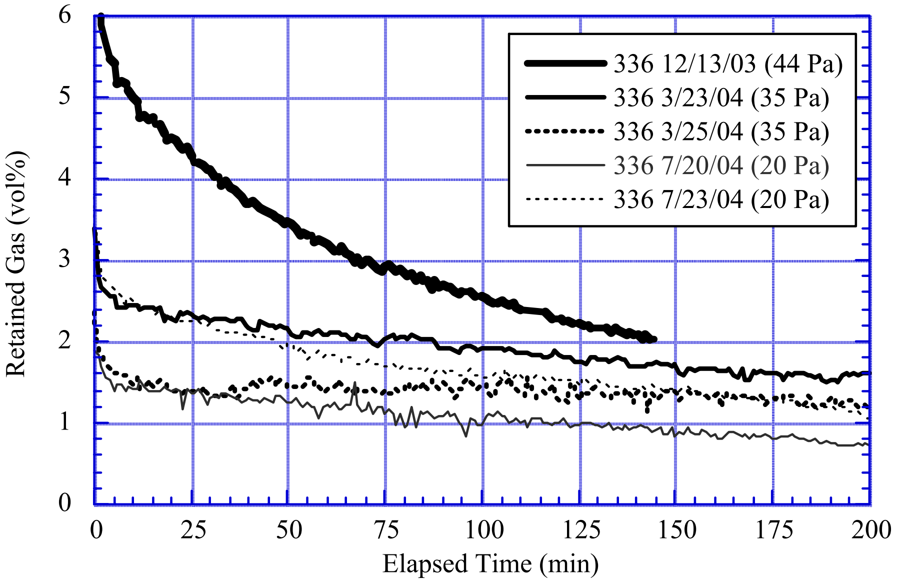

Figure 6.13. Gas-Release Tests in the 336 Building 4PJM System

residual gas retention that releases very slowly. The gas release in the July tests, with 20 Pa Bingham yield stress clay, shows a slightly higher gas-release rate during this gradual residual period than the March tests using 35 Pa Bingham yield stress clay, but still have almost exactly the same overall character. The slow residual release that seems to characterize the 336 4PJM tests may represent the slow erosion of the unmixed, or less well-mixed, volume above the PJM cavern, or of the obstructed region between the PJMs and the tank wall.

6.3.4 APEL 4PJM Gas-Release Test Results

Figures 6.14 through 6.17 compare groups of gas-release tests in the APEL 4PJM system to illustrate how gas-release behavior varies with various parameters. Figure 6.14 illustrates the effect of initial gas fraction, which varied from 3.6 to 5.6 vol%, with a Bingham yield stress of 30 to 33 Pa. The test with 5.6 vol% initial gas fraction shows a persistent long-term residual gas fraction, and other the tests do not. Perhaps the higher initial gas fraction hindered mobilization in these tests. There is little difference between tests with initial gas fractions ranging from 3.6 to 4.2 vol%.

Two other tests with widely different initial gas fractions of 10.7 and 6.4 vol%, but a lower Bingham yield stress of 18 and 20 Pa and a consistency of 14 and 26 cP, are presented in Figure 6.15. For unknown reasons, these results are completely contrary to the expected trends in that the most rapid and complete gas release occurred in the more viscous simulant with the highest initial gas fraction.

The effects of simulant rheology for tests with approximately the same initial gas fraction are shown in Figure 6.16. Generally, the weaker the simulant, the larger the initial gas release and the lower the residual retained gas fraction. This effect is much stronger than observed in the holdup tests presented in Section 5. Figure 6.17 presents the results of three nearly identical tests to assess the repeatability of the APEL 4PJM system. Though the initial gas fraction of the February 13, 2004, test was slightly lower than the other two, the three tests show very similar results.

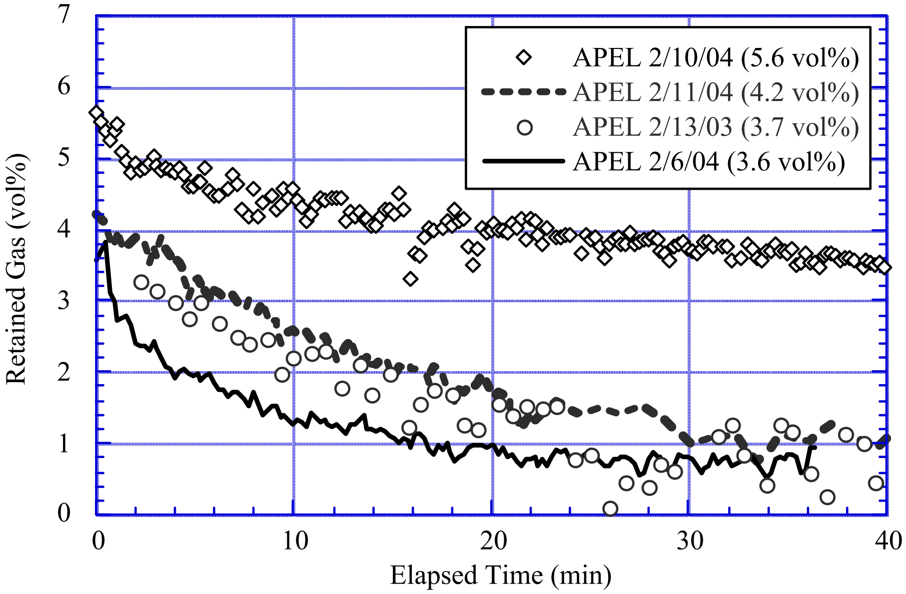

Figure 6.14. Effect of Initial Gas Fraction in Four APEL 4PJM Tests

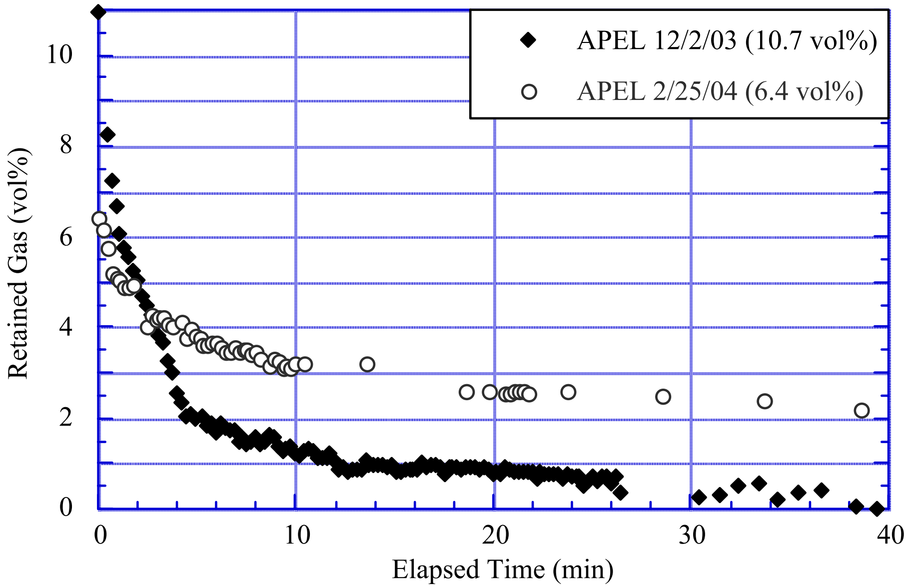

Figure 6.15. Effect of Initial Gas Fraction in 12/2/03 and 2/25/04 APEL 4PJM Tests

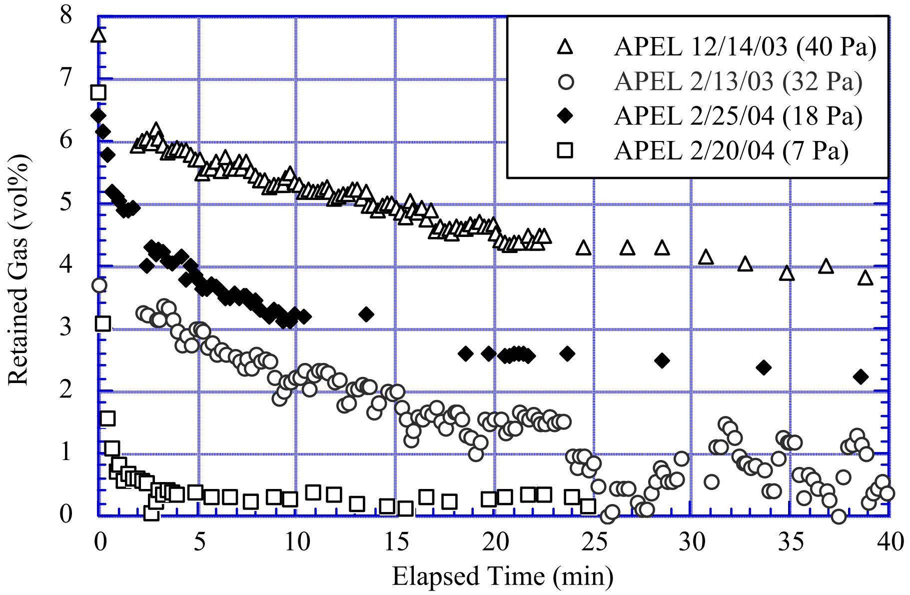

Figure 6.16. APEL 4PJM Gas-Release Tests: Effect of Simulant Rheology

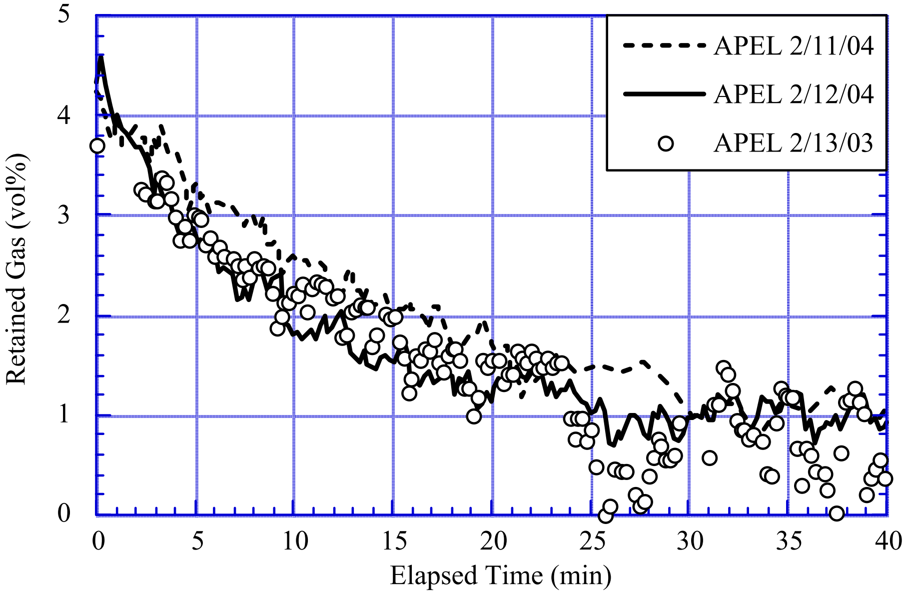

Figure 6.17. APEL 4PJM Gas-Release Tests: Repeatability Series

6.4 Uncertainty Analysis

The data from gas-release tests are subject to the same uncertainties as already described for gas-holdup tests in Section 5.3. Because the simulant level decreases as gas is released, a gas-release test is at least conceptually more influenced by simulant deposition or cake out on tank walls and structure that would increase the apparent gas release. This effect may be strong enough to produce the negative final gas-volume fractions at the end of several tests, as described at the beginning of Section 6. The average of the adjustments made to the five tests is 0.2 vol%. However, this minimum is only enough to bring the final gas fraction up to zero or a perfectly complete release. It is likely that less than 100% of the gas is actually released, and the adjustments should be a little larger.

Another complication that affects gas-release tests is the transition from static conditions during gas growth to PJM operation when the gas release is initiated. Gas accumulation typically occurs with the PJMs vented so that the level inside and outside the PJMs is approximately equal. The PJMs are filled to begin the first cycle, and the minimum simulant surface level following this first fill is the reference for calculating the gas released during subsequent cycles. The problem is that the initial gas-volume fraction calculated from this first minimum level ranges from 0.5 vol% greater to 0.8 vol% less than the static minimum. It is not known whether this is a result of gas release during the initial PJM filling or of mismatched PJM versus tank levels during the static phase or both.

The scatter in the calculated gas-volume fractions was typically within ± 0.2 vol%, comparable to that observed in the gas-holdup tests. However, even with this relatively small scatter, the behavior of the data in the initial part of the gas release was sometimes erratic. Apparently, the vertical movement of gas and the changing flow patterns in the growing PJM cavern in the first few cycles obscures the actual gas release. An example is the APEL 4PJM test on 12/14/03, shown in Figure 6.18. Following the extremely large first-cycle gas release of almost 2 vol%, the gas fraction appears to increase about 0.3 vol% over the first 3 minutes before starting the expected exponential decay. Other examples include LS sequence 14, run 4 and sequence 15, run 2 shown in Figure 6.7. Unfortunately, analysis of the first several PJM cycles, where uncertainty is highest determines the primary time constant for the gas release.

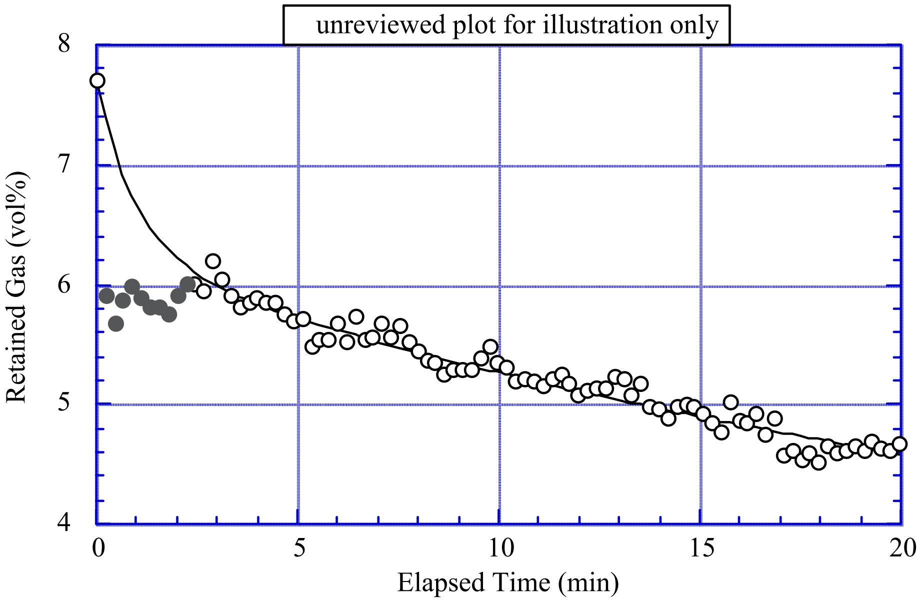

Figure 6.18. Example of Initial Release Behavior—APEL 4PJM, 12/14/03

Overall, combined effects of all sources of error and uncertainty allow the residual gas fraction at the end of a gas-release test to be estimated to ±0.5 vol% (an estimate of zero could indicate +0.5 vol% residual gas). The gas fraction at any time during the gas release probably has the same magnitude of uncertainty. However, the time constant deduced from the first portion of the gas release can be estimated only to within about a factor of 2, as discussed in Section 6.5.

6.5 Data Analysis

This section presents the derivation and application of a gas-release model based on the bubble migration theory of Section 2 but extended to capture additional phenomena evidenced by the test data. Because the analysis in Section 6.2 confirmed that the gas-generation rate is small for the gas-release tests, the rate of change in retained gas volume can be expressed, following Section 2, as

$$\frac{d\alpha}{dt} = -\frac{U_R}{H}\alpha = -\frac{\alpha}{\tau_R} \tag{6.12}$$

where τ_R is a time constant equal to H/U_R. Integrating Eq. (6.12) with $\alpha(t = 0) = \alpha_0$ and defining the peak release rate, $R_0 = \alpha_0/\tau_R$, gives the exponential decay equation and its derivative, respectively, as

$$\alpha(t) = R_0 \tau_R e^{-t/\tau_R} \tag{6.13}$$

$$\frac{d\alpha(t)}{dt} = -R_0 e^{-t/\tau_R} = -\frac{\alpha(t)}{\tau_R} \tag{6.14}$$

The product $R_0\tau_R$ is also the total gas release, i.e., the difference between α_0 and $\alpha(t=\infty)$.

Because gas is released by at least two processes (direct mobilization and erosion of an unmobilized region), each proceeding at different rates, the gas-release test results appear to follow more than one time constant. To analyze the data, we assume that the gas release is the combination of three release rates of the form of Eq. (6.14), each with a different peak rate and time constant that may be written as

$$\frac{d\alpha(t)}{dt} = -\left[R_S e^{-t/\tau_S} + R_M e^{-t/\tau_M} + R_L e^{-t/\tau_L}\right] \tag{6.15}$$

where the subscripts refer to a short, medium, and long time constant. This model represents either three independent regions of slurry, each releasing gas with at different time constant, or one well-mixed region (with the short time constant) that erodes two other non-releasing regions at different rates. Integrating Eq. (6.15) with $\alpha(t=0) = \alpha_0$ yields

$$\alpha(t) = R_S\tau_S e^{-t/\tau_S} + R_M\tau_M e^{-t/\tau_M} + R_L\tau_L e^{-t/\tau_L} \tag{6.16}$$

or, because $R_S\tau_S + R_M\tau_M + R_L\,\tau_L = \alpha_0$,

$$\alpha(t) = \alpha_0\left(F_S e^{-t/\tau_S} + F_M e^{-t/\tau_M} + F_L e^{-t/\tau_L}\right) \tag{6.17}$$

where the $F_k = R_k\tau_k/\,\alpha_0$ are the fractions of the total gas release accounted for by each release rate. Assuming the initial gas fraction is uniform and the hydrostatic pressure is not large, F_k can also approximate the fraction of the total volume subject to each of the release rates.

The six constants, R_S, τ_S, R_M, τ_M, R_L, and τ_L, were determined by minimizing the sum of the squares of difference between Eq. (6.16) and the measured gas-volume fractions, as was done for the gas-holdup tests in Section 5.2. The short time constant depends strongly on the first few data points and therefore has a relatively large variability. The variability is exacerbated by the already high uncertainty in the first few data points resulting from the transition from static conditions to fluctuating levels of the PJM drive cycle. In some cases, the error minimization solution did not find a plausible short time constant, and a value was assigned manually that produced a visually satisfactory fit. In other cases, ignoring a few of the early data points in computing the error produced a good solution. The fit was performed only for the period in which the mixing system was operating at specified conditions. It does not include the post-test degassing period of aggressive sparging and PJM overblows.

The three-rate model of Eq. (6.16) fits the data extremely well, which is not surprising with so many adjustable parameters. In fact, many tests can be fit reasonably well with only two rates (four constants). A few rapid releases require only the short time constant release, and some with a very persistent residual are dominated by the long time constant. Figure 6.19 illustrates how the three rates add together, and Figure 6.20 shows examples of how the model fits the data for two of the scaled prototype tests.

The six constants and the fraction of total release for all the tests are listed in Table 6.3. The three time constants fall into the same ranges for all the tests. The short time constant, corresponding closely to the value of A_R derived in Section 6.2, ranges from 0.5 to 5 minutes, mostly less than 1 minute, the medium value generally from 4 to 50 minutes, and the long time constant from 50 to 1,440 minutes (1 day) with most around 100 minutes. The three peak gas-release rates fall into similar nominal ranges, 0.4 to 20 vol%/min, 0.03 to 0.4 vol%/min, and 0.001 to 0.05 vol%/min.

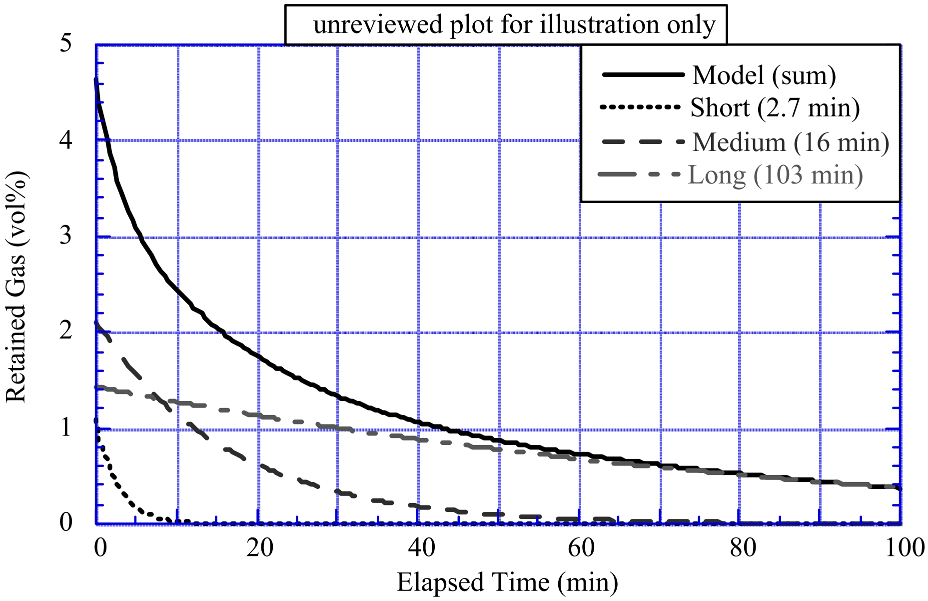

Figure 6.19. Illustration of the Components of the Three-Rate Release Model

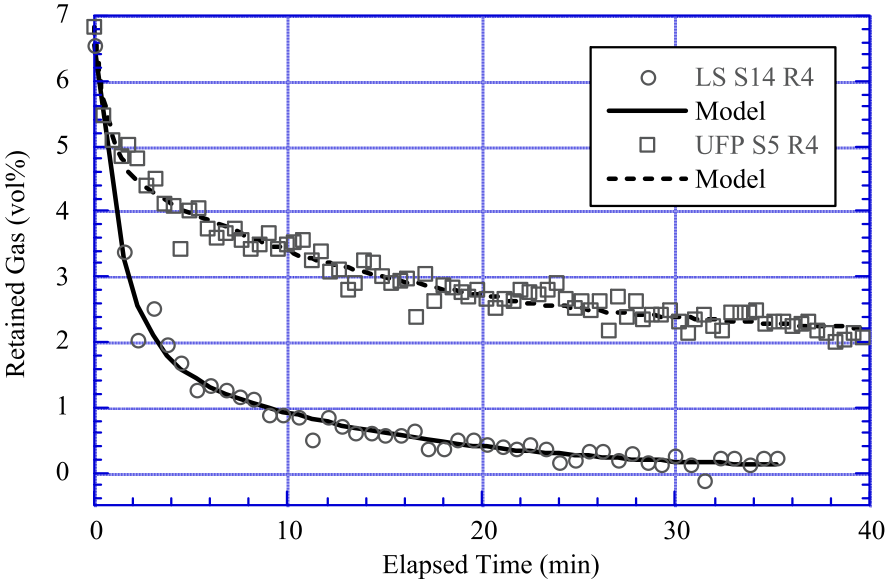

Figure 6.20. Example of the Model Fit to LS Sequence 14, Run 4 and UFP Sequence 5, Run 4 Data

Table 6.3. Gas-Release Model Fits

Test/Date	R_S (vol%/min)	τ_S (min)	F_S %	R_M (vol%/min)	τ_M (min)	F_M %	R_L (vol%/min)	τ_L (min)	F_L %
Lag Storage									
S14 R2 2/6/04	4.5	0.3	48	0.37	4.3	52	-	-	-
S14 R4 2/6/04	3.3	1.3	68	0.17	12	32	-	-	-
S15 R2 2/9/04	2.0	0.7	32	0.34	9	68	-	-	-
S15A R4 2/14/04	1.0	2.7	51	-	-	-	0.028	97	49
UFP									
S5 R2 2/12/04	0.46	3.3	47	-	-	-	0.03	50	53
S5 R4 2/12/04	3.1	0.6	29	0.20	13	40	0.002	1440	31
S6 R2 2/13/04	0.37	5.9	48	-	-	-	0.046	53	52
S6 R4 2/13/04	0.93	4.2	57	-	-	-	0.030	92	43
336 4PJM									
12/12/03	3.7	0.86	36	0.06	30	20	0.02	220	44
3/23/04	0.78	1.1	26	*0.004*	*73*	*8*	0.004	520	66
3/25/04	0.4	1.9	35	-	-	-	0.001	1100	65
7/20/04	0.19	2.1	21	-	-	-	0.005	280	79
7/23/04	0.88	1.3	29	0.02	36	18	0.005	670	89
SRNL 4PJM									
12/12/03	1.5	3.9	57	0.18	24	43	-	-	-
2/27/04	1.3	1.7	20	0.20	46	80	-	-	-
APEL 4PJM									
12/2/03	5.1	1.7	77	0.17	13.6	21	-	-	-
12/14/03	0.96	2.1	25	-	-	-	0.06	98	75
1/26/04	0.96	2.1	72	-	-	-	0.03	30	28
2/6/04	0.5	3.9	58	0.03	43	42	-	-	-
2/10/04	0.36	3.0	19	-	-	-	0.03	155	81
2/11/04	-	-	-	0.23	15	82	0.001	1440	18
2/12/04	-	-	-	0.40	8.2	76	0.002	585	24
2/13/04	-	-	-	0.21	16	100	-	-	-
2/18/04	3.3	1.6	100	-	-	-	-	-	-
2/20/04	25	0.25	92	0.03	19	8	-	-	-
2/25/04	1.1	2.8	49	-	-	-	0.024	134	51

The uncertainty involved in determining the initial time constants is illustrated by the three identical APEL 4PJM gas-release tests on February 6, 11, 12, and 13, 2004. The initial time constants range from 4 to 16 minutes and the gas-release rates from 0.2 to 0.5 vol%/min. This indicates an uncertainty of a factor of two in the time constant defining the initial decay curve.

The relative fractions of the total release represented by each of the three rates and time constants reveal the overall gas-release behavior of a test. A high percentage of the long time constant indicates a long, slow release (e.g., 336 March and July tests shown in Figure 6.14). If at the same time the medium rate has a zero fraction, there may be a fast, deep initial gas release followed by a persistent residual gas holdup (e.g., UFP tests, Figure 6.8). On the opposite end of the spectrum, if the short time constant dominates with only a small or zero fraction of medium or long time constant contribution, the gas release will be quick and complete (e.g., APEL 4PJM 2/20/04 test shown in Figure 6.16). If all three rates have an approximately equal contribution, the gas release is steady but relatively slow (e.g., UFP sequence 5, run 4 in Figure 6.8, 336 12/13/03 test shown in Figure 6.14).

As yet, the physical phenomena represented by the three distinct gas-release rates have not been positively determined. However, as mentioned above, the evidence suggests that the lower gas-release rates and longer time constants are the result of an erosion process where a region of less mobilized simulant is slowly subsumed into or recycled with the well-mixed PJM cavern volume. Gas releases with long time constants were typically observed in the relatively tall and narrow UFP tank and in the 336 4PJM system. In the latter, notes in the test laboratory record book (LRB) describe regions between the PJMs and the tank wall that appeared stagnant during the gas-release tests. Similar gas releases were common with the stiffer simulant (30 to 40 Pa Bingham yield stress) in the dimensionally similar APEL 4PJM tank. At the same time, gas releases were clearly more rapid and complete in the LS sequence 14 tests, in which half of the PJM nozzles were angled upward to enhance mobilization in the upper part of the tank, than in the companion LS sequence 15 tests where all nozzles were angled down.

6.6 Conclusions

The data presented in this section show that gas-release behavior is influenced by simulant rheology (Figure 6.16), gas-bubble size as deduced from the more rapid gas releases in tests that had accumulated gas overnight (Figures 6.7 and 6.8), and somewhat by initial gas content (Figure 6.15). Aggressive sparging was effective in releasing residual retained gas at the end of a test (Figures 6.9 and 6.10), but only partial sparging was used in the scaled prototype vessel tests, so the full effect of sparging was not observed. Gas-release behavior appears to scale reasonably well in the few tests that cover the full range of geometric scales (Figures 6.11 to 6.13). Gas-release behavior is also quite repeatable, as demonstrated in repeated tests within a test stand (Figure 6.17) and as generally characterized by the gas-release model.

Gas generation was negligible during the gas-release tests (Section 6.2), even those conducted less than an hour after a gas-holdup test. This is a major difference from the plant-scale situation, where continuous gas generation could aggravate the stubborn residual retained gas fraction observed in so many release tests. The cause for this residual retained gas is not well understood, but the evidence points to an incomplete mobilization of the simulant above the PJM cavern, possibly aggravated by the buoyancy of the gas-bearing simulant. Probably due to these or similar effects, gas release during holdup tests, which started from a degassed state, differs from the release of gas accumulated over a quiescent period. Even partial sparging tends to reduce the difference and, as is shown in Section 7, full sparging by itself can be very effective at releasing gas.

7.0 Sparger-Induced Gas-Release Tests

Fifteen multitube sparger gas-release tests were performed between June 3 and July 15, 2004, in PNWD's CBT in the 336 Building. Sparger air flow rates and initial retained gas fractions (produced by O_2 generated by H_2O_2 decomposition) were the primary parameters varied during these tests. A complete description of these tests and their results is provided in WTP-RPT-129.[a] Several sparger-only gas-release tests were also conducted in the scaled prototype LS and UFP vessels in the APEL in February 2004.

This section describes the results of analyzing sparger-induced gas-release behavior using the techniques derived in Sections 2, 5, and 6. The test systems are described in Section 7.1, and the results are presented in Section 7.2. Sources of uncertainty are discussed in Section 7.3, data analysis results are summarized in Section 7.4, and the summary and conclusions are given in Section 7.5.

7.1 Sparging Test Description

Sparger-induced gas-release tests followed procedures similar to those used in PJM-induced gas-release tests. Decomposing H_2O_2 generated the retained gas that was to be released in the test (see Section 2). The H_2O_2 was injected while the simulant was mixed with PJMs (including several cycles of PJM overblow) to provide approximately uniform gas generation. After adding a predetermined mass of H_2O_2 to give the desired initial retained gas-volume fraction, the mixing system was shut down to allow gas to accumulate in the simulant.

Retained gas buildup and release was quantified by observing changes in the height of the simulant surface level. The test began by starting the preset sparger tube air flow after the static surface level became steady, indicating that H_2O_2 decomposition was essentially complete. Likewise, sparging was terminated when the dynamic surface level (disturbed by sparging) decreased to an approximately steady value, indicating that gas release had effectively ceased. After sparging was terminated, the simulant was degassed by further sparging and PJM operation, including overblows. In the CBT, this step and initial addition of H_2O_2 required pumping the simulant to another tank and back.

The total absolute gas-retention and release volumes, excluding sparger holdup, were calculated from manual simulant surface-level measurements before and after sparging. Retained gas-volume changes were inferred from simulant volume changes computed from these level changes using an empirical model based on data from a water-fill test. The simulant level at the end of a test after degassing was taken as the zero-gas reference.

During sparging, air bubbles in transit create an essentially constant "sparger holdup" on the order of 0.1 to 0.5 vol%, depending on the number of spargers and the air flow rate. This sparger holdup adds to

---

[a] Poloski AP, S.T Arm, J.A. Bamberger, B. Barnett, R Brown, B.J. Cook, C.W. Enderlin, M.S. Fountain, M Friedrich, B.G. Fritz, R.P. Mueller, F Nigl, Y Onishi, L.A. Schienbein, L.A. Snow, S. Tzemos, M. White, and J.A. Vucelik. 2005. *Technical Basis for Scaling of Air Sparging Systems for Mixing in Non-Newtonian Slurries*. WTP-RPT-129 Rev 0, Battelle—Pacific Northwest Division, Richland, WA.

the retained gas created by H_2O_2 decomposition and is included in the transient analysis in Section 7.4. Sparger test data do not show evidence of long-term holdup after sparging ceases.

In addition to the different dimensions and configurations of the test vessels themselves, the primary variables in the sparger gas-release tests were the number and location of spargers activated, the air flow rates, and the initial gas fraction. The simulant rheological properties also varied somewhat over the test period, generally becoming stiffer as water evaporated into the sparge air. The test vessels and mixing systems are described in Section 4.

7.1.1 CBT Tests

The CBT in the 336 Building used nine spargers arranged in two concentric rings of four each plus a central tube, all spaced so that each one's predicted zone of influence (ZOI) overlapped well into the region of bubbles (ROB) of the others. Sparge tube ends were 6 inches above the tank floor. Sparger air flow rates were set to match the full-scale volume flow at the hydrostatic pressure of the submerged sparge tube exit. Because the simulant depth in the test vessel is less than full-scale, the nominal test air flow rate was about two-thirds of full-scale flow rate at the surface. One test was run at about 1.5 times the nominal air flow rate [1.5 = 1/(2/3)], thereby simulating surface conditions at the full scale to allow assessment of aerosol generation. Several tests were also conducted at one-third of nominal air flow.

Because the CBT had no mixing equipment other than spargers, the H_2O_2 was added to the simulant in the supernatant tank where the four-PJM system could mix the bottom region. The H_2O_2-laden simulant was then pumped into the CBT and allowed to fully decompose, as indicated by the simulant surface level in the tank reaching a steady value. At that point, sparging began at a preset air flow rate and continued until the surface level again became steady, indicating that essentially all releasable gas had left the simulant. To measure the amount of gas not released by sparging, the simulant was again pumped over to the supernatant tank where it was thoroughly degassed by PJM mixing and a series of PJM overblows before being transferred back to the CBT for a final surface-level reading.

Though simulant is transferred back to the CBT from the supernatant tank after H_2O_2 addition and PJM degassing were targeted to match the measured initial pretest tank weight, the actual transfers typically differed by 100 pounds (~0.1% of total) or less. The simulant volume calculations were adjusted for small differences in actual weight using a measured simulant density (1.17 g/mL). The simulant rheology was initially adjusted to a nominal 30-Pa Bingham yield stress. During a month of sparging tests, evaporation gradually stiffened the clay to a Bingham yield stress of 40 Pa. The results of the CBT sparging tests that are analyzed in this section are summarized in Table 7.1.

7.1.2 LS and UFP Scaled Prototype Tests

The LS test vessel has eight sparger tubes placed around the seven outer PJMs in a single ring. The UFP test vessel uses four spargers, three spaced around the three outside PJMs plus a single center tube adjacent to the central PJM. Because both UFP and LS tanks were also served by PJMs, it was not necessary to transfer simulant to another tank to mix in H_2O_2 or to correct for weight discrepancies between transfers. The simulant used in UFP and LS tests had a Bingham yield stress of 36 Pa that stayed constant through both tests.

Table 7.1. 336 CBT Sparging Gas-Release Tests

Test ID[(a)]	Air Flow (acfm)	Simulant Volume (L)	Yield Stress (Pa)	Initial Gas Fraction[(b)] (vol%)	Comment
CBT-040603	204.2	24,000	28	1.5	Full air flow
CBT-040608	202.1		29	2.0	
CBT-040609	202.6		30	1.7	
CBT-040614	203.3		32	1.4	
CBT-040615	206.0		32	1.7	
CBT-040707	171.3		35	1.2	
CBT-040715	206.3		40	0.8	
CBT-040611	68.2		32	2.4	1/3 air flow
CBT-040616	57.8		34	0.7	

(a) Test ID is the date, YYMMDD.

(b) Gas-volume fractions include sparger holdup of 0.1 to 0.5 vol% and assume zero gas retention at the end of the test after PJM degassing.

The LS and UFP tests generally applied partial sparging, where not all the tubes were used, as opposed to full sparging in the CBT, where air was always supplied to all tubes though at different flow rates. Also, instead of running each test with a single configuration like the CBT sparging tests, the LS and UFP sparging tests were generally conducted in steps with increasing numbers of sparge tubes active. For example, UFP sequence 5, run 5 began with sparging only through the center tube. The second step exercised the three outer sparge tubes, and the third step added PJMs. Though these steps were done in a single continuous operation, they are analyzed and presented separately as runs 5a, b, and c, respectively. Similarly, there were two steps in LS sequence 15, run 5. All the LS and UFP tests are listed in Table 7.2.

Table 7.2. UFP and Lag Storage Sparging Gas-Release Tests

Test ID	Total Air Flow (acfm)	Simulant Volume (L)	Yield Stress (Pa), Consistency (cP)	Initial Gas Fraction[(a)] (vol%)	Comment
LS S15A R5a	~14	2,935	35, 26	5.1	Tubes 1, 3, 5 and 7
LS S15A R5b	~24			4.7	All eight tubes
UFP S5 R5a	~3	633 (H/D=1.4)	36, 19-20	5.4	Center tube only
UFP S5 R5b	~9			5.0	Outer tubes (1, 2, 3)
UFP S5 R5c	~9			1.5	Outer tubes (1, 2, 3) plus PJMs
UFP S6 R5b	~6	833 (H/D=1.8)		5.2	Outer tubes (1, 2, 3)

(a) Gas-volume fractions include sparger holdup of 0.1 to 0.5 vol% and assume zero gas retention at the end of the test after PJM degassing.

7.2 Test Results

An example of the gas-release behavior of full-flow sparging tests in the CBT is given by the plot of gas-volume fraction versus time for the test performed on July 7, 2004 (Figure 7.1). This test began with 1.2 vol% retained gas, essentially all of which was released during the test. The initial spike in gas volume to about 1.8 vol% is caused by the rapid formation of short-term gas holdup, approximately 0.7 vol% in this test, caused by injection of the large bubbles. These bubbles rapidly leave the simulant when sparging ceases, and the retained gas volume drops equally rapidly to zero in this case. If no gas were released, the apparent retained gas fraction would rise by the amount of the sparger holdup when sparging started and drop back by an equal amount when sparging stopped. However, retained gas is released during sparger startup and reduces apparent initial sparger holdup to less than the drop in calculated gas fraction when sparging ceases. The UFP and LS tests showed similar phenomena, although lower air flow rates and fewer tubes in operation produced less sparger holdup.

Gas-release rate analysis begins at the initial peak of the gas-volume fraction after sparger holdup forms and typically covers a 20- to 30-minute period thereafter, ending long before the spargers shut down (see Figure 7.1). Hence, the plots presented in this section do not explicitly show the effect of sparger holdup forming initially or being released at the end.

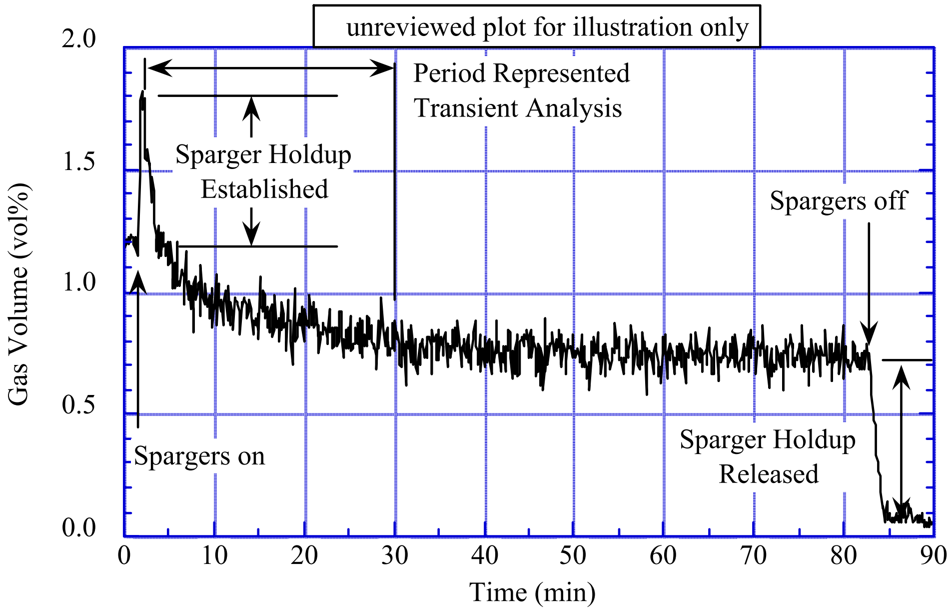

Figure 7.1. Example of Sparger-Induced Gas Release for CBT Test on 7/7/04

7.2.1 CBT Test Results

The gas-release rate depends on the total sparger flow rate. Figure 7.2 compares a full air flow (206 acfm) test on 6/15/04 with a one-third-flow test (68 acfm) on 6/11/04. The initial gas-volume fractions were of similar magnitude (2.1 and 2.6 vol% including sparger holdup) and simulant rheology was essentially the same in both tests. The full-flow results clearly release essentially all the retained gas in about 5 minutes. The one-third-flow test releases much more slowly and, even accounting for 0.5 vol% sparger holdup, about 1 vol% gas remains after 20 minutes.

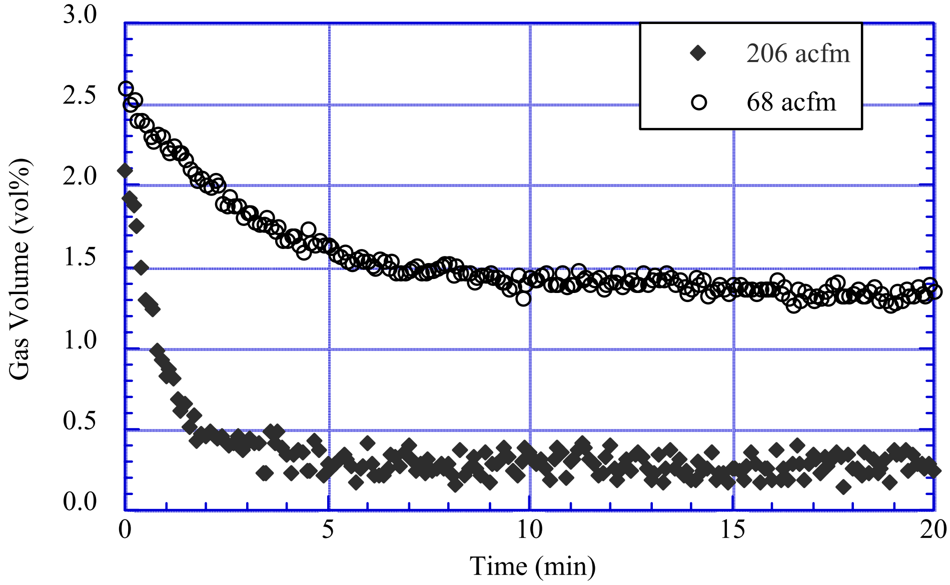

Figure 7.2. Effect of Sparger Air Flow (CBT 6/15 and 6/11)

All the full air flow tests in the CBT showed the same rapid, almost complete gas release regardless of the initial gas fraction. The 6/15/04 test, with over 2 vol% initial gas fraction, is compared with an otherwise similar test on 7/15/04 with only 0.5 vol% initial gas fraction in Figure 7.3. [a] Both release essentially all their gas (except for sparger holdup) in about 5 minutes. The higher the gas content, the higher the release rate.

(a) These initial values include sparger holdup. However, in the 7/15 test, a small gas release apparently occurred before sparging started that lowered the initial value, including sparger holdup, to below the initial gas fraction shown in Table 7.1.

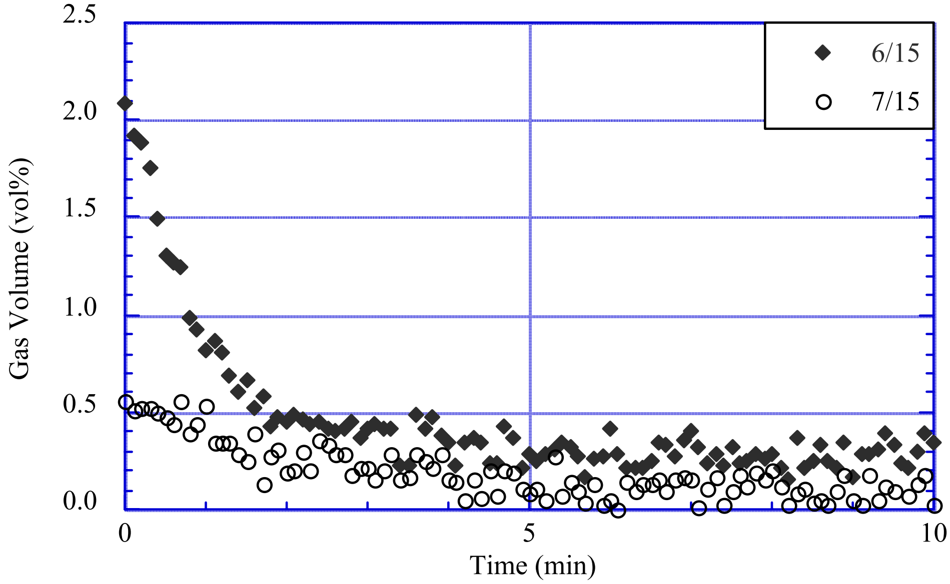

Figure 7.3. Effect of Initial Gas-Volume Fraction (CBT 6/15 and 7/15)

7.2.2 Lag Storage and UFP Sparger Test Results

The difference between partial and full sparging is even more dramatic than a high or low air flow rate through all the spargers. Figure 7.4 compares the results of LS sequence 15A, run 5a, where every other sparge tube was active (four of eight), with run 5b, where all spargers were operating. It is obvious that the partial sparging of run 5a was not effective at releasing gas, while run 5b looks like the full-flow CBT test. The decrease in gas-volume fraction at 15 minutes in run 5b occurred as sparging was shut down, and sparger holdup dissipated.

The UFP tests repeat this trend. UFP sequence 5, runs 5a, b, and c, each represent an increase in mobilization effectiveness and therefore improved ability to release gas, as shown in Figure 7.5. Only the center sparge tube is operating in run 5a, leaving the simulant outside the PJMs essentially undisturbed and the gas release barely perceptible. The three outer spargers of run 5b are much better but still leave a rather large residual retained gas “heel” that is released by adding PJM mixing in run 5c.

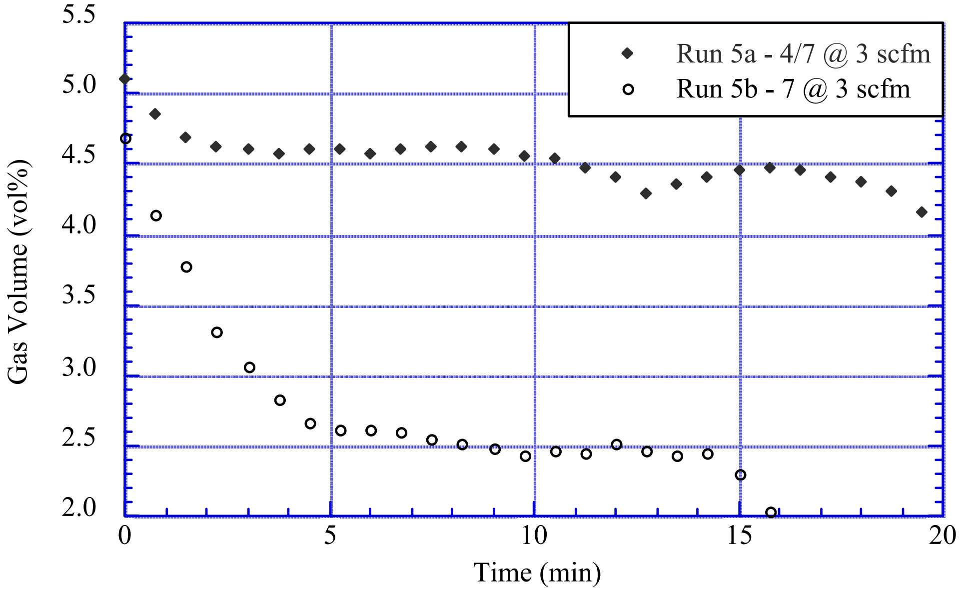

Figure 7.4. Sparge-Induced Gas Release for Lag Storage Sequence 15A, Run 5

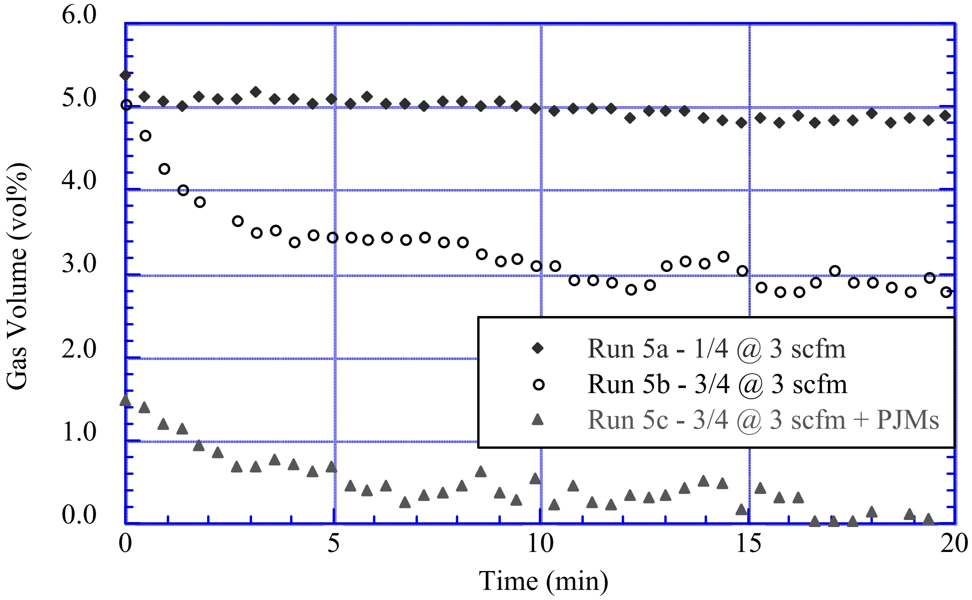

Figure 7.5. Sparge-Induced Gas Release from UFP Sequence 5, Runs 5a, b and c

7.3 Uncertainties

The uncertainties in the CBT tests, which include many of the issues described in the PJM holdup and release tests in Sections 5 and 6, are discussed in detail in WTP-RPT-129.(a) In these tests, the ultrasonic level instruments exhibited a random drift that sometimes became significant over periods approaching an hour. Thus, though the decreasing average surface level showed the progress of the release quite clearly in the early stages, the uncertainty in the absolute gas-volume fraction calculated from measured surface level changes during sparging was on the order of ±0.5vol%.

7.4 Data Analysis

The transient gas-volume fraction during gas release, $\alpha(t)$, was fit to the exponential bubble-rise gas-release model described in Section 2, similar to the application derived in Sections 5 and 6. Sparging tests were fit with two time constants as expressed by

$$\alpha(t) = R_S \tau_S e^{-t/\tau_S} + R_L \tau_L e^{-t/\tau_L} \tag{7.1}$$

where R_S, τ_S, R_L and τ_L are the "short" and "long" gas-release time constants (min), respectively. Because $\alpha_0 = R_S\tau_S + R_L\tau_L$, Eq. (7.1) can also be written as

$$\alpha(t) = \alpha_0 \left(F_S e^{-t/\tau_S} + F_L e^{-t/\tau_L} \right) \tag{7.2}$$

where $F_S = \dfrac{R_S \tau_S}{\alpha_0}$ and $F_L = \dfrac{R_L \tau_L}{\alpha_0}$ are the fractions of the gas release described by the short and long time constants, respectively. Because the long time constant portion includes the transient sparger holdup, it does not accurately represent "sparger heel." In the CBT, after subtracting the effects of sparger holdup, the data indicate that the sparger heel volume was negligible. This is not true for the LS and UFP tests, however, especially with only a few spargers operating.

Figure 7.6 presents the data and curve fit for the same July 7, 2004, CBT test shown in Figure 7.1. Most of the sparging tests show an initial rapid release with a short time constant over the first 10 minutes, followed by a much slower, almost constant, gas-release rate with a much longer time constant (several hours). Some tests simply stop releasing gas after the initial stage.

(a) Poloski AP, S.T Arm, J.A. Bamberger, B. Barnett, R Brown, B.J. Cook, C.W. Enderlin, M.S. Fountain, M Friedrich, B.G. Fritz, R.P. Mueller, F Nigl, Y Onishi, L.A. Schienbein, L.A. Snow, S. Tzemos, M. White, and J.A. Vucelik. . 2005. *Technical Basis for Scaling of Air Sparging Systems for Mixing in Non-Newtonian Slurries*. WTP-RPT-129 Rev 0, Battelle—Pacific Northwest Division, Richland, WA.

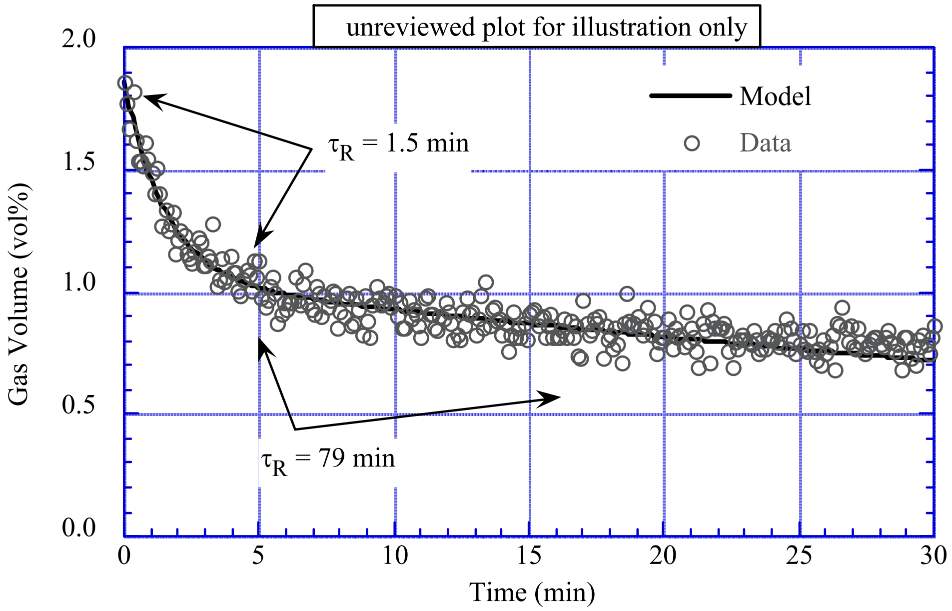

Figure 7.6. Gas-Release Analysis Example for CBT Test, 7/7/04

The results of applying this analysis to all the sparger tests are given in Table 7.3. The short time constant depends strongly on the first few data points and therefore has a relatively large variability.

Table 7.3. Sparging Gas-Release Test Results

Test ID	Air Flow (scfm)[(a)]	Gas Fraction[(b)] (vol%)		Release Time Const. (min)		Comment
		Initial	Final	Fast	Slow	
LS S15A R5a	~14	5.1	4.0	0.6	218	Tubes 1, 3, 5 and 7
LS S15A R5b	~24	4.7	2.4	2.4	1440	All eight tubes
UFP S5 R5a	~3	5.4	4.8	~6	1440	Center tube only
UFP S5 R5b	~9	5.0	2.8	1.3	83	Outer tubes (1, 2, 3)
UFP S5 R5c	~9	1.5	0	5.6	1440	Outer tubes (1, 2, 3) plus PJMs
UFP S6 R5b	~6	5.2	2.7	2.2	228	Outer tubes (1, 2, 3)
CBT-040603	204.2	1.5	-0.1	0.8	-	Full air flow
CBT-040608	202.1	2.0	0.2	0.8	88	
CBT-040609	202.6	1.7	0.1	0.9	54	
CBT-040614	203.3	1.4	0.4	1.0	241	
CBT-040615	206.0	1.7	0.2	0.9	1440	
CBT-040707	171.3	1.2	0	1.5	79	
CBT-040715	206.3	0.8	0	2.2	1440	
CBT-040611	68.2	2.4	0.7	2.8	218	1/3 air flow
CBT-040616	57.8	0.7	-0.1	6.3	-	

(a) LS and UFP sparger flows are given as approximate scfm (~2 to ~3 scfm per tube). The actual flow (acfm) at the tube nozzles would be 15 to 20% less.

(b) Gas-volume fractions include sparger holdup of 0.1 to 0.5 vol% and assume zero gas retention at the end of the test after PJM degassing.

However, regardless of initial gas fraction or the relatively small differences in simulant rheology, full flow, full-coverage sparging seems to consistently result in a gas-release time constant of 1 to 2 minutes. Partial or lower air flow sparging gives time constants of 4 to 10 minutes with a slower-releasing residual. The range of test conditions is too narrow to develop an empirical correlation for the effective bubble rise velocity as a function of test parameters, as was done in Section 5. Nevertheless, the overall results clearly show that sparging is very effective at releasing retained gas.

7.5 Summary and Conclusions

Within the test uncertainty, full-flow sparging released essentially all of the releasable gas over a period of about 10 minutes in every test. Application of the basic bubble-rise gas-release model from Section 2 gives gas-release time constants between 0.9 and 1.5 minutes for the CBT tests and 0.9 to 2.4 minutes for more-or-less full sparging in UFP and LS tests.

Tests using sparging at one-third of full flow in the CBT tests required a longer time, 40 to 60 minutes, compared with approximately 10 minutes for the full-flow tests. Time constants for the one-third-flow tests ranged from 3 to 10 minutes compared with about 1 minute for the full-flow tests. Partial sparging in the UFP and LS tests resulted in incomplete gas release.

8.0 Gas Holdup in Water, Kaolin-Bentonite Clay, and Simulated HLW Matrixes

Hydrogen gas was not used in the majority of gas-retention and release tests because of the experimental difficulties associated with generating H_2 *in situ* in relatively large quantities and the potential safety issues. Therefore, as described in this section, bench-scale tests were completed to compare the relative gas holdup of O_2, H_2, and other gases in various simulants. Section 8.1 provides a test description, and Section 8.2 describes how the data were analyzed and interpreted. The results from water and clay matrixes are presented in Sections 8.3 and 8.4, respectively. Section 8.5 presents the results of a parametric study statistically designed to determine correlations for the coefficient and exponent in the holdup-velocity correlation.

8.1 Test Description

The gas-holdup apparatus consisted of a Perspex column of 15 cm (6 inches) OD and 183 cm (6 ft) high that was filled to a nominal height of 150 cm, providing a volume of 20 L. Gas was introduced into a diffuser at the column base through a rotameter and pressure transducer. Hydrostatic pressure within the column was measured by mounting two pressure transducers through the column wall, 58 cm and either 134.5 or 108.5 cm from the base. The pressure transducers and thermocouples located in the fume hood and column were configured into a data acquisition system.

Water, kaolin-bentonite clay, and simulated AZ-101/102 HLW matrixes were tested in the gas-holdup apparatus with H_2, Ar, O_2, and air at up to five different flow rates. The matrixes were adjusted with sodium nitrate and an antifoaming agent (AFA), product Q2-3183A manufactured by Dow Corning. Table 8.1 summarizes the conditions tested. The gas flow rate was incrementally reduced, allowing

Table 8.1. Gas-Holdup Test Conditions

Matrix	Sodium nitrate concentration (M)	AFA concentration (ppm)
Water	0	100
	0.5	0
	0.5	100
	0.1	0
Kaolin-bentonite clay	0[(a)]	0[(a)]
	0.1	10
	0.01	100
	0.01	10
	0.1	100
	0	100
	0.1	0
Pretreated AZ101/102 HLW simulant	0	0
	0	10
	0	100

(a) Two clays containing no sodium nitrate or AFA but of two rheologies were tested.

15 minutes for achieving a steady state between each reduction. It was found that increasing the flow rate incrementally gave rise to anomalous results, possibly because the slurry was insufficiently sheared.

8.2 Data Analysis

Gas holdup was calculated from the hydrostatic pressures recorded by the pressure transducers. The first step was to calculate the pressure head in the column (P_0) at zero gas flow from the differential pressure between the two pressure transducers (ΔP_{bt}) from the equation:

$$P_0 = \frac{d_{db}}{d_{bt}} \times \Delta P_{bt} + P_b \tag{8.1}$$

where d_{db} is the distance between the diffuser and bottom pressure transducer, d_{bt} is the distance between the top and bottom pressure transducers, and P_b is the pressure recorded by the bottom pressure transducer. The gas holdup (α_i, the volume of retained gas as a fraction of the gas-free slurry) was then calculated by comparing the change in hydrostatic pressure between the diffuser and top pressure transducer upon gas introduction by the equation:

$$\alpha_i = 1 - \left(\frac{P_0 - P_{tg}}{P_0 - P_t} \right) \tag{8.2}$$

where P_{tg} and P_t are pressures recorded by the top pressure transducer with and without gas, respectively.

An error propagation analysis was performed by considering the calibration accuracy of the transducers and rotameter and the variability in the recorded data. The gas superficial velocity was corrected to the rotameter calibration conditions of 1 atm and 21.65ºC. The data were fit to power law equations of the form $\alpha_i = A \times u^n$, where u is the superficial velocity in cm/s. Residual square values were typically greater than 90%, indicating that at least 90% of the variability in the data is due to superficial velocity.

8.3 Water Matrix Test Results

Appendix B provides the gas-holdup data upon which the following discussion is based. Figure 8.1 illustrates the holdup of the four gases (O_2, H_2, Ar, and air) in water. Holdup appears to increase in the order of Ar, H_2, and air/O_2. However, the equation $\alpha_i = 0.0492 \times u^{0.7714}$ can be fit to the results from all gases with a residual square value of 0.95, indicating insignificant difference in holdup between the gases for the same superficial velocity.

The holdup of air in various solutions of sodium nitrate and AFA is illustrated in Figure 8.2. The addition of either AFA or sodium nitrate increases the holdup of air for the same superficial flow rate. There is no discernible difference between the results for 0.5 and 1M sodium nitrate. The addition of a solute was expected to increase the holdup because it reduces the bubble coalescence rate, leading to smaller bubbles and lower rise velocities. Similar trends were observed for the other three gases. As expected, Figure 8.3 shows that solutions of both AFA and sodium nitrate results in higher holdup than in solutions of the reagents alone.

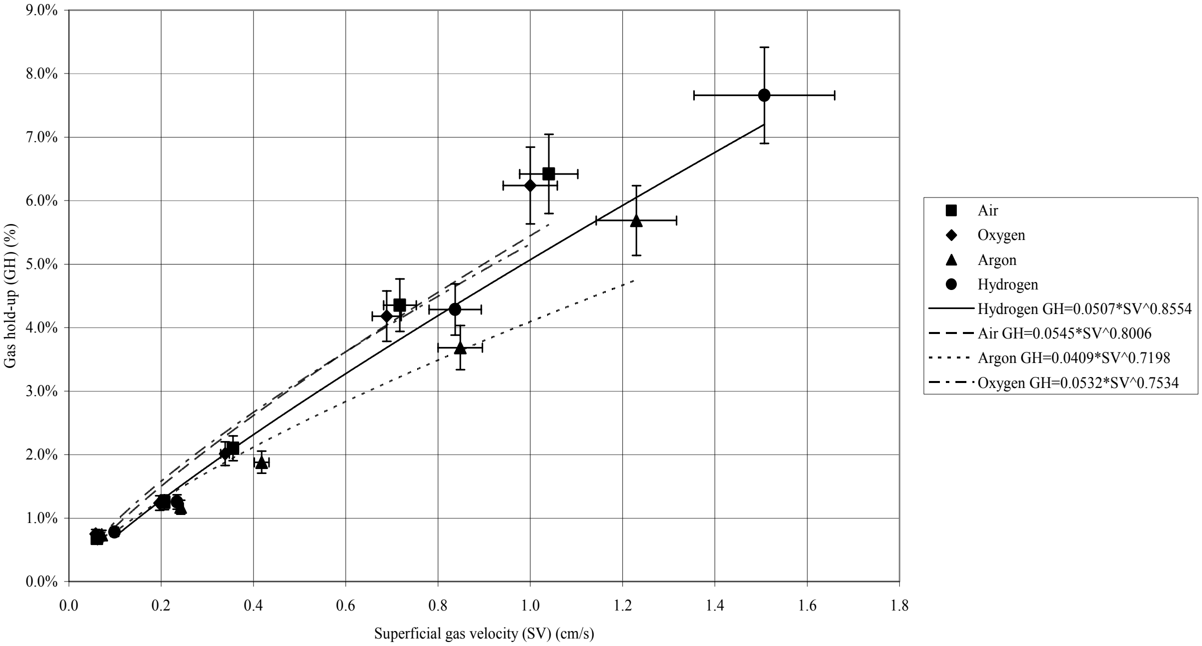

Figure 8.1. Gas Holdup in Water

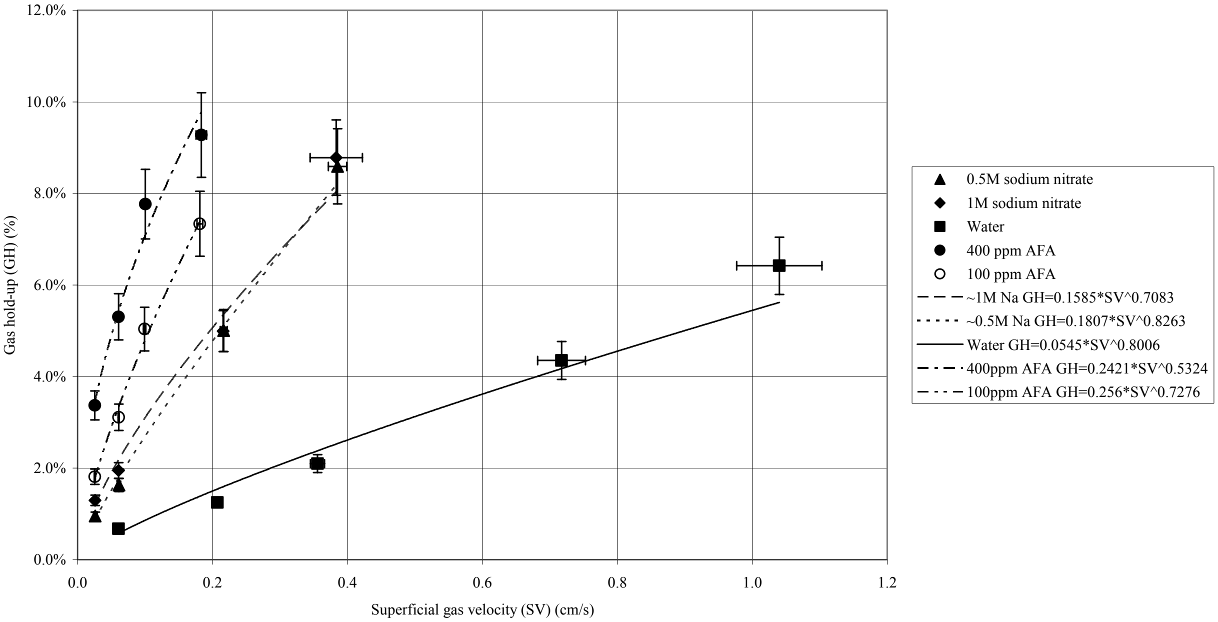

Figure 8.2. Air Holdup in Aqueous Solutions of Sodium Nitrate or AFA

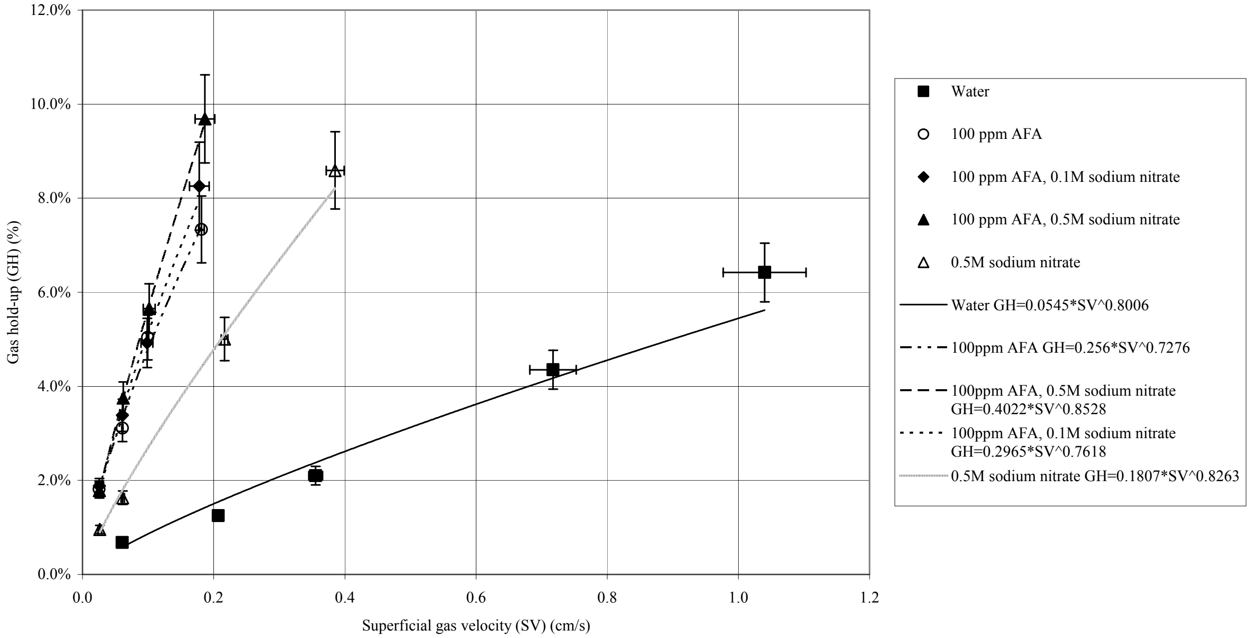

Figure 8.3. Air Holdup in Aqueous Solutions of Sodium Nitrate and AFA

8.4 Clay Matrix Test Results

The gas-holdup results for each velocity are presented in Appendix C. In contrast to the water matrix, there appears to be a significant impact on the holdup in the clay matrix due to the gas type. For example, in clay with a yield stress of ~15 Pa, holdup increases in the order Ar, H_2, air, and O_2, as illustrated in Figure 8.4. All the holdup data can be fit to the equation $\alpha_i = 0.0184 \times u^{0.7813}$ but with a residual square value of 0.5803, indicating a significant impact of the gas type, as confirmed by the residual square values of 0.9920, 0.9719, 0.9470 and 0.9330 derived for the air, Ar, H_2, and O_2 correlations, respectively.

There appears to be little impact of yield stress on air (Figure 8.5), H_2 (Figure 8.6), and O_2 (Figure 8.7) gas holdup. For example, the residual square values of the correlations derived for the individual 7 and 15 Pa correlations for air in Figure 8.5 are 0.9738 and 0.9920, respectively, compared with 0.9596 for the correlation fit to the results from both slurries. However, for argon (Figure 8.8), the impact of yield stress is greater. The residual square values of the correlations derived for the individual 7 and 15 Pa correlations in Figure 8.8 are 0.9960 and 0.9719, respectively, compared with 0.8750 for the correlation fit to the results from both slurries.

The addition of sodium nitrate and AFA to the clay matrix increases the yield stress, which would tend to increase holdup. In addition, solute addition also reduces the bubble coalescence rate, as noted for the water matrix, and this phenomenon would also increase holdup. Figure 8.9 confirms that the effect of adding the solutes at the maximum studied concentrations is to increase the holdup, albeit only upon addition of both solutes.

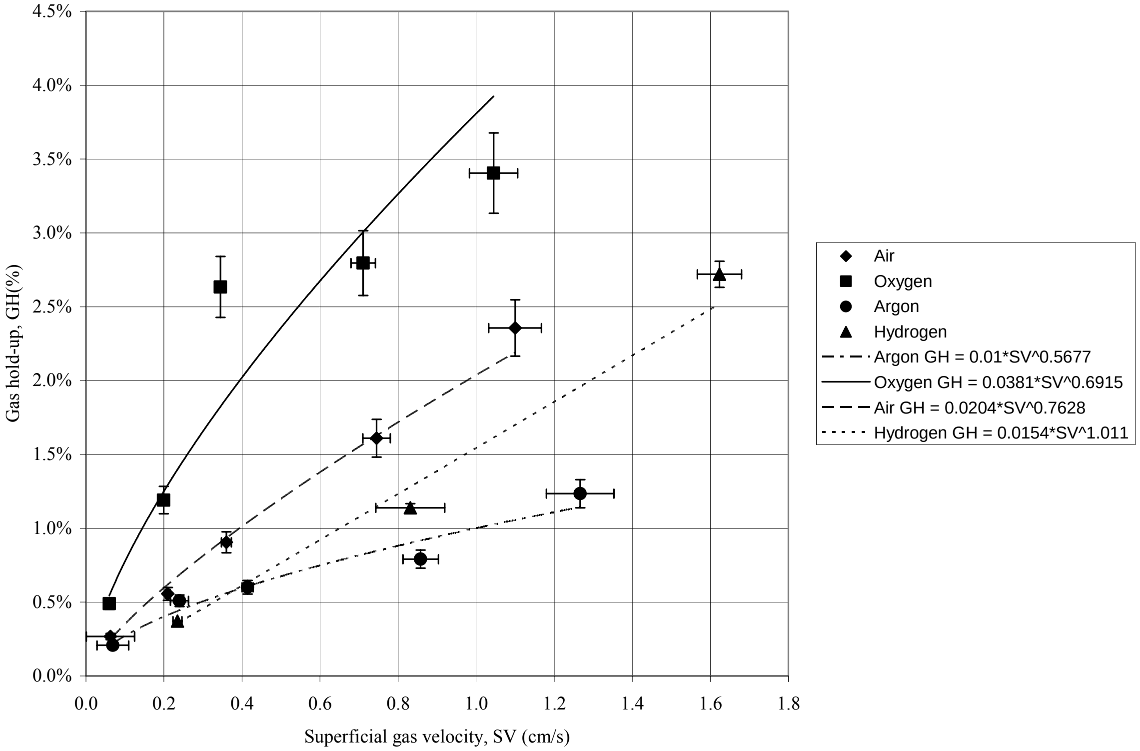

Figure 8.4. Gas Holdup in Kaolin-Bentonite Clay with Yield Stress ~15 Pa

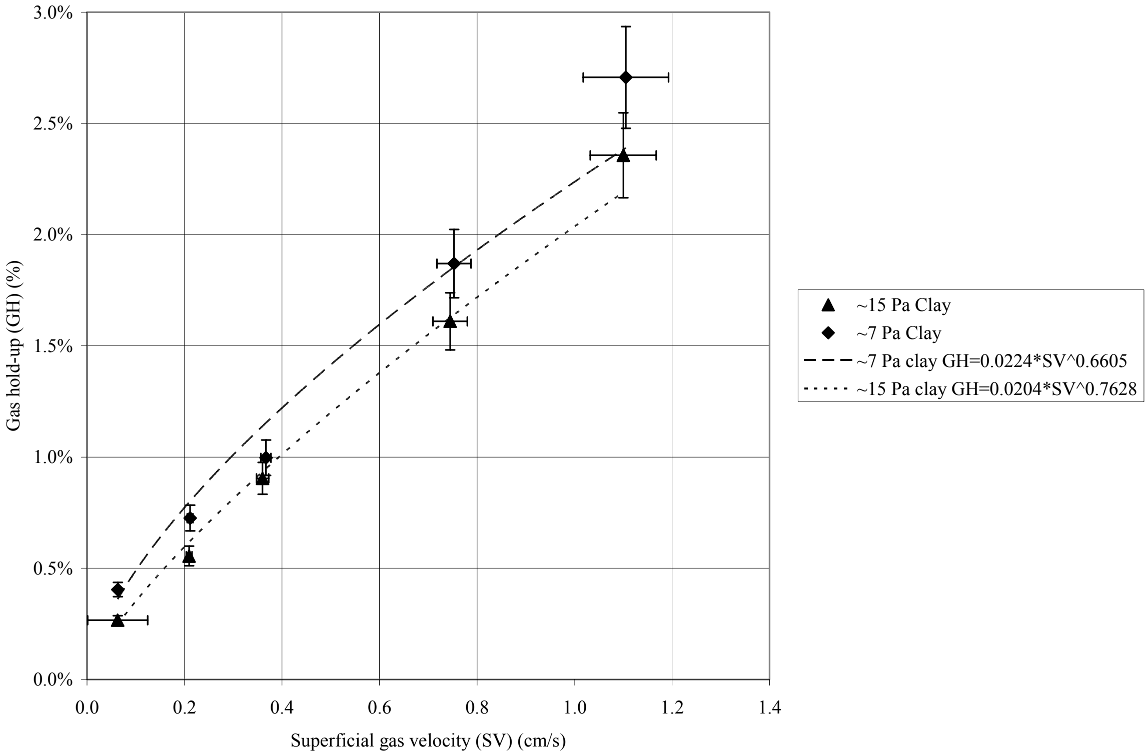

Figure 8.5. Air Holdup in Clay Matrixes of Different Yield Stress

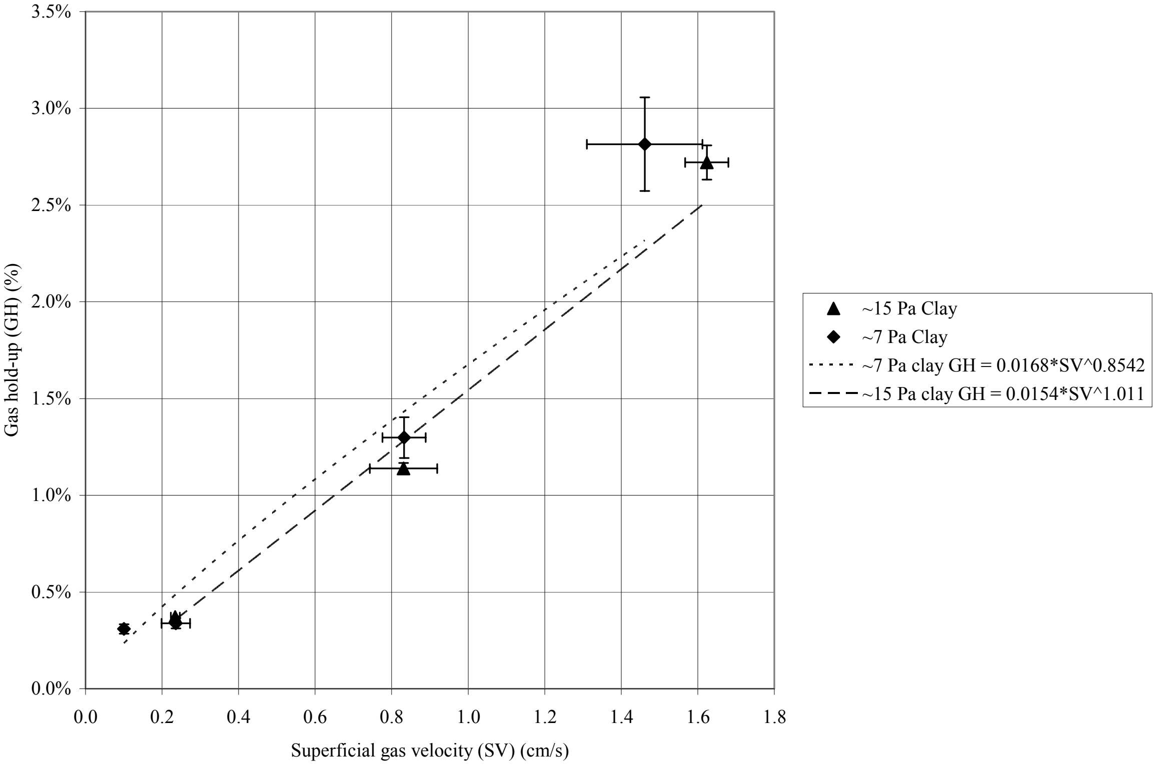

Figure 8.6. Hydrogen Holdup in Clay Matrixes of Different Yield Stress

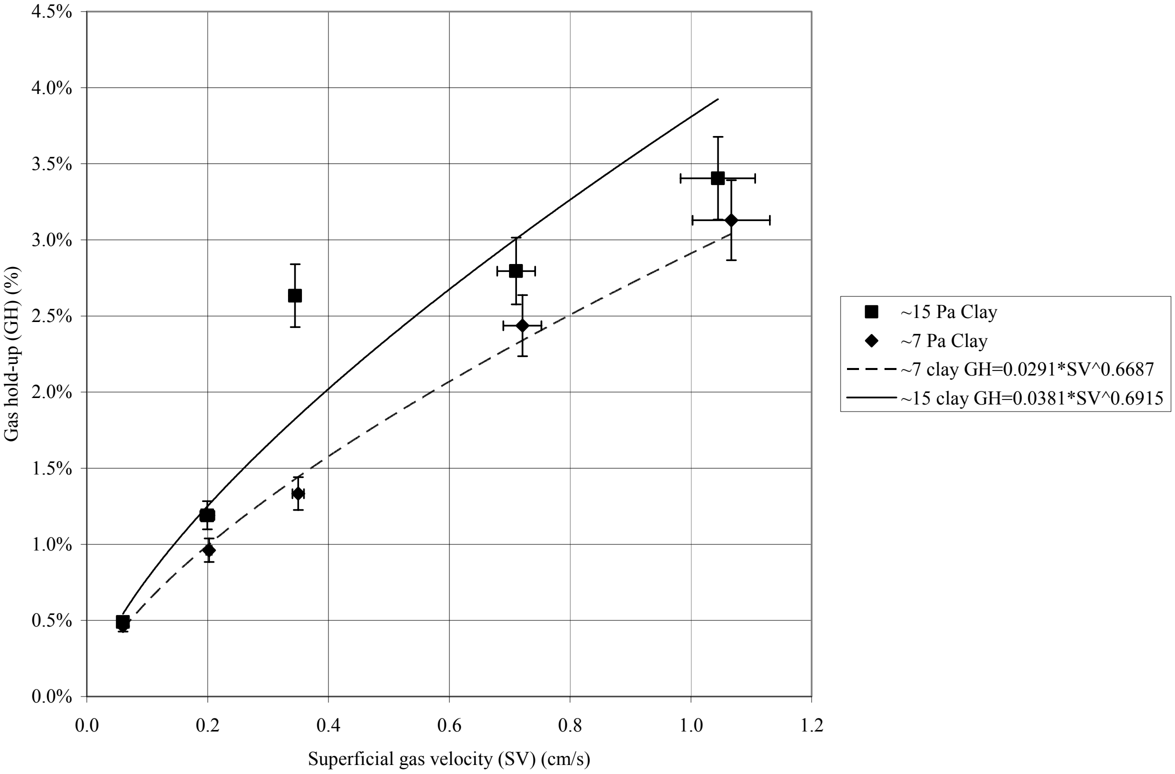

Figure 8.7. Oxygen Holdup in Clay Matrixes of Different Yield Stress

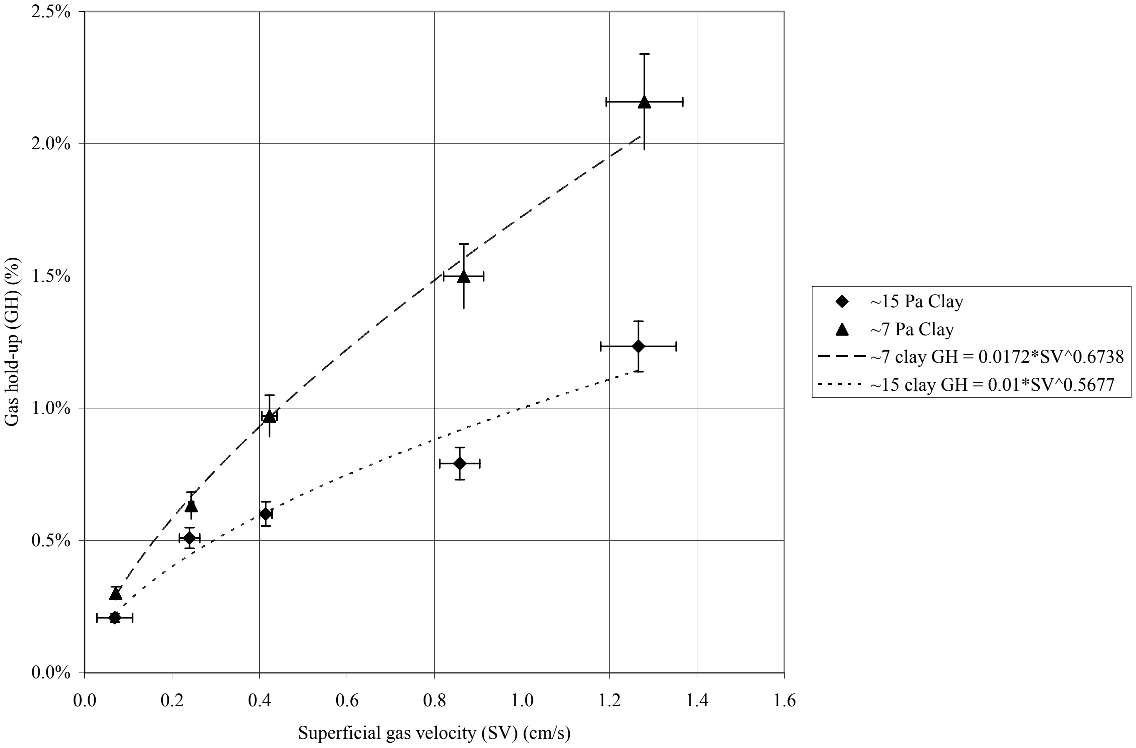

Figure 8.8. Argon Holdup in Clay Matrixes of Different Yield Stress

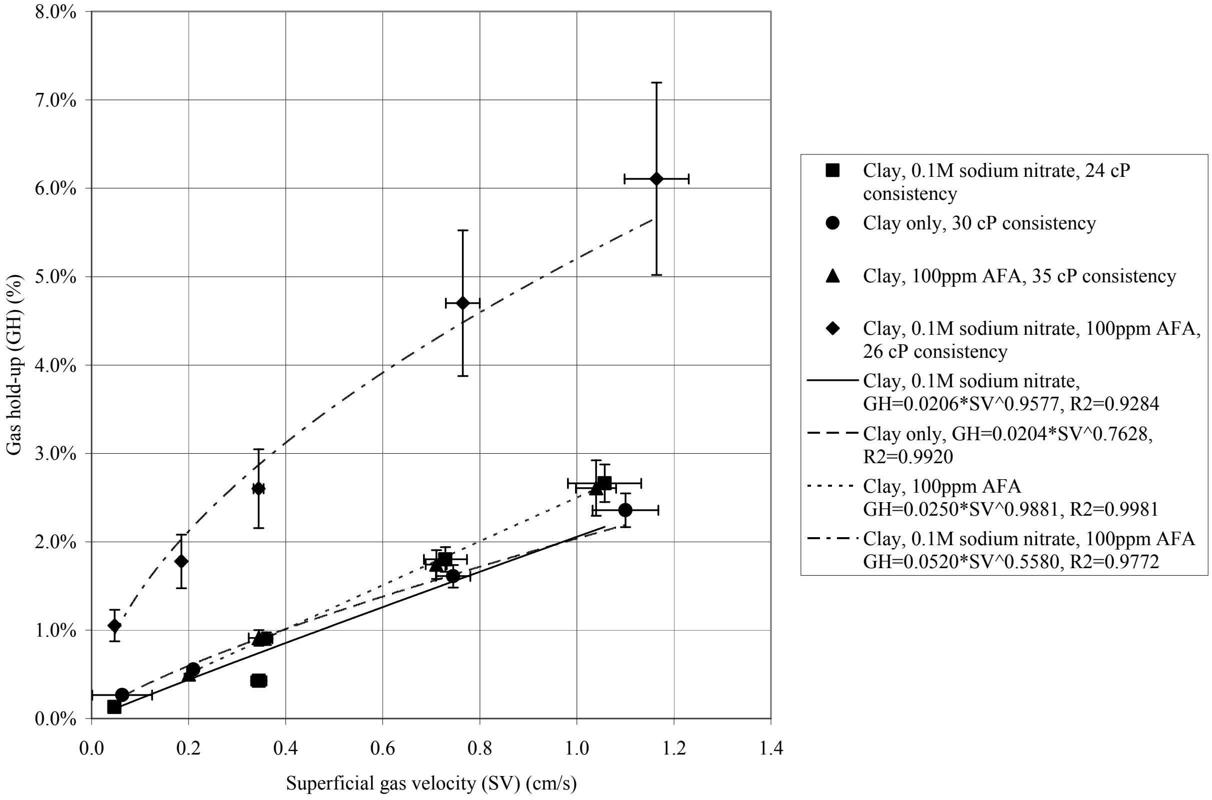

Figure 8.9. Air Holdup in Clay Matrixes with Sodium Nitrate and AFA

8.5 Results of Parametric Study

A statistically designed test strategy was performed to determine correlations for the coefficient and exponent in the holdup-velocity correlation (of the form $\alpha_i = A \times u^n$, where u is the superficial velocity in cm/s) as a function of yield stress and sodium nitrate and AFA concentrations for each gas. The tests and the derived coefficients and exponents fitted to the gas-holdup results used in the statistical analysis are described in Tables 8.2 through 8.5. Appendix C provides the gas holdup for each velocity tested. The tables also provide bubble-rise velocities (gas superficial velocity divided by the holdup, assuming zero liquid velocity) for a single superficial velocity for comparative purposes. Bubble-rise velocities are of the order of 40 cm/s for gas, superficial velocities of approximately 1 cm/s in clay, and of the order of 3 cm/s for velocities of 0.2 cm/s in water.

Table 8.2. Air Holdup in the Parametric Study

Matrix	Yield stress (Pa)	Consistency (cP)	Sodium nitrate concentration (M)	Anti-foaming agent concentration (ppm)	Fitted correlation $\alpha_i=Au^n$		Residual square value	Superficial velocity (cm/s)	Bubble rise velocity (cm/s)
					CoefficientA $(s/cm)^n$	Exponent, n			
Water	0	1	0	0	0.0545	0.8006	0.9679	1.04	16
Water	0	1	0	100	0.2560	0.7276	0.9922	0.18	2.5
Water	0	1	0.5	0	0.1808	0.8265	0.9945	0.39	4.5
Water	0	1	0.5	100	0.4022	0.8528	0.9998	0.19	1.9
Clay	7	14	0	0	0.0224	0.6605	0.9738	1.10	42
Clay	46	19	0.1	10	0.0350	0.7737	0.9816	1.08	24
Clay	23	20	0.01	100	0.0256	0.6779	0.9664	1.04	36
Clay	38	23	0.01	10	0.0245	1.1174	0.9698	1.08	33
Clay	54	26	0.1	100	0.0520	0.5580	0.9772	0.76	16
Clay	13	35	0	100	0.0250	0.9881	0.9981	1.04	40
Clay	51	24	0.1	0	0.0206	0.9577	0.9284	1.06	40
Clay	15	30	0	0	0.0204	0.7628	0.9920	1.10	47

Table 8.3. Argon Gas Holdup in the Parametric Study

Matrix	Yield stress (Pa)	Consistency (cP)	Sodium nitrate concentration (M)	Anti-foaming agent concentration (ppm)	Fitted correlation $\alpha_i=Au^n$		Residual square value	Superficial velocity (cm/s)	Bubble rise velocity (cm/s)
					Coefficient A $(s/cm)^n$	Exponent, n			
Water	0	1	0	0	0.0409	0.7198	0.9483	0.85	23
Water	0	1	0	100	0.0180	0.9762	0.9595	0.22	2.8
Water	0	1	0.5	0	0.1738	0.8262	0.9996	0.33	4.7
Water	0	1	0.5	100	0.3195	0.6842	0.989	0.16	1.7
Clay	7	14	0	0	0.0172	0.6738	0.996	1.28	59
Clay	46	19	0.1	10	0.0223	1.0786	0.9991	1.26	42
Clay	23	20	0.01	100	0.0211	0.4951	0.8916	1.21	42
Clay	38	23	0.01	10	0.0159	1.6273	0.9786	1.22	57
Clay	54	26	0.1	100	0.0384	0.6213	0.9944	1.25	25
Clay	13	35	0	100	0.0211	0.4951	0.8916	1.21	42
Clay	51	24	0.1	0	0.0313	0.675	0.9342	1.22	30
Clay	15	30	0	0	0.0100	0.5677	0.9719	1.27	103

Table 8.4. Hydrogen Gas Holdup in the Parametric Study

Matrix	Yield stress (Pa)	Consistency (cP)	Sodium nitrate concentration (M)	Anti-foaming agent concentration (ppm)	Fitted correlation $\alpha_i=Au^n$		Residual square value	Superficial velocity (cm/s)	Bubble rise velocity (cm/s)
					Coefficient A $(s/cm)^n$	Exponent, n			
Water	0	1	0	0	0.0507	0.8554	0.9879	0.84	20
Water	0	1	0	100	0.2552	0.8728	0.9956	0.39	3.6
Water	0	1	0.5	0	0.1479	0.8136	0.9918	0.58	6.3
Water	0	1	0.5	100	1.0231	1.3365	0.9824	0.25	1.4
Clay	7	14	0	0	0.0168	0.8542	0.9264	0.83	64
Clay	46	19	0.1	10	0.0421	0.5253	0.9269	0.83	29
Clay	23	20	0.01	100	0.0326	0.5318	0.9438	0.74	31
Clay	38	23	0.01	10	0.0274	0.9264	0.9765	0.84	39
Clay	54	26	0.1	100	0.0393	0.5839	0.9160	0.79	31
Clay	13	35	0	100	0.0257	0.9868	0.9967	0.81	36
Clay	50	24	0.1	0	0.0260	1.3333	0.9844	0.83	56
Clay	15	30	0	0	0.0157	1.3914	0.9470	0.83	73

Table 8.5. Oxygen Gas Holdup in the Parametric Study

Matrix	Yield stress (Pa)	Consistency (cP)	Sodium nitrate concentration (M)	Anti-foaming agent concentration (ppm)	Fitted correlation $\alpha_i=Au^n$		Residual square value	Superficial velocity (cm/s)	Bubble rise velocity (cm/s)
					Coefficient A $(s/cm)^n$	Exponent, n			
Water	0	1	0	0	0.0532	0.7534	0.9533	1.0	16
Water	0	1	0	100	0.3085	0.8049	0.9996	0.18	2.3
Water	0	1	0.5	0	0.1989	0.8621	0.9951	0.37	4.1
Water	0	1	0.5	100	0.4583	0.9656	0.9974	0.18	2.1
Clay	7	14	0	0	0.0291	0.6687	0.9946	1.05	44
Clay	46	19	0.1	10	0.0376	1.0700	0.9912	1.09	26
Clay	23	20	0.01	100	0.0230	0.5100	0.8608	1.00	34
Clay	38	23	0.01	10	0.0294	1.1414	0.9964	1.04	33
Clay	54	26	0.1	100	0.0397	0.7197	0.9547	1.03	22
Clay	13	35	0	100	0.0228	0.5528	0.9547	0.98	41
Clay	51	24	0.1	0	0.0254	0.3538	0.7273	1.02	29
Clay	15	30	0	0	0.0381	0.6915	0.9330	1.04	31

A statistical analysis using the JMP statistical software package was performed on the results from the parametric study (both clay and water) to derive the following generalized correlation relating gas holdup to superficial velocity.

$$\alpha_i = \exp\left(\begin{matrix} -2.93 - 0.152\kappa + 2.99[\mathrm{NaNO_3}] + 0.0171[\mathrm{AFA}] + 0.256\kappa[\mathrm{NaNO_3}] - 4.67\times10^{-4}\kappa[\mathrm{AFA}] + \\ 0.0187[\mathrm{AFA}][\mathrm{NaNO_3}] + 3.72\times10^{-3}\kappa^2 + 1.91[\mathrm{NaNO_3}]^2 \end{matrix}\right)u^{0.743}$$

(8.3)

where κ = consistency (cP)
u = superficial velocity (in cm/s, defined as volumetric gas flow rate divided by column cross-sectional area)
$[NaNO_3]$ = sodium nitrate concentration (M)
[AFA] = anti-foaming agent concentration (ppm).

In terms of the average bubble rise velocity throughout the column, u_{cr}, equation 8.3 can be expressed as

$$u_{cr} = \exp\left(\begin{array}{l} 2.93 + 0.152\kappa - 2.99[NaNO_3] - 0.0171[AFA] - 0.256\kappa[NaNO_3] + 4.67\times10^{-4}\kappa[AFA] + \\ 0.0187[AFA][NaNO_3] - 3.72\times10^{-3}\kappa^2 - 1.91[NaNO_3]^2 \end{array}\right)u^{0.257} \tag{8.4}$$

The performance of the statistical correlation is illustrated in Figure 8.10, which compares the actual and predicted gas-holdup values. All of the data points would lie on the plotted straight line of unity slope and zero intercept for a perfect correlation, and the correlation appears to improve at higher gas holdups (less negative values of the natural logarithm of the holdup). The residual square value for the correlation is considered reasonable at 80% and indicates that this percentage of the data variability is accounted for in the correlation. Gas type was described by the molecular weight in the statistical analysis since it affects the gas density and consistency, which were considered the most likely properties affecting holdup. However, gas type is insignificant in explaining the variation in holdup compared to rheology and solute concentration. Including yield stress in the correlation did not significantly improve its performance, and replacing consistency with yield stress led to a lower residual square of 74%. Therefore, consistency is the best rheological parameter for fitting the data from a statistical standpoint. PNWD observed that sodium nitrate and AFA had a significant impact on the rheology, which also affects gas holdup. The effects of rheology and solute addition were separated in the statistical analysis by considering matrices of different rheologies with no added solute. The values for $NaNO_3$ and AFA of 0.5M and 100 ppm, respectively, should be used in the correlation for concentrations greater than these values because experiments showed that there was no significant additional impact on gas holdup at higher concentrations.

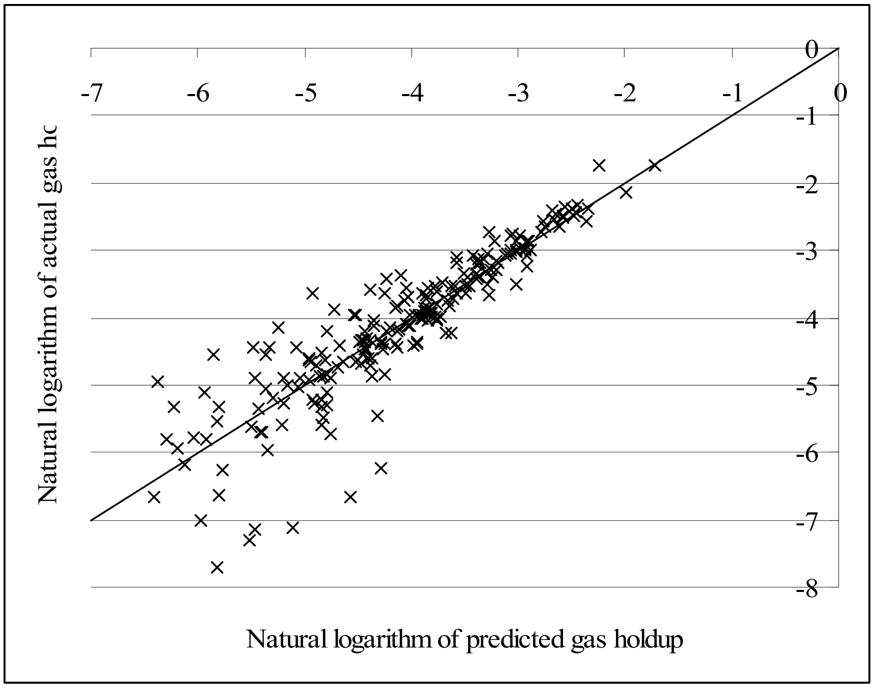

Figure 8.10. Performance of the Statistical Gas-Holdup Correlation

Figure 8.11 compares actual air holdup data for clay matrixes with yield stresses of 15 and 54 Pa, the latter containing 0.1M sodium nitrate and 100 ppm anti-foaming agent. The correlations appear to under-predict the gas holdup, probably because the inherent error in the correlation was introduced as a result of experimental uncertainty.

8.6 Gas Holdup in Pretreated AZ-101 HLW Simulant

Air, Ar, H_2, and O_2 holdup were investigated in pretreated AZ-101 HLW simulant slurry of pH 14 containing sodium dissolved in the liquid portion to a concentration of 0.4M. Tests were then performed with the slurry containing 10 ppm and then 100 ppm anti-foaming agent. The gas-holdup results are presented in Appendix C for each superficial gas velocity.

Figure 8.12 shows that gas holdup in the pretreated AZ-101 high level waste simulant is independent of gas type for air, Ar, and O_2 while H_2 holdup is consistently higher for a given gas velocity. All of the data were correlated by the power law equation $\alpha_i = 0.0208 \times u^{0.3997}$ with a residual square value of 61%. The correlation developed in Section 8.5 predicts the gas holdup to follow the relationship $\alpha_i = 0.111 \times u^{0.743}$, which is also provided in Figure 8.12. The predictive correlation increasingly overpredicts the measured gas holdup. The reasons for the discrepancy are not clear at present.

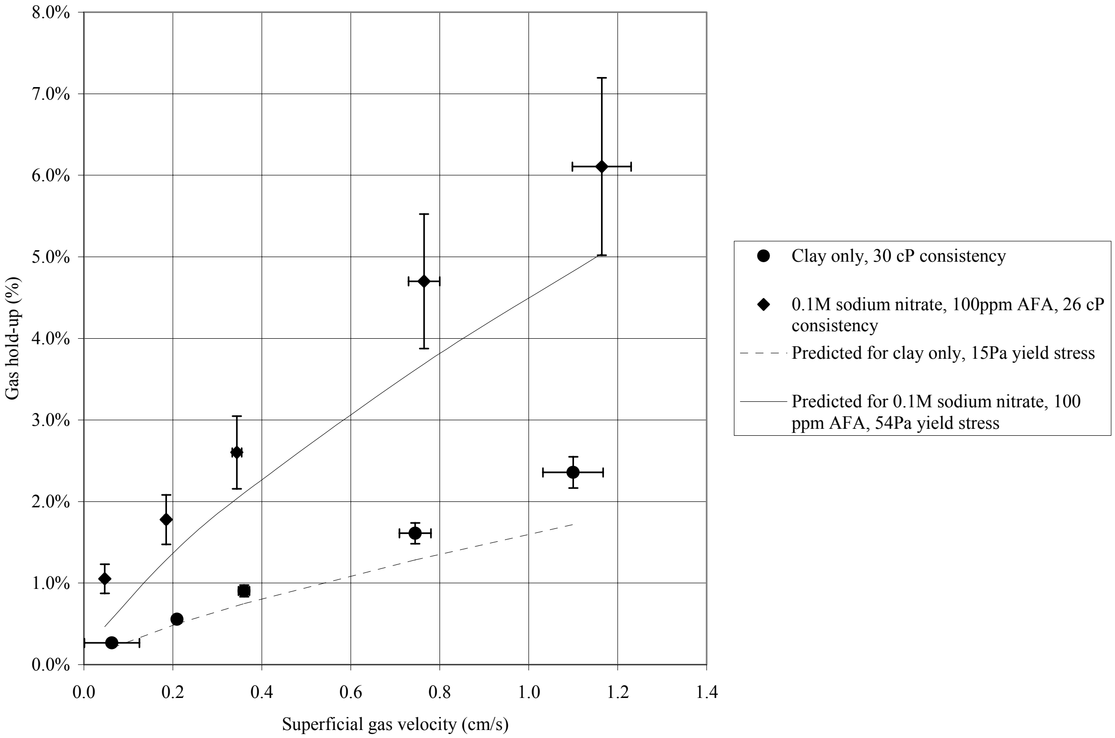

Figure 8.11. Comparison of Actual and Predicted Air Holdup in Clay Matrixes

However, the higher pH of the pretreated AZ-101 HLW simulant compared with clay and differences in the particle surface characteristics may influence bubble coalescence and thereby gas holdup. The predictive correlation is therefore inappropriate for predicting gas holdup in pretreated AZ-101 HLW simulant with no AFA.

Gas holdup in the pretreated AZ-101 HLW simulant containing AFA exhibited trends not previously observed with the clay or water matrixes, and the experiments required a significantly longer time to attain steady state. A steady-state holdup was typically attained within 5 minutes for the water, clay, and pretreated AZ-101 HLW simulant less AFA, but approximately 1 hour was required for the latter matrix after adding AFA. As Figures 8.13 and 8.14 show, gas holdup initially increased with increasing velocity as expected with H_2 holdup again consistently higher than that of air, Ar, and O_2. The predictive correlation predicts the measured values very well, particularly for air, Ar, and O_2 at gas velocities below 0.8 cm/s. Hydrogen holdup is less well predicted, probably because the predictive correlation does not account for gas type, as described in Section 8.5. The improvement in the predictive correlation to predict gas holdup may be because the impact of the AFA on bubble coalescence dominates over the impact of differences between the pretreated AZ-101 HLW simulant and clay.

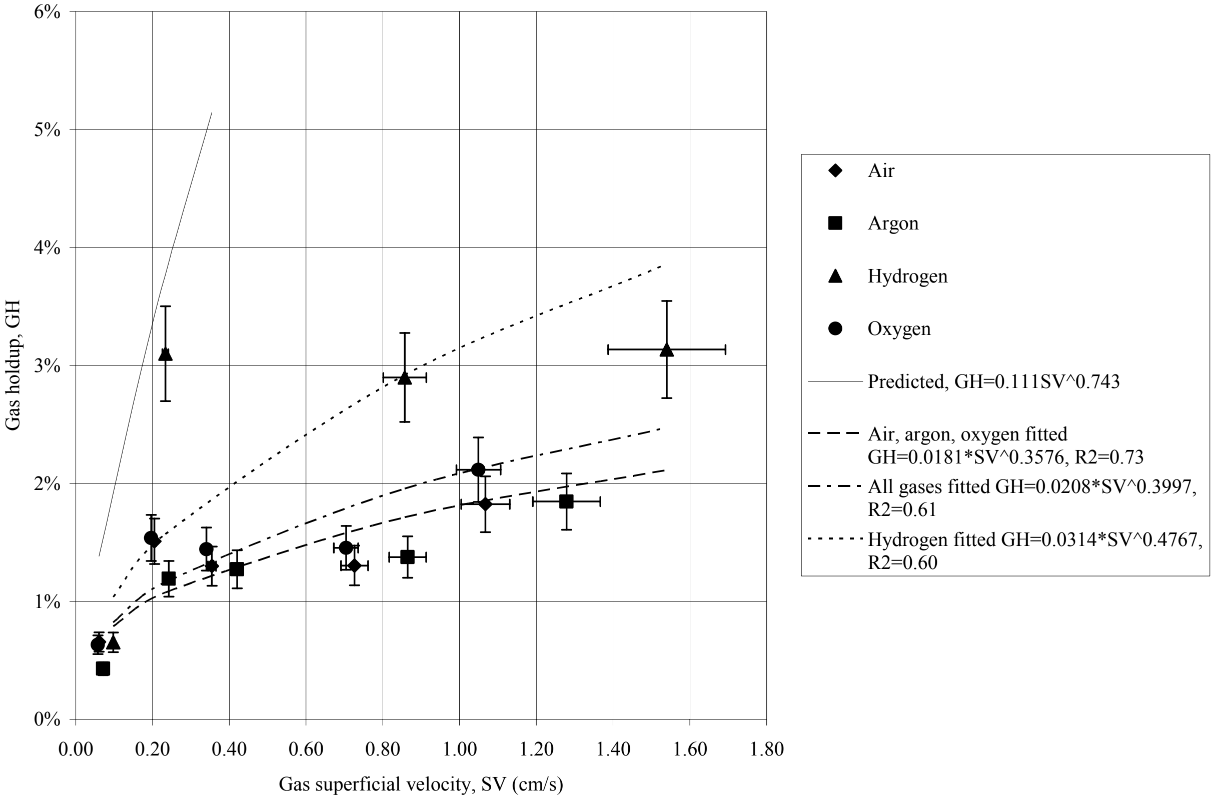

Figure 8.12. Gas Holdup in Pretreated AZ-101 HLW Simulant Slurry (yield stress 7.2 Pa and consistency 7.3 cP)

However, gas holdup decreased with increasing gas velocity for velocities above 0.8 cm/s, a phenomenon not previously observed with either the clay or water and not predicted by the predictive correlation. The predictive correlation therefore increasingly deviates from the measured holdup for velocities above 0.8 cm/s. The reasons for the maximum in gas holdup are not clear, and the same phenomenon occurring for the clay at a higher gas velocity than tested cannot be discounted. The sharpness of the maximum suggests a change in some characteristic of the fluid motion or bubbles related to the bubble velocity. Once again, differences in the particle surface characteristics and pH of the clay and pretreated AZ-101 high-level waste simulant appear to be responsible for the behavior difference because the maximum in holdup was observed after adding AFA to the pretreated AZ-101 HLW simulant while its rheological properties remained essentially the same as before AFA addition. This consideration suggests a change in a bubble characteristic (e.g., shape) that dramatically promoted bubble coalescence. Furthermore, bubble shape would be most affected by the AFA at low velocities because surface tension is dominant in its determination. Gas holdup with AFA approaches that without AFA at velocities higher than those manifesting the holdup maximum, presumably because bubble shape is determined by the inertial forces. The increase in time to steady state for simulated HLW with AFA appears to suggest a change in slurry behavior within the column. For example, an axial recirculation of slurry might also have promoted a lower gas holdup if the bubbles became entrained in an upward flow of material. Evidently, the processes causing the behavior are complicated, and nearly any explanation is speculative.

Further tests with a transparent material (e.g., Laponite) would be useful in examining bubble shape and observing any recirculation.

Figure 8.15 summarizes the air holdup in pretreated AZ-101 high level waste simulant and shows the presence of AFA increasing the gas holdup, particularly at high gas velocities. Also plotted are the results for kaolin-bentonite clay of the closest rheology to the pretreated AZ-101 HLW simulant and apparently shows air holdup in clay and pretreated AZ-101 HLW simulant essentially equivalent for the same rheology on the basis of this result (i.e., the simulant appears to behave as if there were no solute).

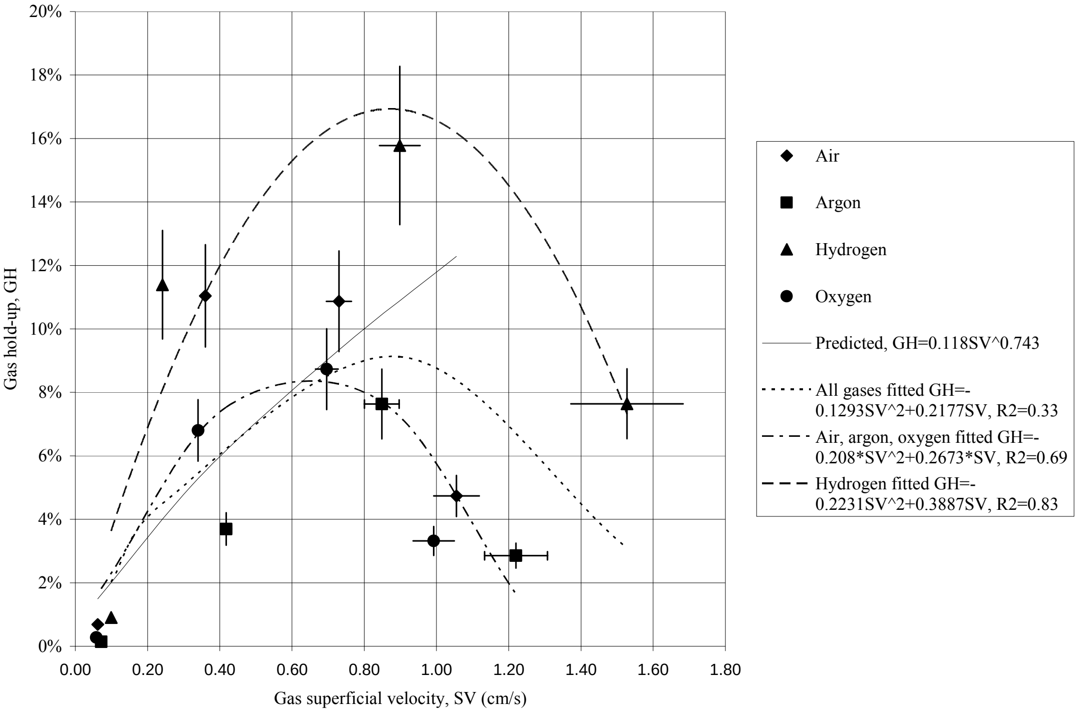

Figure 8.13. Gas Holdup in Pretreated AZ-101 HLW Simulant Slurry Containing 10 ppm AFA (yield stress 7.8 Pa and consistency 8.1 cP)

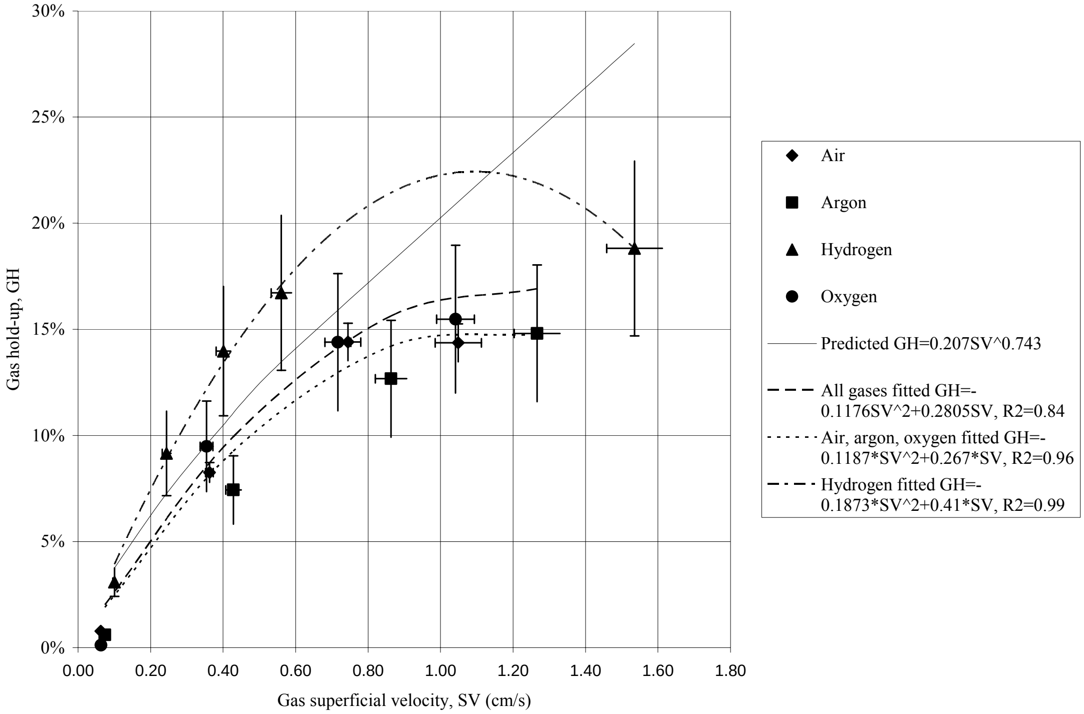

Figure 8.14. Gas Holdup in Pretreated AZ-101 HLW Simulant Slurry Containing 100 ppm AFA (yield stress 5.3 Pa and consistency 7.2 cP)

8.7 Conclusions

A correlation was fitted to the gas-holdup results from water and clay matrixes, which accounts for rheology, AFA, and sodium nitrate concentrations and gas superficial velocity. The effect of gas type was insignificant compared to the other parameters. Gas holdup increases with increasing consistency, solute concentration, and gas superficial velocity.

The correlation fails to predict gas-holdup behavior in pretreated AZ-101 high-level waste simulant with no AFA, assuming solutes in the simulant's supernate are represented by sodium nitrate. However, gas holdup is well predicted by the correlation when the simulant contains AFA up to a superficial velocity of approximately 0.8 cm/s. Gas holdup was observed to decrease with increasing gas superficial velocities above 0.8 cm/s such that the correlation becomes inappropriate at these velocities.

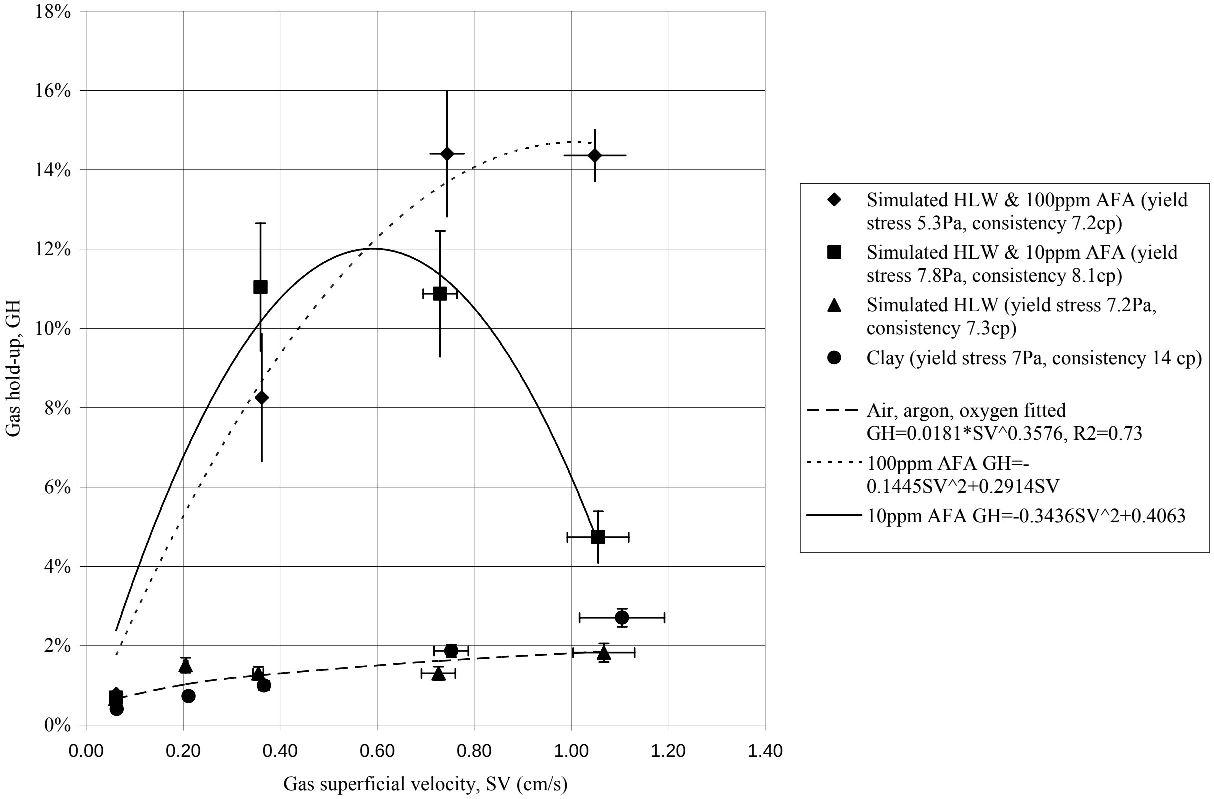

Figure 8.15. Air Holdup in Pretreated AZ-101 HLW Simulant Slurry and Kaolin-Bentonite Clay

9.0 Mass-Transfer Demonstration

Proof-of-concept tests were conducted to demonstrate gas-stripping mass transfer in non-Newtonian simulants, and the results are reported below. Mass-transfer theory is briefly summarized in Section 9.1, experimental methods and test stands are described in Section 9.2, and the results of proof-of-concept tests are presented in Section 9.3. Bench-scale experiments demonstrate the stripping of O_2 from O_2-saturated kaolin-bentonite clay and simulated AZ-01/102 HLW resulting from air sparging at different flow rates, and the results are used to calculate mass-transfer coefficients. A similar proof-of-concept gas-stripping test was conducted with clay simulant in the UFP model vessel.

9.1 Mass-Transfer Theory

According to classical mass-transfer theory (described, for example, in Treybal 1980), the rate of change in concentration of a sparingly soluble solute is proportional to the difference between the instantaneous concentration, C, and that when the solution is saturated, C^*:

$$\frac{dC}{dt} = k_l a\left(C - C^*\right) \tag{9.1}$$

where t is time, k_l is the liquid side mass-transfer coefficient, and a is the interfacial area per unit volume of slurry, which is characteristic of the contact equipment. This equation reasonably assumes the gas-side mass-transfer coefficient is very much larger than that for the liquid side. Integrating Eq. (9.1) above from time zero to t when the concentrations are C^0 and C, respectively, gives

$$\frac{\mathrm{Ln}\left(C^0 - C^*\right)}{\mathrm{Ln}\left(C - C^*\right)} = k_l at \tag{9.2}$$

Eq. (9.2) is rearranged to provide it in a form that enables the mass-transfer coefficient to be determined from experiment:

$$\mathrm{Ln}\left(C - C^*\right) = \mathrm{Ln}\left(C^0 - C^*\right) - k_l at \tag{9.3}$$

Therefore, plotting $\mathrm{Ln}(C\text{-}C^*)$ and t will provide a straight line of slope $k_l a$ and intercept $\mathrm{Ln}(C^0\text{-}C^*)$.

9.2 Test Description

This section describes the equipment and methods used in the bench-scale and UFP vessel mass-transfer experiments. Section 9.2.1 describes the dissolved O_2 monitoring system. The bubble-column used in bench-scale tests with multiple simulants is described in Section 9.2.2, and the UFP vessel configuration used to assess the mass-transfer correlation is described in Section 9.2.3.

9.2.1 Dissolved Oxygen Monitoring System

The dissolved-O_2 concentration was monitored with a FOXY fiberoptic O_2-sensor system manufactured by Ocean Optics Inc. (Dunedin, FL). The system consisted of a personal computer running an application program provided by the vendor providing data acquisition from a spectrometer and light source connected to a probe by a bifurcated optical fiber. The FOXY probes contain a ruthenium complex encapsulated in a sol-gel matrix that is further protected by a silicone overcoat. Oxygen dissolved in the solution to be analyzed diffuses into the sol-gel matrix such that the O_2 in the sol-gel matrix and solution are in dynamic equilibrium. A pulsed blue-light-emitting diode transmits light at ~475 nm through the optical fiber to the probe. The blue light excites the ruthenium complex, which fluoresces, emitting energy at ~600 nm. The fluorescence signal decreases when the excited ruthenium complex encounters an O_2 molecule because the excess energy is transferred to it. Hence, the fluorescence signal strength is directly proportional to the O_2 partial pressure in the sol-gel film. The fluorescence energy is carried back to the spectrometer by the optical fiber.

The system performance was checked in O_2 of purity 99.5% and in nitrogen of purity 99.9% before use as recommended by the manufacturer. Performance was verified in air before and after each simulant was tested to confirm system stability. Performance was considered verified if the reading in air was within 20% of its value, 21 vol%, reported as the composition of the U.S. standard atmosphere (1976) in the Handbook of Chemistry and Physics (CRC Press 2004). The reading in air was typically within 15% of its reported value for the U.S. standard atmosphere.

9.2.2 Bubble Column

Laboratory-scale tests were performed in the dissolved O_2 mass-transfer apparatus schematically illustrated in Figure 9.1. The apparatus consisted of a column 25.4 cm internal diameter and 91.4 cm high. Two FOXY probes were inserted through the column wall at 15.2 cm and 30.5 cm, measured from the column bottom, to protrude 2.5 cm into the column. The gas line fed either air or O_2 through a pressure gauge and rotameter to the base of the column through a ¼ inch (6.4 mm) diameter hole.

The column was first filled with slurry to a height of 50 cm to provide a volume of 25.3 L. Oxygen was then bubbled through the slurry at a nominal flow rate of 50 L/min while the FOXY system monitored the dissolved O_2 concentration increase to the saturation, or equilibrium, condition for an atmosphere of pure O_2 at a pressure of 1 atm. At this point, the O_2 feed was terminated, and air was bubbled through the column at the desired flow rate, set on the rotameter. The air feed was continued until the FOXY system indicated the dissolved O_2 concentration had reduced to a steady value, which was assumed the saturation condition (C^* in Eq. 9.3) for an atmosphere of air containing O_2 at a partial pressure of 0.21 atm.

Three slurries described in Table 9.1 (dilute kaolin-bentonite clay, concentrated kaolin-bentonite clay, and pretreated AZ-101 high level waste simulant) were tested in the bubble column, each at air sparge flow rates of 13.9, 32, and 54.4 L/min corrected to standard temperature and pressure. The slurries were observed to remain fluid throughout the column while sparged.

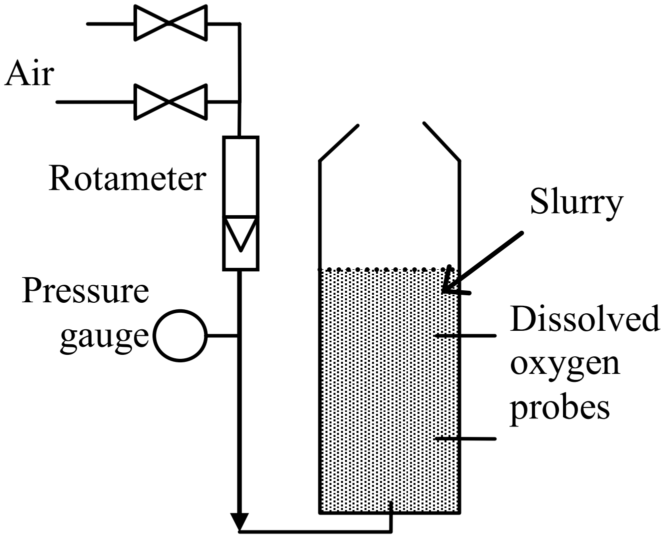

Figure 9.1. Dissolved Oxygen Mass-Transfer Apparatus Schematic

Table 9.1. Slurries Used in the Bubble Column Tests

Slurry	Yield stress (Pa)	Consistency factor (cP)
Dilute kaolin clay	7.3	19
Concentrated kaolin clay	17	30
Pretreated AZ-101 high level waste simulant	11	11

9.2.3 UFP Tank

A single scoping test was performed in December 2003 in the UFP tank with the four lower pulse jets situated equidistantly around two ram heads (as described by Bates et al. 2004). Two O_2-sensing probes were inserted into the tank at elevations of 46 and 97 cm from the base. The tank was filled with kaolin-bentonite clay slurry with a yield stress of 16 Pa and a consistency of 23 cP to provide a slurry H/D of 1.84. Oxygen had been previously dissolved into this slurry by decomposing H_2O_2 in the slurry to generate O_2 gas that then saturated the slurry. Previous testing then reduced the O_2 content to a concentration below saturation. The pulse jets and ram heads were then started at a target velocity of 11 m/s with drive and refill times of 1.2 and 18.8 seconds, respectively, and a total cycle time of 27 seconds once the tank was filled. Air sparging was not immediately initiated to assess the capability of the pulse jets and ram heads alone to reduce the dissolved-O_2 concentration. Air sparging was then initiated at a total flow rate of 2.7 acfm through three sparge tubes to provide a total superficial velocity of 0.22 cm/s.

9.3 Testing Results

Bench-scale mass-transfer experiments were conducted in a bubble column, and the results are presented in Section 9.3.1. The mass-transfer correlations developed from these bench-scale tests were applied to the experimental conditions of a larger-scale test in the UFP tank. The correlation prediction is compared to the UFP test results in Section 9.3.2.

9.3.1 Bubble Column Testing Results

Figures 9.2 through 9.10 illustrate the results from the bubble column testing for the three slurries at the three air flow rates plotted according to Eq. (9.3). In general, the results are consistent with Eq. (9.3). The noise apparent when the O_2 concentration is close to saturation is assumed due to inhomogeneous mixing that accentuates concentration gradients at low concentrations. In general, results from the two probes are consistent. However, at the lowest air flow rate, poor mixing in the bottom of the column is assumed responsible for the fluctuations in the concentration and poorer mass-transfer evident in the results from the bottom probe. Straight lines were fitted over the linear portions of the plots to derive the $k_l a$ products in Table 9.2.

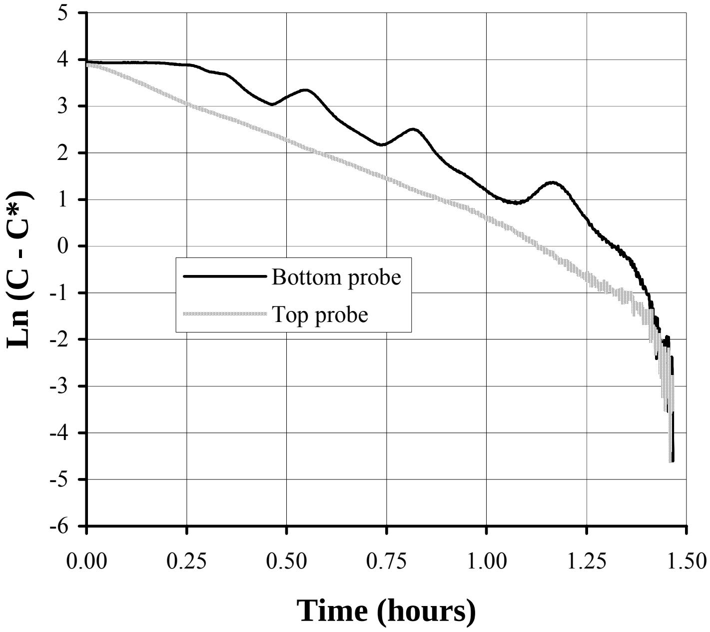

Figure 9.2. Mass-Transfer Results from Bubble Column for Dilute Clay Slurry and an Air Flow Rate of 13.9 L/min

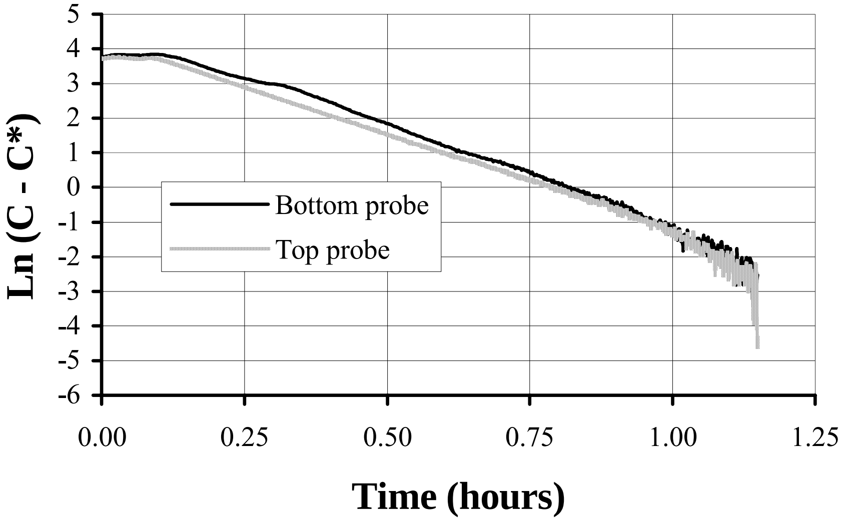

Figure 9.3. Mass-Transfer Results from Bubble Column for Dilute Clay Slurry and an Air Flow Rate of 31.7 L/min

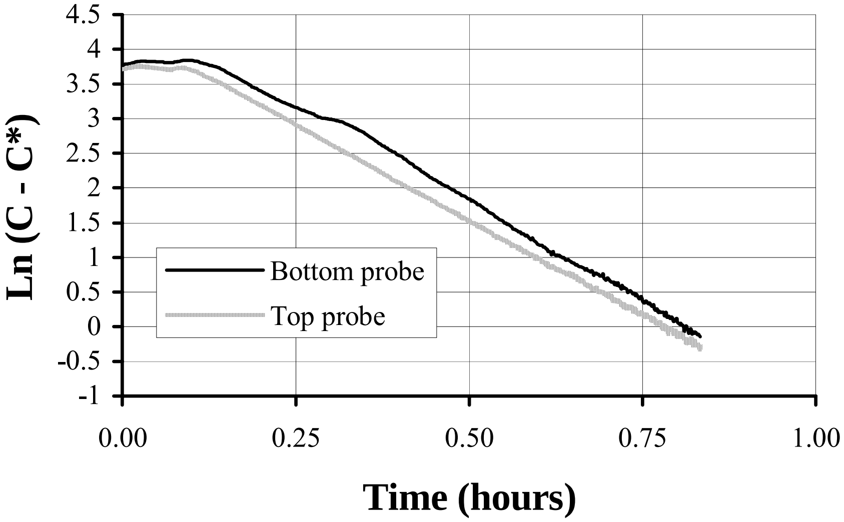

Figure 9.4. Mass-Transfer Results from Bubble Column for Dilute Clay Slurry and an Air Flow Rate of 50.3 L/min

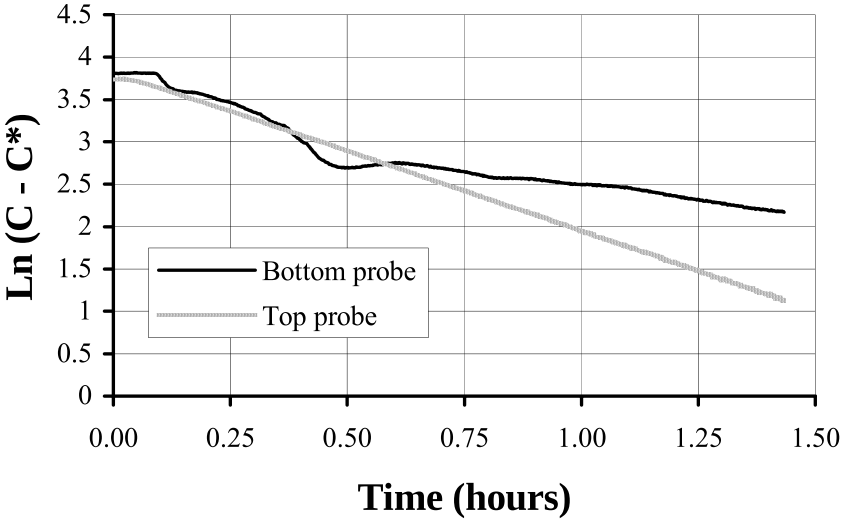

Figure 9.5. Mass-Transfer Results from Bubble Column for Concentrated Clay Slurry and Air Flow Rate of 13.9 L/min

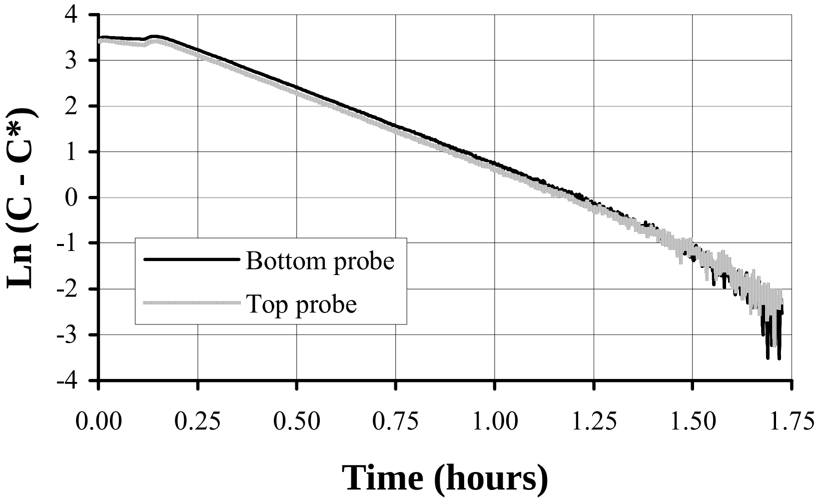

Figure 9.6. Mass-Transfer Results from Bubble Column for Concentrated Clay Slurry and an Air Flow Rate of 30.9 L/min

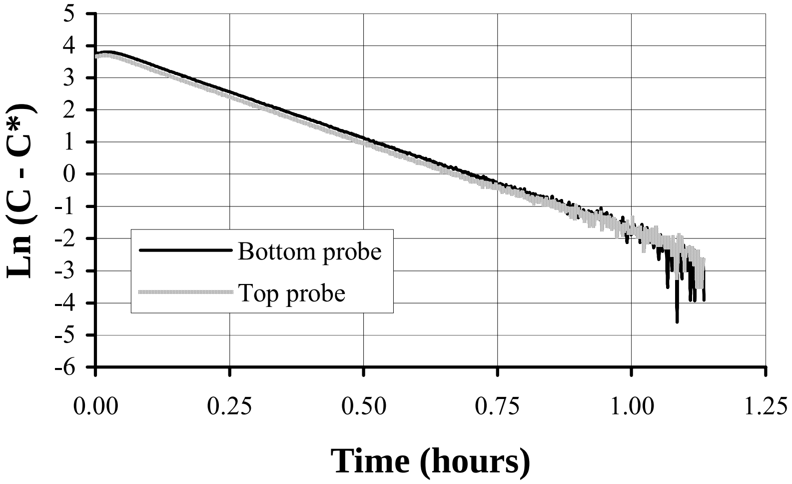

Figure 9.7. Mass-Transfer Results from Bubble Column for Concentrated Clay Slurry and an Air Flow Rate of 50.3 L/min

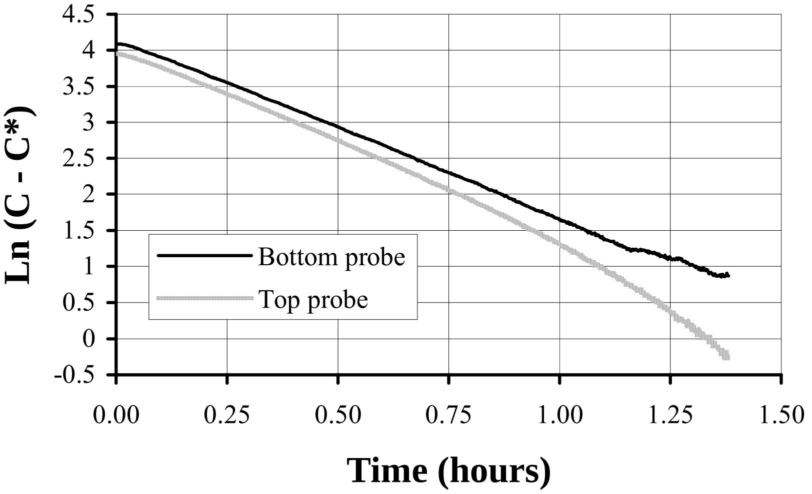

Figure 9.8. Mass-Transfer Results from Bubble Column for Pretreated AZ-101 HLW Simulant and an Air Flow Rate of 13.9 L/min

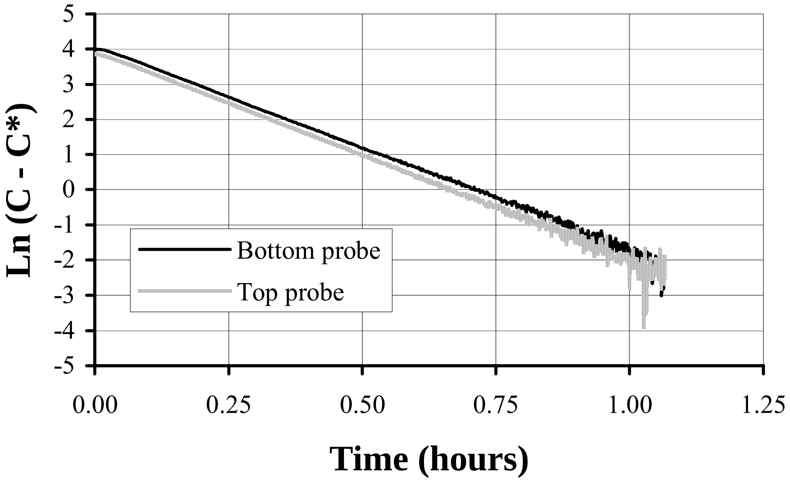

Figure 9.9. Mass-Transfer Results from Bubble Column for Pretreated AZ-101 HLW Simulant and an Air Flow Rate of 31.7 L/min

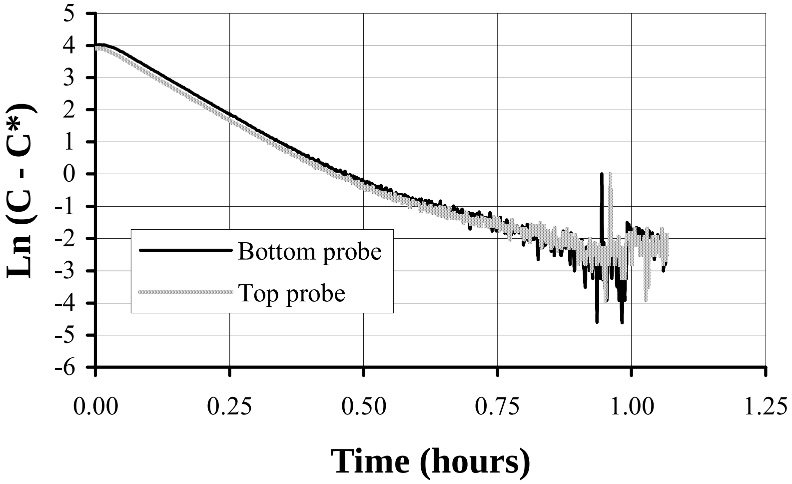

Figure 9.10. Mass-Transfer Results from Bubble Column for Pretreated AZ-101 HLW Simulant and an Air Flow Rate of 51.7 L/min

Table 9.2. Derived Oxygen Mass-Transfer Coefficients

Slurry	Yield Stress (Pa)	Predicted gas holdup (vol%)	Air flow rate (L/min)	$k_l a$ product (/hr)		
				Bottom probe	Top probe	Average
Dilute clay	7.3	1.11	12.9	(a)	3.58	3.6
		1.70	29.5	5.94	5.66	5.8
		2.43	50.3	8.17	8.09	8.1
Concentrated clay	17	1.09	12.9	(a)	1.87	1.9
		2.63	29.5	3.41	3.35	3.4
		4.55	50.3	5.68	5.61	5.6
Pretreated AZ-101 HLW simulant	11	2.26	12.9	2.49	2.69	2.6
		3.49	29.5	5.97	5.96	6.0
		5.01	51.3	9.11	9.08	9.1

(a) Result not obtained because data were inconsistent, as shown in Figures 7.2 and 7.5.

As expected, $k_l a$ products increased with increasing air flow rate and decreasing yield stress. Terasaka and Shibata (2003) found that for non-Newtonian solutions of xanthan and carbopol, the O_2 $k_l a$ product, was correlated by

$$k_l a \propto \alpha_i^{0.73} \sqrt{\frac{D_L}{\tau_0}} \tag{9.4}$$

where α_i is gas holdup (dimensionless fraction), D_L is O_2 diffusivity ($m^2 s^{-1}$), and τ_0 (Pa) is yield stress. The gas holdup is a function of its superficial velocity and rheological properties. The value for each slurry was derived from the bubble-column testing described in Section 8. PNWD assumed an insignificant difference between the specific interfacial areas in the mass transfer and gas-holdup bubble columns in using the correlation from Section 8. Therefore, the data were fitted to a correlation of the same form, assuming the O_2 diffusivity to be the same in all slurries, to provide

$$k_l a = 6130 \alpha_i^{1.125} \tau_0^{-1.1013} \tag{9.5}$$

where α_i is gas holdup (dimensionless fraction), and τ_0 (Pa) is yield stress. The residual square value of the correlation is 87%, indicating that this percentage of variability is accounted for in the correlation. The remaining 13% is probably due to variation in the diffusivities in the slurries and differences in the specific interfacial areas in the mass transfer and gas-holdup bubble columns. Indeed, the correlation fit to only the results for clay ($k_l a = 1748 \alpha_i^{0.894} \tau_0^{-0.862}$) gave a residual square value of 99%, indicating that essentially all of the variability in $k_l a$ is accounted for by considering only yield stress and gas holdup. Thus the clay and pretreated AZ-101 HLW simulant have comparable mass-transfer coefficients for equivalent rheology.

For application to H_2 gas, the $k_l a$ product derived from Eq. (9.5) should be modified to account for the difference in diffusivity between H_2 and O_2:

$$(k_l a)_H = (k_l a)_O \sqrt{\frac{D_{L,H}}{D_{L,O}}} \qquad (9.6)$$

where $(k_l a)_H$ and $(k_l a)_O$ are the $k_l a$ products for H_2 and O_2 gases, respectively, and $D_{L,H}$ and $D_{L,O}$ are the H_2 and O_2 diffusivities, respectively. Application of these results to plant performance will require additional data from the half-scale LS testing and the technical literature on mass transfer in non-Newtonian fluids. Factors that need to be addressed for predicting plant performance include accounting for the following:

- The difference in gas liquid interfacial area per unit volume between test stands and full-scale tanks.
- The difference between the rheological properties of the simulants used and the bounding rheological properties assumed for the plant.
- The difference between the diffusivity of flammable gases in actual waste and the diffusivity of O_2 in the simulants.

9.3.2 UFP Tank Testing Results

Results from the UFP test are illustrated in Figure 9.11. The constant dissolved O_2 concentration for 20 minutes shows that pulse jets alone are ineffective at stripping dissolved O_2. The dissolved O_2 concentration decreased according to theory once air sparging began, providing a $k_l a$ product of 0.70/hr.

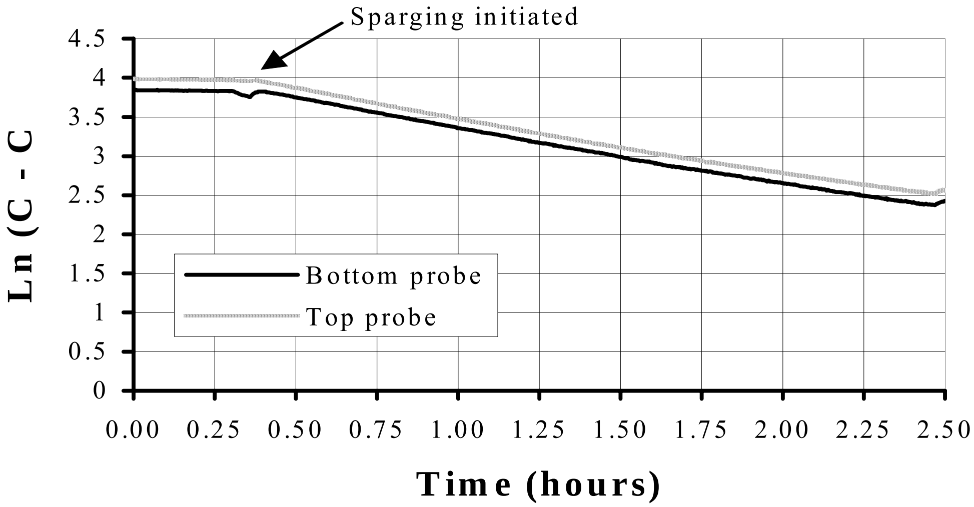

Figure 9.11. Mass-Transfer Results from UFP Tank Test

A holdup of 0.45% was calculated from the correlation presented in Section 8 for a superficial velocity of 0.26 cm/s. The correlation derived from the bubble column data (Eq. 9.5) predicts a *ka* product of 1.27/hr for the UFP tank test, approximately twice the measured value. The correlation derived from the mass-transfer apparatus overestimated the $k_l a$ product in the UFP, probably because of a number of factors, including

- poorer distribution of sparge bubbles in the UFP resulting from a lower mixing intensity
- larger sparge bubbles providing a lower specific interfacial area
- wall effects in the mass-transfer column more significant leading to greater gas-holdup and higher mass-transfer rates than in the UFP tank for the same sparge rate.

10.0 References

Bates JM, JW Brothers, JM Alzheimer, and DE Wallace. 2004. *Test Results for Pulse Jet Mixers in Prototypic Ultrafiltration Feed Process and High-Level Waste Lag Storage Vessels.* WTP-RPT-110 Rev. 0, Battelle—Pacific Northwest Division, Richland WA.

Bontha JR, TE Michener, DS Trent, JM Bates, and MD Johnson. 2003a. *Development and Assessment of the TEMPEST CFD Model of the Pulsed Jet Mixing Systems*. PNWD-3261, Battelle—Pacific Northwest Division, Richland, WA.

Bontha JR, JM Bates, CW Enderlin, and MG Dodson. 2003b. *Large Tank Experimental Data for Validation of the FLUENT CFD Model of Pulsed Jet Mixers*. PNWD-3303, Battelle—Pacific Northwest Division, Richland, WA.

CRC Press. 2004. *Handbook of Chemistry and Physics*, 84th Edition. Boca Raton, FL.

Gauglitz PA, SD Rassat, MR Powell, RR Shah, and LA Mahoney. 1995. *Gas Bubble Retention and Its Effects on Waste Properties: Retention Mechanisms, Viscosity, and Tensile and Shear Strengths*. PNNL-10740, Pacific Northwest National Laboratory, Richland WA.

Gauglitz PA, SD Rassat, PR Bredt, JH Konynenbelt, SM Tingey, and DP Mendoza. 1996. *Mechanisms of Gas Bubble Retention and Release: Results for Hanford Waste Tanks 241-S-102 and 241-SY-103 and Single-Shell Tank Simulants*. PNNL-11298, Pacific Northwest National Laboratory, Richland WA.

Johnson GD, DC Hedengren, JM Grigsby, CW Stewart, JJ Zach, and LM Stock. 2001. *Flammable Gas Safety Issue Resolution.* RPP-7771, CH2MHILL Hanford Group, Inc., Richland, WA.

Poloski AP, PA Meyer, LK Jagoda and PR Hrma. 2004. *Non-Newtonian Slurry Simulant Development and Selection for Pulsed Jet Mixer Testing.* WTP-RPT-111 Rev 0, PNWD-3495, Battelle—Pacific Northwest Division, Richland, WA.

Rassat SD, SM Caley, PR Bredt, PA Gauglitz, DE Reinhart, and SV Forbes. 1998. *Mechanisms of Gas Retention and Release: Experimental Results for Hanford Single-Shell Waste Tanks 241-A-101, 241-S-106, and 241-U-103*. PNNL-11981, Pacific Northwest National Laboratory, Richland WA.

Stewart CW, ME Brewster, PA Gauglitz, LA Mahoney, PA Meyer, KP Recknagle, and HC Reid. 1996. *Gas Retention and Release Behavior in Hanford Single-Shell Waste Tanks.* PNNL-11391, Pacific Northwest National Laboratory, Richland, WA.

Tachiev G, JA Roth, and AR Bowers. January 2000. "Kinetics of Hydrogen Peroxide Decomposition with Complexed and "Free" Iron Catalysts." *International Journal of Chemical Kinetics*, 32(1):24-35.

Terasaka K and H Shibata. 2003. "Oxygen Transfer in Viscous Non-Newtonian Liquids Having Yield Stress in Bubble Columns." *Chemical Engineering Science* 58.

Treybal RE. 1980. *Mass Transfer Operations*. McGraw-Hill, New York.

Wilson DA, ML Restivo, HN Guerrero, TJ Steeper, RE Eibling, EK Hansen, TM Jones, and KR Eberl. 2004. *One-Eighth Scale Pulse Jet Mixer (PJM) – Design Parameter Scale Law Testing*. WSRC-TR-2004-00430/SRNL-RPP-2004-00069 Draft A, Westinghouse Savannah River Company, Aiken, SC.

Appendix A

Determining the Relationship Between Height Measurement and Tank Volume

Appendix A

Determining the Relationship Between Height Measurement and Tank Volume

The U.S. Department of Energy (DOE) Office of River Protection's Waste Treatment Plant (WTP) will process and treat radioactive waste that is currently stored in underground tanks at the Hanford Site. Pulse jet mixers (PJMs) have been selected to mix the high-level waste (HLW) sludge stream in several tanks (e.g., the lag storage [LS] and ultrafiltration feed process [UFP] vessels). Gas-retention and release (GR&R) testing was conducted by Battelle—Pacific Northwest Division (PNWD) using rheologically representative, nonradioactive, non-Newtonian waste simulants in scaled test stands to assess safety-related questions about gas in the waste slurry (gas generated in actual waste is anticipated to be flammable/explosive because of the presence of constituents such as hydrogen). Specifically, there was a desire to understand the amount of gas that could be expected to be retained in the waste slurry during normal operations and the characteristics of gas release upon system restart after occurrence of a loss-of-power event. Thus, the principal quantity of interest in these tests is the volume of gas in the slurry fluid.

To assess the amount of gas within the slurry fluid, the change in volume of the fluid within the tank can be tracked over time during the testing. In the GR&R tests, observations (electronic and manual) were made of the height of the fluid surface in the test-stand tanks. These height observations were subsequently used to determine the volume within the tank. This appendix describes the correlation between the measured height and the volume within each of the tanks in the four test stands operated by PNWD.

A.1 Concepts and Approaches to the Calculations

Understanding the relationship between tank volume and the height of the fluid surface is complicated by the fact that the fluid surface height changes within both the PJMs and the tank and the fact that the PJMs are of an irregular shape (i.e., do not have a constant specific volume). It is useful to first define relevant terms and then to examine a simplified PJM/tank system before discussing two approaches for determining the total volume in a tank.

A.1.1 Terms

4PJM	A four-PJM test stand. The PNWD GR&R tests were conducted with a large-scale system (336 4PJM) and a small-scale system (APEL 4PJM). These tanks do not represent a particular WTP process vessel but were used to examine scaling effects. A third, very-small-scale system was operated by Savannah River National Laboratory but is not discussed here.
Fluid	The fluid in the tank and PJMs that is undergoing testing. May refer to water used in height/volume correlation development or a slurry simulant. See entry for slurry.
GR&R	Gas retention and release; refers to a particular type of PJM mixing test.

H/D	Ratio of fluid surface height (above tank bottom) to tank diameter under static conditions.
Height	Distance measurement made relative to a specified reference. A height measurement specified as “from rim” denotes the distance between the top of the tank rim to the tank fluid level (or other feature within the tank). The “from rim” height is usually reported in inches and was taken using a steel tape. A height measurement specified as “affixed” means that the height value was read from a flexible measuring tape that was firmly attached to the tank wall with Scotch tape. An affixed tape has the zero at an arbitrary vertical position. Affixed tapes were usually read using the centimeter scale (although the tapes had corresponding values in inches). A height measurement specified as “from tank bottom” denotes the distance from the tank bottom (inside the tank) to the tank fluid level (or other feature within the tank). Most often the “from tank bottom” values are actually calculated by subtracting a “from rim” measurement from the total tank height (from bottom of inside of tank to tank rim). The GR&R tests primarily use the “affixed tape” height measurements (usually recording the centimeter value).
Level probe	This most often refers to the Ametek Drexelbrook (Horsham, PA) RF admittance sensors that are installed inside the PJM tubes for determining displacement within the PJM (from which the nozzle velocity can be calculated). Use within a PJM is implied unless it is explicitly stated otherwise (e.g., for a situation where a Drexelbrook level probe was used in the tank directly).
LS	Prototypic lag storage tank or test stand.
PJM	Pulse jet mixer; consists of a number of parts, including a nozzle, cone section, tube section, shoulder section, large riser pipe, and (in some cases) a small riser pipe. The cone, tube, and shoulder sections are of larger diameter and are where the bulk of the fluid displacement occurs. The shoulder of the PJM tube is the rounded portion at the top of the PJM tube. In the UFP and LS test stands, the larger riser pipe is connected to the top of the shoulder section and houses electronics for the PJM level probe within the PJM. The small riser pipe in the UFP and LS test stands is connected above the large riser pipe and is used both for mounting to a frame above the tank and as the connection to the pressure/vent/vacuum manifold. The 336 4PJM test stand has a single large diameter riser pipe with a cross fitting to connect to instrumentation (electronics are external) and the pressure/vent/vacuum supply. The APEL 4PJM system also has a single diameter riser pipe with externally mounted PJM level probe electronics and a tee for connection to the pressure/vent/vacuum supply. The whole of these parts that hang from the mounting frame are also referred to as the “PJM assembly” in this appendix.
PJMs full	When a vacuum is applied to the PJMs, they fill with fluid to a height depending on the fluid density as well as the strength and duration of the vacuum applied. This is the “PJM full” condition (also referred to as the minimum tank level). For the LS, UFP, and 336 4PJM test stands, the fluid flowed up into the flexible air/vacuum supply hose above the top of the tank during PJM full conditions. However, in the APEL 4PJM system, the fluid within the PJM was still within the cylindrical PJM tube section of the PJM assembly under PJM full conditions. When the vacuum is discontinued, the fluid within the PJM may 1) remain at the same height within the

	PJM (i.e., when a solenoid valve isolates the PJM), 2) slowly drain downwards (i.e., if the solenoid valve is leaky), or 3) more rapidly drain downwards (i.e., the PJM is vented to atmosphere). The PJM full condition is important because during operation of the PJMs, this condition is maintained for (typically) a significant portion of each pulse cycle, thereby providing a transiently stable condition at which an observation of the height of the fluid surface can be recorded.
Slurry	Refers to the rheologically representative, nonradioactive, non-Newtonian waste simulants used by PNWD in the PJM mixing tests. The GR&R tests used a bentonite/kaolin/water mixture (i.e., clay slurry) with a composition designed to obtain specific fluid properties (e.g., Bingham yield stress, consistency).
Specific volume	The volume within or displaced by a “container” per unit change in height. Depending on the context, the specific volume may refer to the volume in the tank, the volume within a piece of equipment (e.g., pipe), or the volume displaced by a piece of equipment.
Static	The true static fluid level is the equilibrated level of slurry in a tank with the PJM tubes opened to atmosphere (vented). In this document, “static” denotes a true static (equilibrated) condition where the fluid level is the same within both the tank and the PJMs. A note of caution: at times during testing, operators casually used the term “static” when referring to quiescent conditions with the PJMs full. Similarly, true static conditions may not have been attained even if the PJMs were vented to atmosphere because not enough time was allowed for the fluid to come to equilibrium.
Tank volume	The volume of fluid in a tank, including fluid within the PJMs.
Test stand	This refers to the tank, PJMs, sparge tubes, and other equipment used by PNWD for PJM mixing tests with nonradioactive slurry simulants. The UFP and LS test stands represent scaled versions of the actual WTP vessels for which they are named. The 4PJM test stands are generic systems used to examine scaling effects and are referred to as full-scale (336 4PJM) and small-scale (APEL 4PJM).
UFP	Prototypic ultrafiltration feed process tank or test stand.
Ultrasonic sensor	Continuous ultrasonic sensors from Gems Sensors (Plainville, CT) that are mounted to the PJM frame sitting on the top of the tank. These sensors use high-frequency sound-wave pulses to determine the distance to the surface of the fluid in the tank.

A.1.2 Conceptual Discussion of Height/Tank Volume Relationship

Our understanding of the height/volume correlation is benefited by a conceptual understanding of how the fluid location in a PJM/tank system changes and an examination of the effects of the irregular shape of the PJM assembly on such a correlation.

There are several scenarios for the locations of the fluid surfaces in a tank and in the PJMs (Figures A.1 and A.2). Under nonoperating (quiescent) conditions, the PJMs may either be at equilibrium with the tank or full of fluid; both conditions are depicted in Figure A.1. Depending on the test stand, the fluid surface height in the PJMs when they are full may be either within the cylindrical tube portion or somewhere above the top of the PJM level probe (oftentimes the fluid surface rises above the top of the

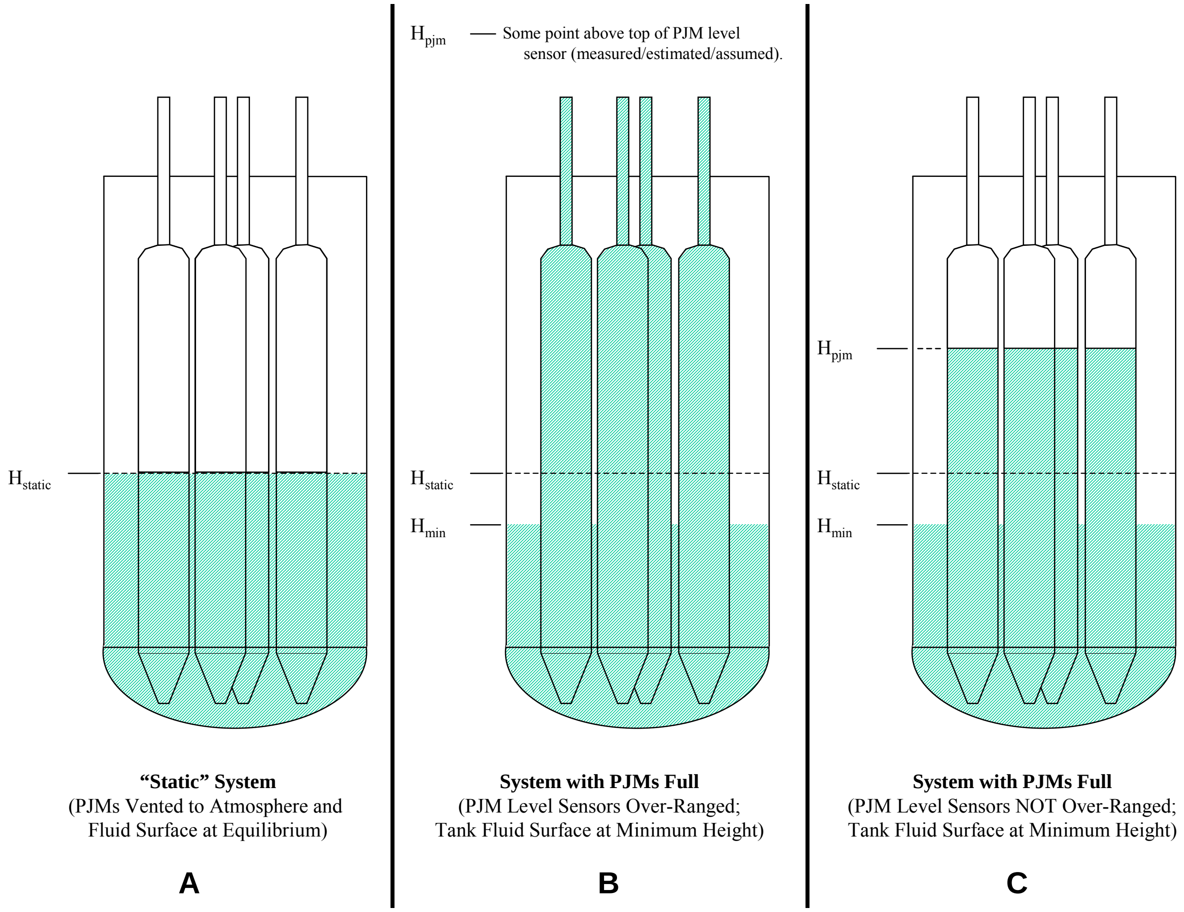

"Static" System (PJMs Vented to Atmosphere and Fluid Surface at Equilibrium)

System with PJMs Full (PJM Level Sensors Over-Ranged; Tank Fluid Surface at Minimum Height)

System with PJMs Full (PJM Level Sensors NOT Over-Ranged; Tank Fluid Surface at Minimum Height)

Figure A.1. Side View of a Tank with PJMs. H_{static} represents the liquid level in the tank for a particular total tank volume under static conditions (same height both in the tank and within the PJMs). For PJM full conditions, that same volume would be distributed such that the tank liquid level is some H_{min} and the liquid level within the PJMs is at H_{pjm}.

tank into the flexible air/vacuum supply hosing). Only the APEL 4PJM test stand operated under conditions shown in Figure A.1 (C). During operation of the PJMs, the PJM full condition (tank fluid surface minimum level) is also maintained for (typically) a significant portion of each pulse cycle. The other operating condition of note is when the PJMs are mostly emptied (but not overblown such that they are completely empty), as shown in Figure A.2 (D). Two non-ideal cases may occur during testing, depending on operator actions or equipment reliability. If the PJMs are vented but not allowed enough time to come to equilibrium, a scenario such as in Figure A.2 (E) may occur. If a vacuum is not maintained (e.g., valves leak), the PJM full condition may not be maintained, as shown in Figure A.2 (F) for the case where the PJM full condition results in fluid above the top of the tank.

The importance of these tank/PJM fill scenarios is in relating a known height of the fluid surface level in the tank to the total volume of slurry in the tank (and PJMs). The conditions under which a tank fluid surface level height observation was taken will require a corresponding height/volume relationship. The PJM full condition is a convenient scenario for making observations because it can be maintained whether the PJMs are operating (as a transiently/cyclically stable condition) or not. However, the correlation of height/volume for the static scenario is more straightforward.

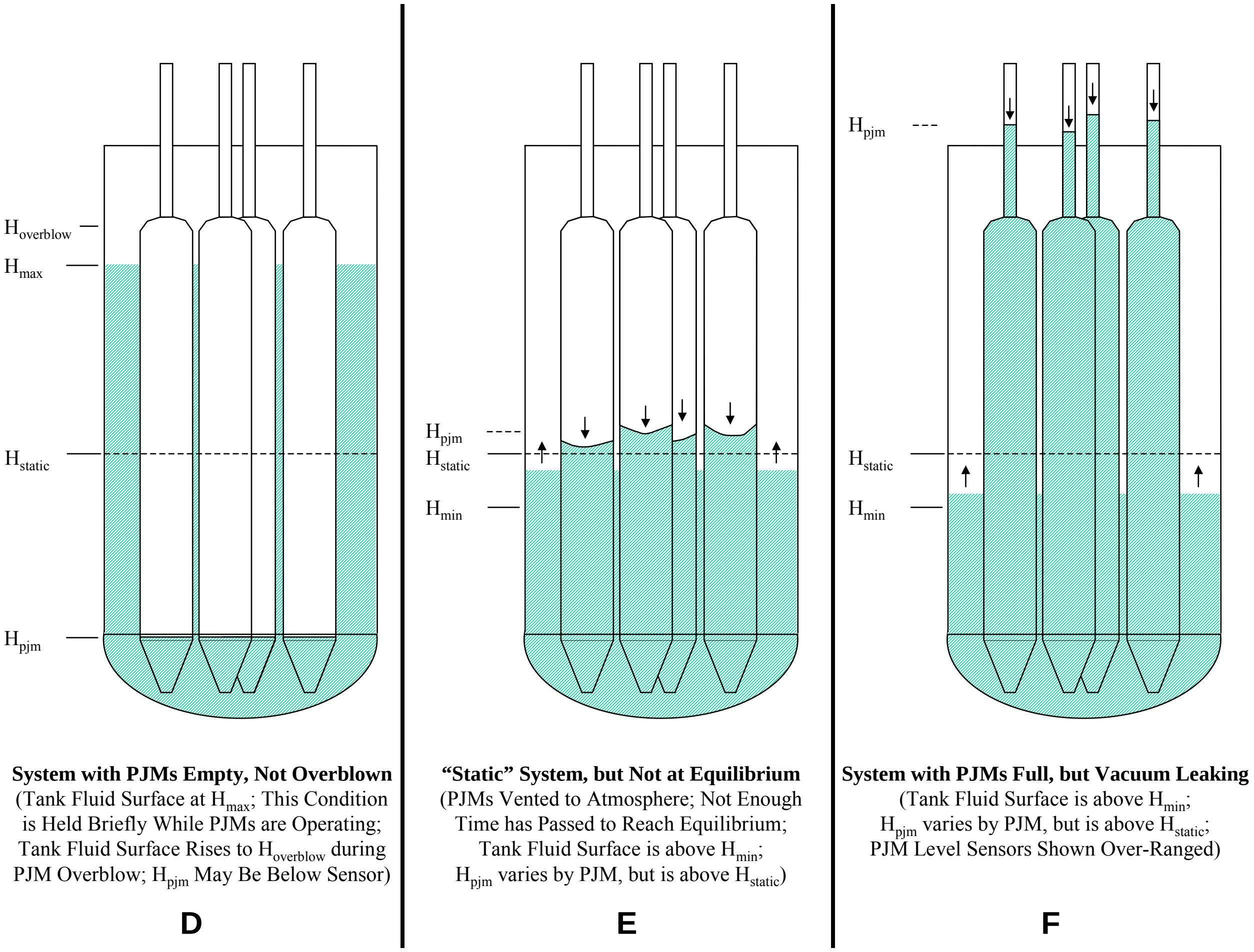

System with PJMs Empty, Not Overblown
(Tank Fluid Surface at H_{max}; This Condition is Held Briefly While PJMs are Operating; Tank Fluid Surface Rises to $H_{overblow}$ during PJM Overblow; H_{pjm} May Be Below Sensor)

"Static" System, but Not at Equilibrium
(PJMs Vented to Atmosphere; Not Enough Time has Passed to Reach Equilibrium; Tank Fluid Surface is above H_{min}; H_{pjm} varies by PJM, but is above H_{static})

System with PJMs Full, but Vacuum Leaking
(Tank Fluid Surface is above H_{min}; H_{pjm} varies by PJM, but is above H_{static}; PJM Level Sensors Shown Over-Ranged)

Figure A.2. Side View of a Tank with PJMs. H_{static} represents the liquid level in the tank for a particular total tank volume under static conditions. When PJMs are operating and the PJMs are "empty," the tank liquid level will be at some H_{max} . Non-ideal conditions (E and F) may mean that the liquid levels are not well defined.

Several points are made clear when examining the height/volume relationships for an idealized PJM/tank configuration (see Attachment A). If a PJM is idealized as a stack of cylinders (the PJM tube and riser pipes) that are within a cylindrical tank, the tank volume can be readily calculated as a function of height. If these ideal PJMs are completely empty or completely full, the height/volume data do not show a linear relationship over the entire tank height. Rather, there is a linear relationship over the vertical extent of each cylindrical part; each segment has a linear relationship with a slope that defines the specific volume (volume per unit change in height) of the tank. For the case where the PJMs are vented to the atmosphere, the height/volume relationship is very close to linear over the entire tank height because it is only affected by the difference in wall thickness of the parts.

A.1.3 Approaches to Determining Total Tank Volume

There are two approaches that can be taken to determine the total tank volume for a tank/PJM system, presuming that the height observation is taken when the PJMs are full. Volume may be calculated by a direct correlation or by a sum of volumes. For height observations made under static conditions, the direct correlation approach applies.

A.1.3.1 Direct Correlation Approach

To obtain a relationship for the volume in a tank based on height observations, a series of measurements that record water volume (or mass) in the tank and the fluid surface level height can be taken (for different heights). Water is a convenient fluid to work with when making these measurements. These height and tank volume (water mass) data can be used in a least-squares regression to obtain a correlation.

Additional considerations apply if this approach is being used to correlate height to tank volume while the PJMs are full. Measurements are needed more frequently around features where the specific volume changes (i.e., at the shoulder between the PJM tube and the riser pipe attached to the top of the PJM tube) than for zones of constant specific volume (i.e., the cylindrical portion of the PJM tube). The transition areas require more measurements because the rate of tank-volume change in these areas is potentially nonlinear, as shown by the ideal system discussed in Section A.1.2. Also, the "PJM full" condition needs to be maintained by applying a constant vacuum to the PJMs while collecting data. This constant vacuum will hold the water level within the PJMs at a (measured) height. This ensures consistency for defining the "PJM full" condition and provides data from which to calculate fluid levels within the PJMs to represent alternative "PJM Full" scenarios.

A.1.3.2 Sum of Volumes Approach

The height/volume correlation can also be obtained using another method, though the data cannot be directly correlated (as in the first approach). Consider the total volume in the tank and PJMs (shown in Figure A.1[C] as an example) as being divided up into two portions: that below the liquid surface (in both the tank and the PJMs) and that above the liquid surface (within the PJMs only). The volume of liquid within the tank and PJMs below the liquid surface (H_{min} in the figure) can be determined from a direct correlation of height and volume data collected under true static conditions, which is an essentially linear correlation over all portions of the PJM (as discussed in Section A.1.2). The volume of liquid within the PJMs above the liquid surface must be determined from a known height of liquid within the PJMs and information about the geometry and dimensions of the PJM assembly. The height of liquid within the PJMs can be determined either from the PJM level probe data or by assuming a height (using operational knowledge as a basis). The total tank volume is the sum of the volume within the PJMs above the liquid surface height plus the volume below the liquid surface height. Mathematically, the static correlation can be added to a piecewise sum of specific volumes times delta heights for the PJM sections above the fluid surface level.

A.2 Correlation Data

Data were collected for each of the four test stands used in the GR&R tests by PNWD. Similar approaches were used for all the test stands, but the details differ because of variations such as tank material (transparent acrylic versus steel) and number of sensors. Manual height measurements were made using either a tape affixed to the side of the tank (UFP, LS, APEL 4PJM) or a steel tape to measure from the top of the tank rim downward (336 4PJM). Measurements were generally taken at a specific location around the circumference of the tank, although other observation stations may exist. The manual height measurements are the primary data of interest; supplemental data in the form of sensor data logged by the data acquisition and control system or video recordings were not used. Water-mass measurements were taken using load cells placed under the tank legs (336 4PJM) or under the water-supply vessel used to add water to the tank (UFP, LS, APEL 4PJM).

A summary of the height and mass data for each test stand is given below, with the actual data in Attachment B. Test-stand diagrams showing dimensions of interest for the height to tank volume correlations are shown in Attachment D. The data for all four test stands are best suited to a sum of volumes approach (Section A.1.3.2) to determine the correlation of height to tank volume.

A.2.1 LS and UFP Tanks

After the GR&R tests were completed in the UFP and LS tanks and the tanks were cleaned and emptied, a series of observations was made for the mass of water in a tank and the corresponding height measurement (LRB #14497, pp. 42-43; LRB #14497, p. 138). Most of these measurements were made under true static conditions where the PJM tubes were vented to the atmosphere. Some measurements were made with the PJMs empty (by overblowing the PJMs and then closing the manifold valves) and with the PJMs full (by applying vacuum to the PJMs and then closing the manifold valves). It was observed during this data collection that when the valves were closed for the “PJM Full” condition, (i.e., after applying a vacuum), water would drain back down from the small riser pipe and flexible hose connected to the system manifold (rather than remaining at a specific height). Additional data listed in Attachment C (LRB #14497, p. 139) were collected for the relationship between the “from rim” heights and the affixed tape heights (at the south side of the tanks) because some height measurements required conversion to the affixed tape scale.

For static conditions, there are five points of height/tank volume data for the UFP tank and nine for the LS tank. For the full PJM condition, there are two points of data for the UFP tank and possibly one for the LS tank. The temperature of the water was not recorded while measuring water mass and tank fill height. Dimensional information pertaining to the height/volume correlations for the UFP and LS tanks was obtained from measurements (LRB #14497, pages 142-143) and standard tables (ASME 1985, 2001; ASTM 2003) and is shown in equipment drawings (Attachment D).

A.2.2 APEL 4PJM Tank

Six observations were made for the mass of water in the APEL 4PJM tank and the corresponding height measurement (LRB #14411, pages 91-92) under static conditions (PJM tubes vented to the atmosphere). The temperature of the water was recorded in the LRB as 19.6°C, which corresponds to a density of 0.998265 g/mL (Perry and Green 1997).

Drawings WS005492-001B(a) and WS005494-001B(b) show that the APEL 4PJM test stand PJM tubes are 5-inch stainless steel (schedule 10—per personal communication with Jagan Bontha, PNWD). The

---

(a) Battelle. August 20, 2003. "4PJM Overall Arrangement (for 5" Pipe)." Drawing WS005492-001B, Battelle—Pacific Northwest Division, Richland, WA.

(b) Battelle. August 20, 2003. "4PJM Support Frame Assay (for 5" Pipe)." Drawing WS005494-001B, Battelle—Pacific Northwest Division, Richland, WA.

PJM tube diameters were obtained from ASME B36.19M-1985 (ASME 1985). The PJM level probes used in the APEL 4PJM test stand have a diameter of 0.57 inch, according to information on a vendor quote (personal communication with Jagan Bontha, PNWD, quote E3070701a provided by Autoline Controls, Inc. for Drexelbrook probe model 700-0002-027-I060.0BA0).

A.2.3 336 4PJM Tank

Eight observations (not including one below the cylindrical portion of the tank) were made for the mass of water in the 336 4PJM tank and the corresponding height measurement (LRB #14471, page 119) under static conditions (PJM tubes vented to the atmosphere). The temperature of the water was also recorded by the data acquisition and control system, with an average value of 28.4°C. Two water samples were collected for subsequent density determination, yielding average measured densities (four measurements for each sample) of 0.994 g/mL at ~27.7°C and 0.995 g/mL at ~26.7°C. The average for the two samples is 0.994625 g/mL (compared with 0.996119 g/mL listed in Perry and Green [1997] for a temperature of 28.4°C). Dimensions for the 336 4PJM test stand were found in reports, measured, or derived (see Attachment D).

The data shown in Attachment B for the 336 4PJM test stand include data logged by the data acquisition and control system and manual observations of values displayed by the data acquisition and control system (as well as the eight manual observations of water mass and water-surface height). The manual observations of the weigh computer readout were (subjectively) deemed the most reliable.

A.3 Volume Calculations for Encountered Geometries

For the sum of volumes approach (Section A.1.3.2), the volume within the PJM above the fluid surface-level height must be calculated. The PJM assembly is made up of essentially three types of PJM parts: cylinder, shoulder, and cone. Equations for the volume of fluid contained within each type of geometry (internal volume) are given in the sections below. Note, however, that the volume of the cone is not required because the minimum height of the tank fluid level is always above the cone section, but the equations are included for completeness. Equations for the volume displaced by a type of part (i.e., as if the part were a solid monolith) are included here as well for completeness. The internal volume equations are the primary concern for the height/tank volume correlation, although equipment within the PJM (the level probe) does displace volume within the PJM. In the diagrams and equations that follow, internal dimensions have a subscript of "i," and outside dimensions have a subscript of "o." Volumes are denoted as "inner" or "displaced."

Each type of part has dimensions in the drawings below. However, the equations for volume are formulated in terms of an arbitrary height, h_{wet}, which represents the wetted height above the bottom of the part. For a completely wetted item, h_{wet} equals the total height of the part.

A.3.1 Cylindrical Parts of the PJM Assembly

Cylindrical parts of the PJM assembly include the riser pipes, pipe collars, most of the PJM tube body, and the PJM level probe. Based on the dimensions in Figure A.3, the volume can be calculated for the cylinders of interest.

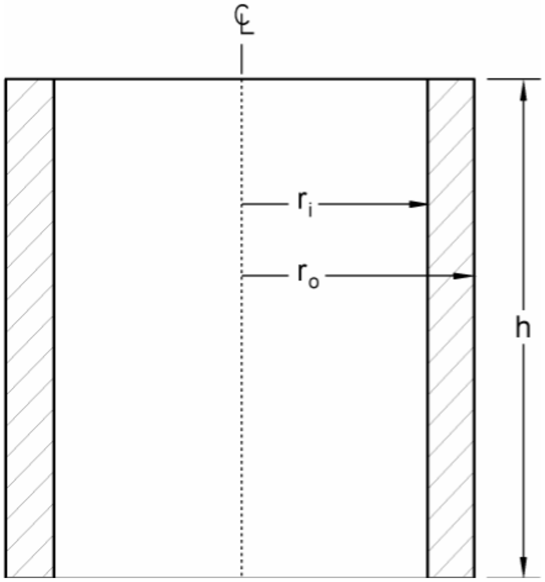

Figure A.3. Section View Through the Center of a Cylindrical Part with a Wall Thickness of $r_o - r_i$.

The volume of a cylinder for a liquid level at an arbitrary height, h_{wet}, above the bottom of the cylinder is

$$V_{\text{inner, cylindrical\_item}} = \pi \cdot r_i^2 \cdot h_{wet} \tag{A.1}$$

$$V_{\text{displaced, cylindrical\_item}} = \pi \cdot r_o^2 \cdot h_{wet} \tag{A.2}$$

For a completely wetted cylindrical item, $h_{wet} = h$ (from Figure A.3).

A.3.2 Shoulder of PJM Tube

From visual observation of the shoulder area of the UFP and LS PJM assemblies, it was determined that the profile of the shoulder looked like a rounded rectangle (i.e., a rectangle with a quarter circle on the right and left sides) as shown in Figure A.4. Design drawings were found that specified a 2:1 elliptical profile (i.e., a where the diameter of major axis = 2 × the diameter of minor axis) for these two test stands (Figure A.5). The reliability of these design drawings with respect to the "as built" system was uncertain. Equations for both profiles are presented; the selected profile for each test stand is discussed in the section on the test stand height/volume correlations.

The volume of the shoulder to an arbitrary height can be determined by integration over a series of cylinders having a thickness, dy, and a radius that is given by the equation for the shoulder profile. The equation of a circle centered at point (x_0, y_0) is

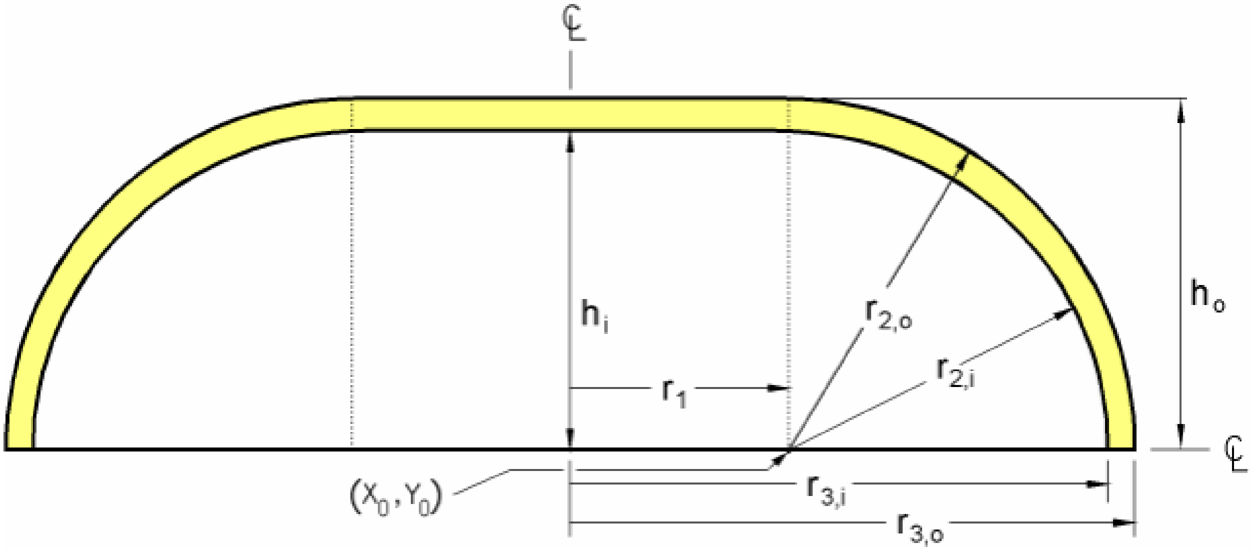

Figure A.4. Section View Through the Center of the PJM Shoulder with a Wall Thickness of $r_{3,o} - r_{3,i}$. This is the observed "rounded rectangle" profile of the shoulder.

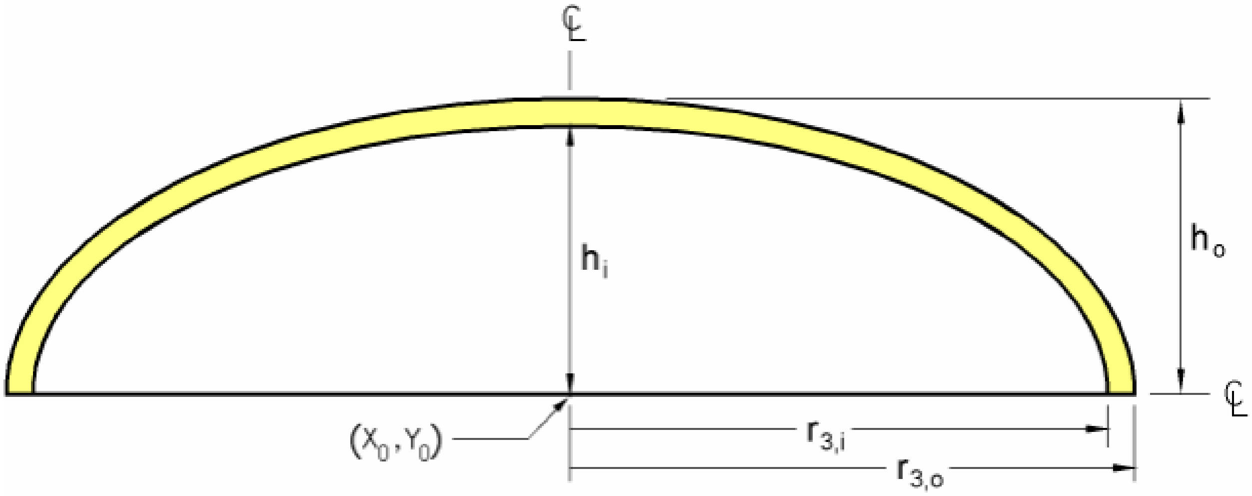

Figure A.5. Section View Through the Center of the PJM Shoulder with a Wall Thickness of $r_{3,o} - r_{3,i}$. This is the profile for a 2:1 elliptical shoulder, per design drawings.

$$(x - x_0)^2 + (y - y_0)^2 = r^2 \tag{A.3}$$

For the case of the rounded rectangle PJM shoulder, $y_0 = 0$ and $r = r_2$, which is a fixed value (either inner or outer, depending on the calculation). Eq. (A.3) can be solved for x, taking the positive root. We then have the x value as a function of height (y in Eq. A.3). At a height of zero, $x = r_3$ and at the top of the shoulder, $x = r_1$. The positive root for x is

$$x = x_0 + (r^2 - y^2)^{\frac{1}{2}} \tag{A.4}$$

The integration equation to obtain the volume of the observed shoulder profile is

$$\text{Volume}_{\text{shoulder,observed}} = \int_0^h \pi \cdot x^2 dy = \int_0^h \pi \cdot \left[x_0 + \left(r^2 - y^2\right)^{\frac{1}{2}} \right]^2 dy \tag{A.5}$$

The integrand can be expanded and then integrated. Using the integral formula from the CRC Handbook (Lide 1992), the volume to an arbitrary wetted height h_{wet} is

$$\text{Volume}_{\text{inner,shoulder,observed}} = \pi \cdot \left[h_{wet} \cdot r_1^2 + h_{wet} \cdot r_{2,i}^2 - \frac{1}{3} \cdot h_{wet}^3 + h_{wet} \cdot r_1 \cdot \left(r_{2,i}^2 - h_{wet}^2\right)^{\frac{1}{2}} + r_1 \cdot r_{2,i}^2 \cdot \sin^{-1}\left(\frac{h_{wet}}{\left|r_{2,i}\right|} \right) \right] \tag{A.6}$$

$$\text{Volume}_{\text{displaced,shoulder,observed}} = \pi \cdot \left[h_{wet} \cdot r_1^2 + h_{wet} \cdot r_{2,o}^2 - \frac{1}{3} \cdot h_{wet}^3 + h_{wet} \cdot r_1 \cdot \left(r_{2,o}^2 - h_{wet}^2\right)^{\frac{1}{2}} + r_1 \cdot r_{2,o}^2 \cdot \sin^{-1}\left(\frac{h_{wet}}{\left|r_{2,o}\right|} \right) \right] \tag{A.7}$$

The volume in an elliptical shoulder can be determined in a similar fashion. The equation for an ellipse centered at (0,0) is

$$\frac{x^2}{a^2} + \frac{y^2}{b^2} = 1 \tag{A.8}$$

For the case of a 2:1 elliptical PJM shoulder, $x_0 = 0$, $y_0 = 0$, $a = r_3$ and $b = ½ \times r_3$ (see Figure A.5). Eq. (A.8) can be solved for x, taking the positive root. We again have the x value as a function of height. At a height of zero, $x = r_3$ and at the top of the elliptical shoulder, $x = 0$. The positive root for x is

$$x = \left(r^2 - 4 \cdot y^2\right)^{\frac{1}{2}} \tag{A.9}$$

The integration equation to obtain the volume of the elliptical shoulder profile is

$$\text{Volume}_{\text{shoulder,elliptical}} = \int_0^h \pi \cdot x^2 dy = \int_0^h \pi \cdot \left[\left(r^2 - 4 \cdot y^2\right)^{\frac{1}{2}} \right]^2 dy = \int_0^h \pi \cdot \left(r^2 - 4 \cdot y^2\right) dy \tag{A.10}$$

Integrating Eq. (A.10):

$$\text{Volume}_{\text{inner,shoulder,elliptical}} = \frac{1}{3} \cdot \pi \cdot h_{wet} \cdot \left(3 \cdot r_{3,i}^2 - 4 \cdot h_{wet}^2\right) \tag{A.11}$$

$$\text{Volume}_{\text{displacement,shoulder,elliptical}} = \frac{1}{3} \cdot \pi \cdot h_{wet} \cdot \left(3 \cdot r_{3,o}^2 - 4 \cdot h_{wet}^2\right) \tag{A.12}$$

For the shoulder volume equations [Eq. (A.6), (A.7), (A.11), and (A.12)], the total height, h, is used in place of h_{wet} when the item is completely wetted.

A.3.3 Correction for Caps/Shoulders

Caps and shoulders have horizontal as well as vertical walls. As shown in Figure A.6 for a cap with a smaller pipe connected to its top, the shaded area is a volume above the total internal height of the cap and below the bottom height of the pipe connected to it. Because this volume is a cylindrical volume element, the easiest way to include it in volume calculations is to extend the bottom height of the upper pipe to the top of the inner wall of the cap or shoulder (e.g., Eq. A.13). If a cap is inverted (smaller pipe connected to the bottom), the same approach is applied except that the top of the pipe is extended upward. No correction is needed for displaced volume, only for volume inside the cap/shoulder/pipe.

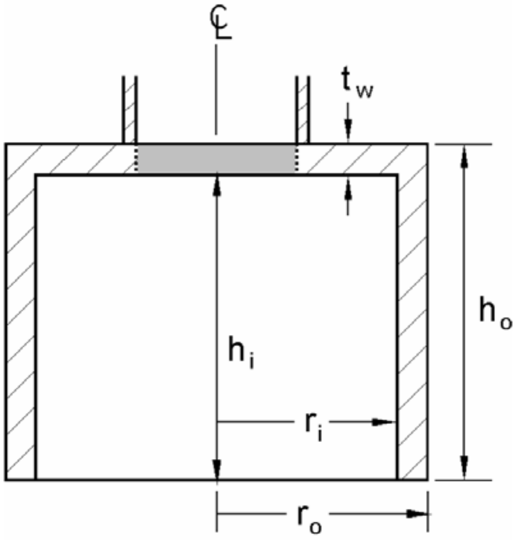

Figure A.6. Section View Through the Center of a Cap with a Pipe Connected to the Top. The shaded area is included in the internal volume for the pipe, not the cap.

$$h_{pipe\_bottom\_theoretical} = h_{pipe\_bottom} + t_w \tag{A.13}$$

A.3.4 Cone of PJM Tube

The cone portion of a PJM assembly is not actually a full cone, but is truncated at the tip of the cone. Thus, the volume within the cone portion of the PJM assembly is determined as the difference between two full cones. Figure A.7 depicts a section view of a full cone with a line to represent where the PJM cone portion is truncated (shaded portion is imaginary) and dimensional quantities that are used in the calculation of cone volume. The only dimensions that are known are the outer diameter of the cone ($r_{1,o}$), the height of the truncated cone (h_3), and the angle of the cone (60°). The cone wall thickness (t_w) is assumed to be the same as for the large diameter pipe that composes the PJM tube body. Other dimensions must be calculated from these quantities using geometric relationships.

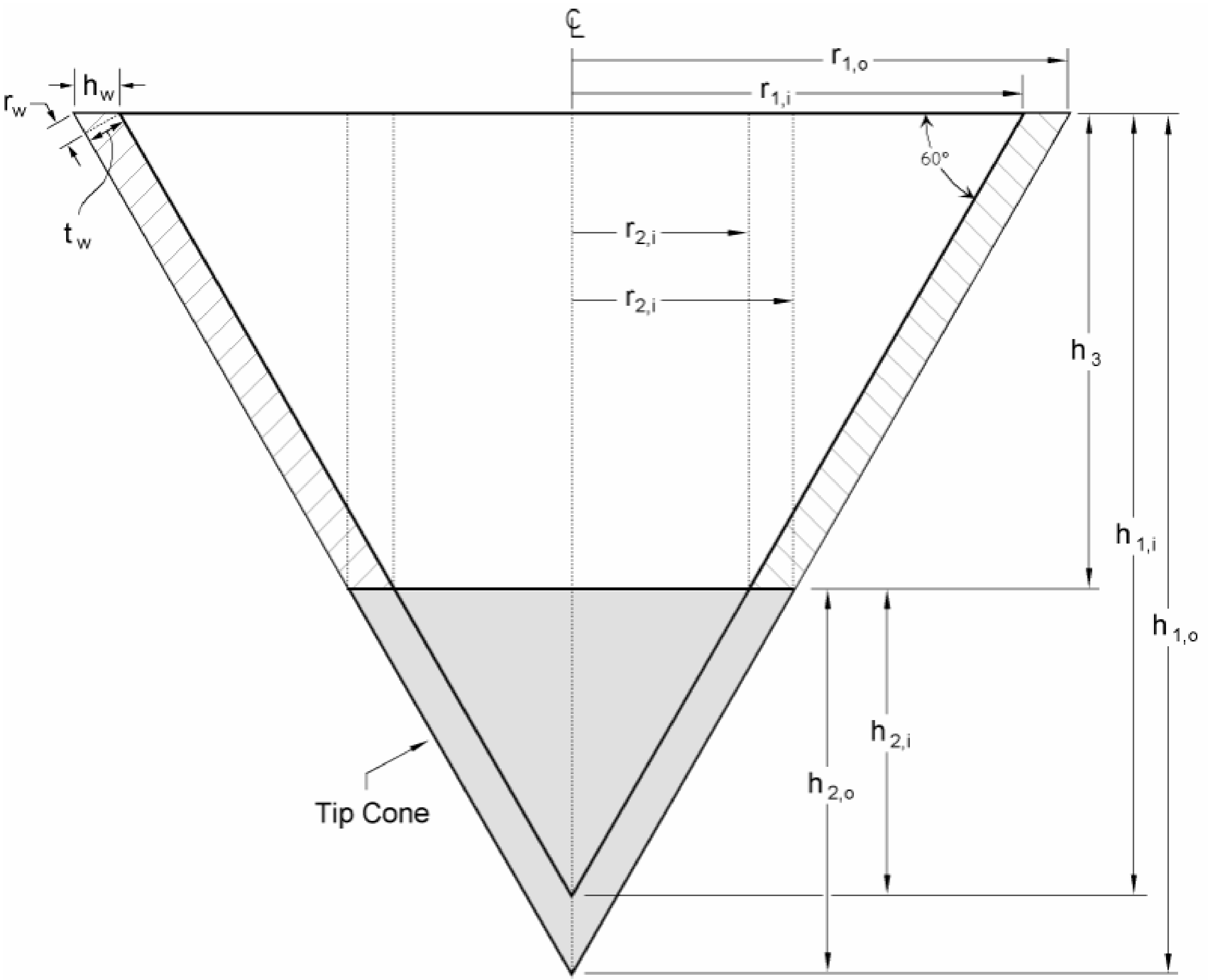

Figure A.7. Section View Through Center of Hollow Cone with a Wall Thickness of t_w. The horizontal line running through the cone represents where the PJM cone portion is truncated (PJM assembly does not include the shaded portion of the cone, or "tip cone").

From geometry, the relationship between the lengths of the sides of a 30-60-90 right triangle (Figure A.8) is known:

$$s = 2 \cdot r \tag{A.14}$$

$$h = r \cdot \sqrt{3} \tag{A.15}$$

Thus, we can calculate "h_w" from the wall thickness:

$$h_w = \left(\frac{2}{\sqrt{3}}\right) \cdot t_w \tag{A.16}$$

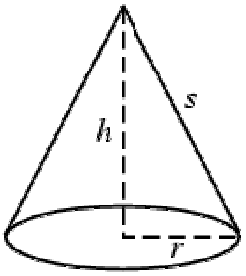

Figure A.8. Depiction of a Cone and the Right Triangle Within the Cone

The inner radius at the base (widest part) of the large cone in Figure A.8 is

$$r_{1,i} = r_{1,o} - h_w \tag{A.17}$$

The volume of a right cone is

$$V_{cone} = \left(\frac{1}{3}\right) \cdot \pi \cdot r^2 \cdot h \tag{A.18}$$

Solving Eq. (A.15) for "r" and substituting into Eq. (A.18) gives

$$V_{cone} = \left(\frac{1}{9}\right) \cdot \pi \cdot h^3 \tag{A.19}$$

The geometry of the tip cone (the portion of the cone in Figure A.7 that is not actually present in the PJM assembly) is used in the calculations for volume of the (truncated) cone section of the PJM. Because it is imaginary, the tip cone height, h_2, does not depend on the wetted height, nor does its volume. The tip cone height is calculated as

$$h_{2,i} = \sqrt{3} \cdot r_{1,i} - h_{3,i} \tag{A.20}$$

$$h_{2,o} = \sqrt{3} \cdot r_{1,o} - h_{3,o} \tag{A.21}$$

The volume for the PJM cone portion (truncated cone) is the difference between the full cone (for the wetted portion) and the tip cone (the shaded part of Figure A.7). For an arbitrary liquid height, the wetted height, h_{wet}, is known and must be added to the height of the tip cone, h_2, to obtain the height of the full cone. If the cone item is completely wetted, then h_{wet} equals h_3.

$$V_{inner,\ cone\_item} = \left(\frac{1}{9}\right) \cdot \pi \cdot \left[\left(h_{wet} + h_{2,i}\right)^3 - h_{2,i}^3\right] \tag{A.22}$$

$$V_{displaced,\ cone\_item} = \left(\frac{1}{9}\right) \cdot \pi \cdot \left[\left(h_{wet} + h_{2,o}\right)^3 - h_{2,o}^3\right] \tag{A.23}$$

A.4 Correlations of Height to Tank Volume

After converting water-mass data to volume (Attachment B) per Equations A.24 and/or A.25, calculations to obtain height/tank volume correlations were performed in three stages. First, linear least squares regression was applied to the height/tank volume data under static conditions to obtain a linear curve fit (the "static correlation") of the form shown in Eq. (A.26). Second, the geometry/dimensions of the PJMs were used to get a piecewise description of the volume within a PJM assembly. Finally, these two pieces were combined and curve fit to obtain height/volume correlation equations valid over a specific vertical span of the tank.

$$\text{Mass of Water in Tank (kg)} = \frac{\text{Mass of Water in Tank (lb)}}{2.20462\ ^{\text{lb}}\!/_{\text{kg}}} \tag{A.24}$$

$$\text{Volume in Tank (L)} = \frac{\text{Mass of Water in Tank (kg)}}{\text{Density of Water (kg/L)}} \tag{A.25}$$

$$V_{\text{static}} = m_{\text{static}} \cdot H_{\text{surface}} + b_{\text{static}} \tag{A.26}$$

The volume within a PJM for portions above the tank-fluid surface level is calculated by a summation of the volume within the different parts of the PJM assembly. Figure A.9 shows a tank in the PJM full condition with arbitrary fluid surface levels of $H_{surface}$ for the surface-level height of the tank fluid and H_{pjm} for the fluid surface-level height within the PJMs. The figure also numbers the parts of the PJM assembly that are located above the tank-fluid surface level. Let $F(h_k)$ represent the function for calculating the volume inside the k^{th} part of the PJM assembly that is above the tank fluid surface level height, $H_{surface}$, where h_k is the delta height for the wetted portion of the k^{th} part. If $H_{k,\,top}$ and $H_{k,\,bottom}$ are the heights of the top and bottom of the k^{th} part, respectively, then h_k can be calculated from Equations A.27, A.28, or A.29. Similarly, let $G(h_k)$ represent the function for calculating the volume displaced by equipment within the k^{th} part of the PJM assembly that is above the surface-level height of the tank fluid. For N_{pjm} number of PJMs in a tank, the volume within the PJMs above the plane represented by the surface-level height of the tank fluid can be calculated from Eq. (A.30). The functions represented by $F(h_k)$ and $G(h_k)$ are presented in Section A.3.

$$h_k = H_{k,\text{top}} - H_{k,\text{bottom}} \qquad \text{for a fully wetted PJM part} \tag{A.27}$$

$$h_k = h_{\text{wet}} = H_{\text{pjm}} - H_{k,\text{bottom}} \qquad \text{for a partially wetted PJM part} \tag{A.28}$$

$$h_k = H_{k,\text{top}} - H_{\text{surface}} \qquad \text{for the PJM part that is intersected by the tank fluid surface} \tag{A.29}$$

$$V_{\text{pjm}} = N_{\text{pjm}} \cdot \left(\sum_k \left[F(h_k) - G(h_k) \right] \right) \tag{A.30}$$

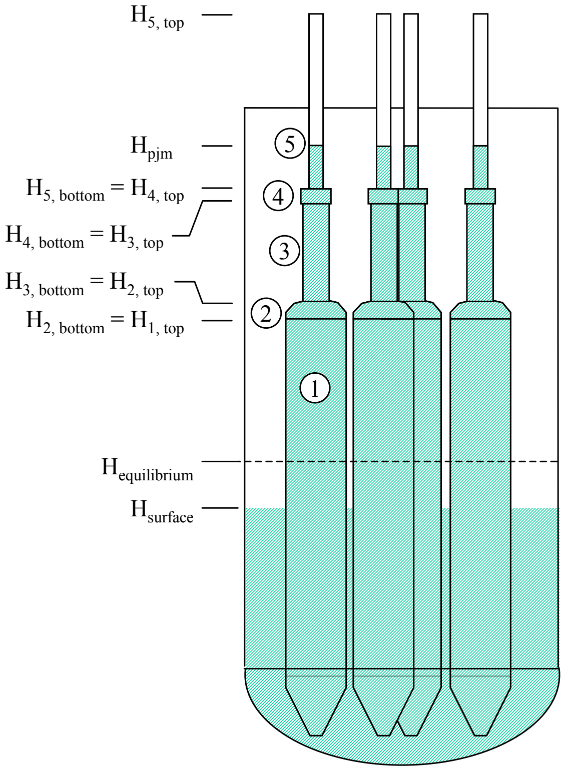

Figure A.9. Side View of Example Tank with PJMs under PJM Full Conditions. Each PJM part above the tank fluid surface is numbered, and the heights of the tops and bottoms ($H_{k,\ top}$ and $H_{k,\ bottom}$) are shown, as are the tank fluid-surface height ($H_{surface}$) and fluid height within the PJMs (H_{pjm}).

The total volume in the tank is then a sum of V_{static} plus V_{pjm}. If V_{static} and V_{pjm} results are calculated at regular intervals (0.5 cm or 0.5 inch, for example) over the height range of interest for a tank, these results can be summed and combined correlations determined by regression. Multiple combined correlations may be appropriate for a tank, depending on the height range where observations will be made and the geometric features of the PJM assembly over the height range.

The correlation equations for static and full PJM conditions are presented in the sections below for each test stand along with test stand-specific information and assumptions.

A.4.1 LS and UFP Test Stands

A.4.1.1 Static Correlation

Height and volume data for the UFP and LS tanks under static conditions are listed in Attachment E (a reorganization of the data in Attachment B). The height data are in terms of the south-side affixed tape scale in units of centimeters. A linear least squares regression was done on the data using the LINEST worksheet function of Microsoft® Excel to obtain height/tank volume correlations under static conditions. The resulting linear curve fit equations for the UFP and LS tanks are shown in Table A.1 (and as Linear Equation #1 on the respective pages of Attachment E).

Table A.1. Height/Volume Correlations for the UFP and LS Test Stands under Static Conditions

Tank	Height/Volume Correlation under Static PJM Conditions	R^2	Eq. #
UFP	Volume in Tank (L) = (5.67571)×(Affixed Tape Height (cm)) + 144.37745	0.999980	(A.31)
LS	Volume in Tank (L) = (24.04534)×(Affixed Tape Height (cm)) + 416.71567	0.999969	(A.32)

A.4.2.2 Height/Tank Volume Correlations with PJMs Full

Attachment F summarizes the heights ($H_{k,\,top}$) of each part of the PJM assemblies for both the UFP and LS test stands and also shows the total internal volume for each part (from the PJM tube upward) calculated using the equations presented in Section A.3. For the UFP and LS test stands, the PJM level probe rod and sensor head are located inside of the PJM assembly and a $^3/_8$-inch OD stainless steel tube encloses the wiring from the sensor head to a tee in the small riser pipe located above the tank rim. The geometry of the PJM level probe "sensor head" (located within the 2-inch pipe above the PJM tube) is unknown, so it was assumed to displace 75% of the volume within the 2-inch fittings. The 75% displacement figure is an estimate based on drawing A-009-0 (Assembly Sketch Level Sensor/PJM Stem Assembly).(a) Dimensions and heights for these internal PJM parts are also included in Attachment F.

Eq. (A.30) was applied for both the UFP and the LS test stands every 0.5 cm from the bottom of the PJM tube to the top of the tank rim (the PJM level probes were over-ranged, so a height of fluid within the full PJM was selected as the top of the tank rim). Linear least squares regression was done on the resulting data using the LINEST worksheet function of Microsoft® Excel to obtain a linear curve fit for each part. Where neighboring parts had similar specific volumes (i.e., the slope of the linear curve fit), those parts were grouped together, and a linear regression was done on the same 0.5-cm interval height/volume data over the height span for that group of parts. The linear regression (linear in the coefficients) for the shoulder part was best modeled by a cubic polynomial rather than a linear curve fit. For some of the GR&R tests in the UFP and LS tanks, the minimum tank-fluid surface-level height intersected both the PJM tube and the PJM shoulder as the volume changed over time. Thus, linear regressions were conducted to determine whether extending the grouped correlations would be acceptable. For the UFP test stand, a linear regression was done to group the entire PJM tube part with the entire shoulder part. For the LS test stand, the cubic curve fit for the PJM shoulder was extended down to include the top 1.6 cm of the PJM tube. The appropriateness of the curve fits was assessed by examining the R^2 regression statistic and the error between the correlation and the volume calculated from Eq. (A.30).

Attachment G shows plots of the data calculated using Eq. (A.30) at 0.5-cm intervals, the abovementioned regressions for each part and for grouped parts, and the error between the regression results and the volumes calculated from Eq. (A.30). A comparison of the volume error for unit changes in height is also included. Recommended choices for the height/total tank volume correlations for height ranges of interest are highlighted. Where available, the recommended correlations are compared to actual data of heights observed when the PJMs were full. The equations for the recommended height/tank

---

(a) PNNL. Drawing A-009-0 (Assembly Sketch Level Sensor/PJM Stem Assembly). Pacific Northwest National Laboratory, Richland, WA.

volume correlations under PJM full conditions are listed in Table A.2. There is an overlap in the height range addressed by LS correlations in Eq. (A.35) and (A.36) because the cubic curve fit for the shoulder was extended 1.6 cm down into the PJM tube part (as mentioned above); both correlations are equally valid in the overlapping region (see Attachment G).

Table A.2. Height/Volume Correlations for the UFP and LS Test Stands for Height Observations Taken when the PJMs are Full

Tank	Affixed Tape Height Range (cm)	**Height/Volume Correlation under PJM Full Conditions** V = Tank Volume with PJMs Full (L) H = Affixed Tape Height on south side (cm)	R^2	Eq.
UFP	11.5 to 101	$V = 4.94161 \times H + 218.81407$	0.999998	(A.33)
	101 to 196.5	$V = 5.66061 \times H + 147.23645$	0.999999	(A.34)
LS	52.6 to 102.6	$V = 18.23469 \times H + 1071.5948$	1.00000	(A.35)
	101 to 117.6	$V = 0.0096806 \times H^3 - 2.98630 \times H^2 + 325.32031 \times H - 9454.7612$	1.00000	(A.36)
	117.6 to 201	$V = 24.01227 \times H + 423.1228$	1.00000	(A.37)

A.4.1.3 Assumptions for LS and UFP Tank Calculations

Assumptions used in determining the height/tank volume correlation when PJMs are full for the UFP and LS test stands are given in Table A.3 along with a brief discussion of the impact of the assumption on the total tank volume. Most of the assumptions pertain to the volume within the PJMs (above the fluid surface height). The impacts of these assumptions on the total tank volume are negligible.

Table A.3. Assumptions and Impacts Pertaining to the Height/Volume Correlations for the UFP and LS Test Stands for Height Observations Taken when PJMs are Full

Assumption for LS & UFP Tank Calculations	Quantities Impacted
Water temperature is 20°C during height/tank volume measurements.	Density of water, volume of water in the tank, and static height/tank volume correlations are all impacted. Using densities from Perry's Chemical Engineers' Handbook (Perry and Green, 1997), there is a 0.02% relative error for a 1°C temperature difference from 20°C and about 0.1% relative error for a 5°C temperature difference from 20°C. Temperature (°C) Density (g/mL) 15 0.999099 19 0.998405 20 0.998204 21 0.997992 25 0.997045 Negligible impact.

Table A.3 (contd)

Assumption for LS & UFP Tank Calculations	Quantities Impacted
During the PJM full condition, the liquid level within the PJMs is at the top of the tank rim (196.5 cm for UFP and 201.0 cm for LS).	Impacts the volume within the PJMs. If the fluid only went as far as the top of the PJM shoulder, then the current calculations would be too high by 1.5 L and 2.8 L for the UFP and LS test stands, respectively. If the fluid rose above the top of the tank rim and into the 1-inch ID clear flexible hose by 2 ft, then the current calculations would be too low by 1.25 L and 2.5 L for the UFP and LS test stands, respectively. Relative to the volume at the lowest H/D setting used in the GR&R tests (or nearest conservative known volume), these latter volumes would give 0.19% and 0.09% error in the absolute volume for the UFP and LS test stands, respectively. Negligible impact on gas-volume fraction.
The 2-in. collars and caps (UFP and LS) are assumed to have an ID equal to the OD of 2-in. pipe.	Impacts the volume within PJMs. Negligible impact.
The 2-in. collars and caps (UFP and LS) are assumed to have an OD equal to 2.75 in. (estimate).	Impacts calculation of wall thickness; thus the volume element in a cap (Section A.3.3). Negligible impact.
The wall thickness of the shoulder or the end plate of a cap is assumed to be the same as that of the PJM tube and cylindrical portion of the cap, respectively.	Impacts the volume element in a cap as discussed in Section A.3.3. For the UFP and LS test stands, the volume elements where the shoulder horizontal wall meets the riser pipe sum to volumes of 0.11 L and 0.22 L total (for all PJMs in the test stand), respectively. Any error in the wall thickness would have a negligible impact. Negligible impact.
The volume in the horizontal wall element of the shoulder or cap is ignored.	Impacts the volume element in a cap as discussed in Section A.3.3. For the UFP and LS test stands, the volume elements where the shoulder horizontal wall meets the riser pipe sum to volumes of 0.11 L and 0.22 L total (for all PJMs in the test stand), respectively. Negligible impact.
Rod portion of PJM level probe (in PJM assembly) is assumed to end at the top of the PJM shoulder.	Impacts the volume within the PJM. If the 2-inch pipe above the PJM shoulder did not contain any level probe equipment, then the current calculations would be too low by 2.6 L and 5.5 L for the UFP and LS test stands, respectively. Relative to the volume at the lowest H/D setting used in the GR&R tests (or nearest conservative known volume), this would be 0.4% and 0.2% error for the UFP and LS test stands, respectively. Negligible impact.

Table A.3 (contd)

Assumption for LS & UFP Tank Calculations	Quantities Impacted
Rod portion of PJM level probe (in PJM assembly) is assumed to be 101 cm (UFP) or 86.5 cm long (LS).	Impacts the volume within PJM, but practically speaking there is no impact because bottom tip of rod is well below the operating region.
The head of PJM level probe (within PJM assembly) is assumed to end at the top of the 2-inch cap above the PJM shoulder (minus wall thickness of cap endplate).	Impacts the volume within PJM. If the 2-inch pipe above the PJM shoulder did not contain any level probe equipment, then the current calculations would be too low by 2.6 L and 5.5 L for the UFP and LS test stands, respectively. Relative to the volume at the lowest H/D setting used in the GR&R tests (or nearest conservative known volume), this would be 0.4% and 0.2% error for the UFP and LS test stands, respectively. Negligible impact.
The head of the PJM level probe (within the PJM assembly) is assumed to comprise 75% of the volume within the 2-inch collar, 2-inch pipe, and 2-inch cap (all of which are directly above the PJM shoulder).	Impacts the volume within PJM. If the 2-inch pipe above the PJM shoulder did not contain any level probe equipment, then the current calculations would be too low by 2.6 L and 5.5 L for the UFP and LS test stands, respectively. Relative to the volume at the lowest H/D setting used in the GR&R tests (or nearest conservative known volume), this would be 0.4% and 0.2% error for the UFP and LS test stands, respectively. Negligible impact.
PJM shoulder is assumed to have the profile shown in Figure A.4 (rounded rectangle).	Impacts the volume within the PJM. For shoulder profiles of the same height, the rounded rectangle profile has 0.4 L and 6.3 L more volume (for all PJMs in the test stand) than a 2:1 ellipse profile for the UFP and LS test stands, respectively. Relative to the volume at the lowest H/D setting used in the GR&R tests (or nearest conservative known volume), this would be 0.06% and 0.22% error for the UFP and LS test stands, respectively. Negligible impact.
During operations, simulant fluid is not lost from the volume calculations as a result of buildup (as a crust) above the maximum fluid height within the PJM or on the tank walls.	Impacts total volume in tank; only impacts calculation of volume within a run. When a new reference volume is established, such an existing non-participating crust volume would not affect subsequent volume calculation. There are insufficient data to quantify the impacts of the failure of this assumption. However, impacts are assumed to be negligible because the tank walls were intermittently wiped with a squeegee during tests, returning the wiped simulant to the bulk and thereby minimizing the impact of simulant coating on tank walls.
The LS measurement at "~H/D = 1.0" was taken at the same tank volume as "Addition #10, Supply Tank Fill #7."	No effect on correlations; used in Attachment G to compare the height/volume correlation for PJM full conditions to actual data.

The impacts of the assumptions are discussed above in terms of absolute volume because the correlations provide total tank volumes. However, volumes in GR&R data reduction are subtracted to obtain the change in volume from a gas-free condition (see discussion in Section 2.2 of the main report). If the same set of assumptions (same basis) applies to both the gas-entrained and gas-free volumes and measurement conditions are the same (e.g., both measured with PJMs full to the same height), then the assumptions (with the exception of #12) will have no impact on the change in volume. If the assumption basis differs, then the change in volume will be impacted. Loss of simulant material as buildup on the tank wall would also impact the change in volume because the gas-entrained volume would be incorrect, but (as discussed in the table) the impact is believed to be negligible because of operational activities. Volumes calculated from the static correlation have the same basis (assumption #1) regardless of height of the fluid surface. A difference in assumption basis will occur when one or both of the tank fluid surface heights (for the gas-free and the gas-entrained states) intersect any PJM part above the top of the PJM tube part because parts above the PJM tube are the ones for which assumptions have been made. Assumptions for the PJM parts above the PJM tube but below the tank fluid surface height are not needed because the volume below the tank-fluid surface height is calculated from the static correlation. The following examples illustrate the scenarios where the same set of assumptions does and does not apply to both the gas-free and the gas-entrained volumes.

If the gas-free volume is calculated at $H_{surface}$ = 90.0 cm and the gas-entrained volume is calculated at $H_{surface}$ = 96.0 cm in the LS tank, then both volumes have the same assumption basis. This is because the assumptions pertaining to PJM internal volume apply to both volume calculations—both heights are below the top of the PJM tube and assumptions #2-#11 apply to PJM parts above the PJM tube.

If the gas-free volume is calculated at $H_{surface}$ = 126.9 cm (top of the 2-inch collar above the PJM shoulder) and the gas-entrained volume is calculated at $H_{surface}$ = 133.0 cm (intersecting the 2-inch pipe) in the LS tank, then the volumes have a different assumption basis. The gas-free volume includes the assumption #10 for the entire length of the 2-inch pipe. For the gas-entrained volume, assumption #10 only applies for 72% of the length of the 2-inch pipe (from a height of 133.0 cm to 148.7 cm). The difference in the assumption basis is the portion of the 2-inch pipe that is submerged (from 126.9 cm to 133.0 cm). Using the LS correlation in Eq. A.37, the change in volume for these gas-free and gas-entrained heights is 146.38 L. If assumption #10 was incorrect and the level probe sensor head only displaced 40% of the volume within the 2-inch pipe (instead of 75%), then the change in volume would be high by 0.37 L. This is a 0.25 % impact on the change in volume.

We can look at the overall impact of assumptions #2 through 11 on the change in volume in the LS tank. The sum of the impacts on total volume for these assumptions equals up to 5.6 L. From a height of 102.6 cm (top of PJM tube) to 155.2 cm (top of 2-inch cap), the change in volume is 1206.6 L using the LS correlations in Table A.3. This is a 0.46% impact on the change in volume.

Most differences in gas-free and gas-entrained height are relatively small and thus there will be small differences in one or two assumptions. In general, the impacts of the assumptions on the change in volume will be negligible.

A.4.2 APEL 4PJM Tank

A.4.2.1 Static Correlation

Height and volume data for observations with water in the APEL 4PJM test stand under static conditions are shown in Attachment E. The height data are in terms of the 0° Station affixed tape in units of centimeters. A linear least squares regression was done on the data using the LINEST worksheet function of Microsoft® Excel to obtain height/tank volume correlations under static conditions. The resulting linear curve fit equation is shown in Table A.4 (and as Linear Equation #1 on the respective page of Attachment E).

Table A.4. Height/Volume Correlation for the APEL 4PJM Test Stand under Static Conditions

Tank	Height/Volume Correlation under Static PJM Conditions	R²	Eq.
APEL 4PJM	Volume in tank [L] = (5.72254)×(affixed tape height [cm]) + 45.99564	0.999961	(A.38)

A.4.2.2 Height/Tank Volume Correlations with PJMs Full

Two operational characteristics simplify the application of Eq. (A.30) to determine the correlation of height to tank volume when the PJMs are full. For the APEL 4PJM tank, both the tank fluid surface level and the fluid level within the PJMs were always within the bounds of a single PJM part—the cylindrical PJM tube. Also, at the PJM full condition, the PJM level probes were not over-ranged (i.e., data on fluid height within the PJM assembly were available) in the APEL 4PJM tank. Given these characteristics, Eq. (A.30) may be applied as the volume within the cylindrical PJM tubes minus the volume displaced by the cylindrical PJM level probe rods over the same delta height, h_k. Rather than doing a linear regression to obtain a linear curve fit, Eq. (A.26) and (A.30) were summed [substituting in Eq. (A.1) and (A.2) for $F(h_k)$ and $G(h_k)$, respectively] to give Eq. (A.39) for the total tank volume as a function of tank-fluid surface-level height and height of fluid within the PJMs. Eq. (A.39) is valid for height observations above the top of the tank dish (approximately 6.0 cm on the 0° station affixed tape) up to 110.0 cm (near the top of the cylindrical PJM tube section).

$$V_{tank} = V_{static} + N_{pjm} \cdot \left(\pi \cdot r_{pjm}^2 - \pi \cdot r_{probe}^2\right) \cdot \left(H_{pjm} - H_{surface}\right) \qquad (A.39)$$

In applying Eq. (A.39), the PJM level probe data recorded by the data-acquisition system must be translated back to the 0° station affixed tape scale, giving H_{pjm}. At an early point in PJM mixing tests (around 8/26/2003), the height of the tips of the PJM level probes (i.e., the start of the active sensor region where the voltage just started to increase from 1 V) were determined on the 0° station affixed tape scale to be at 13.5 cm (personal communication with Jagan Bontha, PNWD), and the top of the dish (the bottom portion of the tank) for the APEL 4PJM tank was noted as 5.1 cm on the 0° station affixed tape scale. The data-acquisition and control system was set to convert the PJM level probe voltage signal to the 0° station affixed tape scale minus an offset of 8 cm, giving H'_{pjm}. Thus, a reading of 1.0 V would display a height (on the 0° station affixed tape scale) nominally equal to the top of the dish. This 8-cm offset was implemented for convenience during operations to prevent driving the liquid level in the PJMs down too far and must be added back to the logged data, H'_{pjm}, to obtain the actual height of the liquid within the PJMs on the 0° station affixed tape scale (Eq. A.40).

$$H_{pjm} = H'_{pjm} + 8\,\text{cm} \tag{A.40}$$

A.4.2.3 Assumptions for APEL 4PJM Tank Calculations

Assumptions used in determining the height/tank volume correlation when PJMs are full for the APEL 4PJM test stand is given in Table A.5 along with a brief discussion of the impact of the assumption on the total tank volume.

Table A.5. Assumptions and Impacts Pertaining to the Height/Volume Correlations for the APEL 4PJM Test Stand for Height Observations Taken when the PJMs are Full

Assumption for APEL 4PJM Tank	Quantity Impacted
During operations, the tank level and level within PJM tubes remains within cylindrical portion of PJM assembly (i.e., the PJM tube).	Not an assumption *per se*, but a constraint on application of Eq. (A.39).
The fluid level within PJM tubes never over-ranges level probe (e.g., PJM levels are always less than 100 cm and greater than 0 cm).	Not an assumption *per se*, but a constraint on application of Eq. (A.39).
During operations, volume of fluid is not lost as a result of buildup (as a crust) above the maximum fluid height within the PJM or on the tank walls.	Impacts total volume in the tank. This only impacts calculation of volume within a run. When a new reference volume is established, such an existing non-participating crust volume would not affect subsequent volume calculations. There are insufficient data to quantify the impacts of the failure of this assumption, but the impact is presumed to be small.

Volumes in GR&R data reduction are subtracted to obtain the change in volume from a gas-free condition (see discussion in Section 2.2 of the main report). Because the APEL 4PJM system is constrained to operate with all fluid heights intersecting the PJM tube portion of the PJM assembly, there would be no impact on the change in volume except those from loss of simulant material to the tank wall.

A.4.3 336 4PJM Test Stand

A.4.3.1 Static Correlation

Height and volume data for the 336 4PJM tank under static conditions is listed in Attachment E (a reorganization of the data in Attachment B). The "height" data are in terms of distance measured down from the top of the tank rim in units of inches. The 336 4PJM tank is opaque (steel); thus, the "from rim" measurement is most convenient. The "from rim" measurement can be converted to a height above the inside tank bottom (by knowing the distance between the tank bottom and the rim), but it is not necessary. A linear least squares regression was done on the data using the LINEST worksheet function of Microsoft Excel to obtain height/tank volume correlations under static conditions. The resulting linear curve fit equations for the 336 4PJM tank is shown in Table A.6 (and as linear equation #1 on the respective page of Attachment E).

Table A.6. Height/Volume Correlations for the 336 4PJM Test Stand under Static Conditions

Tank	Height/Volume Correlation under Static PJM Conditions	R^2	Eq. #
336 4PJM	Volume in Tank (L) = (–296.26055)×(From Rim Height (in.)) + 49485.23	0.999987	(A.41)

A.4.3.2 Height/Tank Volume Correlations with PJMs Full

Attachment F summarizes the heights ($H_{k,\,top}$) of each part of the PJM assemblies for the 336 4PJM test stand and also shows the total internal volume for each part (from the PJM tube upwards) as calculated using the equations presented in Section A.3. In the 336 4PJM test stand, the PJM level probe electronics are located outside of the PJM assembly; thus, only the level probe rod displaces volume within the PJM assembly. Dimensions and heights for the internal PJM parts are also included in Attachment F.

Eq. (A.30) was applied for both the 336 4PJM test stand every 0.5 inches from the bottom of the PJM tube to a point 10 ft above the top of the tank rim (the system typically pulled fluid up above the tank rim, thus over-ranging the PJM level probes). Linear least squares regression was done on the resulting data using the LINEST worksheet function of Microsoft Excel to obtain a linear curve fit for each part. None of the neighboring parts had similar specific volumes, so a height/volume correlation was done for the height span of each PJM part individually. The linear regression (linear in the coefficients) for the shoulder part was best modeled by a cubic polynomial rather than a linear curve fit, but both were calculated for comparison. The appropriateness of the curve fits was assessed by examining the R^2 regression statistic and the error between the correlation and the volume [calculated from Eq. (A.30)].

Attachment G shows plots of the data calculated using Eq. (A.30) at 0.5-inch intervals, the regressions for each part, and the error between the regression results and the volumes calculated from Eq. (A.30). A comparison of the volume error for unit changes in height is also included. Recommended choices for the height/total tank volume correlations for height ranges of interest are highlighted. No data were available with the PJMs full for comparison to the recommended correlations. The equations for the recommended height/tank volume correlations under PJM full conditions are listed in Table A.7.

Table A.7. Height/Volume Correlations for the 336 4PJM Test Stand for Height Observations Taken when the PJMs are Full

Tank	Distance Down from Tank Rim (in.)	**Height/Volume Correlation under PJM Full Conditions** V = Tank Volume with PJMs Full (L) H = Distance Down From Tank Rim (in.)	R^2	Eq. #
336 4PJM	0.0 to 20.5	$V = -296.05543 \times H + 49509.95$	1.00000	(A.42)
	20.5 to 26.25	$V = -0.274568 \times H^3 + 21.62222 \times H^2 - 834.22346 \times H + 53821.27$	1.00000	(A.43)
	26.25 to 147.75	$V = -266.64017 \times H + 48854.91$	1.00000	(A.44)

A.4.3.3 Assumptions for 336 4PJM Tank Calculations

Assumptions used in determining the height/volume correlation when PJMs are full for the 336 4PJM test stand are given in Table A.8 along with a brief discussion of the impact of the assumption on the total tank volume. Most of the assumptions pertain to the volume within the PJMs (above the fluid surface height). The impacts of these assumptions on the total tank volume are negligible or presumed small.

Table A.8. Assumptions and Impacts Pertaining to the Height/Volume Correlations for the 336 4PJM Test Stand for Height Observations Taken when the PJMs are Full

Assumption for 336 4PJM Tank Calculations	Quantities Impacted
The measured density is reasonable to use.	Density of water, volume of water in the tank, and static height/tank volume correlations are all impacted. The measured densities of the water samples exhibit inappropriate trends and are lower than would be expected for pure water (Perry and Green 1997) at the specified temperature. The volumes calculated using the average measured density are about 0.15 to 0.2% too high in terms of relative error. Negligible impact.
The manual observations of the Hardy weigh computer readout for water mass are more reliable than values from the data-acquisition and control system.	The volume of water in the tank and the static height/tank volume correlations are impacted. The manual recording of the DACS display is unreliable because it is a snapshot value, and the person recording data may not have allowed enough time to pass for the system to be at equilibrium. The logged data appear to have an RPD of 0.12 to 0.17% over the entire range of mass recorded. Subjectively, there are more things that can add error to the logged data (electrical noise, distance of signal transmission, analog to digital signal conversion, numerical precision in scaling the signal to engineering units). Negligible impact.
During the PJM full condition, the liquid level within the PJMs rises to a point 10 ft (120 inches) above the top of the tank rim.	Impacts the volume within the PJMs. If this height were incorrect by ±10 ft, then the total volume in the tank currently calculated would be higher or lower by 24.7 L. Relative to the volume in the 336 4PJM tank at the top of the tank dish (a conservative volume), this would be a 0.3% error. Negligible impact.
The 2-inch ID flexible hose rises directly up from the cross where it connects to the PJM assembly (versus traveling horizontally for any distance).	Impacts the volume within PJMs. From observations of a similar system, the horizontal distance that the 2-inch ID flexible hose may travel could be estimated as about 3 ft. In that case, the total volume of the tank would be low by 7.4 L. Relative to the volume in the 336 4PJM tank at the top of the tank dish (a conservative volume), this would be a 0.1% error. Negligible impact.

Table A.8 (contd)

Assumption for 336 4PJM Tank Calculations	Quantities Impacted
The volume within the 2-inch cross of the PJM assembly is negligible.	Impacts the volume within PJMs. If the cross were conceptualized as two 8-inch long cylinders with a 2.067-inch ID, then the total volume of the tank currently calculated would be low by 3.5 L. Relative to the volume in the 336 4PJM tank at the top of the tank dish (a conservative volume), this would be a 0.05% error. Negligible impact.
The rod portion of the PJM level probe (in the PJM assembly) extends below the lowest height where the height/tank volume correlation will be applied.	Impacts the volume within the PJM. At 0.15 L/ft of height (for 4 PJMs), there is negligible impact.
The wall thickness of the shoulder is assumed to be the same as that of the PJM tube.	Impacts the volume within the PJM as discussed in Section A.3.3. For the 336 4PJM test stand, the volume elements where the shoulder horizontal wall meets the riser pipe sum to a volume of 0.05 L total (for 4 PJMs). Any error in the wall thickness would have a negligible impact.
PJM shoulder is assumed to have the profile shown in Figure A.5 (2:1 ellipse).	Impacts the volume within the PJM. A drawing in Appendix A of Bontha et al. (2003a) shows the PJM shoulder profile for the 336 4PJM test stand as a combination of two circle radii of 21.6 and 4.125 in. Yet, in Section 2 of Bontha et al. (2003b), the profile is referred to as a 2:1 ellipse. The 2:1 ellipse profile results in a shoulder volume 2.5 L less than the other profile, which corresponds to an error of 0.03% relative to the volume in the 336 4PJM tank at the top of the tank dish (a conservative volume). Negligible impact.
During operations, simulant fluid is not lost from the volume calculations as a result of buildup (as a crust) above the maximum fluid height within the PJM or on the tank walls.	Impacts total volume in tank; only impacts calculation of volume within a run. When a new reference volume is established, such an existing non-participating crust volume would not affect subsequent volume calculation. There are insufficient data to quantify the impacts of the failure of this assumption, but the impact is presumed to be small.

The impacts of the assumptions are discussed above in terms of absolute volume because the correlations provide total tank volumes. However, volumes in GR&R data reduction are subtracted to obtain the change in volume from a gas-free condition (see discussion in Section 2.2 of the main report). If the same set of assumptions (same basis) applies to both the gas-entrained and gas-free volumes and measurement conditions are the same (e.g., both measured with PJMs full to the same height), then the assumptions (with the exception of #9) will have no impact on the change in volume. If the assumption basis differs, then the change in volume will be impacted. Loss of simulant material as buildup on the tank wall (assumption #9) would also impact the change in volume because the gas-entrained volume would be incorrect. Volumes calculated from the static correlation have the same basis (assumptions #1 and #2) regardless of height of the fluid surface. A difference in assumption basis will occur when one or both of the tank fluid surface heights (for the gas-free and the gas-entrained states) intersect any PJM part above the top of the PJM tube part. Assumptions (3 through 8) for the PJM parts above the PJM tube but below the tank fluid surface height are not needed because the volume below the tank fluid surface height is calculated from the static correlation. Examples are shown for the LS test stand in subsection A.4.1.3 to illustrate the scenarios where the same set of assumptions does and does not apply to both the gas-free and the gas-entrained volumes.

A.5 References

American Society for Testing and Materials (ASTM). 2003. *Standard Specification for Poly(Vinyl Chloride) (PVC) Plastic Pipe, Schedules 40, 80, and 120*. ASTM D 1785-03, ASTM International, West Conshohocken, PA.

American Society of Mechanical Engineers (ASME). 1985. *Stainless Steel Pipe*. ANSI/ASME B36.19M-1985, New York.

American Society of Mechanical Engineers (ASME). 2001. *Welded and Seamless Wrought Steel Pipe*. ASME B36.10M-2000, New York.

Bontha JR, TE Michener, DS Trent, JM Bates, and MD Johnson. 2003a. *Development and Assessment of the TEMPEST CFD Model of the Pulsed Jet Mixing Systems*. PNWD-3261, Battelle – Pacific Northwest Division, Richland, WA.

Bontha JR, JM Bates, CW Enderlin, and MG Dodson. 2003b. *Large Tank Experimental Data for Validation of the FLUENT CFD Model of Pulsed Jet Mixers*. PNWD-3303, Battelle – Pacific Northwest Division, Richland, WA.

Lide DR. 1992. *CRC Handbook of Chemistry and Physics, 73rd edition*. CRC Press, Boca Raton, FL, p. A-32, Eq. 200.

Perry RH and DW Green. 1997. *Perry's Chemical Engineers' Handbook, 7th Edition*. McGraw-Hill, New York.

Appendix A Attachments

Theoretical Tank & PJMs

Pipe & Tank Data

Nominal Size	Schedule	i.d. [inch]	o.d. [inch]	Specific Volume (capacity) [L/cm]	Specific Volume (displacement) [L/cm]
1-inch	40	1.049	1.315	0.005575814	0.008762112
2-inch	40	2.067	2.375	0.021649021	0.028581469
6-inch	40	6.065	6.625	0.186388419	0.222397079
UFP Tank	N/A	34	N/A	5.857538458	N/A

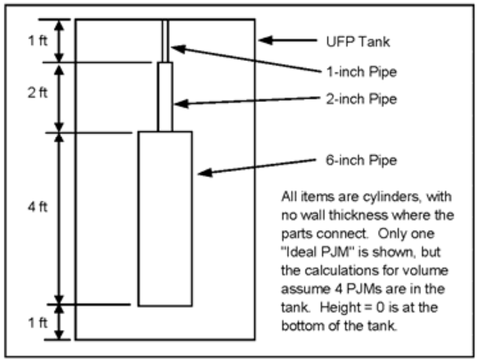

All items are cylinders, with no wall thickness where the parts connect. Only one "Ideal PJM" is shown, but the calculations for volume assume 4 PJMs are in the tank. Height = 0 is at the bottom of the tank.

Plot of Actual Volume in the Tank Under Various Scenarios

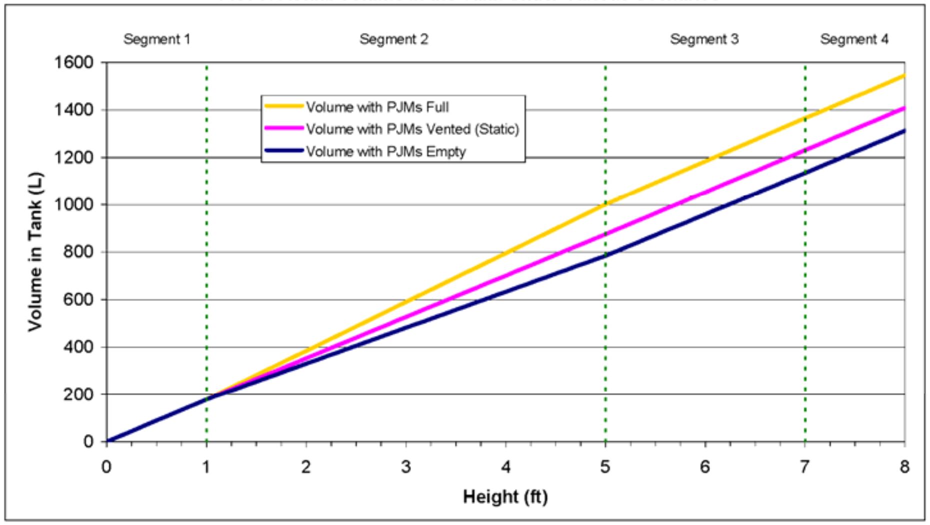

Linear Curve Fits

Affected PJM Part	Segment	Linear Fit Parameters	PJM Condition PJMs Empty	 PJMs Full	 PJMs Vented*
Entire PJM Assembly	0 - Entire Tank Height	slope	5.0778	6.6373	5.7307
		intecept	15.6149	-15.6149	2.5646
		R²	0.999536	0.999729	0.999991
None	1 - From 0 ft to 1 ft Height	slope	5.8575	5.8575	5.8575
		intecept	0.0000	0.0000	0.0000
		R²	1.000000	1.000000	1.000000
PJM Tube	2 - From >1 ft to 5 ft Height	slope	4.9680	6.7471	5.7135
		intecept	27.1147	-27.1147	4.3902
		R²	1.000000	1.000000	1.000000
Large Riser Pipe	3 - From >5 ft to 7 ft Height	slope	5.7432	5.9719	5.8298
		intecept	-91.0353	91.0353	-13.3347
		R²	1.000000	1.000000	1.000000
Small Riser Pipe	4 - From >7 ft to 8 ft Height	slope	5.8225	5.8926	5.8448
		intecept	-107.9500	107.9500	-16.5318
		R²	1.000000	1.000000	1.000000

* When PJMs are vented, the fluid level in the tank and the fluid level within the PJMs are at the same height. This is referred to as "static" conditions.

Attachment A (page 1 of 1)

UFP – MANUALLY RECORDED HEIGHT/WATER MASS DATA (LRB #14497, PAGES 42-43) AND ASSOCIATED CALCULATIONS

Measurements to define the relationship between Tank Fluid Surface Level Height and Tank Volume for the UFP Tank with the Chandelier (3 + 1) PJM configuration (PJMs vented)
Data Collected 2/16/2004

				Calculated Values				South Station		West Station		North Station		East Station			
Time	Measurement/Condition	Initial Scale Weight (kg)	Final Scale Weight (kg)	Weight of Water Added (kg)	Cumulative Weight Added (kg)	Volume in Tank (gallons)	Volume in Tank (L)	Tank Level from Rim (inches)	Tank Level Affixed Tape (cm)	Tank Level from Rim (inches)	Tank Level Affixed Tape (cm)	Tank Level from Rim (inches)	Tank Level Affixed Tape (cm)	Tank Level from Rim (inches)	Tank Level Affixed Tape (cm)	Observer/ Recorder	Comment
ND	Addition #1, Supply Tank Fill #1	560.5	96.0	464.5	464.5	123.0	465.4	55.0	56.6	ND	ND	55.1	56.2	55.1	56.1	AE Capetillo	
14:15	Addition #2, Supply Tank Fill #2	600.0	419.0	181.0	645.5	170.9	646.8	42.5	88.4	ND	ND	42.6	88.0	42.6	87.9	AE Capetillo	
14:20	Addition #2, PJMs Full	N/A	N/A	0	645.5	170.9	646.8	43.2	86.7	ND	ND	43.5	86.4	43.5	86.3	AE Capetillo	
14:28	Addition #2, PJMs Empty	N/A	N/A	0	645.5	170.9	646.8	37.6	100.9	ND	ND	37.9	100.4	37.9	100.3	AE Capetillo	
14:33	Addition #3, Supply Tank Fill #2	419.0	349.5	69.5	715.0	189.3	716.4	37.6	100.8	ND	ND	37.7	100.5	37.8	100.3	AE Capetillo	Cleaned UCL-200-3 at 14:36 & got reading of 102.0 cm
14:38	Addition #4, Supply Tank Fill #2	349.5	283.0	66.5	781.5	206.9	783.1	32.9	112.7	ND	ND	33.2	112.2	33.1	112.1	AE Capetillo	
14:45	Addition #5, Supply Tank Fill #2	283.0	226.0	57.0	838.5	222.0	840.2	29.1	122.5	ND	ND	29.3	122.0	29.3	122.1	AE Capetillo	
ND	Addition #5, PJMs Full	N/A	N/A	0	838.5	222.0	840.2	29.1	122.6	ND	ND	29.2	122.2	29.2	122.0	AE Capetillo	
14:52	Addition #5, PJMs Full	N/A	N/A	0	838.5	222.0	840.2	ND	122.4	ND	ND	ND	121.9	ND	121.7	AE Capetillo	
14:57	Addition #5, PJMs Empty	N/A	N/A	0	838.5	222.0	840.2	ND	135.4	ND	ND	ND	135.0	ND	134.9	AE Capetillo	

ND = No Data Recorded
N/A = Measurement or Calculation is Not Applicable
Shaded cells represent calculated numbers.
Measurements were taken on both the "From Rim" scale and the "Affixed Tape" scale. The South Station is the primary data source.

Conversion Factor for Water Density:	3.7778	kg/gallon
Conversion Factor for Water Density:	8.3287	lb/gallon
Conversion Factor for Water Density:	2.2002	lb/L

Mass measurement equipment
Transcell Tech. Inc., Model TI-600E, S/N: 419056002049, Calibration Due: 08/2004

Affixed Tape Reading (south) at H/D = 1.4:	86.6	cm
Affixed Tape Reading (south) at H/D = 1.8:	121.5	cm

Assumed Temperature (measurement not available):	20.0	°C
Density of Water at assumed Temperature* :	0.998	g/mL

* From Perry, R.H., and D.W. Green. 1997. *Perry's Chemical Engineers' Handbook, 7th Edition*. McGraw-Hill, New York, NY.

LS – MANUALLY RECORDED HEIGHT/WATER MASS DATA (LRB #14497, PAGE 138) AND ASSOCIATED CALCULATIONS

Measurements to define the relationship between Tank Fluid Surface Level Height and Tank Volume for the Lag Storage Tank with the Chandelier (7 + 1) PJM configuration (PJMs vented)
Data Collected 2/18/2004

				Calculated Values				South Station		West Station		North Station		East Station			
Time	**Measurement/Condition**	**Initial Scale Weight (kg)**	**Final Scale Weight (kg)**	**Weight of Water Added (lb)**	**Cumulative Weight Added (lb)**	**Volume in Tank (gallons)**	**Volume in Tank (L)**	**Tank Level from Rim (inches)**	**Tank Level Affixed Tape (cm)**	Tank Level from Rim (inches)	Tank Level Affixed Tape (cm)	Tank Level from Rim (inches)	Tank Level Affixed Tape (cm)	Tank Level from Rim (inches)	Tank Level Affixed Tape (cm)	**Observer/ Recorder**	**Comment**
13:40	Addition #1, Supply Tank Fill #1	1370	191	1179	1179	141.6	535.9	ND	ND	ND	ND	ND	ND	ND	ND	DL Blanchard	
14:04	Addition #2, Supply Tank Fill #2	1428	120	1308	2487	298.6	1130.3	67.5	29.5	67.5	29.2	67.5	29.2	67.4	29.5	DL Blanchard	Affixed Tape measurement originally made in inches
ND	Addition #3, Supply Tank Fill #3	1403	118	1285	3772	452.9	1714.4	57.6	53.8	ND	ND	ND	ND	ND	ND	DL Blanchard	Affixed Tape measurement originally made in inches
ND	Addition #4, Supply Tank Fill #4	1403	115	1288	5060	607.5	2299.8	48.3	78.4	ND	ND	ND	ND	ND	ND	DL Blanchard	Affixed Tape measurement originally made in inches
ND	Addition #5, Supply Tank Fill #5	1375	116	1259	6319	758.7	2872.0	38.9	102.2	38.9	101.8	ND	ND	ND	ND	DL Blanchard/ AE Capetillo	
ND	Addition #6, Supply Tank Fill #6	1363	1051	312	6631	796.2	3013.8	36.4	108.1	36.6	107.8	ND	ND	ND	ND	AE Capetillo	
ND	Addition #7, Supply Tank Fill #6	1051	516	535	7166	860.4	3257.0	32.5	118.4	32.6	117.9	ND	ND	ND	ND	AE Capetillo	
ND	Addition #8, Supply Tank Fill #6	516	123	393	7559	907.6	3435.6	29.6	125.8	29.8	125.2	ND	ND	ND	ND	AE Capetillo	
ND	Addition #9, Supply Tank Fill #7	1457	712	745	8304	997.0	3774.2	24.5	139.5	24.4	139.2	ND	ND	ND	ND	AE Capetillo	
ND	Addition #10, Supply Tank Fill #7	712	120	592	8896	1068.1	4043.2	19.9	150.4	20.0	150.3	ND	ND	ND	ND	AE Capetillo	
ND	Tank Level at ~ H/D = 1.0	N/A	N/A	ND	ND	ND	ND	19.8	150.7	ND	ND	ND	ND	ND	ND	RT Hallen	PJMs were (mostly) full because static water level was above the top of the PJMs.
ND	Tank Level at ~ H/D = 1.0 & PJMs Empty (overblown)	N/A	N/A	ND	ND	ND	ND	10.9	ND	ND	ND	ND	ND	ND	ND	RT Hallen	This south affixed tape value can be calculated from the Rim down measurment and the relationship between rim down & the affixed tape. The resulting value is 173.3 cm.
ND	Tank Level at ~ H/D = 0.74	N/A	N/A	ND	ND	ND	ND	40.2	98.7	ND	ND	ND	ND	ND	ND	RT Hallen	Vacuum was applied but not kept on, so the water drained back to some point less than "PJMs Full" - most likely near the true static liquid level.
ND	Tank Level at ~ H/D = 0.74 & PJMs Empty (overblown)	N/A	N/A	ND	ND	ND	ND	29.8	125.1	ND	ND	ND	ND	ND	ND	RT Hallen	

ND = No Data Recorded
N/A = Measurement or Calculation is Not Applicable
Shaded cells represent calculated numbers.
Measurements were taken on both the "From Rim" scale and the "Affixed Tape" scale. The South Station is the primary data source.

Conversion Factor for Water Density:	3.7778	kg/gallon
Conversion Factor for Water Density:	8.3287	lb/gallon
Conversion Factor for Water Density:	2.2002	lb/L

Mass measurement equipment
Transcell Tech. Inc., Model TI-600E, S/N: 419056002049, Calibration Due: 08/2004

Affixed Tape Reading (south) at H/D = 0.74:	102.1	cm
Affixed Tape Reading (south) at H/D = 1.0:	148.5	cm

Assumed Temperature (measurement not available):	20.0	°C
Density of Water at assumed Temperature* :	0.998	g/mL

* From Perry, R.H., and D.W. Green. 1997. *Perry's Chemical Engineers' Handbook, 7th Edition*. McGraw-Hill, New York, NY.

APEL 4PJM – MANUALLY RECORDED HEIGHT/WATER MASS DATA (LRB #14411, PAGES 91-92) AND ASSOCIATED CALCULATIONS

Measurements to define the relationship between Tank Fluid Surface Level Height and Tank Volume for the APEL 4PJM Tank (PJMs vented)
Data Collected 10/03/2003

Time	Measurement/Condition	0° Station Affixed Tape Reading (cm)	Initial Scale Weight (kg)	Final Scale Weight (kg)	Calculated Values Weight of Water Added (kg)	Calculated Values Cumulative Weight Added (kg)	Calculated Values Volume in Tank (gallons)	Calculated Values Volume in Tank (L)	Observer/ Recorder	Comment
ND	Addition #1	5.1	890.0	813.5	76.5	76.5	20.2	76.6	J Bontha	
ND	Addition #2	25.0	813.5	704.0	109.5	186.0	49.2	186.3	J Bontha	
ND	Addition #3	50.0	704.0	558.0	146	332.0	87.9	332.6	J Bontha	
ND	Addition #4	75.0	558.0	415.0	143	475.0	125.7	475.8	J Bontha	
ND	Addition #5	100.0	415.0	271.5	143.5	618.5	163.7	619.6	J Bontha	
ND	Addition #6	125.2	271.5	130.0	141.5	760.0	201.1	761.3	J Bontha	

ND = No Data Recorded
N/A = Measurement or Calculation is Not Applicable
Shaded cells represent calculated numbers.

Mass measurement equipment:
Transcell Tech. Inc., Model TI-600E, S/N: 419056002049, Calibration Due: 10/2003

Measured Water Temperature:	19.6	°C
Density of Water at measured Temperature* :	0.998265	g/mL

* From Perry, R.H., and D.W. Green. 1997. *Perry's Chemical Engineers' Handbook, 7th Edition*. McGraw-Hill, New York, NY.

Conversion Factor for Water Density:	3.7788	kg/gallon
Conversion Factor for Water Density:	8.3309	lb/gallon
Conversion Factor for Water Density:	2.2008	lb/L

Attachment B (page 3 of 5)

336 4PJM HEIGHT/WATER MASS DATA

Measurements to define the relationship between Tank Fluid Surface Level Height and Tank Volume for the 336 4PJM Tank (PJMs vented)
Data Collected 7/30/2004

MANUALLY RECORDED DATA (LRB # 14471, PAGE 119) AND ASSOCIATED CALCULATIONS

						Calculated Values (Hardy)			Calculated Values (DAS Manual)				
Time	**Measurement/Condition**	**Height of Liquid Level - Distance From Ref. Point (inch)**	**Mass of External Weight added to Tank (lbs)**	**Reading on Hardy weight computer (lbs)**	**Manual Reading of DAS [recorded in LRB] (lbs)**	**Change in Weight (lb)**	**Cumulative Weight Added (lbs)**	**Volume in Tank (L)**	**Change in Weight (lb)**	**Cumulative Weight Added (lb)**	**Volume in Tank (L)**	**Observer/ Recorder**	**Comments**
07:08	Empty Tank	N/A	0	109320	109000	N/A	0.0	0.0	N/A	0.0	0.0	M. White	Tank empty
07:51		N/A	0	109320	109000	N/A	N/A	N/A	N/A	N/A	N/A	M. White	Log on
08:01	Addition #1	162.5	0	113727	113300	4407	4407	2010	4300	4300	1961	M. White	Level at PJM nozzles
08:14	Addition #2	142.2	0	125530	125200	11803	16210	7392	11900	16200	7388	M. White	Level at cylindrical section bottom
08:19		142.2	150	125677	125300	147	N/A	N/A	100	N/A	N/A	M. White	weight on
08:20		142.2	0	125539	125300	-138	N/A	N/A	0	N/A	N/A	M. White	weight off
08:30	Addition #3	117.6	0	141347	141000	15808	32027	14606	15700	32000	14593	M. White	
08:32		117.6	150	141495	141100	148	N/A	N/A	100	N/A	N/A	M. White	weight on
08:33		117.6	0	141349	141000	-146	N/A	N/A	-100	N/A	N/A	M. White	weight off
08:42	Addition #4	100.1	0	152714	152300	11365	43394	19790	11300	43300	19747	M. White	CBT is empty (up to this point water had been pumped out of the CBT to fill the SNT)
08:45		100.1	0	152714	152300	0	N/A	N/A	0	N/A	N/A	M. White	040730-1 sample taken from SNT (using dipper)
08:48		100.1	150	152866	152600	152	N/A	N/A	300	N/A	N/A	M. White	weight on
08:50		100.1	0	152718	152300	-148	N/A	N/A	-300	N/A	N/A	M. White	weight off
09:13	Addition #5	75.8	0	168610	168300	15892	59290	27039	16000	59300	27043	M. White	Now filling SNT with process water from 2-inch building water supply pipe
09:15		75.8	150	168755	168500	145	N/A	N/A	200	N/A	N/A	M. White	weight on
09:16		75.8	0	168608	168300	-147	N/A	N/A	-200	N/A	N/A	M. White	weight off
09:32	Addition #6	52.0	0	184080	183800	15472	74760	34094	15500	74800	34112	M. White	
09:40	Addition #7	41.8	0	190830	190500	6750	81510	37172	6700	81500	37168	M. White	
09:47	Addition #8	30.8	0	197870	197500	7040	88550	40383	7000	88500	40360	M. White	
09:55	Addition #9	21.3	0	203832	203500	5962	94512	43102	6000	94500	43096	M. White	
09:57		21.3	150	203977	203700	145	N/A	N/A	200	N/A	N/A	M. White	weight on
09:59		21.3	0	203829	203500	-148	N/A	N/A	-200	N/A	N/A	M. White	weight off
10:01		N/A	N/A	N/A	N/A	N/A	N/A	N/A	N/A	N/A	N/A	M. White	Log off
10:02		N/A	N/A	N/A	N/A	N/A	N/A	N/A	N/A	N/A	N/A	M. White	040730-2 sample taken from SNT (using dipper)

Attachment B (page 4 of 5)

336 4PJM HEIGHT/WATER MASS DATA (CONTINUED)

REDUCED DAS LOGGED DATA AND ASSOCIATED CALCULATIONS

					Calculated Values (DAS Logged)			
Corresponding LRB-Noted Time	Measurement/Condition	Height of Liquid Level - for LRB-Noted Time (inch)	Average of DAS Logged Data for Specified Time Span (lb)	Std. Dev. of DAS Logged Data for Specified Time Span (lb)	Change in Weight (lb)	Cumulative Weight Added (lb)	Volume in Tank (L)	Time Span (inclusive) **
7:08	Empty Tank	N/A	108929.1	79.7	N/A	N/A	N/A	07:52:26.0 to 07:57:25.5
8:01	Addition #1	162.5	113343.8	76.1	4414.8	4414.8	2013	08:01:06.0 to 08:06:25.5
8:14	Addition #2	142.2	125160.1	73.0	11816.2	16231.0	7402	08:13:38.0 to 08:17:59.0
8:19		142.2	125319.1	69.6	159.0	N/A	N/A	08:18:40.0 to 08:20:06.0
8:20		142.2	125175.8	78.7	-143.3	N/A	N/A	08:20:33.0 to 08:20:53.0
8:30	Addition #3	117.6	140995.2	66.7	15819.5	32066.2	14624	08:30:02.5 to 08:31:33.5
8:32		117.6	141147.8	72.2	152.5	N/A	N/A	08:31:47.0 to 08:33:14.5
8:33		117.6	141015.7	70.0	-132.1	N/A	N/A	08:33:32.0 to 08:34:55.5
8:42	Addition #4	100.1	152381.8	69.2	11366.1	43452.7	19816	08:41:35.5 to 08:48:10.5
8:48		100.1	152532.7	83.8	150.9	N/A	N/A	08:48:32.5 to 08:49:59.5
8:50		100.1	152414.3	107.4	-118.5	N/A	N/A	08:50:15.5 to 08:59:01.0
9:13	Addition #5	75.8	168294.4	114.5	15880.1	59365.3	27073	09:13:03.5 to 09:15:09.0
9:15		75.8	168432.5	151.7	138.1	N/A	N/A	09:15:24.0 to 09:16:13.5
9:16		75.8	168290.6	145.9	-141.9	N/A	N/A	09:16:25.5 to 09:17:30.5
9:32	Addition #6	52.0	183803.9	130.4	15513.3	74874.8	34146	09:31:15.0 to 09:33:38.5
9:40	Addition #7	41.8	190574.0	134.2	6770.1	81644.9	37234	09:39:42.0 to 09:41:31.0
9:47	Addition #8	30.8	197601.8	135.9	7027.9	88672.7	40439	09:47:49.0 to 09:49:23.0
9:55	Addition #9	21.3	203574.4	127.0	5972.6	94645.3	43162	09:54:48.5 to 09:57:14.5
9:57		21.3	203701.2	120.1	126.8	N/A	N/A	09:57:26.0 to 09:59:05.5
9:59		21.3	203552.0	126.7	-149.3	N/A	N/A	09:59:27.0 to 10:00:53.5

** CD Johnson selected the time spans based on the nominal start and end points of each flat section in the plot of "SNT Wt." over time, except for the initial time span, which is an arbitrary 5 minutes worth of data. The "SNT Wt." data between each time span (inclusive of start/end) was averaged to obtain the DAS Logged Data. The data file used is entitled "040730-02Hz-SNT-Vol-Lvl-Wt-Dat1.asc".

ND = No Data Recorded
N/A = Measurement or Calculation is Not Applicable
Shaded cells represent calculated numbers.
The reference point is the top of the tank rim.
The 336 4PJM tank is also referred to as the Supernatant Tank (SNT)

Conversion Factor for Water Density:	3.7651	kg/gallon
Conversion Factor for Water Density:	8.3005	lb/gallon
Conversion Factor for Water Density:	2.1928	lb/L

\ Using average
|-- measured density
/ of both samples

Mass measurement equipment
Weigh computer: Hardy Model HI2151/WC; S/N 4558
Load Cells: BLH Model Z-Blok, 100000 lb; S/N 31713, 31719, and 31721 (3 load cells)

Density measurement by LK Jagoda on 8/6/2004 (LRB # 14472, p. 35)

Sample # 040703-1

Measurement #	Temperature (°C)	Density (g/mL)
1	28.0	0.993
2	27.7	0.993
3	27.7	0.997
4	27.2	0.994
	Average Density:	0.994

Sample # 040703-2

Measurement #	Temperature (°C)	Density (g/mL)
1	26.8	0.994
2	26.8	0.995
3	26.7	0.997
4	26.6	0.994
	Average Density:	0.995

Note: The DAS recorded data for "Lo Temp." (SNT) had a nominal progression as follows:

Time	Temperature (°C)
07:51	28.60
08:45	28.40
08:56	28.30
08:59	28.30
09:00	28.30
09:36	28.30
09:38	28.00
09:42	27.60
09:49	27.20
10:00	26.80
Average of Logged Data:	28.04

Ambient temperature (from DAS) steadily increased from 26.2 °C to 28.5°C over this time, except for a discontinuity at 8:59/9:00 where the temperature suddenly dropped from about 27.5 °C to 27.1 °C.

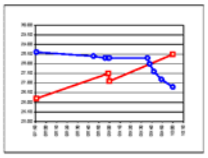

UFP Tank *	
From Rim (inches)	Affixed Tape (cm)
17.5	152.0
28.5	124.1
48.0	74.5
60.0	44.0
76.5	2.1

* Measurements taken 2004-Mar-08
on South Side of UFP Tank by
CD Johnson

Correlation (Linear Fit) of "From Rim" to "Affixed"	
slope	-2.541188
intercept	196.4888
R²	1.000000

Correlation (Linear Fit) of "Affixed" to "From Rim"	
slope	-0.3935166
intercept	77.32161
R²	1.000000

LS Tank **	
From Rim (inches)	Affixed Tape (cm)
20.1	150.0
22.8	143.0
26.9	132.5
32.3	119.0
40.5	98.0
48.8	77.0
57.0	56.0
64.5	37.0
73.1	15.0

** Measurements taken 2004-Mar-17
on South Side of LS Tank by
CD Johnson

Correlation (Linear Fit) of "From Rim" to "Affixed"	
slope	-2.543849
intercept	201.0296
R²	1.000000

Correlation (Linear Fit) of "Affixed" to "From Rim"	
slope	-0.3931051
intercept	79.02577
R²	1.000000

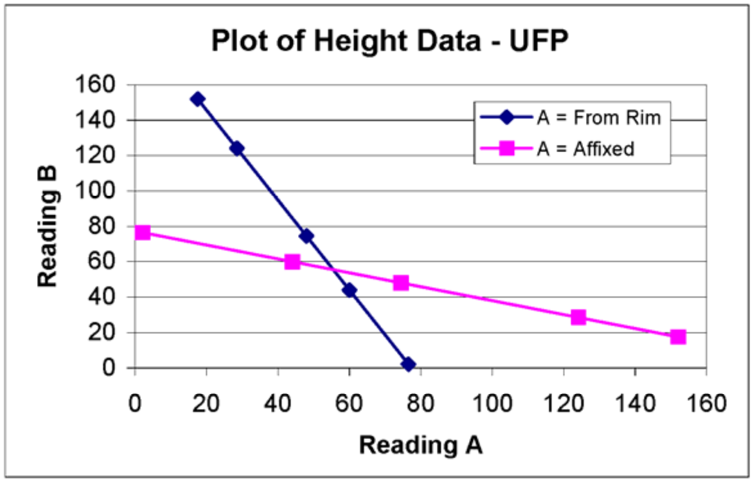

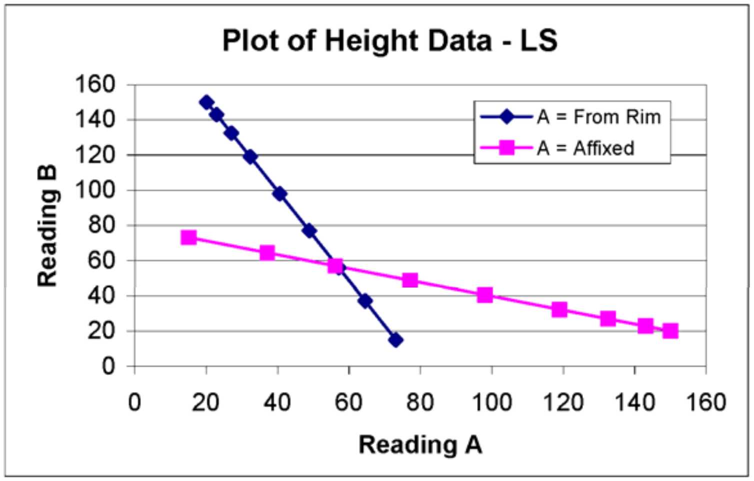

Attachment C (page 1 of 1)

UFP, Chandelier (3+1) Configuration

Not To Scale

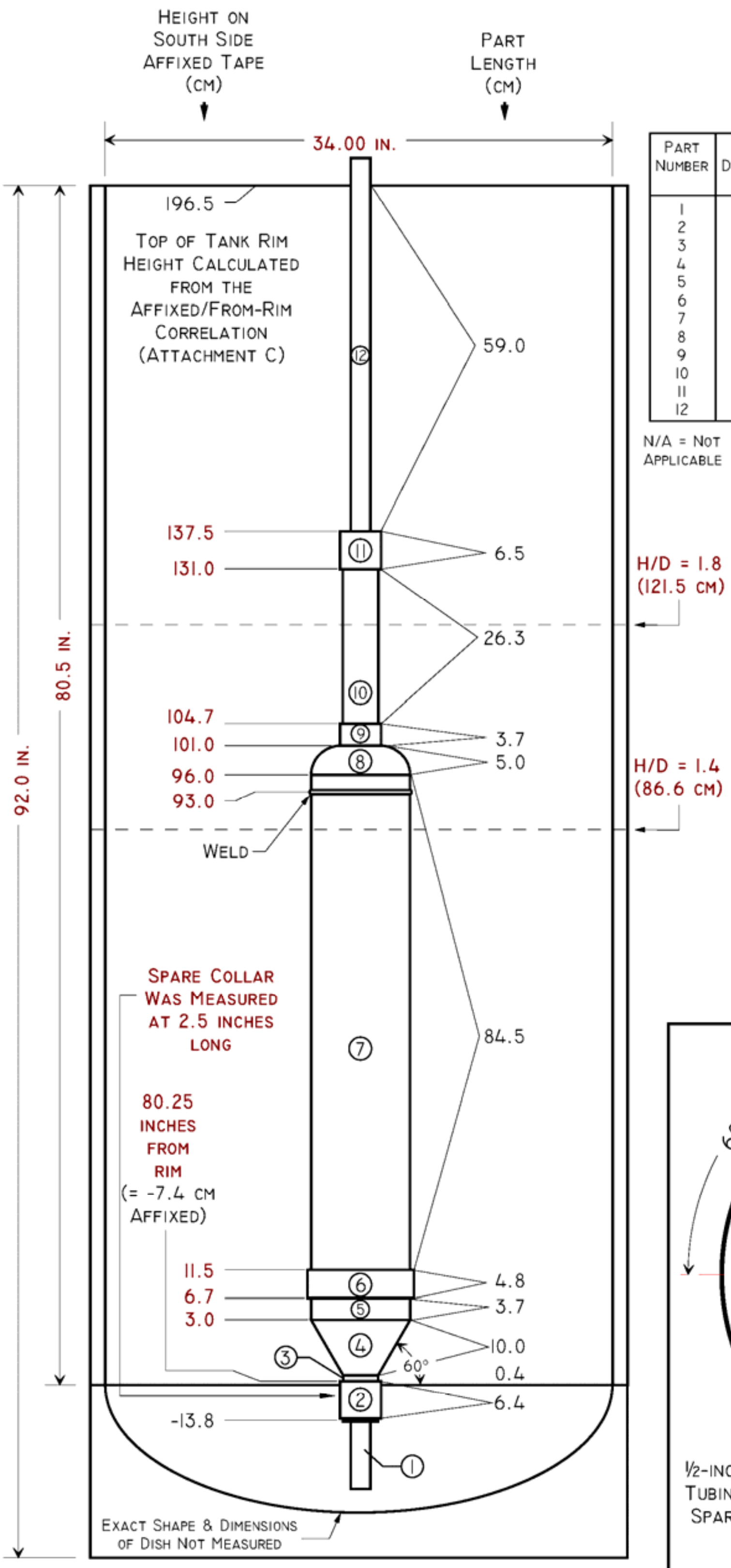

Section View

Part Number	Inside Diameter (inch)	Outside Diameter (inch)	Part Description	Comment(s)
1	--	--	Nozzle	Design Varied
2	2.375	2.750	2-Inch Cap/Collar	Assumed Diameters
3	2.067	2.375	2-Inch Pipe Nipple	O.D. Assumed
4	N/A	N/A	Cone	
5	6.065	6.625	6-Inch Pipe Nipple	O.D. Assumed
6	6.625	7.125	6-Inch Pipe Collar	Assumed Diameters
7	6.065	6.625	6-Inch Pipe	
8	N/A	N/A	Shoulder	
9	2.375	2.750	2-Inch Collar	Assumed Diameters
10	2.067	2.375	2-Inch Pipe	
11	2.375	2.750	2-Inch Cap/Collar	Assumed Diameters
12	0.824	1.050	¾-Inch Pipe	

N/A = Not Applicable

Note 1: The UFP Tank is shown with a typical PJM, representative of all PJMs in the tank (though nozzle configurations differed between center & peripheral PJMs). The PJM level probe & sensor head within the PJM is not shown. Plan view is mainly to show number of PJMs - lateral locations are approximate & some items (recirculation piping, peroxide injection piping, sensors) are not shown.

Note 2: **Bolded** values were measured on 2004-Mar-08 by CD Johnson. PJM part heights were measured by looking through the south side of the UFP tank (clean and empty of clay) and reading the height off the affixed tape. These heights may be up to ±0.5 cm. Data is in LRB 14497, Page 142.

Note 3: Diameters are estimated or are the standard values (ANSI/ASME B36.19M-1985) for schedule 40 pipe (all pipe is schedule 40).

Note 4: Shoulder and Cone are assumed to have the same wall thickness as the 6-inch pipe.

Note 5: Shoulder has the profile of a rectangle with two rounded corners. The left and right sides of the rectangle are quarter circles with a radius of 5 cm (= 101-96).

Note 6: The diameter of a spare Drexelbrook level probe rod was measured as **0.8 inches**. The probe rod length is 101 cm. The top of the probe is assumed to be even with top of the shoulder (i.e., 101 cm).

Note 7: PJM dimensions/details below the top of the cone and lateral placement of PJMs are not important to the height/volume correlations.

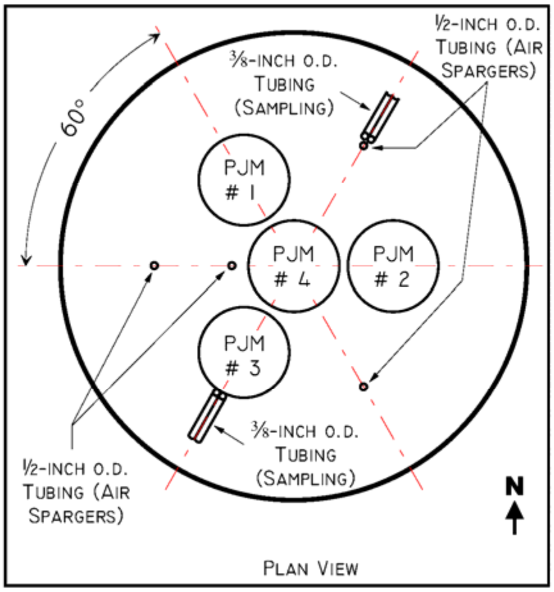

Plan View

Attachment D (page 1 of 4)

LS, CHANDELIER (7+1) CONFIGURATION

NOT TO SCALE

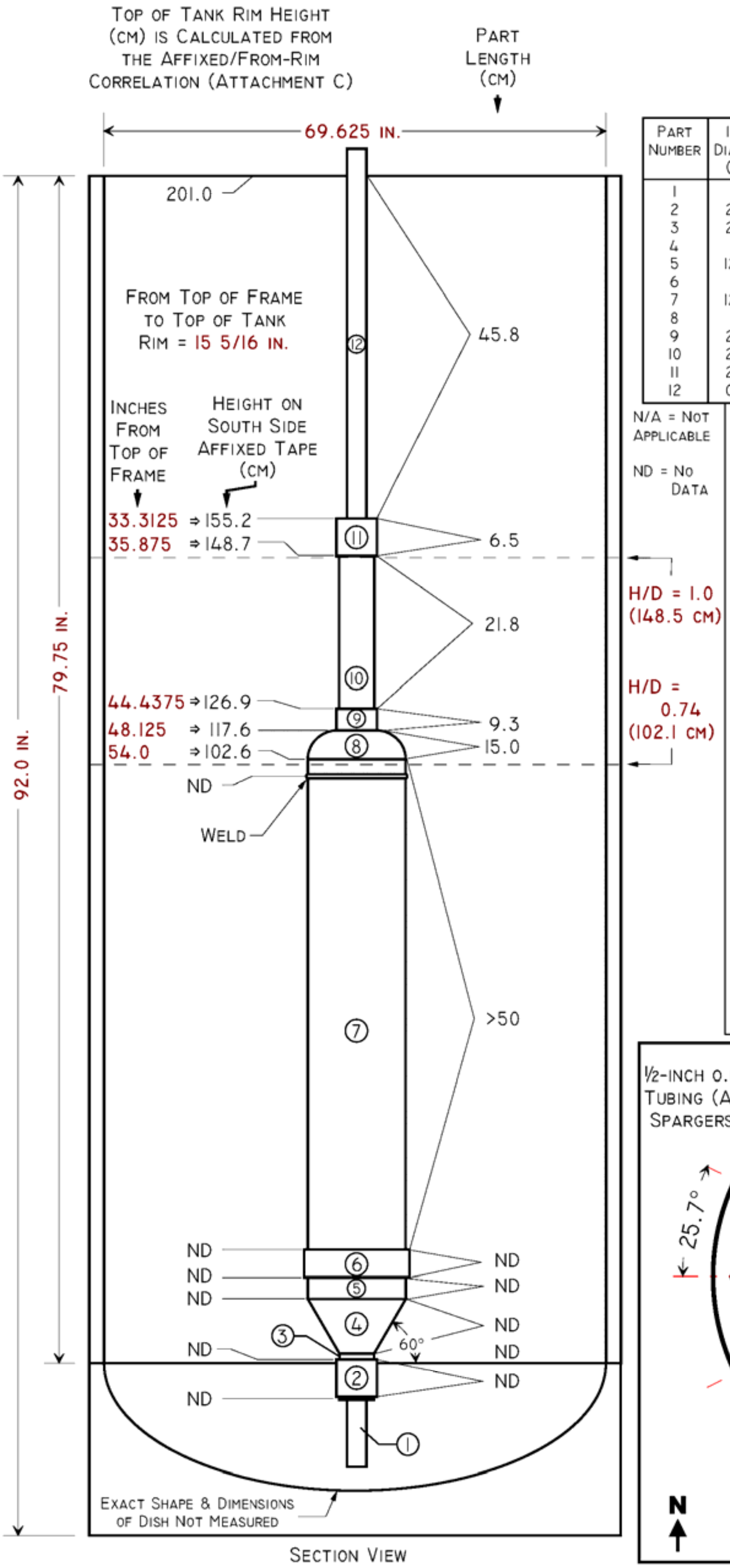

PART NUMBER	INSIDE DIAMETER (INCH)	OUTSIDE DIAMETER (INCH)	PART DESCRIPTION	COMMENT(S)
1	--	--	NOZZLE	DESIGN VARIED
2	2.375	2.750	2-INCH CAP/COLLAR	ASSUMED DIAMETERS
3	2.067	2.375	2-INCH PIPE NIPPLE	O.D. ASSUMED
4	N/A	N/A	CONE	
5	12.000	12.750	12-INCH PIPE NIPPLE	O.D. ASSUMED
6	ND	ND	12-INCH PIPE COLLAR	ASSUMED DIAMETERS
7	12.000	12.750	12-INCH PIPE	
8	N/A	N/A	SHOULDER	
9	2.375	2.750	2-INCH COLLAR	ASSUMED DIAMETERS
10	2.067	2.375	2-INCH PIPE	
11	2.375	2.750	2-INCH CAP/COLLAR	ASSUMED DIAMETERS
12	0.824	1.050	¾-INCH PIPE	

N/A = NOT APPLICABLE

ND = NO DATA

NOTE 1: THE LS TANK IS SHOWN WITH A TYPICAL PJM, REPRESENTATIVE OF ALL PJMS IN THE TANK (THOUGH NOZZLE CONFIGURATIONS DIFFERED BETWEEN CENTER & PERIPHERAL PJMS). THE PJM LEVEL PROBE & SENSOR HEAD WITHIN THE PJM IS NOT SHOWN. PLAN VIEW IS MAINLY TO SHOW NUMBER OF PJMS - LATERAL LOCATIONS ARE APPROXIMATE & SOME ITEMS (RECIRCULATION PIPING, PEROXIDE INJECTION PIPING, SAMPLE COLLECTION PIPING, SENSORS) ARE NOT SHOWN.

NOTE 2: **BOLDED** VALUES WERE MEASURED ON 2004-MAR-17 BY CD JOHNSON. PJM PART HEIGHTS WERE DETERMINED BY MEASURING THE DISTANCE FROM THE PJM ASSEMBLY SUPPORT FRAME TO THE TOP OF THE PART AND THEN SUBTRACTING THE DISTANCE FROM THE FRAME TO THE TOP OF THE TANK RIM. BECAUSE THE TANK CONTAINED CLAY SLURRY, HEIGHTS FOR SOME PARTS COULD NOT BE MEASURED. THE MEASURED HEIGHTS MAY BE UP TO ± 0.125 INCH. DATA IS IN LRB 14497, PAGE 143.

NOTE 3: DIAMETERS ARE ESTIMATED OR ARE THE STANDARD VALUES (ANSI/ASME B36.19M-1985) FOR SCHEDULE 40 PIPE (ALL PIPE IS SCHEDULE 40).

NOTE 4: SHOULDER AND CONE ARE ASSUMED TO HAVE THE SAME WALL THICKNESS AS THE 12-INCH PIPE.

NOTE 5: SHOULDER HAS THE PROFILE OF A RECTANGLE WITH TWO ROUNDED CORNERS. THE LEFT AND RIGHT SIDES OF THE RECTANGLE ARE QUARTER CIRCLES WITH A RADIUS OF 15 CM (= 117.6 - 102.6).

NOTE 6: THE DIAMETER OF A SPARE DREXELBROOK LEVEL PROBE ROD WAS MEASURED AS **0.8 INCHES**. THE PROBE ROD LENGTH IS 101 CM. THE TOP OF THE PROBE IS ASSUMED TO BE EVEN WITH TOP OF THE SHOULDER (I.E., 101 CM).

NOTE 7: PJM DIMENSIONS/DETAILS BELOW THE TOP OF THE CONE AND LATERAL PLACEMENT OF PJMS ARE NOT IMPORTANT TO THE HEIGHT/VOLUME CORRELATIONS.

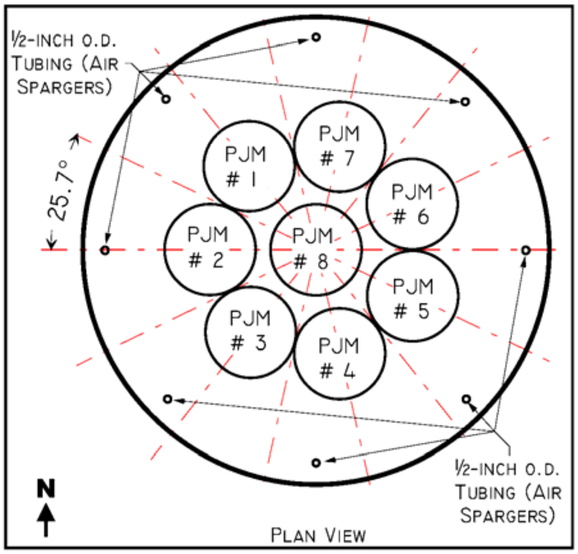

Attachment D (page 2 of 4)

APEL 4PJM Test Stand

Not To Scale

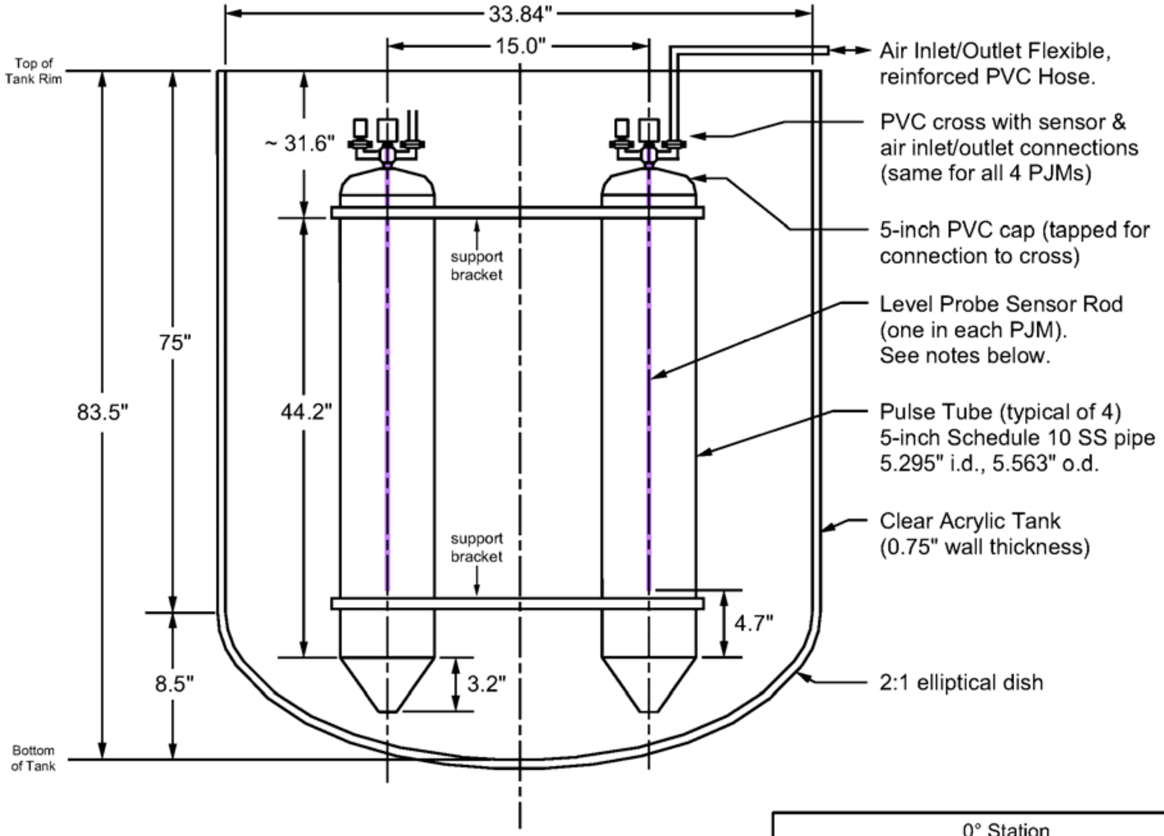

NOTES:

As-built dimensions for the PJMs are in LRB 14411 on pages 64-66. Other dimentions were taken from CAD drawings (Drawing2 WS005492-001B and WS005494-001B) of the test stand. The most important dimension for the height/volume correlation is the PJM tube diameter because the fluid in the PJMs did not rise above the cylindrical PJM tube portion of the PJM assembly during GR&R testing. Lateral position of the PJMs is not important for the height/volume correlation used for the GR&R tests.

The PJM level probes used in the APEL 4PJM test stand have a diameter of 0.57 inch, according to information on a vendor quote (personal communication with Jagan Bontha, PNWD, quote # E3070701a provided by Autoline Controls, Inc. for Drexelbrook probe model 700-0002-027-I060.0BA0).

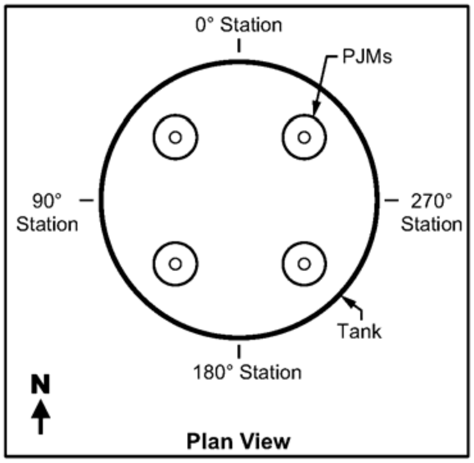

Attachment D (page 3 of 4)

336 4PJM Test Stand

Not To Scale

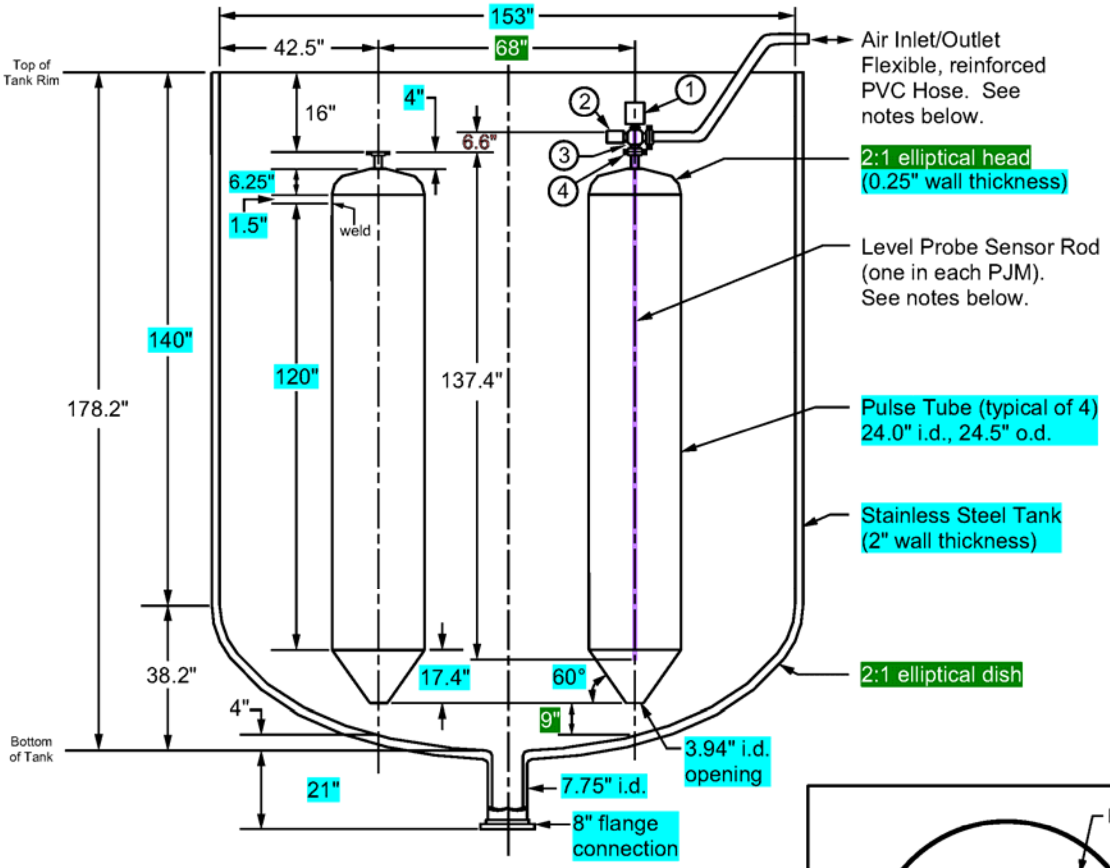

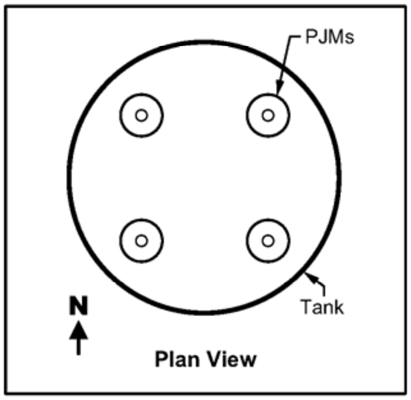

NOTES:

① Level Transmitter for Drexelbrook Level Probe
② Pressure Transmitter
③ 2-inch Schedule 40 Carbon Steel cross
④ 2-inch Schedule 40 Carbon Steel pipe & flanges

123	Dimension from PNWD-3261, Appendix A
123	Dimension from PNWD-3303, Section 2
123	Measured dimension (see notes)
123	Dimension is derived from other dimensions/geometry

Dimensional information on the cross/flange assemblies at the top of the PJMs is not available, other than the fact that they are 2-inch pipe size.

On 2004-Mar-08, CD Johnson measured the diameter of a spare Drexelbrook level probe rod at the APEL facility to be 0.8 inches. Level probes in the SNT PJMs are assumed to have the same diameter.

Mike White measured the vertical location of the Drexelbrook level probe rod (communicated in an e-mail to CD Johnson on 2004-Aug-24 at ~13:00), stating:

> The top of the measuring section of the 144" [long] Drexelbrook level probe for PJM levels is 0.6 +/- 0.1" below the top of the 2->1" pipe bushing it threads into (it threads that far into the bushing). The top of that bushing ranges from 7.0 to 7.3" above the face of the flange on the top of the PJM. That places the 144" point on the probe 6.3 to 6.8" above the flange face.

The diagram above shows the top of the level sensor rod at an average height of 6.6 inches above the flange face.

The flexible hose is 2-inch i.d. according to WH Combs (e-mail sent to CD Johnson on 2004-Aug-24 at ~09:20).

Lateral position of the PJMs is not important for the height/volume correlation used for the GR&R tests.

Attachment D (page 4 of 4)

UFP – Linear Correlations for Height of Liquid Surface vs. Tank Volume under Static Conditions

Measurment ID	Height (South Affixed Tape Reading) (cm)	Volume in Tank (L)	Application of Linear Equation #1 (L)	% Error (between Static Corellation & Actual)
Addition #1, Supply Tank Fill #1	56.6	465.4	465.6	0.0412 %
Addition #2, Supply Tank Fill #2	88.4	646.8	646.1	-0.1057 %
Addition #3, Supply Tank Fill #2	100.8	716.4	716.5	0.0078 %
Addition #4, Supply Tank Fill #2	112.7	783.1	784.0	0.1231 %
Addition #5, Supply Tank Fill #2	122.5	840.2	839.7	-0.0629 %

Description	Linear Equation Number	Slope	Intercept	R^2
Linear Fit of Height (cm) vs. Tank Volume (L) - PJMs Vented	1	5.67571	144.37745	0.999980

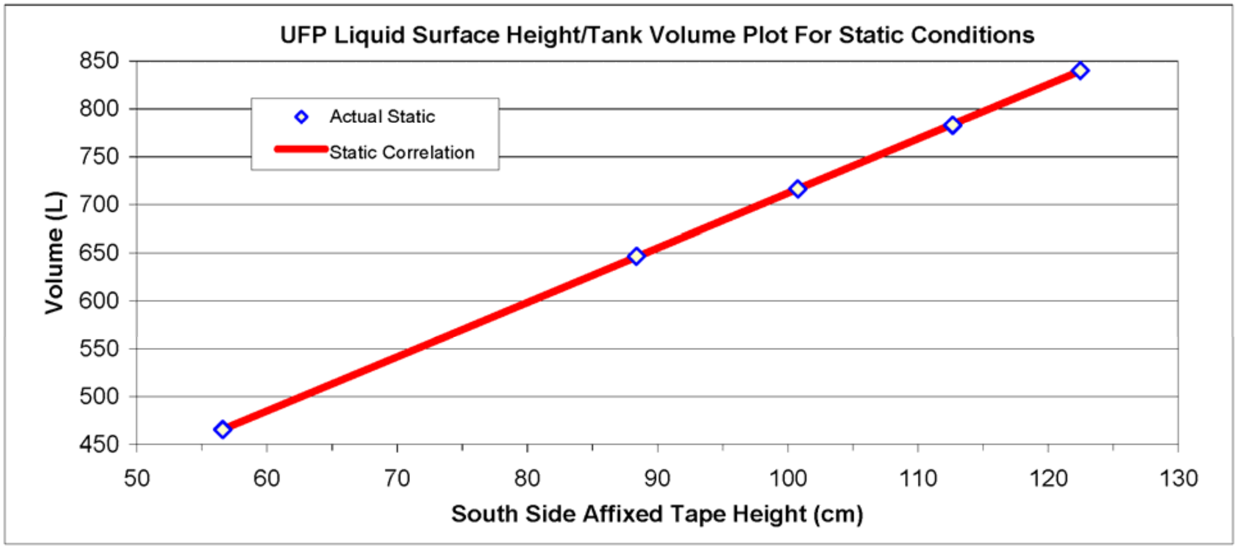

Attachment E (page 1 of 4)

LS – Linear Correlations for Height of Liquid Surface vs. Tank Volume under Static Conditions

Measurment ID	Height (South Affixed Tape Reading) (cm)	Volume in Tank (L)	Application of Linear Equation #1 (L)	% Error (between Static Corellation & Actual)
Addition #1, Supply Tank Fill #1 *	ND	535.9		
Addition #2, Supply Tank Fill #2	29.5	1130.3	1126.7	-0.3213 %
Addition #3, Supply Tank Fill #3	53.8	1714.4	1711.5	-0.1675 %
Addition #4, Supply Tank Fill #4	78.4	2299.8	2302.4	0.1144 %
Addition #5, Supply Tank Fill #5	102.2	2872.0	2874.1	0.0749 %
Addition #6, Supply Tank Fill #6	108.1	3013.8	3016.0	0.0735 %
Addition #7, Supply Tank Fill #6	118.4	3257.0	3263.7	0.2064 %
Addition #8, Supply Tank Fill #6	125.8	3435.6	3441.6	0.1758 %
Addition #9, Supply Tank Fill #7	139.5	3774.2	3771.0	-0.0833 %
Addition #10, Supply Tank Fill #7	150.4	4043.2	4033.1	-0.2501 %

* Measurement not used in determining the linear equation below because there is no data (ND) for the height.

Description	Linear Equation Number	Slope	Intercept	R^2
Linear Fit of Height (cm) vs. Tank Volume (L) - PJMs Vented	1	24.04534	416.71567	0.999969

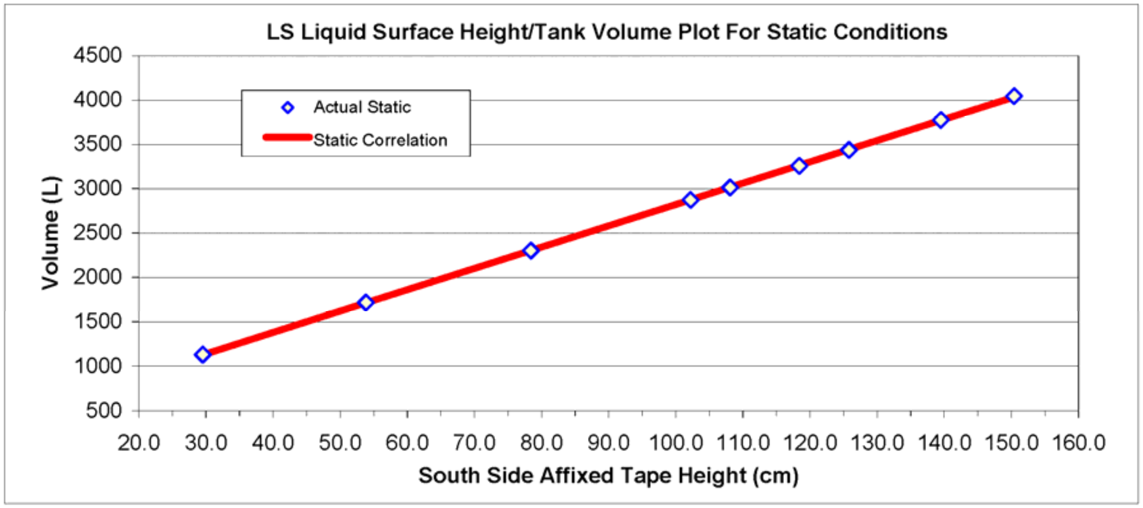

Attachment E (page 2 of 4)

APEL 4PJM – Linear Correlations for Height of Liquid Surface vs. Tank Volume under Static Conditions

Measurment ID	Height (0° Station Affixed Tape Reading) (cm)	Volume in Tank (L)	Application of Linear Equation #1 (L)	% Error (between Static Corellation & Actual)
Addition #1	5.1	76.6	75.2	-1.8952 %
Addition #2	25	186.3	189.1	1.4683 %
Addition #3	50	332.6	332.1	-0.1367 %
Addition #4	75	475.8	475.2	-0.1344 %
Addition #5	100	619.6	618.2	-0.2140 %
Addition #6	125.2	761.3	762.5	0.1493 %

Description	Linear Equation Number	Slope	Intercept	R^2
Linear Fit of Height (cm) vs. Tank Volume (L) - PJMs Vented	1	5.72254	45.99564	0.999961

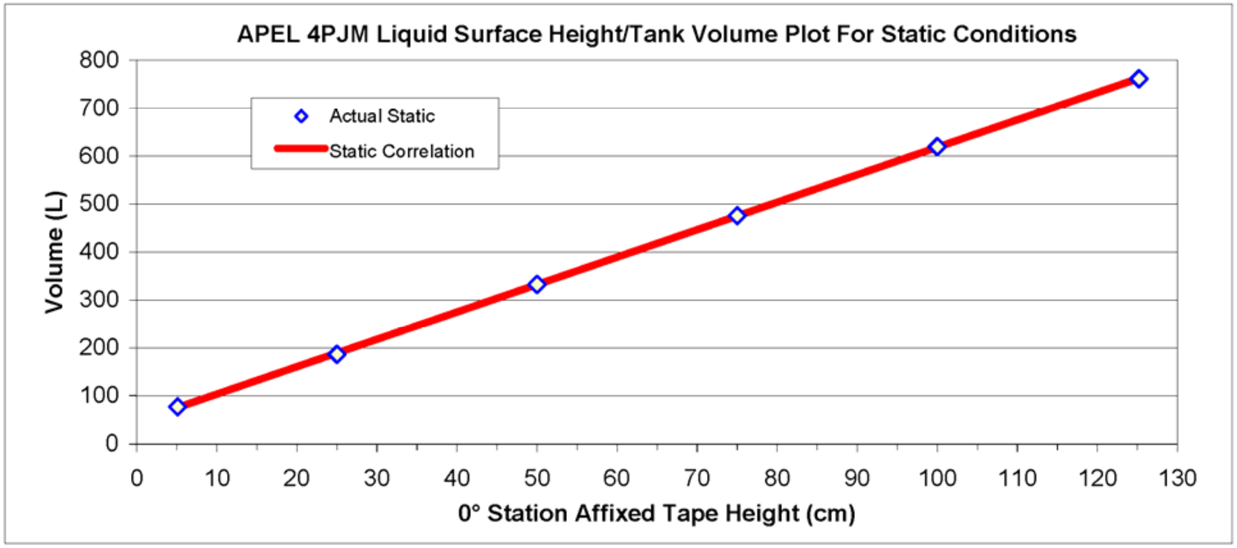

Attachment E (page 3 of 4)

336 4PJM – Linear Correlations for Height of Liquid Surface vs. Tank Volume under Static Conditions

Height/Volume Data and Linear Fit for Static Conditions (Hardy Computer Data)	Height (Distance from Ref. Point) (in.)	Volume in Tank based on Hardy (L)	Application of Linear Equation #1 (L)	% Error (between Static Corellation & Actual)
Addition #1 *	162.5	2010		
Addition #2	142.2	7392	7357.0	-0.4800 %
Addition #3	117.6	14606	14645.0	0.2690 %
Addition #4	100.1	19790	19829.5	0.2021 %
Addition #5	75.8	27039	27028.7	-0.0375 %
Addition #6	52	34094	34079.7	-0.0415 %
Addition #7	41.8	37172	37101.5	-0.1898 %
Addition #8	30.8	40383	40360.4	-0.0551 %
Addition #9	21.3	43102	43174.9	0.1701 %

Height/Volume Data and Linear Fit for Static Conditions (Manually Recorded DAS Data [in LRB])	Height (Distance from Ref. Point) (in.)	Volume in Tank based on DAS (L)	Application of Linear Equation #2 (L)	% Error (between Static Corellation & Actual)
Addition #1 *	162.5	1961.0		
Addition #2	142.2	7387.9	7342.9	-0.6090 %
Addition #3	117.6	14593.4	14632.8	0.2701 %
Addition #4	100.1	19746.7	19818.7	0.3648 %
Addition #5	75.8	27043.4	27019.7	-0.0875 %
Addition #6	52	34112.1	34072.6	-0.1158 %
Addition #7	41.8	37167.5	37095.2	-0.1947 %
Addition #8	30.8	40359.9	40354.9	-0.0122 %
Addition #9	21.3	43096.1	43170.1	0.1717 %

Height/Volume Data and Linear Fit for Static Conditions (DAS Logged Data)	Height (Distance from Ref. Point) (in.)	Volume in Tank based on DAS (L)	Application of Linear Equation #3 (L)	% Error (between Static Corellation & Actual)
Addition #1 *	162.5	2013.3		
Addition #2	142.2	7402.0	7365.0	-0.5009 %
Addition #3	117.6	14623.6	14664.3	0.2784 %
Addition #4	100.1	19816.3	19856.9	0.2046 %
Addition #5	75.8	27073.2	27067.2	-0.0222 %
Addition #6	52	34146.2	34129.1	-0.0500 %
Addition #7	41.8	37233.6	37155.6	-0.2095 %
Addition #8	30.8	40438.6	40419.5	-0.0472 %
Addition #9	21.3	43162.4	43238.4	0.1761 %

* Measurement not used in determining the linear equation below.
The reference point is the top of the tank rim.
PJMs were open to atmosphere during data collection.

Description	Linear Equation Number	Slope	Intercept	R²
Linear Fit of Height (in.) vs. Tank Volume (L) - PJMs Vented, Hardy	1	-296.26055	49485.23057	0.999987
Linear Fit of Height (in.) vs. Tank Volume (L) - PJMs Vented, DAS Manual	2	-296.33751	49482.10343	0.999982
Linear Fit of Height (in.) vs. Tank Volume (L) - PJMs Vented, DAS Logged	3	-296.71973	49558.51051	0.999985

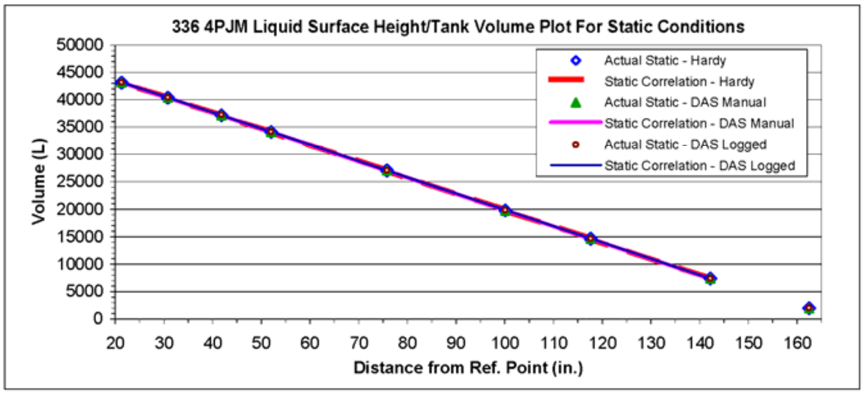

The Hardy weigh computer data was subjectively deemed the most reliable, thus Linear Equation #1 above was used as the static correlation for development of the overall height/volume correlation. The volume within the PJMs above the tank fluid surface level (based on geometry) is added to the volume from the static correlation to obtain an overall height/volume correlation when the PJMs are full.

Attachment E (page 4 of 4)

UFP – Geometry

	Part[¥] --	i.d.[§] (inch)	o.d.[§] (inch)	Height at Top of Part (external) [*] (cm)	Delta Part Height [internal][†] (cm)	Delta Part Height [external] (cm)	Total Internal Volume for Part[‡] (L)	Total Volume Displaced by Part (L)	Internal Part that Displaces volume --
Externally Visible PJM Parts	6" collar	N/A	N/A	11.5	N/A	N/A	N/A	N/A	N/A
	6" pipe (PJM tube)	6.065	6.625	96.0	84.5	84.5	15.7498	18.7926	Level Probe Rod
	shoulder (rnd. rect.)	N/A	N/A	101.0	4.29	5.0	0.6321	0.8660	Level Probe Rod
	2" collar	2.375	2.750	104.7	3.7	3.7	0.1058	0.1418	Level Probe Head
	2" pipe	2.067	2.375	131.0	26.3	26.3	0.5694	0.7517	Level Probe Head
	2" cap	2.375	2.750	137.5	6.5	6.5	0.1858	0.2491	Level Probe Head
	3/4" pipe	0.824	1.050	196.5	59.0	59.0	0.2030	0.3296	3/8" SS tubing

Internal PJM Part	Level Probe Rod[Ω]		0.8	101.0		89.5		0.2902	
	Level Probe Head		N/A	137.02		36.02		0.6304	
	3/8" o.d. SS tubing		0.375	196.5		59.0		0.0420	

N/A = Measurement or Calculation is Not Applicable

[¥] The first part in the list is presented only as a reference for the bottom of the subsequent part, hence the "N/A" values for all but the height at the top of the part.

[§] Values for inside diameter (i.d.) and outside diameter (o.d.) of the stainless steel pipe were obtained from ANSI/ASME B36.19M-1985 ("Stainless Steel Pipe," American Society of Mechanical Engineers, New York, New York. 1985.). The i.d. for a 2-inch collar/cap is estimated as being equal to the o.d. of a 2-inch pipe. The o.d. for a 2-inch collar/cap is assumed to be 2.75 inches. The level probe rod o.d. was measured by CD Johnson (see Attachment D notes) and agreed with observations by Mike White.

[*] See associated drawing (in Attachment D) for dimensional information & sources. This is the height at the top of the part as measured at the external surface. Heights of external parts were measured on 2004-Mar-08 (by CD Johnson) by viewing the PJM assembly from outside the tank (tank was empty & clean) and recording the affixed tape reading. Estimated heights for the parts internal to the PJM (shown above) and the assumed volume occupied by the level probe head (75% of the internal volume) were based on drawing A-009-0 (Assembly Sketch Level Sensor/PJM Stem Assembly). All values are relative to the south side affixed tape scale. It is assumed that when the PJMs are full, the fluid within the PJMs rises to be even with the top of the tank rim.

[†] Where a cap or shoulder mates with a coupling or pipe, this value includes a height element equal to the wall thickness of the cap or shoulder. The horizontal portion of a cap is assumed to have the thickness of the cylindrical walls of the cap. The entire shoulder is assumed to have a wall thickness equal to the wall thickness of the PJM tube.

[‡] Volume displaced by internal parts is not included in this value - this is the total volume within this part for the total height of the part.

[Ω] The PJM level probe rod is 101 cm long, but only the length above the top of the 6" collar is included in the Delta Part Height.

Data for Shoulder & Calculations for Shoulder Volumes

rounded rectangle	Internal	External
qtr. circle radius, r_2 (cm)	4.2888	5.0
central radius, r_1 (cm)	3.4138	3.4138
shoulder height, h (cm)	4.2888	5.0
shoulder volume (L)	0.6321	0.8660

Number of PJMs in Tank =	4

LS – Geometry

	Part[¥] --	i.d.[§] (inch)	o.d.[§] (inch)	Height at Top of Part (external) * (cm)	Delta Part Height [internal][†] (cm)	Delta Part Height [external] (cm)	Total Internal Volume for Part[‡] (L)	Total Volume Displaced by Part (L)	Internal Part that Displaces volume --
Externally Visible PJM Parts	12" collar	N/A	N/A	52.6	N/A	N/A	N/A	N/A	N/A
	12" pipe (PJM tube)	12.000	12.750	102.6	50.0	50.0	36.4829	41.1858	Level Probe Rod
	shoulder (rnd. rect.)	N/A	N/A	117.6	14.05	15.0	7.0297	8.4597	Level Probe Rod
	2" collar	2.375	2.750	126.9	9.3	9.3	0.2658	0.3564	Level Probe Head
	2" pipe	2.067	2.375	148.7	21.8	21.8	0.4719	0.6231	Level Probe Head
	2" cap	2.375	2.750	155.2	6.50	6.5	0.1858	0.2491	Level Probe Head
	3/4" pipe	0.824	1.050	201.0	45.8	45.8	0.1576	0.2559	3/8" SS tubing
Internal PJM Part	Level Probe Rod[Ω]		0.8	117.6		65.0		0.2108	
	Level Probe Head		N/A	154.72		37.12		0.6722	
	3/8" o.d. SS tubing		0.375	201.0		45.8		0.0326	

N/A = Measurement or Calculation is Not Applicable

[¥] The first part in the list is presented only as a reference for the bottom of the subsequent part, hence the "N/A" values for all but the height at the top of the part. The LS tank was full of slurry at the time of part height measurements, hence the top of 12" collar or 60° cone could not be determined. The arbitrary height of 52.6 cm is certainly within the PJM tube section.

[§] Values for inside diameter (i.d.) and outside diameter (o.d.) of the stainless steel pipe were obtained from ANSI/ASME B36.19M-1985 ("Stainless Steel Pipe," American Society of Mechanical Engineers, New York, New York. 1985.). The i.d. for a 2-inch collar/cap is estimated as being equal to the o.d. of a 2-inch pipe. The o.d. for a 2-inch collar/cap is assumed to be 2.75 inches. The level probe rod o.d. was measured by CD Johnson (see Attachment D notes) and agreed with observations by Mike White.

* See associated drawing (in Attachment D) for dimensional information & sources. This is the height at the top of the part as measured at the external surface. Heights of external parts were measured on 2004-Mar-17 (by CD Johnson) as the distance (in inches) from the top of the part to the top of the inner frame, which is 15+5/16" above the tank top rim. The "From Rim" to "Affixed" correlation was applied to get the values used here. Estimated heights for the parts internal to the PJM (shown above) and the assumed volume occupied by the level probe head (75% of the internal volume) were based on drawing A-009-0 (Assembly Sketch Level Sensor/PJM Stem Assembly). All values are relative to the south side affixed tape scale. It is assumed that when the PJMs are full, the fluid within the PJMs rises to be even with the top of the tank rim.

[†] Where a cap or shoulder mates with a coupling or pipe, this value includes a height element equal to the wall thickness of the cap or shoulder. The horizontal portion of a cap is assumed to have the thickness of the cylindrical walls of the cap. The entire shoulder is assumed to have a wall thickness equal to the wall thickness of the PJM tube.

[‡] Volume displaced by internal parts is not included in this value - this is the total volume within this part for the total height of the part.

[Ω] The PJM level probe rod is 86.5 cm long, but only the length above the top of the 12" collar is included in the Delta Part Height.

Data for Shoulder & Calculations for Shoulder Volumes

rounded rectangle	Internal	External
qtr. circle radius, r_2 (cm)	14.048	15.0
central radius, r_1 (cm)	1.1925	1.1925
shoulder height, h (cm)	14.048	15.0
shoulder volume (L)	7.0297	8.4597

Number of PJMs in Tank = 8

336 4PJM – Geometry

	Part [¥] --	i.d. [§] (inch)	o.d. [§] (inch)	Height at Top of Part (external) [*] (inch)	Delta Part Height [internal] [†] (inch)	Delta Part Height [external] (inch)	Total Internal Volume for Part [‡] (L)	Total Volume Displaced by Part (L)	Internal Part that Displaces volume --
Externally Visible PJM Parts	60° cone (24")	N/A	N/A	147.75	N/A	N/A	N/A	N/A	N/A
	24" custom tube	24.000	24.500	26.25	121.5	121.5	900.7200	938.6409	Level Probe Rod
	2:1 elliptical shoulder	N/A	N/A	20.0	6.0	6.25	29.6533	31.5257	Level Probe Rod
	2" pipe	2.067	2.375	16.0	4.25	4.0	0.2337	0.2904	Level Probe Rod
	2" i.d. flexible hose	2.000	N/A	-120.0	136.0	136.0	7.0015	N/A	None
Internal PJM Part	Level Probe Rod [Ω]		0.8	9.4		138.4		0.4487	

N/A = Measurement or Calculation is Not Applicable

[¥] The first part in the list is presented only as a reference for the bottom of the subsequent part, hence the "N/A" values for all but the height at the top of the part. The 2" i.d. flexible hose, Drexelbrook level probe, and a pressure transducer all attach to a cross, which itself connects to a flanged fitting above the PJM shoulder. The volume within the cross and any horizontal run of the 2-inch flexible hose (i.e., as it connects to the cross) is neglected.

[§] Values for inside diameter (i.d.) and outside diameter (o.d.) of the steel pipe were obtained from ASME B36.10M-2000 ("Welded and Seamless Wrought Steel Pipe," American Society of Mechanical Engineers, New York, New York. 2001.). The hose i.d. was provided by Bill (WH) Combs. The level probe rod o.d. was measured by CD Johnson (see Attachment D notes) and agreed with observations by Mike White. The tube i.d. and o.d. are from PNWD-3261, Appendix A.

[*] See associated drawing (in Attachment D) for dimensional information & sources. This is the height at the top of the part as measured at the external surface. All values are relative to the top of the tank rim (= 0 in.), positive direction is down from the rim. It is assumed that when the PJMs are full, the 2-inch i.d. flexible hose fills to a point 10 ft above the top of the tank rim.

[†] Where a cap or shoulder mates with a coupling or pipe, this value includes a height element equal to the wall thickness of the cap or shoulder. The horizontal portion of a cap is assumed to have the thickness of cyldrical walls of the cap. The entire shoulder is assumed to have a wall thickness equal to the wall thickness of the PJM tube.

[‡] Volume displaced by internal parts is not included in this value - this is the total volume within this part for the total height of the part.

[Ω] The PJM level probe rod is 144 inches long, but only the length above the top of the 60° cone is included in the Delta Part Height.

Data for Shoulder & Calculations for Shoulder Volumes

2:1 elliptical shoulder	Internal	External
major radius, r_3 (in.)	12	12.25
shoulder height, h (in.)	6	6.25
shoulder volume (L)	29.7	32.2

Number of PJMs in Tank =	4

UFP – Height / Volume Correlations

LINEAR CURVE FITS FOR TOTAL TANK VOLUME OVER RANGE OF EACH PART				
Height at Top of Part **	**Part**	**Slope**	**Intercept**	**R²**
(cm, south affixed)	**--**	**(L/cm)**	**(L)**	**--**
11.5	6" collar	--	--	--
96	6" pipe (PJM tube)	4.943128	218.67355	1.00000
101	shoulder (rnd. rect.)	5.185563	195.06584	0.99953
104.7	2" collar	5.647129	148.76886	1.00000
131	2" pipe	5.654055	148.04371	1.00000
137.5	2" cap	5.647129	148.95118	1.00000
196.5	3/4" pipe	5.664799	146.52155	1.00000

Tank Volume* Correlations (shaded correlations are recommended)

Segment: (all heights are on the south side affixed tape scale)	1 + 2 + 3 Linear Fit For Segment from Height of 11.5 cm to 196.5 cm	1 + 2 Linear Fit For Segment from Height of 11.5 cm to 101.0 cm	1 Linear Fit For Segment from Height of 11.5 cm to 96.0 cm	2 Cubic Fit For Segment from Height of 96.0 cm to 101.0 cm	3 Linear Fit For Segment from Height of 101.0 cm to 196.5 cm
R²	0.998877	0.999998	0.999999	0.999999	1.000000
Slope (m)	5.32757	4.94161	4.94033	N/A	5.66061
Intercept (i)	196.9601	218.8141	218.8589	N/A	147.2365
Cubic Constant 1 (a)	N/A	N/A	N/A	0.0158435	N/A
Cubic Constant 2 (b)	N/A	N/A	N/A	-4.60439	N/A
Cubic Constant 3 (c)	N/A	N/A	N/A	450.99589	N/A
Cubic Constant 4 (d)	N/A	N/A	N/A	-14185.6755	N/A

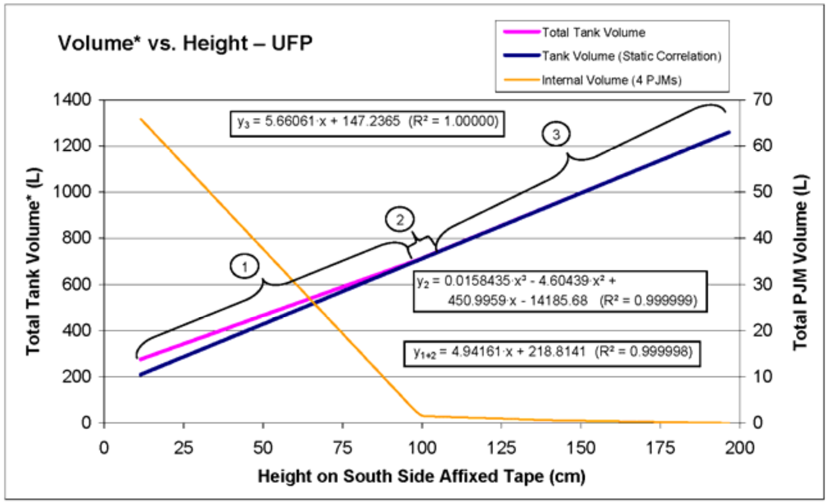

Equations on the plot above are for each numbered segment as identified by the subscript on the "y" and are valid only for the range of "x" specified in the Tank Volume Correlations table above.

* Total Tank Volume includes static volume plus volume inside PJMs above the level of the fluid surface in the tank.

** Height is location on the south side affixed tape for the top of the part, as measured externally.

ASSESSMENTS OF CORRELATIONS (TOTAL VOLUME)	**Height** (affixed tape, south side)	**Tank Volume*** From Segment Correlation	**Tank Volume*** From Static + Geometry	**Difference**	**Percent Error** (between models)
(Segment) / (Fit Type)	**(cm)**	**(L)**	**(L)**	**(L)**	**--**
(1 + 2 + 3) / (Linear)	11.5	258.227	275.520	17.292	6.2763 %
(1 + 2 + 3) / (Linear)	96.0	708.406	693.214	-15.193	-2.1916 %
(1 + 2 + 3) / (Linear)	101.0	735.044	719.129	-15.915	-2.2132 %
(1 + 2) / (Linear)	11.5	275.643	275.520	-0.123	-0.0447 %
(1 + 2) / (Linear)	96.0	693.208	693.214	0.006	0.0008 %
(1 + 2) / (Linear)	101.0	717.916	719.129	1.212	0.1686 %
(1) / (Linear)	11.5	275.673	275.520	-0.153	-0.0556 %
(1) / (Linear)	96.0	693.131	693.214	0.083	0.0120 %
(2) / (Cubic)	96.0	693.205	693.214	0.009	0.0013 %
(2) / (Cubic)	101.0	719.124	719.129	0.005	0.0007 %
(3) / (Linear)	101.0	718.958	719.129	0.171	0.0238 %
(3) / (Linear)	196.5	1259.546	1259.654	0.108	0.0086 %
(1 + 2) / (Linear)	95.0	688.267	688.271	0.004	0.0006 %
(1 + 2) / (Linear)	96.0	693.208	693.214	0.006	0.0008 %
(1 + 2) / (Linear)	100.0	712.975	713.513	0.538	0.0754 %
(1 + 2) / (Linear)	101.0	717.916	719.129	1.212	0.1686 %
(1) / (Linear)	95.0	688.190	688.271	0.080	0.0117 %
(1) / (Linear)	96.0	693.131	693.214	0.083	0.0120 %
(2) / (Cubic)	100.0	713.535	713.513	-0.023	-0.0032 %
(2) / (Cubic)	101.0	719.124	719.129	0.005	0.0007 %
(3) / (Linear)	119.0	820.849	820.876	0.027	0.0033 %
(3) / (Linear)	120.0	826.510	826.530	0.021	0.0025 %

COMPARISON TO ACTUAL VOLUME (PJMS FULL)	**Height** (affixed tape, south side)	**Tank Volume*** Actual Data (see Attachment B)	**Tank Volume*** Static + Geometry Correlation	**Difference**	**% Error** (between Actual & Model)
Tank Level	**(cm)**	**(L)**	**(L)**	**(L)**	**--**
~ H/D = 1.4	86.7	646.8	647.25	0.46	0.0709 %
			647.2	-0.39	-0.0606 %
~ H/D = 1.8	122.5	840.2	840.7	0.49	0.0577 %
			840.66	-0.48	-0.0572 %

ASSESSMENTS OF CORRELATIONS (DELTA VOLUME)	**Δ Height**	**Δ Volume** (From Segment Correlation)	**Δ Volume** (From Static + Geometry)	**Difference**	**% Error** (between models)
(Segment) / (Fit Type)	**(cm)**	**(L)**	**(L)**	**(L)**	**--**
(1 + 2) / (Linear)	96 – 95	4.942	4.943	0.002	0.0308 %
(1 + 2) / (Linear)	101 – 100	4.942	5.616	0.675	12.0125 %
(1) / (Linear)	96 – 95	4.940	4.943	0.003	0.0566 %
(2) / (Cubic)	101 – 100	5.588	5.616	0.028	0.4981 %
(3) / (Linear)	120 – 119	5.661	5.654	-0.007	-0.1158 %

Attachment G (page 1 of 3)

LS – Height / Volume Correlations

LINEAR CURVE FITS FOR TOTAL TANK VOLUME OVER RANGE OF EACH PART				
Height at Top of Part **	Part	Slope	Intercept	R²
(cm, south affixed)	--	(L/cm)	(L)	--
52.6	12" collar	--	--	--
102.6	12" pipe (PJM tube)	18.234691	1071.59478	1.00000
117.6	shoulder (rnd. rect.)	20.171107	866.18297	0.99825
126.9	2" collar	23.988178	426.28459	1.00000
148.7	2" pipe	24.002042	424.52514	1.00000
155.2	2" cap	23.988178	426.58685	1.00000
201	3/4" pipe	24.023518	421.10208	1.00000

Tank Volume* Correlations (shaded correlations are recommended)

Segment: (all heights are on the south side affixed tape scale)	1 + 2 + 3 Linear Fit For Segment from Height of 52.6 cm to 201.0 cm	1 Linear Fit For Segment from Height of 52.6 cm to 102.6 cm	2 Linear Fit For Segment from Height of 102.6 cm to 117.6 cm	2' Cubic Fit For Segment from Height of 101.0 cm to 117.6 cm	3 Linear Fit For Segment from Height of 117.6 cm to 201.0 cm
R²	0.996207	1.000000	0.998253	1.000000	1.000000
Slope (m)	21.95497	18.23469	20.17111	N/A	24.01227
Intercept (i)	753.8802	1071.5948	866.1830	N/A	423.1228
Cubic Constant 1 (a)	N/A	N/A	N/A	0.0096806	N/A
Cubic Constant 2 (b)	N/A	N/A	N/A	-2.98630	N/A
Cubic Constant 3 (c)	N/A	N/A	N/A	325.32031	N/A
Cubic Constant 4 (d)	N/A	N/A	N/A	-9454.7612	N/A

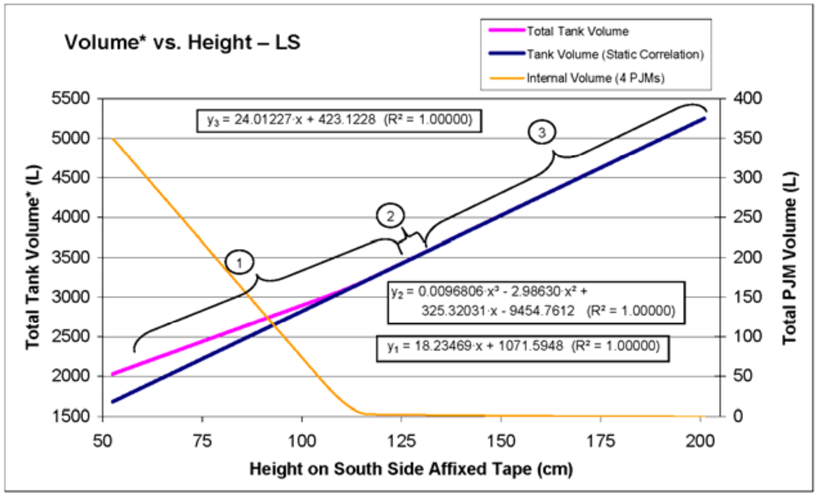

Equations on the plot above are for each numbered segment as identified by the subscript on the "y" and are valid only for the range of "x" specified in the Tank Volume Correlations table above.

* Total Tank Volume includes static volume plus volume inside PJMs above the level of the fluid surface in the tank.

** Height is location on the south side affixed tape for the top of the part, as measured externally.

COMPARISON TO ACTUAL VOLUME (PJMs FULL)	Height (affixed tape, south side)	Tank Volume* Actual Data (see Attachment B)	Tank Volume* Static + Geometry Correlation	Difference	% Error (between Actual & Model)
Tank Level	(cm)	(L)	(L)	(L)	--
~ H/D = 0.74	98.7	No Data	2871.37	--	--
			2871.4	--	--
~ H/D = 1.0 †	150.7	4043.2	4041.61	-1.64	-0.0407 %
			4041.77	1.48	0.0365 %

† Actual volume is estimated as the volume at the end of LS Addition #10, Supply Tank Fill #7.

ASSESSMENTS OF CORRELATIONS (TOTAL VOLUME)	Height (affixed tape, south side)	Tank Volume* From Segment Correlation	Tank Volume* From Static + Geometry	Difference	Percent Error (between models)
(Segment) / (Fit Type)	(cm)	(L)	(L)	(L)	--
(1 + 2 + 3) / (Linear)	52.5	1906.516	2028.358	121.841	6.0069 %
(1 + 2 + 3) / (Linear)	102.5	3004.265	2940.639	-63.625	-2.1637 %
(1 + 2 + 3) / (Linear)	117.5	3333.589	3244.890	-88.699	-2.7335 %
(1) / (Linear)	52.5	2028.916	2028.358	-0.558	-0.0275 %
(1) / (Linear)	102.5	2940.651	2940.639	-0.011	-0.0004 %
(2) / (Linear)	102.5	2933.721	2940.639	6.918	0.2353 %
(2) / (Linear)	117.5	3236.288	3244.890	8.602	0.2651 %
(2) / (Cubic)	101.0	2913.232	2913.288	0.057	0.0019 %
(2) / (Cubic)	102.5	2940.658	2940.639	-0.018	-0.0006 %
(2) / (Cubic)	117.5	3244.903	3244.890	-0.013	-0.0004 %
(3) / (Linear)	117.5	3244.564	3244.890	0.326	0.0100 %
(3) / (Linear)	201.0	5249.588	5249.829	0.241	0.0046 %
(1 + 2 + 3) / (Linear)	99.0	2927.422	2876.820	-50.602	-1.7590 %
(1 + 2 + 3) / (Linear)	100.0	2949.377	2895.054	-54.323	-1.8764 %
(1) / (Linear)	101.0	2913.299	2913.288	-0.010	-0.0003 %
(1) / (Linear)	102.0	2931.533	2931.522	-0.011	-0.0004 %
(2) / (Cubic)	101.0	2913.232	2913.288	0.057	0.0019 %
(2) / (Cubic)	102.0	2931.530	2931.522	-0.008	-0.0003 %
(2) / (Cubic)	115.0	3186.174	3186.129	-0.045	-0.0014 %
(2) / (Cubic)	116.0	3209.084	3209.059	-0.026	-0.0008 %
(3) / (Linear)	129.0	3520.705	3520.789	0.083	0.0024 %
(3) / (Linear)	130.0	3544.717	3544.791	0.073	0.0021 %

ASSESSMENTS OF CORRELATIONS (DELTA VOLUME)	Δ Height	Δ Volume (From Segment Correlation)	Δ Volume (From Static + Geometry)	Difference	% Error (between models)
(Segment) / (Fit Type)	(cm)	(L)	(L)	(L)	--
(1 + 2 + 3) / (Linear)	100 – 99	21.955	18.234	-3.721	-20.4067 %
(1) / (Linear)	102 – 101	18.235	18.234	-0.001	-0.0037 %
(2) / (Cubic)	102 – 101	18.298	18.234	-0.064	-0.3528 %
(2) / (Cubic)	116 – 115	22.911	22.930	0.020	0.0855 %
(3) / (Linear)	130 – 129	24.012	24.002	-0.010	-0.0426 %

336 4PJM – Height / Volume Correlations

LINEAR CURVE FITS FOR TOTAL TANK VOLUME OVER RANGE OF EACH PART				
Height at Top of Part **	Part	Slope	Intercept	R²
(inch)	--	(L/in.)	(L)	--
147.75	60° cone (24")	--	--	--
26.25	24" custom tube	-266.640169	48854.91182	1.00000
20	2:1 elliptical shoulder	-274.767898	49059.39579	0.99981
16	2" pipe	-296.073547	49510.24440	1.00000
-120	2" i.d. flexible hose	-296.054627	49509.94168	1.00000

Tank Volume* Correlations (shaded correlations are recommended)

Segment: (all heights are distances down from tank rim)	1 + 2 + 3 Linear Fit For Segment from Height of 0 in. to 147.75 in.	1 Linear Fit For Segment from Height of 26.25 in. to 147.75 in.	2 Linear Fit For Segment from Height of 20.5 in. to 26.25 in.	2 Cubic Fit For Segment from Height of 20.5 in. to 26.25 in.	3 Linear Fit For Segment from Height of 0.0 in. to 20.5 in.
R²	0.999898	1.000000	0.999811	1.000000	1.000000
Slope (m)	-268.45772	-266.64017	-274.76790	N/A	-296.05543
Intercept (i)	49039.3635	48854.9118	49059.3958	N/A	49509.9457
Cubic Constant 1 (a)	N/A	N/A	N/A	-0.2745679	N/A
Cubic Constant 2 (b)	N/A	N/A	N/A	21.62222	N/A
Cubic Constant 3 (c)	N/A	N/A	N/A	-834.22346	N/A
Cubic Constant 4 (d)	N/A	N/A	N/A	53821.2656	N/A

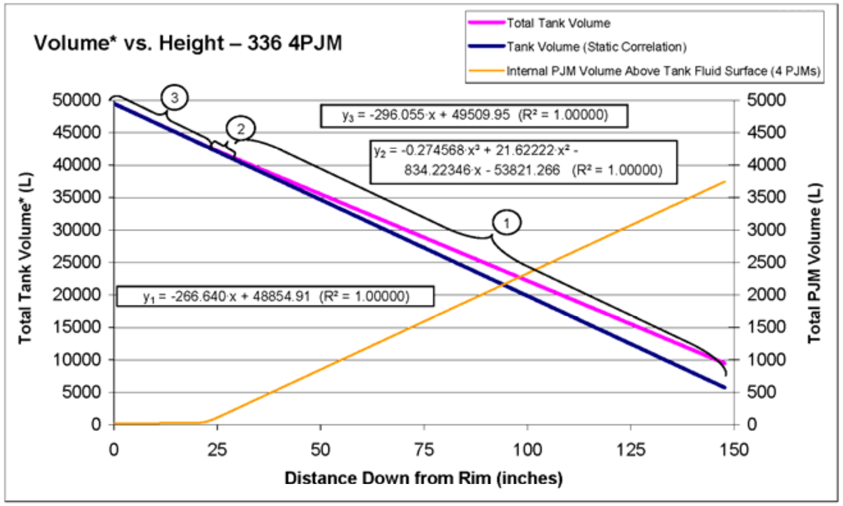

Equations on the plot above are for each numbered segment as identified by the subscript on the "y" and are valid only for the range of "x" specified in the Tank Volume Correlations table above.

* Total Tank Volume includes static volume plus volume inside PJMs above the level of the fluid surface in the tank.

** Height is distance down from tank rim to top of part as measured externally.

ASSESSMENTS OF CORRELATIONS (TOTAL VOLUME)	Height (distance down from tank rim)	Tank Volume* From Segment Correlation	Tank Volume* From Static + Geometry	Difference	Percent Error (between models)
(Segment) / (Fit Type)	(in.)	(L)	(L)	(L)	--
(1 + 2 + 3) / (Linear)	0.0	49039.363	49509.942	470.578	0.9505 %
(1 + 2 + 3) / (Linear)	26.5	41925.234	41788.947	-136.287	-0.3261 %
(1 + 2 + 3) / (Linear)	147.5	9441.850	9525.487	83.637	0.8780 %
(1) / (Linear)	26.5	41788.947	41788.947	0.000	0.0000 %
(1) / (Linear)	147.5	9525.487	9525.487	-0.000	-0.0000 %
(2) / (Linear)	20.5	43426.654	43440.986	14.332	0.0330 %
(2) / (Linear)	26.0	41915.430	41922.272	6.841	0.0163 %
(2) / (Cubic)	20.5	43440.986	43440.986	0.000	0.0000 %
(2) / (Cubic)	23.0	42731.613	42731.613	-0.000	-0.0000 %
(2) / (Cubic)	26.0	41922.272	41922.272	-0.000	-0.0000 %
(3) / (Linear)	0.0	49509.946	49509.942	-0.004	-0.0000 %
(3) / (Linear)	20.5	43440.809	43440.986	0.177	0.0004 %
(1) / (Linear)	30.0	40855.707	40855.707	0.000	0.0000 %
(1) / (Linear)	31.0	40589.067	40589.067	0.000	0.0000 %
(1) / (Linear)	60.0	32856.502	32856.502	0.000	0.0000 %
(1) / (Linear)	61.0	32589.862	32589.862	0.000	0.0000 %
(2) / (Cubic)	21.0	43295.199	43295.199	-0.000	-0.0000 %
(2) / (Cubic)	22.0	43009.905	43009.905	-0.000	-0.0000 %
(2) / (Cubic)	25.0	42189.444	42189.444	0.000	0.0000 %
(2) / (Cubic)	26.0	41922.272	41922.272	-0.000	-0.0000 %
(3) / (Linear)	15.0	45069.114	45069.122	0.008	0.0000 %
(3) / (Linear)	16.0	44773.059	44773.068	0.009	0.0000 %

COMPARISON TO ACTUAL VOLUME (PJMS FULL)	Height (distance down from tank rim)	Tank Volume* Actual Data (Hardy computer)	Tank Volume* From Static + Geometry	Difference	% Error (between Actual & Model)
Tank Level	(in.)	(L)	(L)	(L)	--
--------- No measurements with PJMs full were taken, hence a comparison is not possible. ---------					

ASSESSMENTS OF CORRELATIONS (DELTA VOLUME)	Δ Height	Δ Volume (From Segment Correlation)	Δ Volume (From Static + Geometry)	Difference	% Error (between models)
(Segment) / (Fit Type)	(in.)	(L)	(L)	(L)	--
(1) / (Linear)	31 – 30	-266.640	-266.640	-0.000	0.0000 %
(1) / (Linear)	61 – 60	-266.640	-266.640	0.000	-0.0000 %
(2) / (Cubic)	22 – 21	-285.294	-285.294	-0.000	0.0000 %
(2) / (Cubic)	26 – 25	-267.172	-267.172	-0.000	0.0000 %
(3) / (Linear)	16 – 15	-296.055	-296.055	0.001	-0.0003 %

Attachment G (page 3 of 3)

Appendix B

Empirical Holdup Model

Appendix B

Empirical Holdup Model[a]

The gas-holdup tests performed in the scaled prototype lag storage (LS) and ultra-filtration process (UFP) vessels and the 4PJM test stands in the Battelle—Pacific Northwest Division Applied Process Engineering Laboratory (APEL) and 336 Buildings and at Savannah River National Laboratory (SRNL) provide data with a range of variables and scales that are potentially amenable to empirical modeling to predict holdup in other systems. This appendix describes the process of model development and the resulting model. The final results are summarized in Section 5.4 of the main report.

B.1 Data Selection

The holdup data were recorded in 15 tests in the five test vessels during December 2003 through July 2004. The actual data values available for empirical modeling are listed in Table B.1. The holdup data in the first column represent averages of the once-per-cycle measurements over the last 20 PJM cycles for each gas-generation rate. The actual raw data from which the averages were computed were used to derive the empirical model. The second column contains the apparent bubble-rise velocity calculated from the holdup by the formula shown (from Eq. 2.14 in the main report). A bubble-rise velocity calculation is associated with each of the holdup data points. The values of the other variables are uniform for each test. Only two holdup measurements were available for the SNRL 4PJM test. The total number of data points used is 262: 120 for scaled prototype tests and 142 for the 4PJM series.

The scaled prototype tests and 4PJM tests represent two distinct populations of data. The scaled prototype LS and UFP tests used variations in their mixing systems that are not described by the variables listed. The notes at the bottom of Table B.1 show how sparging and recirculation varied in each test. The effects of sparging and recirculation cannot be isolated, however, because the LS sequence 14 test also used different PJM nozzle angles along with sparging, while LS sequence 15 used recirculation but changed to normal PJM nozzle design. Likewise, UFP sequence 5 had a shallow simulant depth with recirculation while UFP sequence 6 had deep simulant but changed to sparging. It could be said that each of these tests used some manner of enhanced mixing in addition to PJMs, though the effectiveness of individual methods cannot be compared directly.

The 4PJM tests were designed specifically to investigate the effects of scale. Each test is not only geometrically equivalent, but the PJM cycle time also follows the length scale; hence, there is only one independent variable available to describe the physical scale. The simulant rheology and gas-generation rate were varied within both the 336 and APEL 4PJM tests. Though intended to be uniform, the PJM nozzle velocities and drive times varied enough within and between tests to qualify as a potential influence on the holdup and bubble-rise velocity.

(a) The empirical holdup models given in this section must be used with careful consideration of scaling principles. They should only be applied to tank configurations, operational modes, and slurry conditions representative of the tests that were modeled.

Table B.1. Holdup-Data Summary

						PJM System Variables						
Test	**Holdup α_{SS} (Vol%)**	**$U_R = g_v H/\alpha_{SS}$ (m/min)**	**Gas Gen. g_v (ml/L-min)**	**Depth H (m)**	**(H/D)**	**Cycle Time t_C (min)**	**Drive Time t_D (min)**	**Number (N_{PJM})**	**Nozzle Vel. U_0 (m/s)**	**Nozzle Dia d_0 (m)**	**Yield stress τ_y (Pa)**	**Consistency κ (cP)**
Scaled Prototype Tests												
LS S14, R3a (a)	0.591	0.357	1.622	1.31	0.74	0.75	0.06975	8	17	0.0243	36	27
LS S14, R3b (a)	1.171	0.411	3.722	1.31	0.74	0.75	0.06975	8	17	0.0243	36	27
LS S15A, R3a (b)	0.790	0.267	1.620	1.31	0.74	0.75	0.079	8	16	0.0243	35	26
LS S15A, R3b (b)	1.397	0.312	3.373	1.31	0.74	0.75	0.079	8	16	0.0243	35	26
UFP S5, R3 (c)	3.430	0.142	4.196	1.2	1.4	0.45	0.033	4	15.7	0.0209	36	19
UFP S6, R3 (d)	3.465	0.158	3.669	1.55	1.8	0.45	0.033	4	16.4	0.0209	36	20
4PJM Tests												
336 12/16/03	3.682	0.129	1.434	3.45	0.9	1	0.15	4	8.5	0.1	44	23
336 7/22/04	1.616	0.172	0.817	3.45	0.9	1	0.158	4	8.3	0.1	20	18
APEL 12/15/03	1.613	0.175	3.719	0.77	0.9	0.22	0.0242	4	10.3	0.022	40	21
APEL 1/27/04	0.867	0.328	3.726	0.77	0.9	0.22	0.025	4	10.4	0.022	13	22
APEL 2/19/04	1.067	0.259	3.631	0.77	0.9	0.22	0.0264	4	9.9	0.022	7	9
APEL 2/25/04a	0.913	0.297	3.550	0.77	0.9	0.22	0.025	4	10.5	0.022	18	14
APEL 2/25/04b	1.347	0.407	7.210	0.77	0.9	0.22	0.025	4	10.5	0.022	18	14
SRS 12/13/03	1.272	0.126	4.052	0.4	0.9	0.11	0.0198	4	8.7	0.011	16	19
Data Range												
Maximum	3.68	0.41	7.21	3.45	1.8	1.0	0.16	8	17	0.10	44	27
Minimum	0.59	0.13	0.82	0.4	0.74	0.11	0.02	4	8.3	0.011	7	9

(a) LS Seq. 14 had half the PJM nozzles canted upward at 45 degrees with four of eight spargers operating and no recirculation.

(b) LS Seq. 15 had all PJM nozzles canted downward with four recirculation nozzles operating and no spargers.

(c) UFP Seq. 5 had one recirculation nozzle operating and no sparging.

(d) UFP Seq. 6 had one center sparger operating and no recirculation.

B.2 Model Selection

The objective of this process is to derive the best empirical model that predicts the apparent bubble-rise velocity, U_R, from the other variables shown in Table B.1. Criteria to determine which model is “best” are part of the iterative process. Mathematically, several models can be generated to predict the same variable. However, some models are more statistically stable than others.

A stepwise forward regression process was used to determine the “best” model. Stepwise forward regression begins with a 1-parameter model plus its intercept. Variables eligible for the model are chosen by their level of significance to U_R, the outcome that the model attempts to predict. All possible one-parameter models with some minimum significance are created and then ranked using calculated model criteria. Three of these criteria are the mean squared error (MSE), the correlation (R^2), and Mallow’s C_p (C_p). The best model is the one with the lowest MSE, the highest R^2, and C_p approaching the number of parameters in the model (plus intercept), p. Once the process determines the best one-parameter model, the best two-parameter model is derived in the same manner, and then the best three-parameter model, and so forth. At some point, the remaining variables not selected are not eligible to enter into the model, and the collection of models thus created is evaluated.

The primary evaluation criterion for the set of models is the lack of fit. Despite having the previous three criteria met, the model may not be “stable.” A lack of fit test compares the error associated with the model (difference between data and prediction) to the portion of the random error that cannot be explained by the model (pure error). If the error associated with the model is relatively large compared to the pure error, the model is either not appropriate or unstable. The predictions that would be generated from this model would have considerable uncertainty and be unreliable. This means that using input values different from the data used to create the model, even within the data range, might lead to nonsense predictions.

In the process of selecting the best models for predicting U_R, the complex relationships among the predictor variables rendered many models that seemed “best” according to selection criteria to be unstable when the lack of fit was tested. After much deliberation and iteration, three models were selected based on the criteria that were previously described. The criteria were derived from the two distinct populations of data plus the combined data set. A linear form was chosen for the model, i.e.,

$$U_R(P_i) = A + BP_1 + CP_2 + \ldots.. + X(P_nP_m) + \ldots.$$

where P_i are the data variables, A is the intercept, and B, C, … , X are model parameters. The last term illustrates an interaction between variables P_n and P_m. A log form of the model where the parameters become powers of the variables was discarded because of the complexity of the resulting interaction terms and the very large (and very small) numerical values of the parameters.

B.3 Model Using All Data

The model chosen using all the data is expressed in Eq. (B.1).[(a)] The model had MSE= 0.0013, $R^2 = 0.883$, and $C_p = 9.7$ (p = 12). The lack of fit indicated the model is appropriate (stable), with a p-value = 0.689 (p-values <= .05 indicate an inappropriate, or unstable model). The model estimates for each parameter, and the standard error for that parameter estimate, are shown in Table B.2. The standard error for the estimate shows its uncertainty, since it is an estimate. Figure B.1 shows the actual data versus the predicted values.

$$\begin{aligned} U_R = &- 19.96 + 0.0415g_v - 22.27D + 4.85N_{PJM} + 0.1474U_0 + 820d_0 + 0.0436\tau_y \\ &+ 0.0145\kappa + 0.00845(N_{PJM}\, g_v) - 0.00326(\kappa\, g_v) + 7.064(d_0\, D) - 0.0122(\tau_y\, N_{PJM}) \end{aligned} \tag{B.1}$$

Within this model, the gas generation rate, tank diameter, number of PJMs, nozzle velocity, and nozzle diameter, have the most impact, based on the level of significance.

Table B.2. Parameter Estimates Using All Data

Term	**Estimate**	**Std. Error**
Intercept	-19.96598	3.231394
Gas generation rate, g_v	0.0415082	0.007534
Tank diameter, D	-22.27025	3.142376
No. of PJMs, N_{PJM}	4.8495217	0.806995
PJM nozzle velocity,U_0	0.1474069	0.021491
PJM nozzle diameter,d_0	820.02102	112.1936
Simulant yield stress, τ_y	0.0436196	0.02222
Simulant consistency, κ	0.0145248	0.005567
Interactions		
($N_{PJM}\, g_v$)	0.0084502	0.004718
($\kappa\, g_v$)	-0.003259	0.001445
(d_0 D)	7.064022	1.905245
($\tau_y\, N_{PJM}$)	-0.012221	0.00555

B.4 Model Using 4PJM Data

The model using this 4PJM data only is given in Eq. (B.2). The model had MSE= 0.00086, $R^2 = 0.91$, and $C_p = 8$ (p = 8). The model was sufficiently stable that no lack-of-fit test was necessary. The model estimates for each parameter, and their associated standard error, are shown in Table B.3. Figure B.2 shows the actual data vs the predicted values.

$$\begin{aligned} U_R = &- 4.111 + 0.155g_v + 103t_D + 0.435U_0 + 0.0197\tau_y - 0.00162\kappa \\ &- 0.00693(\tau_y\, g_v) - 12.23(U_0\, t_D) \end{aligned} \tag{B.2}$$

(a) Rounding the parameter values to fewer significant digits than listed in Table B.2 did not significantly alter the metrics of the fit.

Based on the level of significance, the gas generation rate, drive time, and nozzle velocity have the highest impact within this model.

B.5 Model Using LS and UFP Data

The rest of the data involved the LS and UFP locations, which were deemed to behave more similarly to each other than to the 4PJM data. The model chosen using this set data in log space, expressed in Eq. (B.3), had MSE= 0.00173, $R^2 = 0.85$, and $C_p = 3.48$ ($p = 4$). All terms had an a strong impact on the model. The lack of fit indicated the model is appropriate (stable) with a p-value = 0.628 (p-values <= .05 indicate an inappropriate, or unstable model). The model estimates for each parameter, and their associated standard error, are shown in Table B.4. Figure B.3 shows the actual data versus the predicted values.

$$U_R = -2.91 + 0.0228 g_v + 0.0631 \tau_y + 0.036 \kappa \qquad \text{(B.3)}$$

This model illustrates the difficulty in using data from the LS and UFP tests to describe holdup behavior. It predicts that the bubble-rise velocity increases with the stiffness of the simulant. This nonphysical behavior is the result of attempting to model the differences in mixing system with variables that do not describe them directly. Here the lag storage tests had the best mixing and produced the highest bubble-rise velocity, but also had slightly stiffer clay. This model should not be used to scale up these data.

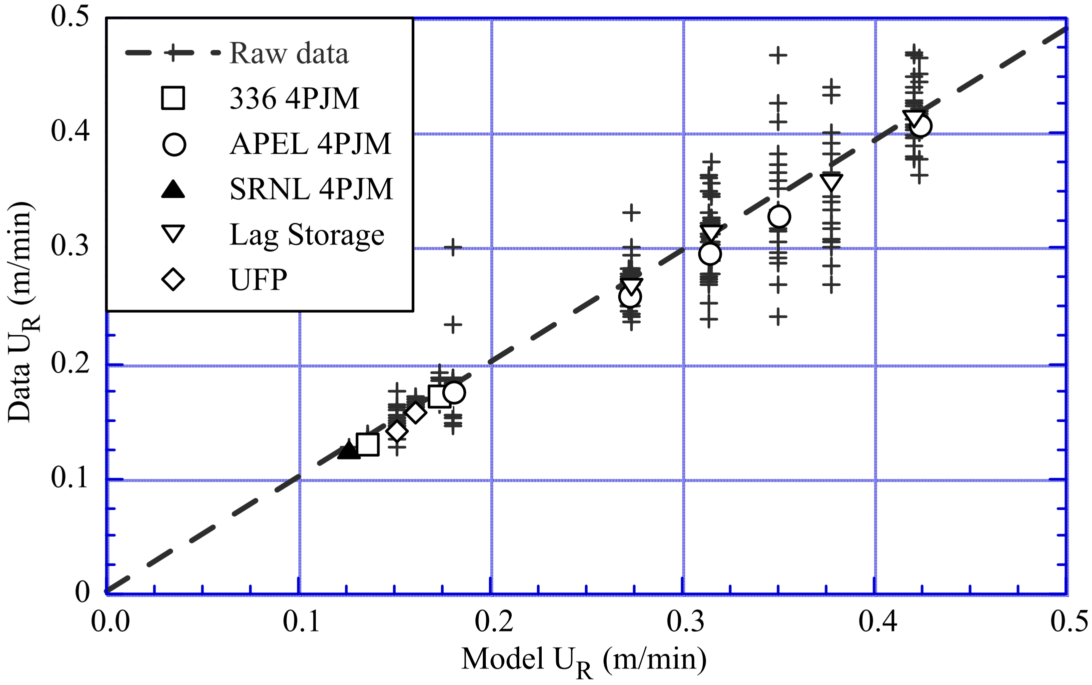

Figure B.1. Empirical Model for U_R Using All the Data

Table B.3. Parameter Estimates Using 4PJM Data

Term	Estimate	Std. Error
Intercept	-4.111	1.87707
Gas generation rate, g_v	0.1549639	0.069996
PJM drive time, t_D	102.99914	64.0176
PJM nozzle velocity,U_0	0.4346703	0.197537
Simulant yield stress, τ_y	0.019678	0.014082
Simulant consistency, κ	0.0016209	0.001261
Interactions		
(τ_y g_v)	-0.006933	0.003951
(U_0 t_D)	-12.22513	7.727429

Table B.4. Parameter Estimates Using LS and UFP Data

Term	Estimate	Std. Error
Intercept	-2.907444	0.325432
Gas-generation rate, g_v	0.0228	0.004769
Simulant yield stress, τ_y	0.0631165	0.008888
Simulant consistency, κ	0.0359864	0.001481

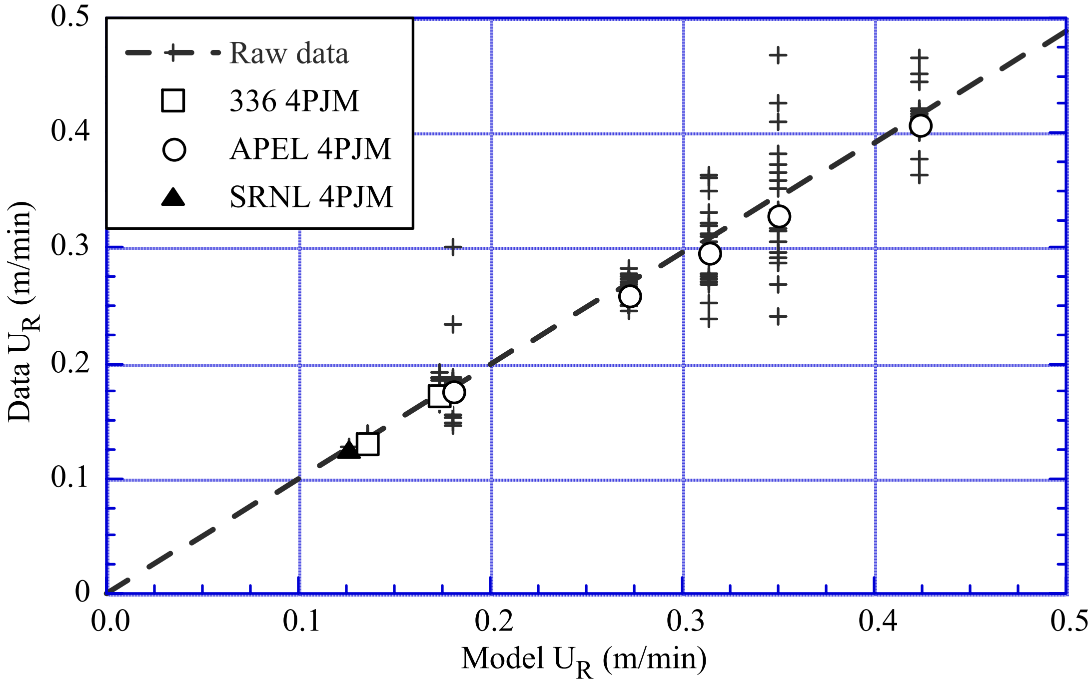

Figure B.2. Empirical Model for U_R Using Only 4PJM Data

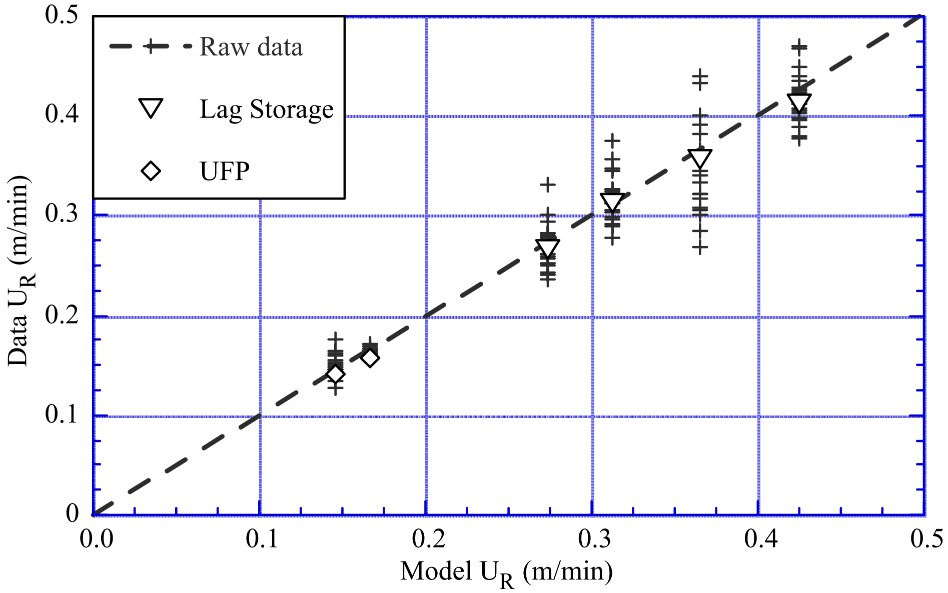

Figure B.3. Empirical Model for U_R Using Only LS and UFP Data

Appendix C

Bubble Column Gas Holdup

Appendix C: Bubble Column Gas Holdup

Matrix	**Yield Stress (Pa)**	**Consistency (cp)**	**Sodium nitrate concentration (M)**	**Anti-foaming agent concentration (ppm)**	**Gas**	**Superficial velocity (cm/s)**	**Gas Holdup (%)**	**Bubble rise velocity (cm/s)**
Water	0	1	0	0	Air	0.06	0.68	8.9
						0.21	1.2	17
						0.36	2.1	17
						0.72	4.4	16
						1.04	6.4	16
Water	0	1	0.5	0	Air	0.03	0.96	2.7
						0.06	1.6	3.8
						0.22	5.0	4.3
						0.39	8.6	4.5
Water	0	1	1	0	Air	0.03	1.3	2.0
						0.06	2.0	3.1
						0.22	5.0	4.3
						0.38	8.8	4.4
Water	0	1	0.1	100	Air	0.03	1.9	1.4
						0.06	3.4	1.8
						0.10	4.9	2.0
						0.18	8.3	2.2
Water	0	1	0.5	100	Air	0.03	1.8	1.4
						0.06	3.8	1.7
						0.10	5.7	1.8
						0.19	9.7	1.9

Matrix	Yield Stress (Pa)	Consistency (cp)	Sodium nitrate concentration (M)	Anti-foaming agent concentration (ppm)	Gas	Superficial velocity (cm/s)	Gas Holdup (%)	Bubble rise velocity (cm/s)
Water	0	1	0	0	Argon	0.07	0.74	9.7
						0.24	1.2	21
						0.42	1.9	22
						0.85	3.7	23
						1.23	5.7	22
Water	0	1	0.5	0	Argon	0.02	0.74	3.0
						0.05	1.6	3.4
						0.18	4.2	4.4
						0.33	7.0	4.7
Water	0	1	0.1	100	Argon	0.02	1.5	1.5
						0.05	3.3	1.6
						0.09	4.6	1.9
						0.16	7.8	2.0
Water	0	1	0.5	100	Argon	0.02	2.5	0.90
						0.05	4.0	1.3
						0.09	5.8	1.5
						0.16	9.6	1.7
Water	0	1	0	0	Hydrogen	0.10	0.78	13
						0.23	1.3	19
						0.84	4.3	20
						1.51	7.7	20
Water	0	1	0.5	0	Hydrogen	0.10	2.2	4.6

Matrix	**Yield Stress (Pa)**	**Consistency (cp)**	**Sodium nitrate concentration (M)**	**Anti-foaming agent concentration (ppm)**	**Gas**	**Superficial velocity (cm/s)**	**Gas Holdup (%)**	**Bubble rise velocity (cm/s)**
						0.24	5.1	4.8
						0.40	7.1	5.7
						0.58	9.1	6.3
Water	0	1	0.1	100	Hydrogen	0.10	3.0	3.2
						0.23	7.7	3.1
						0.39	12	3.3
						0.56	18	3.1
Water	0	1	0.5	100	Hydrogen	0.04	1.4	2.7
						0.10	3.9	2.6
						0.25	17	1.4
Water	0	1	0	0	Oxygen	0.06	0.75	7.7
						0.20	1.2	16
						0.34	2.0	17
						0.69	4.2	16
						1.00	6.2	16
Water	0	1	0.5	0	Oxygen	0.02	0.87	2.9
						0.06	1.6	3.6
						0.21	4.7	4.3
						0.37	9.0	4.1
Water	0	1	1	0	Oxygen	0.02	1.3	1.9
						0.06	2.0	2.9
						0.20	4.6	4.5
						0.36	9.2	4.0

Matrix	Yield Stress (Pa)	Consistency (cp)	Sodium nitrate concentration (M)	Anti-foaming agent concentration (ppm)	Gas	Superficial velocity (cm/s)	Gas Holdup (%)	Bubble rise velocity (cm/s)
Water	0	1	0.1	100	Oxygen	0.02	1.7	1.5
						0.06	3.5	1.7
						0.10	5.1	1.9
						0.18	8.2	2.2
Water	0	1	0.5	100	Oxygen	0.02	1.3	1.9
						0.06	3.0	2.0
						0.10	5.1	1.9
						0.18	8.4	2.1
Clay	7	14	0	0	Air	0.06	0.72	8.8
						0.21	0.75	29
						0.75	2.0	39
						1.10	2.6	42
						0.36	1.2	31
Clay	46	19	0.1	10	Air	0.05	0.39	14
						0.21	1.0	21
						0.74	2.6	29
						1.08	4.4	24
						0.35	1.4	26
Clay	23	20	0.01	100	Air	0.05	0.30	15
						0.17	0.97	18
						0.70	1.8	39
						1.04	2.9	36
						0.31	0.99	32

Matrix	**Yield Stress (Pa)**	**Consistency (cp)**	**Sodium nitrate concentration (M)**	**Anti-foaming agent concentration (ppm)**	**Gas**	**Superficial velocity (cm/s)**	**Gas Holdup (%)**	**Bubble rise velocity (cm/s)**
Clay	38	23	0.01	10	Air	0.06	0.13	46
						0.22	0.34	66
						0.75	1.9	40
						1.08	3.2	33
						0.36	0.66	55
Clay	54	26	0.1	100	Air	0.05	1.1	4.5
						0.19	1.8	10
						0.76	4.7	16
						1.16	6.1	19
						0.34	2.6	13
Clay	13	35	0	100	Air	0.20	0.50	40
						0.34	0.91	38
						0.71	1.7	41
						1.04	2.6	40
Clay	51	24	0.1	0	Air	0.05	0.13	36
						0.34	0.43	81
						0.73	1.8	40
						1.06	2.7	40
Clay	15	30	0	0	Air	0.06	0.27	24
						0.21	0.56	38
						0.36	0.91	40
						0.74	1.6	46
						1.10	2.4	47

Matrix	Yield Stress (Pa)	Consistency (cp)	Sodium nitrate concentration (M)	Anti-foaming agent concentration (ppm)	Gas	Superficial velocity (cm/s)	Gas Holdup (%)	Bubble rise velocity (cm/s)
Clay	7	14	0	0	Argon	0.07	0.30	24
						0.24	0.63	39
						0.42	0.97	44
						0.87	1.5	58
						1.28	2.2	60
Clay	46	19	0.1	10	Argon	0.20	0.41	50
						0.38	0.76	50
						0.84	1.8	48
						1.26	3.0	42
Clay	23	20	0.01	100	Argon	0.19	0.77	25
						0.35	1.0	36
						0.79	1.9	42
						1.21	2.9	42
Clay	38	23	0.01	10	Argon	0.24	0.26	95
						0.48	0.38	130
						0.83	1.2	72
						1.22	2.1	57
Clay	54	26	0.1	100	Argon	0.20	1.3	16
						0.38	2.0	19
						0.83	3.3	25
						1.25	4.9	25
Clay	13	35	0	100	Argon	0.19	0.77	25

Matrix	Yield Stress (Pa)	Consistency (cp)	Sodium nitrate concentration (M)	Anti-foaming agent concentration (ppm)	Gas	Superficial velocity (cm/s)	Gas Holdup (%)	Bubble rise velocity (cm/s)
						0.35	1.0	36
						0.79	1.9	42
						1.21	2.9	42
Clay	51	24	0.1	0	Argon	0.22	1.2	18
						0.39	1.5	26
						0.83	2.4	35
						1.22	4.1	30
Clay	15	30	0	0	Argon	0.07	0.21	33
						0.24	0.51	47
						0.41	0.60	69
						0.86	0.80	110
						1.27	1.2	106
Clay	7	14	0	0	Hydrogen	0.10	0.31	33
						0.24	0.34	70
						0.83	1.3	64
						1.46	2.8	52
Clay	46	19	0.1	10	Hydrogen	0.08	1.2	7.1
						0.23	2.0	11
						0.83	2.9	29
						1.62	6.6	25
Clay	23	20	0.01	100	Hydrogen	0.21	1.5	14
						0.74	2.4	31
						1.43	4.3	33

Matrix	Yield Stress (Pa)	Consistency (cp)	Sodium nitrate concentration (M)	Anti-foaming agent concentration (ppm)	Gas	Superficial velocity (cm/s)	Gas Holdup (%)	Bubble rise velocity (cm/s)
Clay	38	23	0.01	100	Hydrogen	0.09	0.36	26
						0.84	2.1	39
						1.51	4.5	33
						0.21	0.52	41
Clay	54	26	0.1	100	Hydrogen	0.08	0.99	8.2
						0.79	2.5	31
						1.53	6.4	24
						0.23	1.6	14
Clay	13	35	0	100	Hydrogen	0.11	1.6	6.9
						0.19	0.48	39
						0.81	2.2	36
						1.49	3.6	41
Clay	50	24	0.1	0	Hydrogen	0.07	0.08	94
						0.19	0.33	58
						0.83	1.5	56
						1.53	5.6	27
Clay	15	30	0	0	Hydrogen	0.10	0.5	230
						0.23	0.37	63
						0.83	1.1	73
						1.62	2.7	60
Clay	7	14	0	0	Oxygen	0.20	0.07	300
						0.35	0.08	430
						0.71	0.13	560

Matrix	**Yield Stress (Pa)**	**Consistency (cp)**	**Sodium nitrate concentration (M)**	**Anti-foaming agent concentration (ppm)**	**Gas**	**Superficial velocity (cm/s)**	**Gas Holdup (%)**	**Bubble rise velocity (cm/s)**
						1.05	0.20	530
Clay	46	19	0.1	10	Oxygen	0.06	0.19	30
						0.20	0.54	36
						0.34	1.3	26
						0.75	2.9	26
						1.09	4.2	26
Clay	23	20	0.01	100	Oxygen	0.04	0.60	7.5
						0.17	0.72	23
						0.31	0.96	32
						0.67	1.9	35
						1.00	3.0	33
Clay	38	23	0.01	100	Oxygen	0.05	0.090	55
						0.20	0.55	37
						0.37	0.92	40
						0.73	1.9	38
						1.04	3.1	34
Clay	54	26	0.1	100	Oxygen	0.04	0.47	9.2
						0.16	1.1	16
						0.30	1.2	25
						0.67	3.2	21
						1.03	4.7	22
Clay	13	35	0	100	Oxygen	0.05	0.49	10

Matrix	Yield Stress (Pa)	Consistency (cp)	Sodium nitrate concentration (M)	Anti-foaming agent concentration (ppm)	Gas	Superficial velocity (cm/s)	Gas Holdup (%)	Bubble rise velocity (cm/s)
						0.19	0.77	25
						0.33	1.2	28
						0.67	1.9	35
						0.98	2.4	41
Clay	51	24	0.1	0	Oxygen	0.04	1.1	4.1
						0.17	1.1	16
						0.32	1.3	25
						0.69	2.1	33
						1.02	3.5	29
Clay	15	30	0	0	Oxygen	0.06	0.49	12
						0.20	1.2	17
						0.34	2.6	13
						0.71	2.8	25
						1.04	3.4	31
Simulated HLW	7.2	7.3	0	0	Air	0.06	0.23	26
						0.21	0.53	39
						0.36	0.46	78
						0.73	0.46	160
						1.07	0.64	170
Simulated HLW	7.8	8.1	0	10	Air	0.06	0.69	9.0
						0.36	11	3.3
						0.73	11	6.7

Matrix	Yield Stress (Pa)	Consistency (cp)	Sodium nitrate concentration (M)	Anti-foaming agent concentration (ppm)	Gas	Superficial velocity (cm/s)	Gas Holdup (%)	Bubble rise velocity (cm/s)
						1.06	4.7	22
Simulated HLW	5.3	7.2	0	100	Air	0.06	0.78	8.0
						0.36	8.3	4.4
						0.74	14	5.2
						1.05	14	7.3
Simulated HLW	7.2	7.3	0	0	Argon	0.07	0.43	17
						0.24	1.2	20
						0.42	1.3	33
						0.86	1.4	63
						1.28	1.8	69
Simulated HLW	7.8	8.1	0	10	Argon	0.07	0.14	50
						0.42	3.7	11
						0.85	7.6	11
						1.22	2.9	43
Simulated HLW	5.3	7.2	0	100	Argon	0.07	0.60	13
						0.43	7.4	5.8
						0.86	13	6.8
						1.27	15	8.6
Simulated	7.2	7.3	0	0	Hydrogen	0.10	0.65	15

Matrix	**Yield Stress (Pa)**	**Consistency (cp)**	**Sodium nitrate concentration (M)**	**Anti-foaming agent concentration (ppm)**	**Gas**	**Superficial velocity (cm/s)**	**Gas Holdup (%)**	**Bubble rise velocity (cm/s)**
HLW								
						0.23	3.1	7.5
						0.86	2.9	30
						1.54	3.1	49
Simulated HLW	7.8	8.1	0	10	Hydrogen	0.10	0.91	11
						0.24	11	2.1
						0.90	16	5.7
						1.53	7.6	20
Simulated HLW	5.3	7.2	0	100	Hydrogen	0.10	3.1	3.3
						0.24	9.2	2.7
						0.40	14	2.9
						0.56	17	3.4
						1.54	19	8.2
Simulated HLW	7.2	7.3	0	0	Oxygen	0.06	0.63	9.1
						0.20	1.5	13
						0.34	1.4	24
						0.70	1.5	49
						1.05	2.1	50
Simulated HLW	7.8	8.1	0	10	Oxygen	0.06	0.27	21
						0.34	6.8	5.0

Matrix	Yield Stress (Pa)	Consistency (cp)	Sodium nitrate concentration (M)	Anti-foaming agent concentration (ppm)	Gas	Superficial velocity (cm/s)	Gas Holdup (%)	Bubble rise velocity (cm/s)
						0.70	8.7	8.0
						0.99	3.3	30
Simulated HLW	5.3	7.2	0	100	Oxygen	0.06	0.12	51
						0.35	9.5	3.7
						0.72	14	5.0
						1.04	15	6.7

Distribution

No. of
Copies

OFFSITE

4 Savannah River National Laboratory
Dan Burns
Westinghouse SA
Aiken, South Carolina 29808-0001

Richard Edwards
Westinghouse SA
Aiken, South Carolina 29808-0001

Hector Guerrero
Westinghouse SA
Aiken, South Carolina 29808-0001

David Wilson
Westinghouse SA
Aiken, South Carolina 29808-0001

No. of
Copies

ONSITE

17 Battelle – Pacific Northwest Division

S. T. Arm	P7-28
M. S. Fountain	P7-27
C. E. Guzman-Leong	K5-22
B. K. Hatchell	K5-22
D. E. Kurath	P7-28
P. A. Meyer	K7-15
C. D. Johnson	K6-96
S. D. Rassat (2)	K6-28
R. L. Russell (2)	K6-24
C. W. Stewart (2)	K7-15
Project Office (2)	P7-28
Information Release (2)	K1-06

5 Bechtel National, Inc.

H. Abodishish	H4-02
S. M. Barnes	H4-02
J. F. Doyle (2)	H4-02
G. L. Smith	H4-02